

Purification and Characterisation of Isoprene Monooxygenase from *Rhodococcus* sp. AD45

Leanne Sims

**A thesis submitted to the School of Environmental Sciences in
fulfilment of the requirements for the degree of Doctor in Philosophy**

September 2020

**University of East Anglia
School of Environmental Sciences
Norwich, UK**

©This copy of the thesis has been supplied on condition that anyone who consults it is understood to recognize that its copyright rests with the author and that use of any information derived therefrom must be in accordance with current UK Copyright Law. In addition, any quotation or extract must include full attribution

Abstract

Isoprene is a volatile organic compound (VOC) produced by many plants. Isoprene emissions account for one third of total VOCs from biogenic and anthropogenic sources, equal to that of methane. Atmospheric isoprene affects retention of greenhouse gases, air quality and climate. Recently, research has focussed on the role of bacteria in moderating isoprene emissions. Several diverse taxa of bacteria have been isolated capable of using isoprene as a sole carbon and energy source, including the model organism used here, *Rhodococcus* sp. AD45, a Gram positive bacterium isolated from freshwater sediment.

The ability to utilise isoprene is dependent upon a multistep pathway. The initial step is oxidation of isoprene to epoxy isoprene, catalysed by a four-component soluble di-iron monooxygenase (SDIMO), isoprene monooxygenase (IsoMO). IsoMO is a six protein complex comprising an oxygenase containing the di-iron active site (IsoABE), a Rieske-type ferredoxin (IsoC), NADH reductase (IsoF) and a coupling/effector protein (IsoD), homologous to the soluble methane monooxygenase and alkene/aromatic monooxygenases.

In this thesis, results of whole-cell characterisation of the isoprene monooxygenase within *Rhodococcus* sp. AD45 will be presented. This includes the kinetics, substrate range and inhibition of the enzyme by alkynes. The isoprene monooxygenase from *Rhodococcus* sp. AD45 was found to degrade a range of alkene and aromatic compounds, and was not inhibited by acetylene, despite being inhibited by alkynes of a longer carbon chain length.

The individual components of isoprene monooxygenase were also purified and characterised separately using a range of homologous and heterologous expression systems and purification techniques. Following this, reconstitution of the active complex was attempted, and potential avenues for future research were investigated based on the key findings of this research.

Access Condition and Agreement

Each deposit in UEA Digital Repository is protected by copyright and other intellectual property rights, and duplication or sale of all or part of any of the Data Collections is not permitted, except that material may be duplicated by you for your research use or for educational purposes in electronic or print form. You must obtain permission from the copyright holder, usually the author, for any other use. Exceptions only apply where a deposit may be explicitly provided under a stated licence, such as a Creative Commons licence or Open Government licence.

Electronic or print copies may not be offered, whether for sale or otherwise to anyone, unless explicitly stated under a Creative Commons or Open Government license. Unauthorised reproduction, editing or reformatting for resale purposes is explicitly prohibited (except where approved by the copyright holder themselves) and UEA reserves the right to take immediate 'take down' action on behalf of the copyright and/or rights holder if this Access condition of the UEA Digital Repository is breached. Any material in this database has been supplied on the understanding that it is copyright material and that no quotation from the material may be published without proper acknowledgement.

Table of Contents

| | |
|---|------|
| Abstract | ii |
| Table of Contents | iii |
| List of Tables | x |
| List of Figures | xii |
| Declaration..... | xxiv |
| Acknowledgements | xxv |
| Abbreviations | xxvi |
| 1. Introduction..... | 1 |
| 1.1. Isoprene | 1 |
| 1.1.1. The global significance of isoprene | 1 |
| 1.1.2. Isoprene Biosynthesis | 2 |
| 1.1.3. Isoprene Degradation | 7 |
| 1.1.4. Bacterial degradation of isoprene | 9 |
| 1.2. <i>Rhodococcus</i> sp. AD45..... | 13 |
| 1.2.1. Isolation and Taxonomy | 13 |
| 1.2.2. Isoprene degradation by <i>Rhodococcus</i> sp. AD45 | 14 |
| 1.2.3. Curing <i>Rhodococcus</i> sp. AD45 of the isoprene degradation cluster containing megaplasmid..... | 17 |
| 1.2.4. Isoprene monooxygenase in <i>Rhodococcus</i> sp. AD45..... | 18 |
| 1.3. Soluble Diiron Monooxygenases (SDIMOs) | 19 |
| 1.3.1. SDIMOs..... | 19 |
| 1.3.2. Soluble diiron monooxygenase components..... | 22 |
| 1.4. Project Aims | 26 |
| 2. Materials and Methods..... | 28 |
| 2.1 Materials..... | 28 |
| 2.2 Buffers and antibiotic stock solutions | 28 |
| 2.3 Preparation of media and cultivation of bacterial strains | 28 |
| 2.3.1 Growth of <i>Escherichia coli</i> | 30 |
| 2.3.2 Preparation and transformation of chemically competent <i>Escherichia coli</i> strains | 30 |
| 2.3.3 Growth of <i>Rhodococcus</i> sp. AD45 and AD45-ID..... | 31 |
| 2.3.4 Preparation and transformation of electrocompetent <i>Rhodococcus</i> sp. AD45-ID | 33 |
| 2.3.5 Growth of <i>Xanthobacter</i> sp. Py2 | 34 |
| 2.4 Extraction of nucleic acids | 35 |

| | | |
|--------|--|----|
| 2.4.1 | Plasmid extraction from <i>Escherichia coli</i> (mini- and midi-prep) | 35 |
| 2.4.2 | Genomic DNA extraction from <i>Rhodococcus</i> sp. AD45 | 35 |
| 2.5 | Nucleic acid manipulation techniques | 36 |
| 2.5.1 | Quantification of DNA | 36 |
| 2.5.2 | Polymerase Chain Reaction (PCR) | 36 |
| 2.5.3 | Cloning of PCR products into pJETblunt1.2 | 37 |
| 2.5.4 | DNA restriction digests | 37 |
| 2.5.5 | Dephosphorylation | 37 |
| 2.5.6 | DNA purification | 37 |
| 2.5.7 | DNA ligations | 37 |
| 2.5.8 | Sequencing of DNA | 37 |
| 2.5.9 | Agarose gel electrophoresis | 38 |
| 2.6 | Harvesting of cells | 38 |
| 2.7 | Preparation of cell extract | 38 |
| 2.7.1 | Quantification of protein content | 39 |
| 2.7.2 | SDS-PAGE | 39 |
| 2.8 | Fast Isoprene Sensor | 40 |
| 2.8.1 | Quantification of gaseous substrates in the headspace using the Fast Isoprene Sensor | 41 |
| 2.8.2 | Whole-cell assay for alkene degradation by <i>Rhodococcus</i> sp. AD45 using the Fast Isoprene Sensor | 42 |
| 2.8.3 | <i>Rhodococcus</i> sp. AD45 cell lysate assay for alkene degradation | 42 |
| 2.8.4 | Calculating the kinetic constants K_S and V_{max} for isoprene degradation by whole cells of <i>Rhodococcus</i> sp. AD45 containing isoprene monooxygenase | 42 |
| 2.9 | Oxygen electrode | 43 |
| 2.9.1 | Preparation of alkenes and aromatics for substrate specificity assays | 43 |
| 2.9.2 | Oxygen electrode based whole-cell assay to determine substrate specificity of isoprene monooxygenase from <i>Rhodococcus</i> sp. AD45 | 43 |
| 2.10 | Gas chromatography | 44 |
| 2.10.1 | Preparation of alkynes for inhibition assays | 44 |
| 2.11 | Chromatographic Purification | 44 |
| 2.11.1 | Affinity chromatography | 45 |
| 2.11.2 | Anion exchange chromatography | 45 |
| 2.11.3 | Hydrophobic interaction chromatography | 46 |
| 2.11.4 | Size exclusion chromatography | 46 |
| 2.11.5 | Concentration and buffer exchange of protein solutions | 46 |
| 2.12 | Spectroscopic techniques | 46 |

| | | |
|--------|---|----|
| 2.12.1 | Absorbance spectroscopy..... | 46 |
| 2.12.2 | Electron Paramagnetic Resonance (EPR) Spectroscopy..... | 47 |
| 2.12.3 | Circular Dichroism spectroscopy..... | 47 |
| 2.13 | Mass spectrometry techniques..... | 47 |
| 2.13.1 | Liquid chromatography-mass spectrometry (LC-MS) analysis..... | 47 |
| 2.13.2 | Inductively coupled plasma mass spectrometry (ICP-MS)..... | 48 |
| 2.14 | Cyclic voltammetry..... | 48 |
| 3. | Characterisation of isoprene monooxygenase in whole cells of <i>Rhodococcus sp. AD45</i> | 49 |
| 3.1. | Introduction..... | 49 |
| 3.2. | Expression of isoprene monooxygenase in <i>Rhodococcus sp. AD45</i> during growth on isoprene and succinate..... | 50 |
| 3.2.1. | Development of an assay to quantify degradation of isoprene by whole-cell suspensions of <i>Rhodococcus sp. AD45</i> | 50 |
| 3.2.2. | The effect of growth substrate on expression of the isoprene monooxygenase in <i>Rhodococcus sp. AD45</i> | 52 |
| 3.2.3. | Homologous expression of isoprene monooxygenase in <i>Rhodococcus sp. AD45-ID</i> | 54 |
| 3.2.4. | Quantification of isoprene degradation by <i>Rhodococcus sp. AD45</i> and <i>AD45-ID</i> expressing pTipQC1:IsoEx..... | 56 |
| 3.2.5. | Quantifying <i>Rhodococcus sp. AD45</i> isoprene monooxygenase activity using the Fast Isoprene Sensor and an oxygen electrode..... | 57 |
| 3.3. | Whole cell kinetics of isoprene and propylene degradation by <i>Rhodococcus sp. AD45</i> and <i>Xanthobacter sp. Py2</i> | 59 |
| 3.3.1. | Development of Fast Isoprene Sensor assays for whole-cell enzyme kinetics of isoprene and propylene degradation..... | 59 |
| 3.3.2. | Whole-cell kinetics for isoprene and propylene degradation by <i>Rhodococcus sp. AD45</i> expressing isoprene monooxygenase..... | 59 |
| 3.3.3. | Whole-cell kinetics for isoprene and propylene degradation by <i>Xanthobacter sp. Py2</i> expressing alkene monooxygenase..... | 61 |
| 3.3.4. | Comparison of isoprene degradation by <i>Rhodococcus sp. AD45</i> with other isoprene monooxygenases..... | 63 |
| 3.3.5. | Comparison of isoprene degradation by <i>Rhodococcus sp. AD45</i> with other soluble diiron monooxygenases..... | 64 |
| 3.4. | Substrate specificity of isoprene monooxygenase from <i>Rhodococcus sp. AD45</i> .. | 65 |
| 3.4.1. | Assay parameters to determine substrate specificity of isoprene monooxygenase from <i>Rhodococcus sp. AD45</i> | 65 |
| 3.4.2. | Oxidation of terminal alkenes by isoprene monooxygenase in whole cells of <i>Rhodococcus sp. AD45</i> | 66 |

| | | |
|--------|--|----|
| 3.4.3. | Activity of isoprene monooxygenase in whole-cell suspensions of <i>Rhodococcus</i> sp. AD45 with cyclic alkenes, dienes and aromatic compounds | 67 |
| 3.4.4. | Comparison of <i>Rhodococcus</i> sp. AD45 isoprene monooxygenase substrate specificity with that of other isoprene monooxygenases..... | 69 |
| 3.4.5. | Comparison of substrate specificity of isoprene monooxygenase in whole-cells of <i>Rhodococcus</i> sp. AD45 to that of other SDIMOs | 70 |
| 3.5. | Inhibition of isoprene monooxygenase in <i>Rhodococcus</i> sp. AD45 by alkynes..... | 72 |
| 3.5.1. | Development of an assay to quantify isoprene monooxygenase inhibition by alkynes | 72 |
| 3.5.2. | Inhibition of isoprene monooxygenase in whole cells of <i>Rhodococcus</i> sp. AD45 by terminal C ₂ -C ₈ alkynes | 73 |
| 3.5.3. | Inhibition by alkynes of alkene epoxidation by isoprene monooxygenase in <i>Rhodococcus</i> sp. AD45 | 74 |
| 3.5.4. | The alkyne inhibition profile of <i>Rhodococcus</i> sp. AD45 isoprene monooxygenase compared to other isoprene monooxygenases..... | 75 |
| 3.5.5. | Inhibition of isoprene monooxygenase by terminal alkynes and comparison with studies on other SDIMOs..... | 76 |
| 3.6. | Conclusions | 79 |
| 4. | Purification and characterisation of IsoC: The Rieske protein component of isoprene monooxygenase from <i>Rhodococcus</i> sp. AD45 | 80 |
| 4.1. | Introduction | 80 |
| 4.2. | Cloning <i>isoC</i> from <i>Rhodococcus</i> sp. AD45 into the pTipQC1 plasmid for expression in <i>Rhodococcus</i> sp. AD45-ID..... | 81 |
| 4.3. | Production of IsoC in the <i>Rhodococcus</i> sp. AD45-ID homologous expression system | 84 |
| 4.4. | Purification of IsoC from <i>Rhodococcus</i> sp. AD45-ID containing pTipQC1: <i>isoC</i> | 87 |
| 4.4.1. | Partial purification of IsoC by immobilised metal affinity chromatography . | 87 |
| 4.4.2. | Purification of IsoC from <i>Rhodococcus</i> sp. AD45 by gel filtration chromatography..... | 89 |
| 4.5. | Spectroscopic characterisation of purified IsoC from <i>Rhodococcus</i> sp. AD45..... | 91 |
| 4.5.1. | Absorbance spectra of oxidised and reduced IsoC from <i>Rhodococcus</i> sp. AD45 | 91 |
| 4.5.2. | Circular dichroism spectroscopy of purified IsoC from <i>Rhodococcus</i> sp. AD45 | 92 |
| 4.5.3. | Electron paramagnetic resonance spectroscopy of IsoC from <i>Rhodococcus</i> sp. AD45 | 94 |
| 4.6. | Characterisation of IsoC from <i>Rhodococcus</i> sp. AD45 by mass spectrometry..... | 95 |
| 4.6.1. | LC-MS analysis of IsoC from <i>Rhodococcus</i> sp. AD45..... | 95 |
| 4.6.2. | ICP-MS analysis of IsoC from <i>Rhodococcus</i> sp. AD45 | 96 |

| | | |
|--------|---|-----|
| 4.7. | Electrochemical characterisation of IsoC from <i>Rhodococcus</i> sp. AD45 using cyclic voltammetry..... | 97 |
| 4.7.1. | Determination of the midpoint potential of IsoC from <i>Rhodococcus</i> sp. AD45 | 97 |
| 4.7.2. | Comparison of N-terminally His tagged and untagged IsoC from <i>Rhodococcus</i> sp. AD45 | 98 |
| 4.8. | Conclusions | 101 |
| 5. | Purification and characterisation of IsoD: The coupling protein component of isoprene monooxygenase from <i>Rhodococcus</i> sp. AD45..... | 102 |
| 5.1. | Introduction | 102 |
| 5.2. | Cloning <i>isoD</i> from <i>Rhodococcus</i> sp. AD45 into the pTipQC1 expression plasmid for expression in <i>Rhodococcus</i> sp. AD45-ID..... | 102 |
| 5.2.1. | Amplification of <i>isoD</i> from <i>Rhodococcus</i> sp. AD45 genomic DNA | 103 |
| 5.2.2. | Production of IsoD in the <i>Rhodococcus</i> sp. AD45-ID homologous expression system | 104 |
| 5.2.3. | Attempted purification of IsoD from <i>Rhodococcus</i> sp. AD45-ID containing pTipQC1: <i>isoD</i> using immobilised metal chromatography | 107 |
| 5.3. | Cloning <i>isoD</i> from <i>Rhodococcus</i> sp. AD45 into the pET51b plasmid for expression in <i>Escherichia coli</i> | 110 |
| 5.3.1. | Amplification of <i>isoD</i> from <i>Rhodococcus</i> sp. AD45 genomic DNA | 110 |
| 5.3.2. | Production of IsoD in the <i>Escherichia coli</i> heterologous expression system | 112 |
| 5.4. | Purification of IsoD from <i>Escherichia coli</i> Rosetta 2 cells containing pET51b: <i>isoD</i> | 114 |
| 5.4.1. | Affinity chromatography and anion exchange partial purification of IsoD . | 114 |
| 5.4.2. | Purification of IsoD by gel filtration chromatography | 118 |
| 5.4.3. | Hydrophobic interaction chromatography purification of IsoD..... | 119 |
| 5.4.4. | Enterokinase cleavage of the N-terminal Strep-II Tag from recombinant IsoD | 121 |
| 5.4.5. | Preventing anomalous migration of IsoD in SDS-PAGE analysis..... | 123 |
| 5.5. | Absorbance spectrum of IsoD from <i>Rhodococcus</i> sp. AD45..... | 124 |
| 5.6. | LC-MS analysis of IsoD from <i>Rhodococcus</i> sp. AD45..... | 125 |
| 5.7. | Conclusions | 126 |
| 6. | Purification and characterisation of IsoF: The reductase component of isoprene monooxygenase from <i>Rhodococcus</i> sp. AD45..... | 127 |
| 6.1. | Introduction | 127 |
| 6.2. | Cloning <i>isoF</i> from <i>Rhodococcus</i> sp. AD45 into the pTipQC1 expression plasmid for expression in <i>Rhodococcus</i> sp. AD45-ID..... | 128 |
| 6.2.1. | Amplification of <i>isoF</i> from <i>Rhodococcus</i> sp. AD45 genomic DNA..... | 128 |

| | | |
|--------|--|-----|
| 6.2.2. | Production of IsoF in the <i>Rhodococcus</i> sp. AD45-ID homologous expression system | 129 |
| 6.2.3. | Attempted purification of IsoF from <i>Rhodococcus</i> sp. AD45-ID containing pTipQC1: <i>isoF</i> | 131 |
| 6.3. | Cloning <i>isoF</i> from <i>Rhodococcus</i> sp. AD45 into the pET21a plasmid for expression in <i>Escherichia coli</i> | 135 |
| 6.3.1. | Production of the pET21a: <i>isoF</i> plasmid..... | 135 |
| 6.3.2. | Production of IsoF in the <i>Escherichia coli</i> Rosetta 2 (pLysS) heterologous expression system | 136 |
| 6.4. | Cloning <i>isoF</i> from <i>Rhodococcus</i> sp. AD45 into the pET20MBP plasmid for expression in <i>Escherichia coli</i> as a maltose binding protein fusion | 139 |
| 6.4.1. | Production of the pET20MBP: <i>isoF</i> expression plasmid | 139 |
| 6.4.2. | Production of MBP-IsoF fusion in the <i>Escherichia coli</i> heterologous expression system | 140 |
| 6.5. | Attempted purification of MBP-IsoF from <i>Escherichia coli</i> Rosetta 2 cells | 141 |
| 6.5.1. | Affinity chromatography purification of MBP-IsoF | 141 |
| 6.5.2. | Anion exchange chromatography purification of MBP-IsoF..... | 144 |
| 6.5.3 | Removal of MBP from the IsoF fusion protein with Tobacco Etch Virus protease | 148 |
| 6.6. | Characterisation of the purified protein..... | 149 |
| 6.6.1. | Absorbance spectrum of the purified protein | 149 |
| 6.6.2. | NADH:ferricyanide reductase activity of the purified protein..... | 150 |
| 6.6.3. | LC-MS analysis of the purified protein..... | 151 |
| 6.7. | Purification of the reductases from soluble methane monooxygenase of <i>Methylosinus trichosporium</i> OB3b, alkene monooxygenase of <i>Rhodococcus rhodochrous</i> sp. B-276 and isoprene monooxygenase of <i>Rhodococcus</i> sp. AD45 as GST-fusions | 152 |
| 6.7.1. | Construction of the pGEX- <i>isoF</i> plasmid for expression of GST-IsoF in <i>Escherichia coli</i> | 153 |
| 6.7.2. | Production of GST-MmoC, GST-AmoD and GST-IsoF in the <i>Escherichia coli</i> heterologous expression system | 154 |
| 6.8. | Comparison of activity of GST-reductase fusion proteins and the cleaved reductases..... | 160 |
| 6.8.1. | NADH:ferricyanide reductase activity assay..... | 160 |
| 6.9. | Purification of the reductase from toluene 4-monooxygenase of <i>Pseudomonas mendocina</i> sp. KR1 | 162 |
| 6.10. | Reduction of purified IsoC using purified reductase fusion proteins..... | 164 |
| 6.11. | Conclusions..... | 165 |
| 7. | Reconstitution of the active isoprene monooxygenase complex from <i>Rhodococcus</i> sp. AD45..... | 167 |

| | | |
|--------|---|-----|
| 7.1. | Introduction | 167 |
| 7.2. | Purification of the oxygenase component of isoprene monooxygenase from <i>Rhodococcus</i> sp. AD45..... | 168 |
| 7.2.1. | Cloning <i>isoABE</i> from <i>Rhodococcus</i> sp. AD45 into the pTipQC2S2 vector for expression in <i>Rhodococcus</i> sp. AD45-ID | 168 |
| 7.2.2. | Purification protocol for IsoABE from <i>Rhodococcus</i> sp. AD45-ID (pTipQC2S2:IsoEx). | 169 |
| 7.3. | Characterisation of purified IsoABE from <i>Rhodococcus</i> sp. AD45..... | 171 |
| 7.3.1. | Absorbance spectrum of purified IsoABE..... | 171 |
| 7.3.2. | ICP-MS analysis of IsoABE from <i>Rhodococcus</i> sp. AD45 | 172 |
| 7.4. | Following isoprene monooxygenase activity in <i>Rhodococcus</i> sp. AD45: from whole cells to purified protein | 174 |
| 7.4.1. | Development of whole cell assays to monitor isoprene monooxygenase activity in <i>Rhodococcus</i> sp. AD45..... | 174 |
| 7.4.2. | Development of cell lysate assays to monitor isoprene monooxygenase activity in <i>Rhodococcus</i> sp. AD45..... | 175 |
| 7.4.3. | Addition of purified protein components to isoprene monooxygenase activity assays using <i>Rhodococcus</i> sp. AD45-ID (pTipQC2S2:IsoEx). | 179 |
| 7.5. | Reconstitution of the active isoprene monooxygenase complex from <i>Rhodococcus</i> sp. AD45..... | 180 |
| 7.6. | Conclusions | 182 |
| 8. | Conclusions and future prospects..... | 183 |
| 8.1. | Whole cell characterisation of isoprene monooxygenase..... | 183 |
| 8.2. | Purification and characterisation of the Rieske protein, IsoC..... | 183 |
| 8.3. | Purification and characterisation of the coupling protein, IsoD | 184 |
| 8.4. | Purification of SDIMO reductases..... | 184 |
| 8.5. | Reconstitution of the active complex | 185 |
| 8.6. | Future prospects..... | 185 |
| | References | 188 |
| | Appendix I..... | 210 |
| | List of solubilities | 210 |

List of Tables

| | |
|--|-----|
| Table 1.1: Genes and gene products of the isoprene degradation cluster from <i>Rhodococcus</i> sp. AD45..... | 17 |
| Table 2.1: Bacterial strains and plasmids used in this study. | 29 |
| Table 2.2: Components used to produce 12 % and 15 % SDS-PAGE resolving gels, and those used for the 4 % stacking gels..... | 39 |
| Table 3.1: Effect of cell suspension concentration on isoprene degradation rate of <i>Rhodococcus</i> sp. AD45 grown on isoprene in 2 mL vials. n=1 | 51 |
| Table 3.2: Effect of cell suspension concentration on isoprene degradation rate of <i>Rhodococcus</i> sp. AD45 grown on isoprene in 30 mL vials. n=3 | 51 |
| Table 3.3: Effect of temperature on isoprene degradation rate of <i>Rhodococcus</i> sp. AD45 grown on isoprene. n=3 (22/30 °C), n=1 (37 °C) | 52 |
| Table 3.4: Different levels of isoprene degradation by different <i>Rhodococcus</i> sp AD45 or AD45-ID grown on isoprene (iso) or succinate (succ) against a buffer control. n=1..... | 53 |
| Table 3.5: Difference in rate of isoprene degradation between whole cell suspensions of <i>Rhodococcus</i> sp. AD45 grown on isoprene (AD45iso), AD45-ID expressing the pTipQC1 empty expression vector (QC1 MT), the same vector expressing the isoABCDEF gene cluster from <i>Rhodococcus</i> sp. AD45 (QC1 IsoEx) and a buffer control. n=1..... | 57 |
| Table 4.1: Primer sequences used for polymerase chain reaction amplification of <i>isoC</i> from <i>Rhodococcus</i> sp. AD45 genomic DNA and cloning into expression vectors. | 81 |
| Table 4.2: Results of ICP-MS analysis of purified N-terminally 6His-tagged IsoC, showing the number of equivalents of each element per mole of protein. | 97 |
| Table 5.1: Primer sequences used for polymerase chain reaction amplification of <i>isoD</i> from <i>Rhodococcus</i> sp. AD45 genomic DNA and subsequent cloning into expression vectors. .. | 103 |
| Table 5.2: Primer sequences used for polymerase chain reaction amplification of <i>isoD</i> from <i>Rhodococcus</i> sp. AD45 genomic DNA and cloning into the pET51b expression vector..... | 110 |
| Table 6.1: Primer sequences used for polymerase chain reaction amplification of <i>isoF</i> from <i>Rhodococcus</i> sp. AD45 genomic DNA and cloning into expression vectors. | 129 |
| Table 6.2: Primer sequences used for polymerase chain reaction amplification of <i>isoF</i> from <i>Rhodococcus</i> sp. AD45 genomic DNA and cloning into the pGEX-2T expression vector.... | 153 |
| Table 7.1: Results of ICP-MS analysis of purified IsoABE, showing the number of equivalents of each element per mole of protein monomer. Where multiple isotopes of elements have been used the mean value is presented. | 173 |

| | |
|---|-----|
| Table 7.2: <i>Rhodococcus</i> sp. AD45 cell lysate isoprene degradation activity over as measured at timepoints (h) after cell breakage (n=1)..... | 177 |
| Table 7.3: Rate of isoprene degradation by cell lysate of <i>Rhodococcus</i> sp. AD45-ID (pTipQC2S2:IsoEx) with addition of IsoABE after various stages of purification. Experiments performed by Dr C. Lockwood (Murrell Group, University of East Anglia). | 179 |

List of Figures

| | |
|---|----|
| Figure 1.1: The isoprene cycle. Where known, relative contribution is indicated by thickness of arrows. Sources of isoprene are indicated by up arrows, and sinks by down arrows. Image taken from McGenity et al., 2018..... | 2 |
| Figure 1.2: Products of isoprene metabolism (taken from Nicholson, 2005). | 5 |
| Figure 1.3: The two known pathways of isoprene biosynthesis (image taken from McGenity et al., 2018)..... | 6 |
| Figure 1.4: Ozonolysis of isoprene. * indicates Criegee intermediates. Taken from Nguyen et al. (2016)..... | 9 |
| Figure 1.5: Proposed pathway for isoprene degradation in <i>Rhodococcus</i> sp. AD45 Taken from van Hylckama Vlieg et al. (2000) | 16 |
| Figure 1.6: Isoprene gene cluster arrangement in <i>Rhodococcus</i> sp. AD45, <i>Gordonia</i> sp. i37 and <i>Mycobacterium</i> sp. AT1. Image taken from Johnston et al. (2017), line at base represents 5 kbp..... | 16 |
| Figure 1.7: Subunits of the isoprene monooxygenase enzyme. The catalytic subunit IsoA is highlighted in blue. Iron cofactors components shown in red, sulphur as yellow circles, and FAD as a yellow diamond..... | 18 |
| Figure 1.8: Electron transfer in SDIMOs. Image adapted from Orville et al. (2003) | 21 |
| Figure 1.9: Relationship between catalytic subunits (IsoA) of isoprene monooxygenase at an amino acid level between different strains isolated on isoprene as a sole carbon and energy source. Taken from Larke-Mejía (2018)..... | 23 |
| Figure 1.10: Difference in conformation of coupling protein when interacting with the oxygenase of sMMO and To4MO. Oxygenase subunits shown in red (alpha), blue (beta) and yellow (gamma, coupling protein shown in turquoise. Crystal structures for sMMO and To4MO taken from (Lee et al., 2013) and (Acheson et al., 2017) respectively. | 24 |
| Figure 1.11: Predictions for binding between the oxygenase (yellow and grey) and the Rieske protein (red) and coupling protein (green). Image taken from (Liang and Lippard, 2014). A) Rieske protein and oxygenase, B) in the presence of 2-fold excess of coupling protein and C) in the presence of the same amounts of Rieske protein and coupling protein. | 26 |
| Figure 2.1: Diagram of fermenter growth of bacterial strains using gaseous isoprene as a carbon source. Image credit R. Dawson (Murrell Lab, University of East Anglia)..... | 33 |
| Figure 2.2: Output data from the fast isoprene sensor (FIS) (A) and how peak areas are converted to isoprene concentrations (B) and degradation rates (C). | 41 |

| | |
|---|----|
| Figure 3.1: SDS-PAGE gel showing polypeptide profile of <i>Rhodococcus</i> sp. AD45 grown on succinate (S) or isoprene (I). Highlighted bands were confirmed by extraction and analysis by mass spectrometry. Taken from Crombie et al., 2015. | 53 |
| Figure 3.2: Polypeptide profiles of different <i>Rhodococcus</i> sp. AD45 and AD45-ID cultures as determined by SDS-PAGE gel electrophoresis. AD45-ID cells contained pTipQC1 plasmid as either an empty vector (MT) or <i>isoABCDEF</i> expression vector (IsoEx). IsoA and IsoE peptides are highlighted by red and blue arrows respectively. | 55 |
| Figure 3.3: The effect of thiostrepton concentration (1 - 50 $\mu\text{g ml}^{-1}$) on induction of protein expression from the pTipQC1 IsoEx plasmid. IsoWT shows the polypeptide profile of cell-free extract from <i>Rhodococcus</i> sp. AD45 grown on isoprene. MT shows the profile of cell-free extract from <i>Rhodococcus</i> sp. AD45-ID containing the empty pTipQC1 vector. IsoA and IsoE bands are highlighted with red and blue arrows respectively..... | 55 |
| Figure 3.4: The effect of OD ₅₄₀ at induction (numbered samples) on protein expression from the pTipQC1 IsoEx plasmid. IsoWT = polypeptide profile of cell-free extract of <i>Rhodococcus</i> sp. AD45 grown on isoprene. MT = profile of cell free extract of <i>Rhodococcus</i> sp. AD45-ID containing the empty pTipQC1 vector. IsoA and IsoE bands are highlighted with red and blue arrows respectively. | 56 |
| Figure 3.5: Output of the Clark-type electrode (blue line) and where endogenous rates (black solid line) and induced rates (black dotted line) are calculated after addition of potential substrates (black arrows). | 59 |
| Figure 3.6: Whole-cell kinetics of isoprene degradation by <i>Rhodococcus</i> sp. AD45 expressing isoprene monooxygenase. Filled circles show the raw data, and empty circles the data fitted to the Michaelis-Menten equation. | 60 |
| Figure 3.7: Whole-cell kinetics of propylene degradation by <i>Rhodococcus</i> sp. AD45 expressing isoprene monooxygenase. Filled circles show the raw data, and empty circles show the data fitted to the Michaelis-Menten equation..... | 61 |
| Figure 3.8: Whole-cell kinetics of isoprene degradation by <i>Xanthobacter</i> sp. Py2 cells expressing alkene monooxygenase. Filled circles show the raw data, and empty circles the data fitted to the Michaelis-Menten equation. | 62 |
| Figure 3.9: Whole-cell kinetics of propylene degradation by <i>Xanthobacter</i> sp. Py2 expressing alkene monooxygenase. Filled circles show the raw data, and empty circles the data fitted to the Michaelis-Menten equation. | 63 |

| | |
|---|----|
| Figure 3.10: The rate of terminal alkene-induced oxygen uptake of whole-cell suspensions of <i>Rhodococcus</i> sp. AD45 grown on either isoprene (AD45iso, blue bars) or succinate (AD45succ, orange bars). AD45iso cells contain isoprene monooxygenase, whereas AD45succ cells do not and are used as a negative control. All substrates were added at 100 μM | 67 |
| Figure 3.11: The rate of substrate-induced oxygen uptake of whole-cell suspensions of <i>Rhodococcus</i> sp. AD45 grown on either isoprene (AD45iso, blue bars) or succinate (AD45succ, orange bars). AD45iso cells contain isoprene monooxygenase, whereas AD45succ cells do not and are used as a negative control. Substrates tested are dienes, cyclic alkenes and aromatic compounds, all of which were added at a concentration of 100 μM | 68 |
| Figure 3.12: Comparison of whole-cell substrate specificity of the isoprene monooxygenase from <i>Rhodococcus</i> sp. AD45 and <i>Variovorax</i> sp. WS11, shown as a % activity in comparison to the specific activity of the enzymes for isoprene. Specific activity for <i>Rhodococcus</i> sp. AD45 was 23.13 $\text{nmol min}^{-1} \text{mg dw cells}^{-1}$, whereas for <i>Variovorax</i> sp. WS11 it was 31.52 $\text{nmol min}^{-1} \text{mg dw cells}^{-1}$ | 69 |
| Figure 3.13: Inhibition of isoprene degradation by <i>Rhodococcus</i> sp. AD45 by the addition of DMSO | 73 |
| Figure 3.14: Inhibition by alkynes of isoprene degradation by <i>Rhodococcus</i> sp. AD45 grown on isoprene | 74 |
| Figure 3.15: Comparison of inhibition of isoprene degradation by whole cells of <i>Rhodococcus</i> sp. AD45 grown on isoprene by alkynes against the terminal alkene-induced rate of oxygen consumption of the same cell type. | 75 |
| Figure 3.16: Comparison of inhibition of isoprene degradation by whole cells of <i>Rhodococcus</i> sp. AD45 and <i>Variovorax</i> sp. WS11. | 76 |
| Figure 4.1: pJET1.2/blunt cloning system (image taken from https://www.thermofisher.com/order/catalog/product/K1231#/K1231 , ThermoFisher Scientific) | 81 |
| Figure 4.2: pTip expression system for protein production in <i>Rhodococcus</i> sp. AD45-ID. A) pTip series vector map. B) Multiple cloning site of Type 1 pTip vectors. (Images taken from https://www.hssnet.co.jp/e/2/2_7_22.html)..... | 83 |
| Figure 4.3: pTipQC1: <i>isoC</i> vector map | 83 |
| Figure 4.4: Polypeptide profiles of <i>Rhodococcus</i> sp. AD45-ID expressing pTipQC1: <i>isoC</i> as determined by SDS-PAGE gel electrophoresis. AD45-ID cultures were either non-induced | |

| | |
|---|----|
| (NI) or induced with 1 µg mL ⁻¹ thiostrepton (I) to produce the IsoC protein, which has been indicated with an arrow. | 84 |
| Figure 4.5: Polypeptide profiles of IsoC purification by 1 ml HisTrap spin-columns. CL is cell lysate, FT is the flow through, W is the wash and E is the elution. The IsoC bands have been highlighted by an arrow. | 85 |
| Figure 4.6: Polypeptide profiles of <i>Rhodococcus</i> sp. AD45-ID expressing pTipQC1: <i>isoC</i> as determined by SDS-PAGE gel electrophoresis. The number of hours after induction with 1 µg ml ⁻¹ thiostrepton has been labelled and the band corresponding to the IsoC polypeptide has been highlighted with a box..... | 85 |
| Figure 4.7: Absorbance spectroscopy of partially purified IsoC from <i>Rhodococcus</i> sp. AD45-ID expressing pTipQC1: <i>isoC</i> . 1 (blue line) shows the spectrum of the sample where the culture was grown and induced as normal. The culture producing sample 2 (orange line) was supplemented with additional iron and sulphur, and the culture producing sample 3 (grey line) was both supplemented as for culture 2 and exposed to a 20 minute cold shock on ice..... | 86 |
| Figure 4.8: Purification of IsoC using a 5 ml HisTrap column and a stepped benchtop elution as demonstrated by SDS-PAGE gel electrophoresis. The concentration of imidazole used in each elution step is presented above the relevant lanes and given as mM concentrations. Polypeptide bands corresponding to IsoC have been highlighted by an arrow. | 88 |
| Figure 4.9: HPLC trace of a gradient elution of IsoC on a 5 mL HisTrap column using an AKTApure HPLC system. The concentration of the imidazole in the elution buffer (green line) varies from 40 – 500 mM (0 – 100 % buffer B) over the gradient. | 88 |
| Figure 4.10: Purification of IsoC using a 5 mL HisTrap column and a gradient elution from 40 – 500 mM imidazole over 50 mL using an AKTApure HPLC system. Polypeptide profiles of fractions from the purification process were visualised using SDS-PAGE gel electrophoresis and InstantBlue staining. | 89 |
| Figure 4.11: Trace from AKTApure HPLC system showing IsoC purification using gel filtration chromatography. The peak which corresponds to IsoC has been highlighted with an arrow. Elution peaks checked by SDS-PAGE gel are numbered 1-4..... | 90 |
| Figure 4.12: Polypeptide profiles of fractions from the final gel filtration purification step to obtain pure IsoC. The three lanes on the far-right show fully purified and concentrated IsoC samples..... | 90 |

| | |
|--|-----|
| Figure 4.13: Absorbance spectra of purified N-terminally 6His-Tagged IsoC as purified (oxidised, solid line) and reduced by an excess of sodium dithionite (dotted line) between 300 and 700 nm..... | 91 |
| Figure 4.14: A: Circular dichroism spectra of oxidised (unbroken line) and reduced (dotted line) purified IsoC with an N-terminal 6His-tag. B: The difference between the CD spectra of oxidised and reduced IsoC..... | 93 |
| Figure 4.15: EPR spectrum of reduced IsoC..... | 94 |
| Figure 4.16: LC-MS analysis of purified N-terminally 6His-tagged IsoC. Expected mass 13782 Da..... | 95 |
| Figure 4.17: Cyclic voltammetry analysis of purified N-terminally 6His-tagged IsoC with poly-lysine as a co-adsorbant. Peaks are highlighted by arrows. | 97 |
| Figure 4.18: Gel filtration step of untagged IsoC purification. Sample 2 is <i>Rhodococcus</i> sp. AD45-ID (pTipQC2S2:IsoEx) cell lysate. Sample 3 is the load for the gel filtration column. Samples 4 – 17 are elution fractions from the column. Image credit: Dr C. Lockwood, Murrell Group, University of East Anglia..... | 99 |
| Figure 4.19: Absorbance spectrum of purified untagged IsoC as purified between 300 and 700 nm | 100 |
| Figure 4.20: Cyclic voltammetry analysis of purified untagged IsoC with poly-lysine as a co-adsorbant. Image credit: Dr C. Lockwood, Murrell Group, University of East Anglia | 100 |
| Figure 5.1: pTipQC1: <i>isoD</i> vector map for expression of <i>isoD</i> from <i>Rhodococcus</i> sp. AD45 in <i>Rhodococcus</i> sp. AD45-ID | 104 |
| Figure 5.2: Polypeptide profiles of <i>Rhodococcus</i> sp. AD45-ID expressing pTipQC1: <i>isoD</i> as determined by SDS-PAGE gel electrophoresis. AD45-ID cultures were either non-induced (NI) or induced with 1 $\mu\text{g mL}^{-1}$ thiostrepton (I) to produce the IsoD protein, which has been indicated with an arrow. | 105 |
| Figure 5.3: Polypeptide profiles of IsoD purification by 1 mL HisTrap spin-columns as determined by SDS-PAGE. CL is cell lysate, FT is the flow through, W is the wash and E is the elution. The band predicted to correspond to IsoD has been highlighted by an arrow..... | 105 |
| Figure 5.4: Polypeptide profiles of <i>Rhodococcus</i> sp. AD45-ID expressing pTipQC1: <i>isoD</i> as determined by SDS-PAGE. The OD ₅₄₀ at induction and concentration of thiostrepton used to induce ($\mu\text{g mL}^{-1}$) are labelled for each profile and the band predicted to correspond to the IsoD polypeptide has been highlighted with an arrow. | 106 |

| | |
|---|-----|
| Figure 5.5: HPLC trace of a gradient elution of IsoD on a 5 mL HisTrap column using an AKTApure HPLC system. The concentration of imidazole in the elution buffer (green line) varied from 40 – 500 mM (0 – 100 % buffer B) over the gradient. | 108 |
| Figure 5.6: A: Purification of IsoD using a 5 mL HisTrap column and a linear gradient elution from 40 – 500 mM imidazole over 50 mL using an AKTApure HPLC system. Polypeptide profiles of fractions were visualised using SDS-PAGE and InstantBlue staining. B: The pooled fractions highlighted in A after spin-concentrating as visualised by SDS-PAGE. | 108 |
| Figure 5.7: Attempted purification of IsoD using a 5 mL HisTrap column and a gradient elution from 40 – 500 mM imidazole over 50 mL using an AKTApure HPLC system. Polypeptide profiles of fractions were visualised using SDS-PAGE. | 109 |
| Figure 5.8: pET51b expression system for recombinant protein expression in <i>Escherichia coli</i> . A) pET51b vector map. B) Multiple cloning site for the pET51b vector. Images from https://www.merckmillipore.com/GB/en/product/pET-51b+-DNA-Novagen,EMD_BIO-71553#anchor_VMAP | 111 |
| Figure 5.9: pET51b: <i>isoD</i> vector map for expression of isoD from <i>Rhodococcus</i> sp. AD45 in <i>Escherichia coli</i> | 112 |
| Figure 5.10: Polypeptide profiles of <i>Escherichia coli</i> BL21 (DE3) expressing pET51b: <i>isoD</i> as determined by SDS-PAGE. BL21 (DE3) cultures were either non-induced (NI) or induced (I) with 50 µM IPTG to produce the IsoD protein, which has been indicated with an arrow... | 113 |
| Figure 5.11: Polypeptide profiles of <i>Escherichia coli</i> Rosetta 2 (pLysS) cells expressing pET51b: <i>isoD</i> as determined by SDS-PAGE. Rosetta 2 (pLysS) cultures were either non-induced (NI) or induced (I) with 50 µM IPTG to produce the IsoD protein, which has been indicated with an arrow. | 114 |
| Figure 5.12: HPLC trace of a single-step elution of IsoD on a 5 mL StrepTactin-XT column with 10 mM biotin using an AKTApure HPLC system. | 115 |
| Figure 5.13: SDS-PAGE analysis of fractions from HPLC purification of IsoD using a 5 mL StrepTactin-XT column in a single step elution with 10 mM Biotin using an AKTApure HPLC system. | 116 |
| Figure 5.14: HPLC trace of purification of IsoD using a 1 mL Q Sepharose column using an AKTApure system. The concentration of NaCl in the elution buffer (green line) varied from 0 – 1 M (0 – 100 % buffer B) over the gradient. | 117 |
| Figure 5.15: SDS-PAGE analysis of fractions from HPLC purification of IsoD using a 1 mL Q-Sepharose column. The band corresponding to IsoD has been indicated with an arrow. ... | 117 |

| | |
|--|-----|
| Figure 5.16: HPLC trace of purification of IsoD using a Superdex 200 pg 10/300 gel filtration column using an AKTApure system. | 118 |
| Figure 5.17: SDS-PAGE analysis of fractions from HPLC purification of IsoD using a Superdex 200 pg 10/300 gel filtration column. The band corresponding to IsoD has been indicated with an arrow. | 119 |
| Figure 5.18: SDS-PAGE analysis of IsoD sample before and after addition of 2 M ammonium sulfate. The sample with ammonium sulfate added was centrifuged and both the pellet (Precipitate) and supernatant (Phenyl Sepharose load) were analysed. | 120 |
| Figure 5.19: HPLC trace of IsoD purification after StrepII-tag removal using a 5 mL StrepTactin-XT column. | 121 |
| Figure 5.20: SDS-PAGE analysis of fractions from HPLC purification of IsoD after StrepII tag removal using a 5 mL StrepTactin-XT column. | 122 |
| Figure 5.21: SDS-PAGE analysis of the purified IsoD sample under different buffer and salt conditions and after freezing. | 123 |
| Figure 5.22: Comparison of IsoD purification by gel filtration one (orange line) or three (blue line) days after cell breakage. The peaks associated with standard and aggregated IsoD have been labelled with arrows. | 124 |
| Figure 5.23: Absorption profile of IsoD. | 124 |
| Figure 5.24: LC-MS analysis of purified N-terminally StrepII-tagged IsoD. Expected mass 14,735 Da. | 125 |
| Figure 6.1: pTipQC1: <i>isoF</i> vector map for expression of <i>isoF</i> from <i>Rhodococcus</i> sp AD45 in <i>Rhodococcus</i> sp. AD45-ID. | 129 |
| Figure 6.2: Polypeptide profiles of <i>Rhodococcus</i> sp. AD45 expressing pTipQC1: <i>isoF</i> as determined by SDS-PAGE. AD45-ID cultures were either non-induced (N) or induced with 1 $\mu\text{g ml}^{-1}$ thiostrepton (I) to produce a His-tagged IsoF protein, which has been indicated with an arrow. | 130 |
| Figure 6.3: Polypeptide profiles of IsoF partial purification by 1 mL HisTrap spin-columns as determined by SDS-PAGE. CL is cell lysate, FT is flow through, W is wash and E is elution. The band predicted to correspond to IsoF has been indicated with an arrow. | 131 |
| Figure 6.4: Attempted purification of IsoF from <i>Rhodococcus</i> sp. AD45 (pTipQC1: <i>isoF</i>) using a 5 mL HisTrap column and stepped elution with 125 – 500 mM imidazole. Polypeptide profiles of fractions were visualised using SDS-PAGE and InstantBlue staining. | 131 |
| Figure 6.5: Absorbance spectrum of IsoF partially purified by HisTrap column in comparison to the equivalent purification of IsoC. | 132 |

Figure 6.6: Ammonium sulfate precipitation of proteins in *Rhodococcus* sp. AD45-ID (pTipQC1:*isoF*) cell lysate. Each lane represents the non-precipitated proteins of that trial.133

Figure 6.7: HPLC trace of a gradient elution of IsoF on a 130 mL Q-Sepharose column on an AKTApure system. The concentration of NaCl in the elution buffer (green line) varied from 0 – 550 mM (0 – 55 % buffer B) in a 260 mL gradient, followed by a 1 M step of the same volume.....134

Figure 6.8: Attempted identification of fractions containing His-tagged IsoF from the anion exchange purification step using 1 mL HisTrap spin columns. L is load, FT is flow through, E is elution.134

Figure 6.9: pET21a:*isoF* vector map for expression of *isoF* from *Rhodococcus* sp. AD45 in *Escherichia coli* Rosetta 2 (pLysS)135

Figure 6.10: Polypeptide profiles of whole cells of *Escherichia coli* Rosetta 2 (pLysS) expressing pET21a:*isoF* as determined by SDS-PAGE. *Escherichia coli* Rosetta 2 cultures were either non-induced (N) or induced with 100 µM IPTG (I) to produce untagged IsoF protein, which has been indicated with an arrow.....136

Figure 6.11: Polypeptide profiles of *Escherichia coli* Rosetta 2 (pLysS) expressing pET21a:*isoF* as determined by SDS-PAGE. The temperature at induction (°C), time of induction (h) and IPTG concentration (µM) were altered in an attempt to optimise soluble IsoF production. W samples were from whole cells, whereas S samples were soluble extract only.137

Figure 6.12: Polypeptide profile of *Escherichia coli* Rosetta 2 (pLysS) expressing pET21a:*isoF* as determined by SDS-PAGE. The time after induction (h) is indicated at the top. W samples were whole cells, I samples were insoluble fractions of cell extract, S samples were soluble fractions of cell extract. The culture was induced with 100 µM IPTG at 25 °C.....138

Figure 6.13: Polypeptide profile of *Escherichia coli* Rosetta 2 (pLysS) expressing pET21a:*isoF* as determined by SDS-PAGE. The time after induction (h) is indicated at the top. W samples were whole cells, I samples were insoluble fractions of cell extract, S samples were soluble fractions of cell extract. The culture was induced with 25 (left) or 50 (right) µM IPTG at 18 °C.....139

Figure 6.14: pET20MBP:*isoF* vector map for production of IsoF from *Rhodococcus* sp. AD45 as an MBP fusion in *Escherichia coli* Rosetta 2 (pLysS).140

Figure 6.15: Polypeptide profile of *Escherichia coli* Rosetta 2 (pLysS) expressing pET20MBP:*isoF* as determined by SDS-PAGE. The time after induction (h) is indicated at the

| | |
|--|-----|
| top. W samples were whole cells, I samples were insoluble fractions of cell extract, S samples were soluble fractions of cell extract. NI samples were non-induced, I samples were induced with 100 μ M IPTG at 30 $^{\circ}$ C..... | 141 |
| Figure 6.16: HPLC trace of a step elution of MBP-IsoF on a 5 mL MBPTrap column using an AKTApure system. The elution buffer contained 10 mM maltose. | 142 |
| Figure 6.17: Purification of MBP-IsoF using a 5 mL MBPTrap column and step elution with 10 mM maltose using an AKTApure HPLC system. Polypeptide profiles of fractions were visualised using SDS-PAGE and InstantBlue staining. | 142 |
| Figure 6.18: Absorbance spectrum of the most concentrated fraction from an MBPTrap purification of MBP-IsoF both before (C11) and after (C11-SPUN) centrifugation to remove precipitated protein. The 420 nm absorbance spectrum feature has been highlighted with an arrow. | 143 |
| Figure 6.19: HPLC trace of a gradient elution of MBP-IsoF on a 130 mL Q-Sepharose column using an AKTApure HPLC system. The concentration of NaCl was varied from 0 – 550 mM over a 260 mL gradient, followed by a step of the same volume at 1 M..... | 145 |
| Figure 6.20: Purification of MBP-IsoF using a 130 mL Q-Sepharose column using an AKTApure HPLC system. Polypeptide profiles of fractions were visualised using SDS-PAGE and InstantBlue staining. L is the load and FT is the flow through..... | 145 |
| Figure 6.21: Absorbance spectra of the two flow through fractions from the 130 mL Q-Sepharose anion exchange column (1A1 and 1A2) used to partially purify MBP-IsoF. The maximum at 420 nm indicative of the presence of an iron-sulfur cluster has been indicated with an arrow..... | 146 |
| Figure 6.22: Spin concentration columns containing the A – flow through and B – concentrated flow through of the Q-Sepharose anion exchange column used to partially purify MBP-IsoF. The level of precipitation after concentration can be clearly seen in the increased opacity of B. | 147 |
| Figure 6.23: HPLC trace of attempted purification of MBP-IsoF using a 1 mL Blue Sepharose column using an AKTApure HPLC system. The concentration of NaCl in the elution buffer (green line) varied from 0 – 1 M over the 20 mL gradient. | 147 |
| Figure 6.24: Attempted purification of MBP-IsoF using a 1 mL Blue Sepharose column and a linear gradient elution from 0 – 1 M NaCl over a 20 mL gradient using an AKTApure HPLC system. Polypeptide profiles of fractions were visualised using SDS-PAGE and InstantBlue staining. L is the load, FT is the flow through and E is the elution. | 148 |

Figure 6.25: Polypeptide profiles of the MBP-IsoF before (uncut) and after (cut) cleavage of the fusion protein with TEV protease. The resulting sample was applied to two affinity chromatography columns using an AKTApure HPLC system: a 5 mL MBPTrap (MBP) and 5 mL HisTrap (IMAC) column. The flow through from MBP was the load for IMAC, and the load (L), flow through (FT) and elution (E) are presented. The flow through from the IMAC column was concentrated (Conc IsoF). All samples were visualised by SDS-PAGE.....149

Figure 6.26: Absorbance spectra of the resulting protein sample from the attempted IsoF purification (HisTrapFT) and the concentrated sample (Concentrated). The maximum at 420 nm indicating the presence of an iron sulphur cluster has been indicated with an arrow..150

Figure 6.27: Ferricyanide reductase activity of the protein sample believed to be IsoF in the presence and absence (+/-) of NADH. Control reactions not containing ferricyanide are indicated by (NF).151

Figure 6.28: LC-MS analysis of the protein product of attempted IsoF purification from an MBP fusion produced in *Escherichia coli* Rosetta 2 (pLysS). Expected mass 37,512.42 Da. 152

Figure 6.29: Vector map of pGEX-ISOF for expression of the isoprene monooxygenase from *Rhodococcus* sp. AD45 as a GST fusion in *Escherichia coli* Rosetta 2 (pLysS).....153

Figure 6.30: Polypeptide profiles of *Escherichia coli* Rosetta 2 (pLysS) expressing pGEX-MMOC, pGEX-AMOD or pGEX-IsoF as determined by SDS-PAGE. Cultures were wither non-induced (N) or induced with 100 μ M IPTG at 30 $^{\circ}$ C to produce the GST fusion proteins. Soluble refers to the soluble fraction of the cell extract, whereas the insoluble is the insoluble fraction of the cell extract. "N" samples were the soluble fraction. The size of expected GST-reductase fusions has been indicated with an arrow.....155

Figure 6.31: Polypeptide profiles of *Escherichia coli* Rosetta 2 (pLysS) expressing pGEX-IsoF, pGEX-MMOC or pGEX-AMOD as determined by SDS-PAGE. The IPTG concentration used to induce gene expression (μ M) and time after induction at 30 $^{\circ}$ C (h) are indicated. All samples were soluble extract from the cells.156

Figure 6.32: Polypeptide profiles of GST fusions of IsoF, MmoC and AmoD by 5 mL GSTrap columns using an AKTApure HPLC system, as determined by SDS-PAGE. The size of the expected GST-reductase fusions has been indicated by an arrow.....157

Figure 6.33: Absorbance spectrum of GST-IsoF fusion partially purified by GSTrap column. Inset is zoomed in to show spectroscopic feature at 420 nm.158

Figure 6.34: Absorbance spectra of purified GST fusions of both MmoC (orange line) and AmoD (yellow line). Inset is zoomed in to show the spectroscopic features after the A_{280} peak of protein more clearly.....158

| | |
|---|-----|
| Figure 6.35: Polypeptide profiles of the partial purification of GST-IsoF using a 5 mL GSTrap column and an AKTApure HPLC (Load, Flow through and Elution) as determined by SDS-PAGE. Samples of the elution fraction were incubated overnight at 4 °C (E-4C), room temperature (E-RT) and room temperature in the presence of thrombin to cleave the GST (E-RT+Thrombin). The thrombin alone is also present to show where this polypeptide band lies..... | 159 |
| Figure 6.36: Polypeptide profiles of the purification of A) AmoD and B) MmoC as determined by SDS-PAGE. A) The <i>Escherichia coli</i> Rosetta 2 (pLysS) (pGEX-AMOD) soluble cell extract (Load) was applied to a 5 mL GSTrap affinity chromatography column and eluted with the addition of reduced glutathione (Elution). This was incubated in the presence and absence (+/-) of thrombin at room temperature overnight, followed by another GSTrap purification step, where both the flow through (FT) and elution (E) were analysed. B) The <i>Escherichia coli</i> Rosetta 2 (pLysS) (pGEX-MMOC) soluble cell extract (Load) was applied to a 5 mL GSTrap affinity chromatography column and eluted with the addition of reduced glutathione (Elution). This was incubated in the presence of thrombin at room temperature overnight (Elution+Th)..... | 160 |
| Figure 6.37: NADH:ferricyanide reductase activity of IsoF as a GST fusion (GST-IsoF), and after cleavage of the GST tag with thrombin (GST/IsoF) as monitored by the change in absorbance at 420 nm. The activity of thrombin alone was also monitored to account for the level which could be attributed to the presence of thrombin in the cleaved IsoF sample. | 161 |
| Figure 6.38: NADH:ferricyanide reductase activity of GST-AmoD and –MmoC fusion proteins (uncut) and those cleaved with thrombin (cut) as monitored by the change in absorbance at 420 nm. Volumes given are the amount of protein sample added to a 1 mL total reaction volume..... | 162 |
| Figure 6.39: Polypeptide profiles of T4moF purification protocol. Lanes 2-7 are the Q-Sepharose elution fractions, Lanes 8-17 are the MBPTrap elution fractions. Image credit Dr C Lockwood (Murrell Group, University of East Anglia)..... | 163 |
| Figure 6.40: Absorbance spectrum of purified T4moF. Image credit Dr C. Lockwood (Murrell Group, University of East Anglia)..... | 164 |
| Figure 6.41: Reduction of purified IsoC by SDIMO reductases..... | 165 |
| Figure 7.1: pTipQC2S2:IsoEx vector map for expression of <i>isoABCDEF</i> in <i>Rhodococcus</i> sp. AD45-ID, producing an N-terminally StrepII-tagged IsoA protein..... | 168 |

| | |
|--|-----|
| Figure 7.2: HPLC trace of a one-step elution of IsoABE from a 5 mL Strep-TactinXT column using an AKTApure system. The peak corresponding to the IsoABE elution has been highlighted with an arrow. | 170 |
| Figure 7.3: Polypeptide profile of IsoABE purification from <i>Rhodococcus</i> sp. AD45-ID (pTipQC2S2:IsoEx) using a 5 mL StrepTactin-XT column as visualised by SDS-PAGE and InstantBlue staining. | 170 |
| Figure 7.4: Purification of IsoABE using size exclusion chromatography. Polypeptide profiles of fractions were visualised using SDS-PAGE and InstantBlue staining. Image credit C. Lockwood..... | 171 |
| Figure 7.5: Absorbance spectrum of IsoABE as purified between 250 and 700 nm. | 172 |
| Figure 7.6: Protein yield of various cell lysis methods conducted on <i>Rhodococcus</i> sp. AD45 cells grown on isoprene. F/T – Freeze/Thaw 3x, S – Sonication, L – Lysozyme, FP – French Press. | 176 |
| Figure 7.7: Difference in rate of isoprene degradation by <i>Rhodococcus</i> sp. AD45 cell lysate samples diluted to different protein concentrations using phosphate buffer. | 176 |
| Figure 7.8: The effect of NaCl addition on the isoprene degradation activity of <i>Rhodococcus</i> sp. AD45-ID cell lysate..... | 178 |
| Figure 7.9: Attempted reconstitution of purified isoprene monooxygenase in 50 mM phosphate buffer pH 7.0 using purified protein as monitored by isoprene depletion using a Fast Isoprene Sensor over A) 18 min and B) 180 min. | 181 |
| Figure 7.10: Attempted reconstitution of purified isoprene monooxygenase in 50 mM phosphate buffer pH 7.0 containing 200 mM NaCl as monitored by isoprene depletion using a Fast Isoprene Sensor over A) 18 min and B) 180 min..... | 182 |

Declaration

I declare that the work presented in this thesis was conducted by me under the direct supervision of Professor J. Colin Murrell. Results obtained by, or with help from, others has been acknowledged in the relevant section. None of the work presented has been previously submitted for any other degree.

Leanne Sims

Acknowledgements

I would like to thank the BBSRC and the Norwich Doctoral Training Partnership for funding my PhD project. I am grateful to my supervisor, Professor Colin Murrell, for his support and guidance. I am also indebted to the other members of my supervisory team, Professor Nick Le Brun and Dr Andrew Crombie for their advice and help.

I would like to acknowledge the support of Dr Dimitri Svistunenko for EPR analysis, Dr Leon Jenner for assistance in LC-MS and ICP-MS analysis. I would like to thank members of the ELSA and Le Brun groups, past and present, for their technical and emotional support. I would particularly like to thank Dr Colin Lockwood for his endless guidance and patience.

Finally, I would like to thank my closest family and friends for supporting me through the last four years. In particular, to my husband Matt and friends Claire, Em and Lisa, whose emotional support and help to switch off made finishing this project possible.

Abbreviations

| | |
|------------------------|---|
| A | absorbance |
| Amp^R | ampicillin resistance |
| ATP | adenosine triphosphate |
| bis | N,N'-methylenebisacrylamide |
| BMM | bacterial multicomponent monooxygenases |
| bp | base pairs |
| BVOC | biogenic volatile organic compounds |
| CD | circular dichroism |
| Chl^R | chloramphenicol resistance |
| CL | cell lysate |
| CoA | coenzyme A |
| CTAB | cetyl trimethylammonium bromide |
| CV | column volumes |
| Da | Daltons |
| DMAPP | dimethylallyl diphosphate |
| DMS | dimethyl sulfide |
| DMSO | dimethylsulfoxide |
| DNA | deoxyribonucleic acid |
| DTT | dithiothreitol |
| dw | dry weight |
| E | elution |
| EDTA | ethylenediaminetetraacetic acid |
| EPR | electron paramagnetic resonance |
| F/T | freeze thaw |
| FAD | flavin-adenine dinucleotide |
| FID | flame ionization detector |
| FIS | Fast Isoprene Sensor |
| FP | French press |
| FT | flow through |
| g | grams |
| g | acceleration due to gravity |
| G | giga |

| | |
|------------------------|--|
| GMBA | 2-glutathionyl-2-methyl-3-butenolate |
| GST | glutathione S-transferase |
| h | hours |
| HEPES | 4-(2-hydroxyethyl)-1-piperazineethanesulfonic acid |
| HGMB | 1-hydroxy-2-glutathionyl-2-methyl-2-butene |
| HIC | hydrophobic interaction chromatography |
| HPLC | high performance liquid chromatography |
| Hz | hertz |
| I | induced |
| ICP-MS | inductively coupled plasma mass spectrometry |
| IMAC | immobilised metal affinity chromatography |
| IPP | isopentenyl diphosphate |
| IPTG | Isopropyl β -D-1-thiogalactopyranoside |
| k | kilo |
| L | litre |
| LB | Luria-Bertani |
| LC-MS | liquid chromatography-mass spectrometry |
| M | molar |
| m | metre/milli |
| m/z | mass to charge ratio |
| MACR | methacrolein |
| MBP | maltose binding protein |
| MCS | multiple cloning site |
| MEP | methylerythritol phosphate |
| min | minutes |
| mol | mole |
| MPa | megapascals |
| MVA | mevalonate |
| MVK | methyl vinyl ketone |
| n | nano |
| NAD⁺ | nicotinamide adenine dinucleotide (oxidised form) |
| NADH | nicotinamide adenine dinucleotide (reduced form) |
| NADPH | nicotinamide adenine dinucleotide phosphate (reduced form) |
| NI | non-induced |

| | |
|-------------------------|---|
| OD | optical density |
| p | pico |
| PAGE | polyacrylamide gel electrophoresis |
| PCR | polymerase chain reaction |
| pMMO | particulate methane monooxygenase |
| POZ | primary ozonides |
| ppbv | parts per billion by volume |
| ppmv | parts per million by volume |
| psi | pounds per square inch |
| RNA | ribonucleic acid |
| ROS | reactive oxygen species |
| rpm | revolutions per minute |
| rRNA | ribosomal RNA |
| SDIMO | soluble diiron monooxygenase |
| SDS | sodium dodecyl sulfate |
| s | seconds |
| SHE | standard hydrogen electrode |
| SIP | stable isotope probing |
| sMMO | soluble methane monooxygenase |
| SOA | secondary organic aerosols |
| SOB | super optimized broth |
| TBE | Tris-Borate-EDTA (buffer) |
| TCE | trichloroethylene |
| TEMED | N,N,N',N'-tetramethyl-ethane-1,2-diamine |
| TEV | tobacco etch virus |
| thio^R | thiostrepton resistance |
| To4MO | toluene 4-monooxygenase |
| TOF | time of flight |
| Tris | tris(hydroxymethyl)aminomethane |
| V | volts |
| v/v | volume to volume |
| W | Watts/wash (when used on SDS-PAGE labels) |
| w/v | weight to volume |
| WT | wild type |

| | |
|------------|------------------------|
| α | alpha |
| β | beta |
| γ | gamma |
| ϵ | extinction coefficient |
| μ | micro |
| Ω | ohm |

1. Introduction

1.1. Isoprene

1.1.1. The global significance of isoprene

Isoprene is an abundant biogenic volatile organic compound (BVOC) with the systematic chemical name 2-methyl-1,3-butadiene (C₅H₈). Isoprene is a volatile liquid with a boiling point of 34 °C. It is released to the atmosphere in huge quantities, estimated to account for 550 ± 100 Tg of atmospheric carbon released per year (Guenther *et al.*, 2006, 2012), a similar quantity to global emissions of methane. Isoprene accounts for approximately one third of the global reactive BVOC flux (Guenther *et al.*, 2012), including 30 % of total VOC emissions in Europe and 50 % of reactive BVOC emissions (Jenkin *et al.*, 2015).

Over 90 % of the isoprene emitted to the atmosphere comes from terrestrial plants, with trees and shrubs being the highest contributors within this category (reviewed in McGenity *et al.*, 2018, Murrell *et al.*, 2020). Atmospheric concentrations vary greatly over both spatial and temporal parameters (Guenther *et al.*, 2006). Multiple studies have found that isoprene is emitted in a diurnal cycle in a variety of plant species (Funk *et al.*, 2003; Harley *et al.*, 2014), and is linked to both thermal tolerance (Sharkey *et al.*, 2008) and protection against reactive oxygen and nitrogen species (Vickers *et al.*, 2009), in addition to plant growth regulation (Jones *et al.*, 2016) and reducing insect herbivory (Laothawornkitkul *et al.*, 2008).

Along with isoprene emission from plants, many other taxa emit isoprene, including phytoplankton (Srikanta Dani *et al.*, 2017), microalgae (Exton *et al.*, 2013), fungi (Bäck *et al.*, 2010), bacteria (Kuzma *et al.*, 1995; Fall and Copley, 2000) and animals, where it has been found in human breath, and tissue slices taken from rat kidney and liver (Gelmont *et al.*, 1981). Anthropogenic isoprene emissions may also increase due to increased planting of high isoprene-emitting plants such as oil palm (Hardacre *et al.*, 2013), which will be expanded on later.

The presence of two carbon-carbon double bonds makes isoprene highly reactive (Pacífico *et al.*, 2009). This reactivity means that isoprene is very short-lived in the atmosphere (minutes to hours) (Guenther *et al.*, 2006). Isoprene is known to impact on atmospheric chemistry through interactions with hydroxyl radicals. These interactions reduce the available atmospheric pool of radicals, preventing their interaction with methane and therefore increasing the atmospheric retention time of methane (Collins *et al.*, 2002).

Isoprene also impacts air quality (Ashworth *et al.*, 2013) and formation of cloud condensation nuclei (Carlton *et al.*, 2009).

In addition to atmospheric attenuation of isoprene, both terrestrial and marine environments have been demonstrated to be potentially significant sinks of atmospheric isoprene, though this process is less well understood (reviewed in McGenity *et al.*, 2018). The isoprene cycle, therefore, must account for multiple sinks of isoprene, including both atmospheric chemical attenuation and degradation in both marine and terrestrial environments. This is currently difficult to model due to the gap in understanding of what is degrading isoprene in these environments and how.

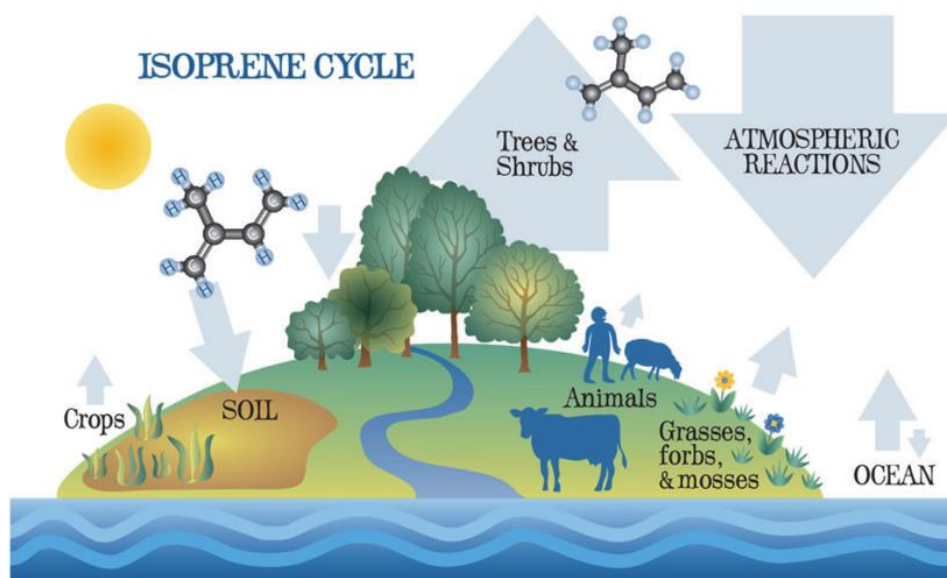


Figure 1.1: The isoprene cycle. Where known, relative contribution is indicated by thickness of arrows. Sources of isoprene are indicated by up arrows, and sinks by down arrows. Image taken from McGenity *et al.*, 2018.

1.1.2. Isoprene Biosynthesis

Atmospheric hydrocarbons are known to have negative effects, so many people are surprised to learn that humans contribute less atmospheric hydrocarbon emissions than vegetation does (Purves *et al.*, 2004). In addition to this, biogenic isoprene emissions are around 500 Tg C year⁻¹, which is approximately equal to methane emission from all sources (Guenther *et al.*, 2006).

The vast majority of atmospheric isoprene is emitted from plants, with the main producers being trees and shrubs (Sharkey *et al.*, 2008). Despite this huge emission from a single taxonomic group, the variation in isoprene emissions even between members of the same genus is surprising. Some oak (genus: *Quercus*) species produce isoprene (*Q. pubescens*, *Q. robur*, *Q. petraea* and *Q. coccifera*), whereas other oak species have not been demonstrated to emit any isoprene at all (*Q. cerris*, *Q. glabra*, *Q. ilex* and *Q. suber*) (Pacífico *et al.*, 2009). One of the highest known emitters of isoprene is oil palm (*Elais guineensis*), with an isoprene emission potential of 172.9 µg per cm² of leaf surface (Cronn and Nutmagul, 1982) (a full comparison of recorded isoprene emission in plants can be found at <http://es.lancs.ac.uk/cnhgroup/iso-emissions.pdf>, Hewitt group, University of Lancaster).

For high-emitting plants, up to 1 - 2 % of the total fixed carbon may be directed towards isoprene production (Sharkey *et al.*, 2008). Isoprene is an “energy-expensive” molecule to produce, with synthesis of one molecule requiring 20 ATP and 14 NADPH molecules to produce it (Sharkey and Yeh, 2001). Despite this, the benefits of isoprene production to the plant are still unclear. Some research has suggested a role in heat tolerance. Sunlight causes large temperature variations in leaves of up to 10 °C throughout the day (Hanson *et al.*, 1999; Singsaas *et al.*, 1999; Wise *et al.*, 2004). Isoprene is synthesised in leaves using carbon directly from the Calvin cycle of photosynthesis, and is believed to protect against sudden changes in temperature caused by sunlight known as heat flecks (Sharkey *et al.*, 2008). Exogenous isoprene supplied to plants in which isoprene synthesis was inhibited with fosmidomycin has been shown to impart a higher tolerance to heat stress (Sharkey *et al.*, 2001). Isoprene may also act to protect against oxidative stress, as isoprene counters the reduced photosynthetic capacity caused by reactive oxygen species (ROS) (reviewed in Sharkey *et al.*, 2008). However, contrasting research has suggested that ozone damage to plants can be worsened by the presence of isoprene, where organic hydroperoxides (ROOH) are produced by the reaction of ozone with isoprene. These ROOH are toxic to the cell and result in more damage to the plant than the presence of ozone alone (Hewitt *et al.*, 1990).

The reduced photosynthesis observed when plants are under heat stress is mediated by ROS. Some have suggested that isoprene protects against heat stress indirectly by protecting against ROS in both environmental and laboratory conditions. However, this is disputed as not all effects of heat stress are explained by ROS (Sharkey *et al.*, 2008). Conversely, it has been demonstrated that isoprene dissolved in a model membrane had effects on membrane stability similar to a 10 °C decrease in temperature, suggesting an

anchoring and stabilising effect of isoprene on the lipid bilayer (Siwko *et al.*, 2007). Isoprene is also known to have a role in plant growth regulation (Terry *et al.*, 1995; Jones *et al.*, 2016) and the reduction of herbivory by insects (Laothawornkitkul *et al.*, 2008). Other roles have been suggested for isoprene, including removing toxic and/or unwanted metabolites (Rosenstiel *et al.*, 2004), dissipating excess energy when leaves are subjected to an excess of sunlight (Magel *et al.*, 2006) and as an opportunistic way to use DMADP (Owen and Penuelas, 2005), however these have been disputed as futile cycles which would be very uncommon (Sharkey *et al.*, 2008).

Volatiles are emitted in human breath, and isoprene is the most abundant hydrocarbon (Gelmont *et al.*, 1981). Isoprene has also been reportedly found in human milk, blood and faeces (reviewed in de Lacy Costello *et al.*, 2014). Other animals also produce isoprene, including rats, where isoprene is emitted from tissue slices of kidney and liver (Gelmont *et al.*, 1981). Outside of the animal kingdom, isoprene production is linked to dimethyl sulfide (DMS) production in marine phytoplankton. DMS is another antioxidant molecule (Sunda *et al.*, 2002). In general, the marine phytoplankton studied emit either DMS or isoprene, with phytoplankton in colder waters being more likely to emit DMS, and those in warmer waters more likely to emit isoprene (Srikanta Dani and Loreto, 2017). Isoprene emission has been linked to photosynthesis in diatoms, however the carbon cost is significantly lower in plants, as it requires less than 0.0005 % of photosynthetically fixed carbon (Srikanta Dani *et al.*, 2017). Some microalgae (Exton *et al.*, 2013), fungi (Bäck *et al.*, 2010), and bacteria (Kuzma *et al.*, 1995; Fall and Copley, 2000) have also been shown to produce isoprene. Bacterial isoprene production has been recorded in species of the genera *Streptomyces*, *Pseudomonas*, *Serratia* and *Enterobacter* (Schöller *et al.*, 1997, 2002). The highest levels of bacterial isoprene production were found in *Bacillus* (Fall and Copley, 2000), where most of the research into bacterial isoprene production has been focussed.

Isoprene production is achieved through two distinct pathways. These pathways provide the precursors for the biosynthesis of isoprenoids, which encompass a wide range of molecules also known as terpenes/terpenoids produced by all free-living organisms. These important biomolecules contain two or more isoprene units and include carotenoids, chlorophylls, archaeal lipids, sterols and some hormones (reviewed in McGenity *et al.*, 2018). These products formed from isoprene metabolism include a wide range of desirable compounds for scents, flavours, colours and even clinically active steroid-based compounds which can act on problems such as breast cancer and enlarged prostates (Figure 1.2) (Nicholson, 2005). The two known pathways of isoprene biosynthesis are the mevalonate

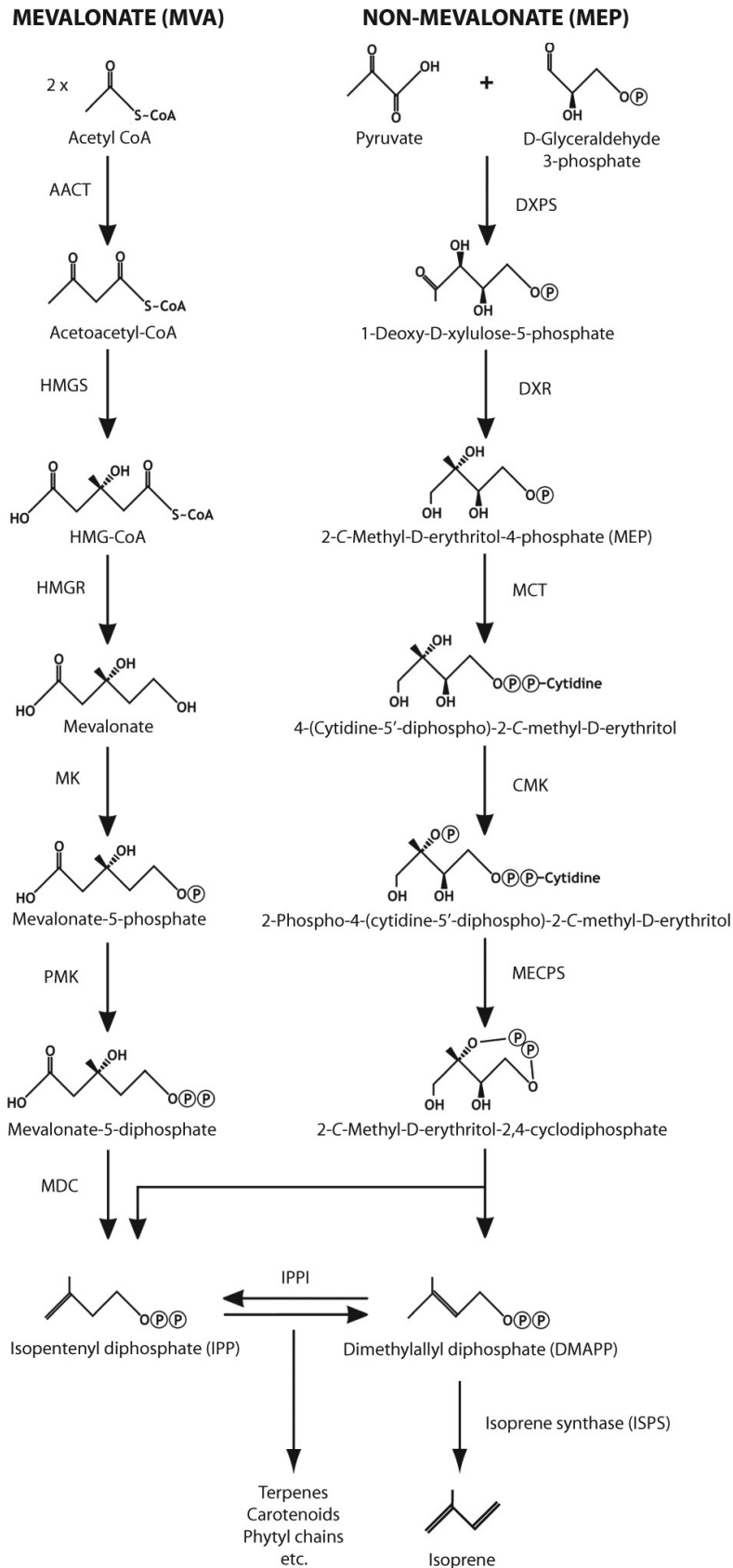


Figure 1.3: The two known pathways of isoprene biosynthesis (image taken from McGenity *et al.*, 2018)

Humans are increasing isoprene emissions in other ways, such as increased planting of high isoprene emitters such as oil palm due to a high demand for palm oil (Misztal *et al.*, 2010). The current drive towards biofuel is also driving up isoprene emissions, with key crops such as poplar, willow and eucalyptus being high producers of isoprene and being planted in areas where previously low emitting agricultural crops and grassland would have grown (Ashworth *et al.*, 2013). Whether this increase in isoprene producing crops will have a significant impact on the levels of isoprene production and associated climate impacts is debated, as the also-increasing CO₂ levels are known to decrease isoprene emissions, suggesting the net effect could be minimal (Hantson *et al.*, 2017).

Isoprene is also a useful compound in itself with a range of industrial applications, including as a fuel additive, production of synthetic rubber, adhesives and elastomers (Bentley *et al.*, 2014). Current isoprene production methods rely on petrochemical sources, however some research is focussing on microbial expression of isoprene synthase genes for bio-based isoprene synthesis (reviewed in Ye *et al.*, 2016). Specifically, the use of microbial fermentation to produce isoprene has been demonstrated. *Clostridium ljungdahlii* was successfully used to produce isoprene from low-value fructose and syngas feedstocks by having the bacterium produce proteins from the eukaryotic genes for isoprene synthesis via the MVA pathway, which requires less energy than the MEP pathway. Whilst this system increased the level of isoprene production by *Clostridium ljungdahlii* 4 – 5 fold, the yield was still low and needed to be increased before this method would be economically viable (Diner *et al.*, 2018). The highly volatile nature of isoprene makes full recovery of any product unlikely, and environmental emissions are likely to continue to increase, with an estimated global burden of isoprene increase of 8 % by 2100 (Sharkey and Monson, 2014).

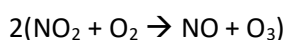
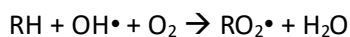
1.1.3. Isoprene Degradation

Despite the negative effects of atmospheric isoprene being well documented, degradation of isoprene remains a comparatively understudied topic. Degradation of isoprene is generally split into two categories, chemical attenuation and biological degradation. The former has been studied far more extensively, with the latter being an expanding field in environmental microbiology.

Chemical attenuation of isoprene

Chemical attenuation of atmospheric isoprene may have conflicting effects on climate. The highly reactive nature of the two alkene bonds leads to atmospheric isoprene affecting levels of other atmospheric trace gases such as methane through a rapid interaction with hydroxyl radicals. The reduced pool of available radicals indirectly leads to an increased retention time of, for example, the potent greenhouse gas methane in areas of high organic compound concentrations, such as isoprene (Collins *et al.*, 2002).

Isoprene also reacts with NO_x species in polluted environments, which leads to an increase in tropospheric ozone levels. In the atmosphere, cycling between NO and NO₂ (combined referred to as NO_x) is dependent on sunlight, with all NO_x species existing in the NO₂ form at night. When no atmospheric hydrocarbons are present, this equilibrium solely determines the amount of ozone produced (Jacob, 1999). In the presence of atmospheric hydrocarbons, such as isoprene, hydroxyl radicals (•OH) can react to form peroxide radicals (RO₂•). These cause conversion of NO to NO₂, which allows more ozone production. These reactions are outlined in the equations below, with one full cycle accounting for the oxidation of a single C-H bond leading to three molecules of ozone formed (equations taken from Sharkey *et al.*, 2008).



The tropospheric ozone formed in this reaction is not only another greenhouse gas but also has a negative impact on human respiratory health (Bromberg and Koren, 1995). In addition to this, isoprene itself is classified as a possible carcinogen (Yoon *et al.*, 2002) and inhalation has been linked to severe respiratory irritation in humans (Purves *et al.*, 2004). In contrast, isoprene can also mitigate levels of tropospheric ozone in non-polluted environments, where reduced NO_x concentrations cause alternative reactions which reduce ozone concentration (Trainer *et al.*, 1987). These ozonolysis reactions accounts for removal of 10 % of emitted isoprene from the atmosphere (Nguyen *et al.*, 2016). However, this reaction is slow and photo-oxidation of atmospheric isoprene is predominantly due to aforementioned reactions with hydroxyl radicals (Claeys *et al.*, 2004). Ozonolysis proceeds

by ozone reacting at either carbon-carbon double bond of isoprene, resulting in production of two primary ozonides (POZ). These decompose to produce methacrolein (MACR), methyl vinyl ketone (MVK), formaldehyde (HCHO) and up to nine Criegee intermediates (Figure 1.4). These Criegee intermediates can undergo immediate decay to form hydroxyl radicals, or become stabilised, where further reactions result in other products, including hydrogen peroxide, formaldehyde, formic acid and sulfuric acid. This stabilisation is the case for CH_2OO^* , which is the simplest Criegee intermediate produced due to the presence of isoprene (Nguyen *et al.*, 2016).

Both the ozonolysis and interaction with hydroxyl radicals to chemically attenuate atmospheric isoprene can cause formation of secondary organic aerosols (SOA), which contribute to the formation of cloud condensation nuclei, which in turn can have a localised cooling effect (Pacifico *et al.*, 2009). These secondary organic aerosols of isoprene and other atmospheric hydrocarbons are also well documented as the source of the blue haze over some forest ecosystems (Went, 1960).

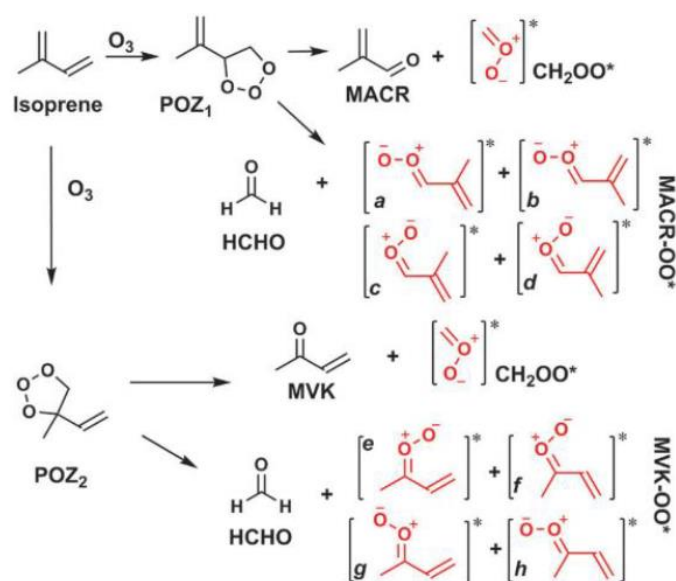


Figure 1.4: Ozonolysis of isoprene. * indicates Criegee intermediates. Taken from Nguyen *et al.* (2016).

1.1.4. Bacterial degradation of isoprene

After identification of plants as the source of isoprene, researchers suggested that microorganisms surrounding plants may provide a sink for organic volatiles produced by them (Rasmussen, 1970). These compounds were later confirmed as providing a source of

carbon and energy for microbial metabolism (Rasmussen and Hutton, 1972). Identification of soils as being a significant sink for atmospheric isoprene was first published by Cleveland and Yavitt (1997). Bacterial isoprene degradation was found to be dependent on the initial concentration of isoprene, temperature, availability of oxygen and soil characteristics including depth, moisture, pH and amount of organic matter (Cleveland and Yavitt, 1998). The abundance of isoprene-degrading microorganisms has been estimated at 10^5 cells per gram dry weight of soil based on colony counts on a basal salt medium with isoprene as a sole carbon source (Cleveland and Yavitt, 1998). However, the real number is likely to be far higher as bacteria may be able to co-oxidise isoprene without growing on it and very few of the bacteria in any environmental sample are able to be cultivated. Isoprene consumption by these microbes was suggested as a significant sink, accounting for removal of up to 5 % of isoprene emitted globally (20.4 Tg per year) based on an estimated biome area and active soil depth from studies into tropical, temperate and boreal forest soil in addition to cultivated land (Cleveland and Yavitt, 1997, 1998).

A range of bacteria have been isolated on volatile and gaseous hydrocarbons as a growth substrate, including species of the genera *Mycobacteria*, *Nocardia*, *Xanthobacter* and *Pseudomonas* (van Ginkel *et al.*, 1987). *Xanthobacter* sp. Py2 was found to oxidise isoprene, but not to grow on it as a sole carbon source (van Ginkel *et al.*, 1986). This suggested that some of the observed isoprene consumption observed could be due to co-oxidation by bacteria containing soluble diiron monooxygenases (SDIMOs). Subsequently, multiple groups successfully isolated Actinobacteria capable of growing on isoprene as a sole carbon source, including *Nocardia*, *Arthrobacter* and *Rhodococcus* species, in addition to the Proteobacterium *Alcaligenes* (van Ginkel, de Jong, *et al.*, 1987; Ewers *et al.*, 1990; Cleveland and Yavitt, 1997, 1998).

More recently, many isoprene degrading bacteria have been isolated from a wide range of both marine and terrestrial environments, and Actinobacteria have often been found to dominate in isolation studies. One study investigating the isoprene degraders in both tropical and temperate seawaters in addition to estuary sediments found that the Actinobacteria, and particularly *Rhodococcus*, were present across all sampling sites, were most commonly isolated from and dominated enrichments from, sediments. Isolates of other phyla were also identified, including Proteobacteria (genera *Xanthobacter*, *Rhodanobacter* and a *Shinella*-like organism) and Bacteroidetes (genus *Dyadobacter*). Most of the isolates obtained were capable of degrading some N-alkanes, and their growth could be supported by the low levels of isoprene produced by microalgae, though the growth

supported was slow (Alvarez *et al.*, 2009). Isolation of isoprene degrading bacteria from a selection of coastal, estuarine and marine environments resulted in isolates exclusively from the Actinobacteria phylum or Alpha-proteobacteria class. The *Gordonia* sp. i37 and *Mycobacterium* sp. AT1 Actinobacterial isolates were studied more extensively, and found to contain two SDIMOs each, however only one of these was sufficiently similar to the isoprene monooxygenase of *Rhodococcus* sp. AD45 to be predicted as having a role in isoprene metabolism (Johnston *et al.*, 2017).

In terms of terrestrial isolation studies, two isolates discovered from garden soil and horse chestnut leaves were both found to be *Rhodococcus* sp. (El Khawand *et al.*, 2016). *Rhodococcus* sp. were also exclusively isolated in work on poplar leaves and soil (Crombie *et al.*, 2018). Both of these studies utilised isoprene concentrations far higher than found naturally, between 150 and 10,000 ppmv. Atmospheric isoprene concentrations have regularly been recorded as less than 5 ppbv (Hewitt and Street, 1992; Klinger *et al.*, 1998; Harrison *et al.*, 2013), though below the forest canopy this has been recorded as increasing up to 40 ppbv (Wiedinmyer *et al.*, 2001, 2005). The highest recorded environmental isoprene concentrations have been found in the intercellular spaces of plant leaves, around the stomata where isoprene is released, reaching up to 30 ppmv (Fall and Monson, 1992; Singaas *et al.*, 1997). Following on from this, isolation of isoprene degrading bacteria from willow soil using a much lower isoprene concentration of 25 ppmv resulted in a wider range of isolates, including the 11 *Rhodococcus* sp., a *Gordonia* and *Nocardioides* from the Actinobacteria phylum, and *Ramlibacter*, *Variovorax* and *Sphingopyxis* which are all Gram negative and belong to the Proteobacteria phylum (Larke-Mejía *et al.*, 2019; Dawson *et al.*, 2020). Isoprene degraders have also been found in contaminated soil from a waste rubber dumping site, including *Alcaligenes*, *Klebsiella* and *Pseudomonas* species (Srivastva *et al.*, 2015). Further research assessed the potential of several soil and leaf isolates as a bioremediation tool in isoprene-contaminated areas based on whole-cell kinetics of isoprene degradation. Bacteria were isolated from soil samples sourced from a tropical dry deciduous forest, using isoprene vapour as a carbon source. Both Gram positive and negative isolates were identified from the genera *Pseudomonas*, *Arthrobacter*, and *Bacillus*. Enrichment of leaf washings for isoprene degraders led to isolates of the genera *Sphingobacterium*, *Sphingobium*, *Pseudomonas* and *Pantoea*. Of these combined soil and leaf isolates, it was found that the *Pseudomonas* sp. were the most efficient isoprene degraders (Singh *et al.*, 2019), however the molecular basis of isoprene degradation remains understudied.

Using DNA stable isotope probing (SIP), a range of studies have aimed to explore the taxonomic diversity of isoprene degrading bacteria. In marine sediment samples, 16S RNA amplicon sequencing suggested a high prevalence of Actinobacteria, with over 99 % of the labelled community belonging to the genus *Mycobacterium* after 12 days incubated with ¹³C-labelled isoprene. After 15 days, the community was found to be more diverse, but Actinobacteria was the only phylum highly enriched in heavy fractions (Johnston *et al.*, 2017). Another study on garden soil and horse chestnut leaves incubated soil microcosms in 5000 ppmv isoprene for 15 days. At the beginning of the experiment, 16S rRNA analysis suggested that 50 % of the bacteria present belonged to the phylum Proteobacteria, and 40 % comprised Planctomycetes, Actinobacteria, Bacteroidetes, Chloroflexi and Firmicutes. In contrast, after 15 days of enrichment *Rhodococcus* sp. accounted for 88 % of the labelled 16S rRNA. Some Beta-Proteobacteria were also enriched, namely *Comamonas* and *Variovorax* spp., though these only accounted for 0.7 % of the microbial community after enrichment. Other known isoprene-degrading genera *Pseudomonas* and *Klebsiella* were investigated, however these were unlabelled and not found, respectively (El Khawand *et al.*, 2016).

A subsequent DNA-SIP experiment using poplar leaves and soil utilised lower isoprene concentrations, at 500 ppmv. In this case *Rhodococcus* was again enriched and accounted for 78 % of the sample, whereas the Comamonadaceae, the family to which both *Variovorax* and *Comamonas* belong, was enriched and accounted for 3 % of the sample. A second DNA-SIP in this study used an even lower concentration of isoprene, 150 ppmv. This resulted in lower enrichment of *Rhodococcus* (74 %), and higher enrichment of the Comamonadaceae (16 %), suggesting that prior heavy bias towards Actinobacterial isolation could have been due to the high concentrations of isoprene used (Crombie *et al.*, 2018). The lowest and most close to environmental concentration of isoprene used in a DNA-SIP to date was 25 ppmv in a study of willow tree soil. In this case, the Actinobacteria were only enriched to 4.5 %, whereas the Comamonadaceae accounted for 76 % of the enriched microbial community after 6 days, mostly belonging to the genera *Ramlibacter* and *Variovorax* (Larke-Mejía *et al.*, 2019).

One study has also investigated the microbial isoprene degraders of Malaysian oil palm phyllosphere and the surrounding soil. Oil palm was selected as it is one of the highest isoprene producers (Kesselmeier and Staudt, 1999), and the crop is cultivated on approximately 85 % of agricultural land in Malaysia (Ibragimov *et al.*, 2019), making an understanding of the associated microbial community vital to understand the impact

increasing oil palm plantations may have on global isoprene levels. This experiment utilised the lower isoprene concentration explained above of 25 ppmv, but had very different results. Based on 16S rRNA amplicon sequencing, rather than the anticipated high abundance of *Rhodococcus*, *Variovorax* and *Gordonia* as found in previous research, the dominant genera in enriched soil samples were *Rhodoblastus*, *Pelomonas*, *Novosphingobium* and *Sphingomonas*. These genera had a 19 – 90 fold higher relative abundance than in the unenriched samples. Conversely, the phyllosphere samples resulted in enrichment of *Gordonia* and *Zoogloea* (Carrión *et al.*, 2020). The *Gordonia* identification was anticipated due to previous isolation of other members of the genera during growth on isoprene as a sole carbon source (Larke-Mejía *et al.*, 2019). However, the *Zoogloea* identified by 16S rRNA amplicon sequencing was the first member of the order *Rhodocyclales* identified as a potential isoprene degrader, which suggested that the diversity of isoprene degraders may be much wider than previously thought (Carrión *et al.*, 2020).

Rhodococcus has been identified as an important genus of isoprene degrader across multiple environments. *Rhodococcus* sp. have been isolated from soil and leaves of isoprene emitting trees (El Khawand *et al.*, 2016; Crombie *et al.*, 2018), a range of other soil environments (Ewers *et al.*, 1990; Murphy, 2017), plant-associated marine sediments, (Alvarez *et al.*, 2009; Johnston *et al.*, 2017) and freshwater sediments (van Hylckama Vlieg *et al.*, 1998). The most recent molecular ecology studies of isoprene degraders suggest that *Rhodococcus* sp. are selected for in high isoprene concentrations, which make it a promising organism for biotechnological and bioremediation applications in isoprene research. The *Rhodococcus* sp. AD45 strain isolated from freshwater sediment on isoprene as a sole carbon source (van Hylckama Vlieg *et al.*, 1998) is to date the most extensively characterised isoprene degrading isolate, and will be used here as a model organism for bacterial isoprene degradation.

1.2. *Rhodococcus* sp. AD45

1.2.1. Isolation and Taxonomy

Rhodococcus sp. AD45 was isolated from freshwater sediment using isoprene as a sole carbon source (van Hylckama Vlieg *et al.*, 1998). *Rhodococcus* sp. AD45 is a Gram-positive Actinobacterium and is capable of growth on a range of carbon substrates, including phenol, 3-methyl-1-butanol, glycerol, 1,2-propanediol and ethanol (van Hylckama Vlieg *et*

al., 1998). In general, bacteria of the genus *Rhodococcus* are metabolically versatile, and multiple species within the genus have been identified as capable of degrading isoprene and C₂-C₄ gaseous hydrocarbons (Shennan, 2006). This metabolic versatility of the genus has led to an extensive amount of research focussing on their potential as biotechnological and bioremediation tools. A total of seven *Rhodococcus* strains were recently isolated from soil contaminated by oil deposits in Western Siberia, and all were found to be effective petroleum degraders. These *Rhodococcus* strains were capable of degrading a wide range of contaminants, including crude oil, diesel fuel, higher chain length alkanes (C₉, C₁₀ and C₁₆), phenol and benzene (Puntus *et al.*, 2019). Another isolation study investigating river sediments close to a petrochemical site found 34 Gram positive isolates. Of these 16 were capable of degrading the wide range of aromatic hydrocarbons tested, and of these, 6 were species of *Rhodococcus* (Narancic *et al.*, 2012). Other *Rhodococcus* species have been studied more intensely for their biodegradation potential, such as *Rhodococcus rhodochrous* B-276, which has been studied for its potential in bioremediation of areas contaminated with chlorinated alkenes (Mattes *et al.*, 2010), and *Rhodococcus erythropolis* JE 77, which was identified as a trichloroethylene degrader (Ewers *et al.*, 1990). Importantly, *Rhodococcus rhodochrous* B-276 also contains an alkene monooxygenase, which belongs to the SDIMO protein family. This protein has been purified and investigated for its biotechnological potential due to its capability to produce chiral epoxides in a regioselective manner (Smith *et al.*, 1999; Fosdike *et al.*, 2005; Perry and Smith, 2006). In addition, genetic tools have been developed for protein expression in *Rhodococcus erythropolis*, using the pTip plasmid expression system (Nakashima and Tamura, 2004b) This system could successfully express proteins at a wide temperature range, between 4 and 30 °C. This system has successfully been used to express proteins which were previously insoluble when recombinantly produced in *Escherichia coli* (Nakashima and Tamura, 2004a).

1.2.2. Isoprene degradation by *Rhodococcus* sp. AD45

Until characterization of *Rhodococcus* sp. AD45 began, nothing was known about the molecular basis for isoprene degradation by bacteria. van Hylckama Vlieg *et al.* (2000) identified a gene cluster encoding a range of proteins involved in isoprene degradation, which was later found to be on a 300 kbp circular megaplasmid (Crombie *et al.*, 2015). The proposed isoprene degradation pathway involves an initial oxidation step of isoprene to epoxyisoprene, catalysed by a four-component soluble diiron monooxygenase (SDIMO)

isoprene monooxygenase (van Hylckama Vlieg *et al.*, 2000). The epoxide formed by isoprene monooxygenase in *Rhodococcus* sp. AD45 is 1,2-epoxy-2-methyl-3-butene (van Hylckama Vlieg *et al.*, 2000), which contrasts studies into isoprene degradation in *Nocardia* where both this epoxide and the 1,2-3,4-diepoxy-2-methylbutane were found. However, it is interesting to note that this second compound cannot be further metabolised by the *Nocardia* sp. (van Ginkel, de Jong, *et al.*, 1987). The highly electrophilic nature of epoxides and instability in aqueous solution causes covalent modifications to bacterial cell components, with toxic effects (van Hylckama Vlieg *et al.*, 1998). Such toxicity is a major stumbling block in the bioremediation of toxic alkenes such as trichloroethylene, and initiated the initial interest in *Rhodococcus* sp. AD45. Despite being a Gram-positive bacterium in which glutathione is comparatively rare, the next step in the isoprene degradation pathways is conjugation to glutathione, via the glutathione transferase IsoI, to yield 1-hydroxy-2-glutathionyl-2-methyl-2-butene (HGMB) (van Hylckama Vlieg *et al.*, 2000). Conversely, other metabolic pathways for alkenes include epoxide conjugation to coenzyme M (Allen *et al.*, 1999). Following this, two oxidation steps are performed by IsoH, forming 2-glutathionyl-2-methyl-3-butenolate (GMBA). The final steps to incorporate GMBA into central carbon metabolism remain unknown, however it has been proposed that a GMBA-CoA thioester could be formed, and IsoJ may facilitate the removal of glutathione from this compound. This would result in a 2-methyl-3-butenyl-CoA, which could be degraded by β -oxidation and feed into central metabolism via the Krebs cycle (van Hylckama Vlieg *et al.*, 2000, Figure 1.5).

The only enzymes of the isoprene degradation pathway that have been purified and biochemically characterised are the glutathione transferase (IsoI) and the dehydrogenase (IsoH). During the study, van Hylckama Vlieg *et al.* (1999) found that IsoI is a homodimer and accounts for approximately 8 % of the total protein in cells grown on isoprene as a sole carbon source. IsoI was also found to be active on a range of epoxides, however the range of glutathione conjugates of epoxides which serve as a substrate for IsoH were much lower, with only the epoxypropane-glutathione conjugate being an alternative IsoH substrate, although the rate was eight-fold lower than with HGMB (van Hylckama Vlieg *et al.*, 1999). Despite some work being carried out on purified glutathione transferase (IsoI) and dehydrogenase (IsoH), no characterisation of the isoprene monooxygenase has been carried out.

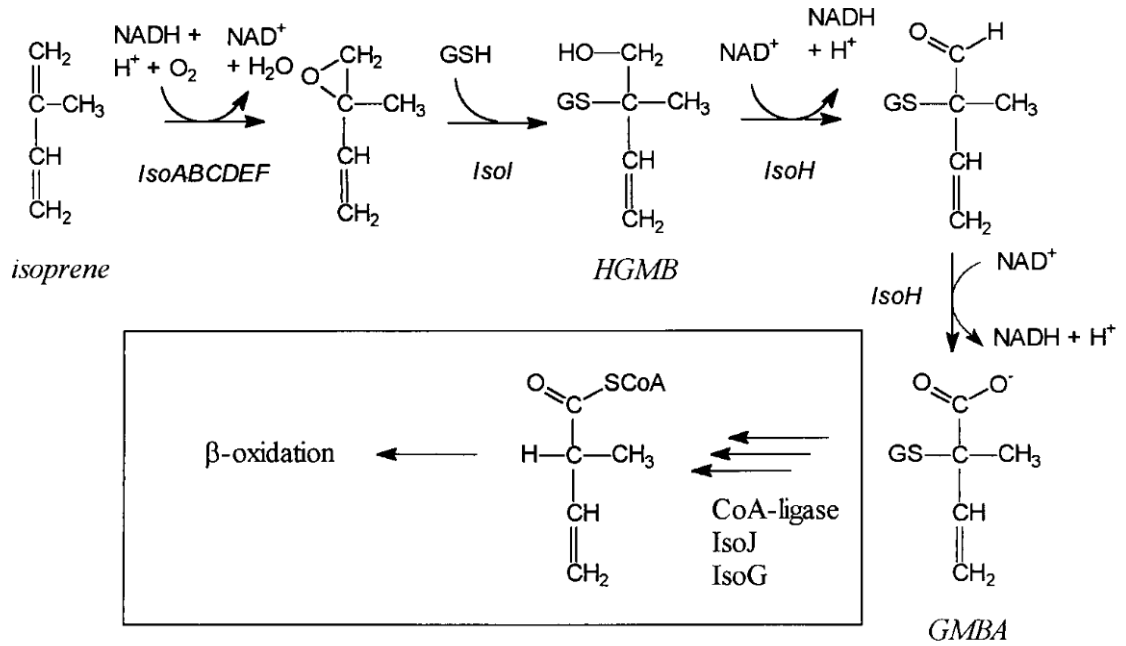


Figure 1.5: Proposed pathway for isoprene degradation in *Rhodococcus* sp. AD45
Taken from van Hylckama Vlieg *et al.* (2000).

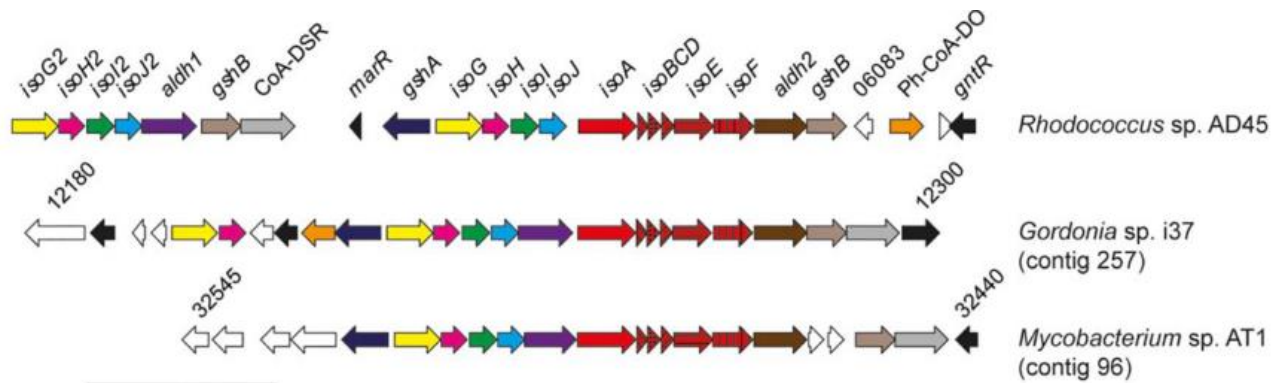


Figure 1.6: Isoprene gene cluster arrangement in *Rhodococcus* sp. AD45, *Gordonia* sp. i37 and *Mycobacterium* sp. AT1. Image taken from Johnston *et al.* (2017), line at base represents 5 kbp.

Homologues of the isoprene degradation cluster of *Rhodococcus* sp. AD45 have since been identified in other isoprene-degrading bacterial isolates. When compared with *Mycobacterium* and *Gordonia* isolates from estuarine sediments, the enzymes showed a 55 - 87 % amino acid similarity between strains and all clusters contained the two glutathione synthase genes flanking the isoprene monooxygenase genes. Where the *Rhodococcus* sp. AD45 isoprene degradation cluster underwent a duplication event involving *isoGHII*, only *isoG* and *isoH* are duplicated in *Gordonia* sp. i37, and there is no duplication in

Mycobacterium sp. AT1 (Johnston *et al.*, 2017, Figure 1.6). The gene products for the isoprene degradation cluster are presented in Table 1.1

Table 1.1: Genes and gene products of the isoprene degradation cluster from *Rhodococcus* sp. AD45.

| Gene | Identification | Reference |
|------------------|------------------------------------|---|
| <i>marR</i> | transcriptional regulator | Crombie <i>et al.</i> , 2015 |
| <i>gshA</i> | glutamate cysteine ligase | Crombie <i>et al.</i> , 2015 |
| <i>isoG</i> | putative racemase | van Hylckama Vlieg <i>et al.</i> , 2000 |
| <i>isoH</i> | NAD-dependent HGMB-dehydrogenase | van Hylckama Vlieg <i>et al.</i> , 2000 |
| <i>isoI</i> | glutathione S-transferase | van Hylckama Vlieg <i>et al.</i> , 2000 |
| <i>isoJ</i> | glutathione S-transferase | van Hylckama Vlieg <i>et al.</i> , 2000 |
| <i>isoA</i> | oxygenase α -subunit | van Hylckama Vlieg <i>et al.</i> , 2000 |
| <i>isoB</i> | oxygenase γ -subunit | van Hylckama Vlieg <i>et al.</i> , 2000 |
| <i>isoC</i> | Rieske-type ferredoxin | van Hylckama Vlieg <i>et al.</i> , 2000 |
| <i>isoD</i> | coupling protein | van Hylckama Vlieg <i>et al.</i> , 2000 |
| <i>isoE</i> | oxygenase β -subunit | van Hylckama Vlieg <i>et al.</i> , 2000 |
| <i>isoF</i> | reductase | van Hylckama Vlieg <i>et al.</i> , 2000 |
| <i>aldh2</i> | aldehyde dehydrogenase | Crombie <i>et al.</i> , 2015 |
| <i>gshB</i> | glutathione synthetase | Crombie <i>et al.</i> , 2015 |
| <i>Ph-CoA-DO</i> | CoA-disulfide reductase | Crombie <i>et al.</i> , 2015 |
| <i>gntR</i> | Putative transcriptional regulator | Crombie <i>et al.</i> , 2015 |

1.2.3. Curing *Rhodococcus* sp. AD45 of the isoprene degradation cluster containing megaplasmid

As described in section 1.2.2, the isoprene degradation cluster of *Rhodococcus* sp. AD45 is encoded on a 300 kbp circular megaplasmid. The full cluster of isoprene degradation genes has been removed from *Rhodococcus* sp. AD45 through curing of the megaplasmid containing them. This was achieved by transforming *Rhodococcus* sp. AD45 with a pNV18-based vector. The megaplasmid was found to be unstable in the presence of this vector, and both the megaplasmid and isoprene oxidising ability were lost after prolonged incubation with kanamycin. The pNV18-based plasmid was then removed by 20 transfers without antibiotic at a high temperature (34 °C) (Crombie *et al.*, 2018). This new strain is

referred to as *Rhodococcus* sp. AD45-ID and provides a potential homologous host for expression of enzymes from the megaplasmid involved in the degradation of isoprene. The cured strain is incapable of oxidation of, or growth on, isoprene as a sole carbon source, and has been successfully complemented with an isoprene monooxygenase from an environmental sample expressed on a pTipQC2 expression vector (Crombie *et al.*, 2018). This expression system was originally produced for use in *Rhodococcus erythropolis*, and it can be used to express proteins at temperatures down to 4 °C when required to aid in protein folding (Nakashima and Tamura, 2004a).

1.2.4. Isoprene monooxygenase in *Rhodococcus* sp. AD45

Isoprene monooxygenase is a 4-component soluble diiron monooxygenase, containing an oxygenase, a reductase, a coupling protein and a Rieske protein. It catalyses the epoxidation of isoprene to 1,2-epoxy-2-methyl-3-butene (van Hylckama Vlieg *et al.*, 2000, Figure 1.7).

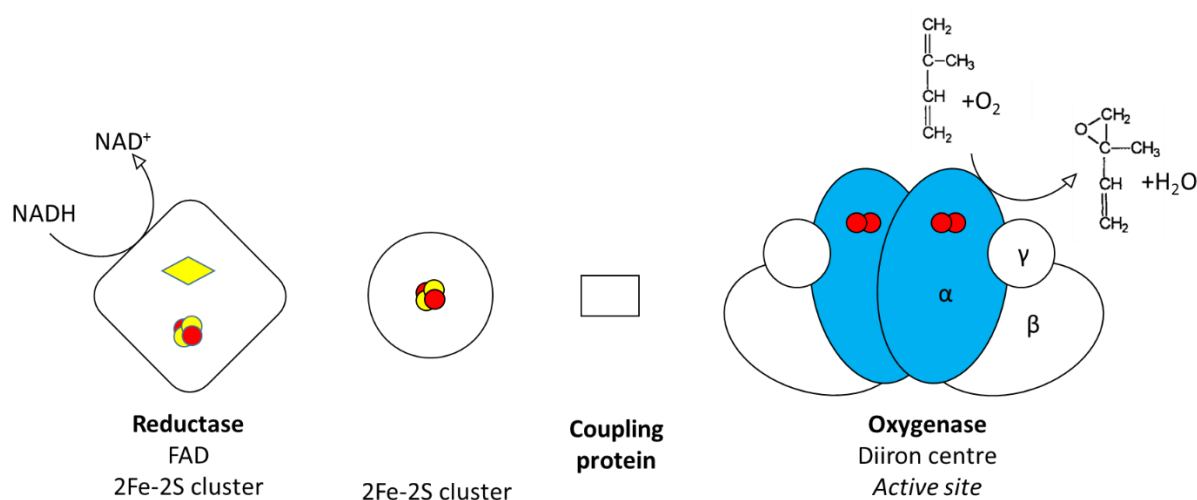


Figure 1.7: Subunits of the isoprene monooxygenase enzyme. The catalytic subunit IsoA is highlighted in blue. Iron cofactors components shown in red, sulfur as yellow circles, and FAD as a yellow diamond.

The active site is situated in the alpha subunit of the oxygenase (IsoA), where most molecular work has focussed. This includes an $\Delta isoA$ mutant has been demonstrated to be incapable of oxidising or growing on isoprene as a sole carbon source (Crombie *et al.*, 2015), and *isoA* gene probes have been developed to identify putative isoprene degraders in environmental samples (El Khawand *et al.*, 2016; Carrión *et al.*, 2018).

The *isoA* primers developed by El Khawand *et al.* (2016) were used to explore potential isoprene degraders from marine and estuarine samples found by Johnston *et al.* (2017). They found that the most abundant *isoA* sequences were associated with the Actinobacteria genera *Mycobacteria*, *Gordonia* and *Rhodococcus*, and the Alpha-proteobacteria genus *Loktanella*. All of the strains isolated from these environments contained *isoA* as identified by the use of the *isoA* primers, suggesting the use of isoprene monooxygenase for growth on isoprene.

Subsequently, Carrión *et al.* (2018) further refined the *isoA* primer set in light of the increasing number of isoprene degraders isolated, which had resulted in a larger diversity of known *isoA* sequences which the previous primer set could not identify, including the identification of Gram negative isoprene degraders of the genera *Variovorax*, *Ramlibacter* and *Sphingopyxis* (Larke-Mejía *et al.*, 2019).

The *Variovorax* sp. WS11 isolated from willow soil and capable of growth on isoprene as a sole carbon and energy source is the only other organism which has been partially characterised in terms of the isoprene monooxygenase enzyme. The *isoABCDEF* gene cluster was successfully expressed using the pTipQC1 expression system in *Rhodococcus* sp. AD45-ID, and an *isoA* mutant was demonstrated to be incapable of growth on isoprene. Further to this, a range of alkene and aromatic compounds were demonstrated to be substrates for the isoprene monooxygenase based on oxygen uptake in their presence (Dawson *et al.*, 2020).

Despite the previous work studying the isoprene degradation pathway in *Rhodococcus* sp. AD45 (van Hylckama Vlieg *et al.*, 1999, 2000) and the characterisation of isoprene monooxygenase in *Variovorax* sp. WS11 (Dawson *et al.*, 2020), to date no isoprene monooxygenase enzyme has been purified and biochemically characterised, which is a knowledge gap this project aimed to fill.

1.3. Soluble Diiron Monooxygenases (SDIMOs)

1.3.1. SDIMOs

Soluble diiron monooxygenases are a subset of the larger protein group of bacterial multicomponent monooxygenases (BMMs) (Wang *et al.*, 2015). The BMMs are an enzyme family which can selectively oxidise a range of hydrocarbons, including alkenes, alkanes, aromatics and halogenated versions of these compounds (Colby *et al.*, 1977; Whited and

Gibson, 1991; Small and Ensign, 1997; Coleman *et al.*, 2011). Many of these compounds are environmentally and industrially relevant, so the BMMs have been the subject of research into stereoselective oxidation for industry (Champreda *et al.*, 2006; Holmes and Coleman, 2008; Lock *et al.*, 2017; Sheldon and Woodley, 2018; Petkevičius *et al.*, 2019) and investigated for their bioremediation potential (Newman and Wackett, 1997; Sullivan *et al.*, 1998; Martin *et al.*, 2014). The most extensive research has been conducted into soluble methane monooxygenase (sMMO), which is capable of oxidising over 50 substrates (Colby *et al.*, 1977; Jiang *et al.*, 2010), and generates one of the most powerful natural oxidants at its active site in order to oxidise methane (Rosenzweig, 2015). In stark contrast, many members of the BMM enzyme family are still poorly biochemically characterised, if examined at all (reviewed in Osborne and Haritos, 2019).

The BMMs are all soluble enzymes containing a diiron centre and comprise a minimum of a hydroxylase, reductase and regulatory subunit (Tinberg *et al.*, 2011). These characteristics are shared by the related archaeal multicomponent monooxygenases, and these two groups combined are referred to as the soluble diiron monooxygenases (SDIMOs) (Osborne and Haritos, 2019).

Soluble diiron monooxygenases are generally split into three- and four-component systems (Leahy *et al.*, 2003). The three-component systems contain the minimum components outlined above. The hydroxylase will be referred to as the oxygenase here, as many SDIMOs will not hydroxylate C-H bonds, as the sMMO “hydroxylase” was named for, and homologues are often referred to in the literature (Furuhashi *et al.*, 1986; van Ginkel and de Bont, 1986; McClay *et al.*, 2000). In addition, the regulatory subunit is called the coupling or effector protein (Hemmi *et al.*, 2001; Mitchell *et al.*, 2002; Sazinsky *et al.*, 2004; Champreda *et al.*, 2006), and the coupling protein nomenclature will be used here. The additional component in the four-component systems is a Rieske-type ferredoxin, which aids in electron transfer from the NADH:acceptor reductase to the oxygenase (Pikus *et al.*, 1996; Small and Ensign, 1997; Cafaro *et al.*, 2002; Moe *et al.*, 2006; Elsen *et al.*, 2007) (Figure 1.8).

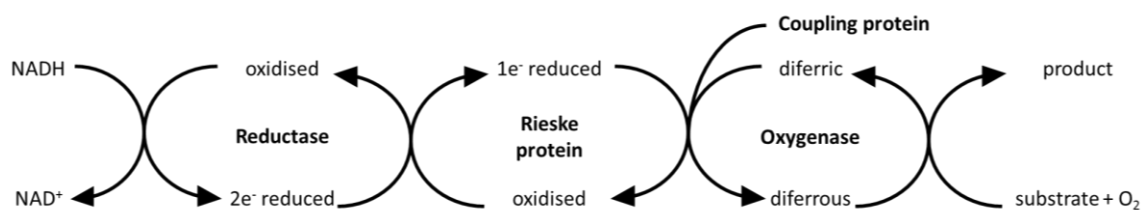


Figure 1.8: Electron transfer in SDIMOs. Image adapted from Orville *et al.* (2003).

The three-component SDIMOs are broadly categorized into three groups, the soluble methane monooxygenases, phenol hydroxylases, and alkene monooxygenase of *Rhodococcus rhodochrous* B-276 (Leahy *et al.*, 2003). The alkene monooxygenase of *Rh. rhodochrous* B-276 was of interest because it was the only known SDIMO with a dimer of dimers ($\alpha\beta$)₂, rather than a dimer of trimers ($\alpha\beta\gamma$)₂ making up the oxygenase component (Miura and Dalton, 1995). However, as more SDIMOs have been discovered this group has expanded with more Actinomycete enzymes, all of which are also encoded by a four-gene cluster. These include the mycobacterial binuclear iron monooxygenase (MimABCD), which plays a role in the metabolism of both propane and acetone, however is generally studied for its biotechnologically important ability to oxidise phenol to hydroxyquinone (Furuya *et al.*, 2013) and the alkane monooxygenases of *Gordonia* sp. TY-5, *Mycobacterium* sp. TY-6 and *Pseudonocardia* sp. TY-7 (Kotani *et al.*, 2006).

In all cases, the oxygenase alpha subunit contains the diiron site for hydrocarbon oxidation. This diiron centre is held in a bundle of four helices (Rosenzweig *et al.*, 1997; Sazinsky *et al.*, 2004; Bailey, McCoy, *et al.*, 2008). The electrons are transferred from NAD(P)H through the reductase component, either straight to the oxygenase component or via the Rieske-type ferredoxin (Lund *et al.*, 1985; Small and Ensign, 1997; Liang and Lippard, 2014). The substitution of components from different SDIMOs and altering oxygenase sequences has been investigated to confer variations in activity (Stirling and Dalton, 1979; Sieber *et al.*, 2001; Champreda *et al.*, 2004; Tee and Schwaneberg, 2007). This has been a source of interest in prospecting for SDIMOs as biocatalysts, as this shuffling may be useful for optimising enzyme systems for specific enantiomerically selective reactions (reviewed in Holmes and Coleman, 2008).

Isoprene monooxygenase falls within the four-component category, where the best characterised example is the toluene 4-monooxygenase from *Pseudomonas mendocina* KR1, which was the first identified aromatic oxygenase of the SDIMOs (Pikus *et al.*, 1996).

However, isoprene monooxygenase is more closely related to the alkene monooxygenase from *Xanthobacter* sp. Py2 (van Hylckama Vlieg *et al.*, 2000; Crombie *et al.*, 2015).

1.3.2. Soluble diiron monooxygenase components

The Oxygenase component

The oxygenase component of isoprene monooxygenase is predicted to comprise six subunits, two of each an alpha, beta and gamma subunit (Figure 1.7) based on the data obtained from other four component SDIMOs, including alkene monooxygenase, toluene 2- and toluene 4-monooxygenase (Newman and Wackett, 1995; Pikus *et al.*, 1996; Small and Ensign, 1997). Structural analysis of the oxygenase components from soluble methane monooxygenase (Rosenzweig *et al.*, 1993), toluene 4-monooxygenase (Acheson *et al.*, 2017) and the toluene/*o*-xylene monooxygenase (Sazinsky *et al.*, 2004) revealed that the alpha subunit is catalytic, and the beta and gamma subunits are structural. Due to this, the alpha subunit of the oxygenase component has been a target of numerous mutagenesis studies in attempts to improve the regioselective nature of SDIMO reactions (reviewed in Nichol *et al.*, 2015). These have mainly been focussed on the soluble methane monooxygenase from *Methylosinus trichosporium* sp. OB3b (Smith *et al.*, 2002; Borodina *et al.*, 2007; Sigdel *et al.*, 2015; Lock *et al.*, 2017), toluene 4-monooxygenase from *Pseudomonas mendocina* sp. KR1 (Pikus *et al.*, 2000; Mitchell *et al.*, 2002; Tao *et al.*, 2005), and alkene monooxygenase from *Rhodococcus rhodochrous* sp. B-276 (Perry and Smith, 2006).

Phylogenetic analysis has been carried out on the IsoA protein sequence to understand the relationship between isoprene monooxygenases of environmental isolates. This revealed that there is a clustering of the sequences from Gram-negative isolates distinct from those of the Gram-positive isolates. Interestingly, within this analysis it was identified that the alkene monooxygenase from *Xanthobacter* sp. Py2 aligns more closely with the isoprene monooxygenases than the toluene monooxygenases, falling between the sequences from the isoprene monooxygenases from Gram positive and Gram negative isolates. This suggested that the distinction between sub-groups of four-component SDIMOs may be less clear than expected, and further biochemical characterisation of the enzymes in question could be required, as grouping according to amino acid sequence is not appropriate alone for identifying the enzymes' preferred substrate (Larke-Mejía, 2018, Figure 1.9).

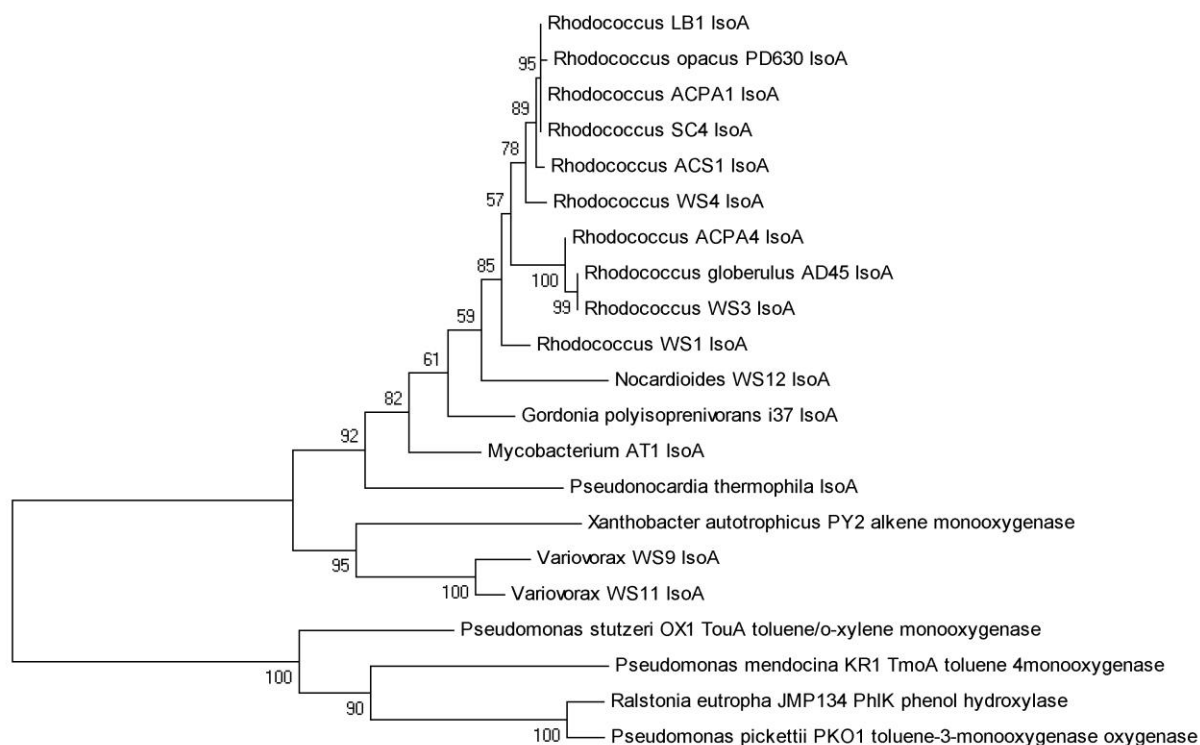


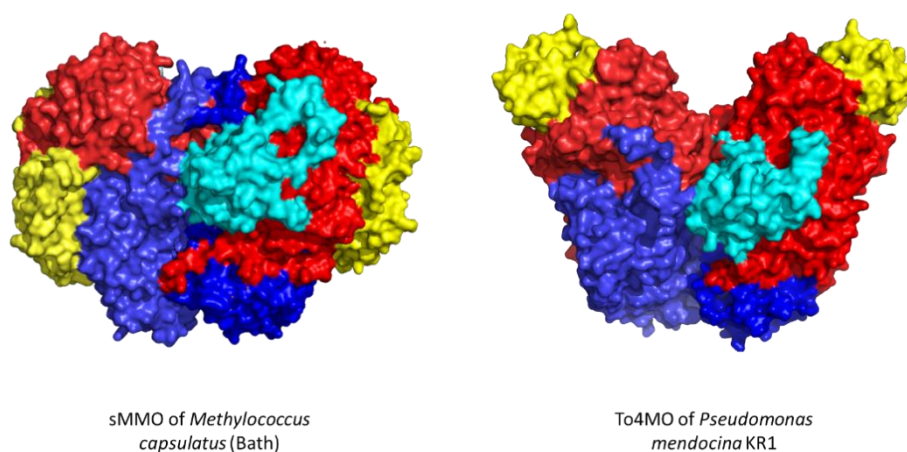
Figure 1.9: Relationship between catalytic subunits (IsoA) of isoprene monooxygenase at an amino acid level between different strains isolated on isoprene as a sole carbon and energy source. Taken from Larke-Mejía (2018).

The Coupling Protein

The coupling protein of SDIMOs has no cofactors, but plays a key role in modulating catalysis through a variety of interactions. These increase the rate and efficiency of the steady state reaction (Green and Dalton, 1986; Fox *et al.*, 1989; Pikus *et al.*, 1996; Mitchell *et al.*, 2002), but seem to reduce the activity when presence in excess (Fox *et al.*, 1991; Hemmi *et al.*, 2001). Coupling proteins have been shown to decrease the reduction potential of the active site (Paulsen *et al.*, 1994), and alter the spectroscopic features of the diiron centre (Hendrich *et al.*, 1990; Fox *et al.*, 1991, 1993). These small effector proteins are suspected to act as a gate for O₂ and substrate access to the active site (Wallar and Lipscomb, 2001), and affect both substrate specificity and regiospecificity (Froland *et al.*, 1992).

The structure of SDIMO coupling proteins always contains an unstructured N-terminal tail. This N-terminal tail is believed to be important in oxygenase interactions; it forms a ring structure on the surface of sMMO from *Methylococcus capsulatus* (Bath) which is thought to be important in controlling substrate access to the active site (Rosenzweig, 2013).

However, the crystal structure solved for the four-component SDIMO toluene 4-monooxygenase in the presence of the substrate and coupling protein suggests that this is not true for all of the SDIMO coupling proteins (Acheson *et al.*, 2017) (Figure 1.10). Binding of the coupling protein to the oxygenase of toluene 4-monooxygenase from *Pseudomonas mendocina* KR1 leads to a conformational change of the oxygenase to make the active site more accessible for both oxygen and the substrate (Acheson *et al.*, 2017).



The coupling protein (T4moD) has also been demonstrated, using fluorescence anisotropy, to bind to a single site of the Rieske protein (T4moC) of the toluene 4-monooxygenase system (Moe *et al.*, 2006). This study also determined that there is no protein complex formed between the coupling protein and reductase, and in addition that an increased presence of reductase lowers the binding affinity of the coupling protein to the Rieske protein in the toluene 4-monooxygenase system.

Some research has suggested the potential for the dimerization of coupling proteins (Fox *et al.*, 1991; Brandstetter *et al.*, 1999). Later deletions of N-terminal residues suggested that the presence of the N-terminus in T4moD reduces self-dimerization (Moe *et al.*, 2006). However, deletion of up to 10 N-terminal residues did not significantly reduce the activity of a toluene 4-monooxygenase complex reconstituted from purified proteins, and so the functional importance of dimerization remains unclear.

The triangular shape of T4moD is mainly formed by two antiparallel beta-sheets. The backbone crosses the connecting corner between them three times at glycine residues Gly-36, Gly-54 and Gly-85, which are conserved across many SDIMOs (Hemmi *et al.*, 2001). These glycine residues are believed to confer the conformational flexibility required for the

backbone to change direction in the range of recorded protein-protein interactions of this vital component (Lountos *et al.*, 2005).

The Reductase Component

The reductase is responsible for the first step in the electron transfer chain of SDIMOs, oxidising NADH to NAD⁺ and transferring the two electrons to either the Rieske protein or the hydroxylase through the use of a [2Fe-2S] cluster and FAD cofactors.

The reductase has often posed unique challenges in the purification and characterisation of SDIMOs. Numerous papers describe incidences of inclusion bodies, low yield and rapid loss of activity of reductases from soluble methane monooxygenase (Blazyk and Lippard, 2004), toluene/*o*-xylene monooxygenase (Cafaro *et al.*, 2002), toluene 4-monooxygenase (Studts *et al.*, 2000) and alkene monooxygenase (Champreda *et al.*, 2004). In the case of the alkene monooxygenase of *Xanthobacter autotrophicus* sp. Py2, the other three purified components had to be complemented with a toluene 4-monooxygenase reductase to confer activity, as the reductase could not be purified (Champreda *et al.*, 2004). The requirement of NADH for the reductase activity on the Rieske protein or hydroxylase is an intriguing issue for any biotechnological applications for SDIMO enzymes, as this is an expensive precursor and cycling NADH/NAD⁺ is often difficult to implement in industrial settings.

The structure of the soluble methane monooxygenase reductase from *Methylococcus capsulatus* (Bath) was resolved using NMR by expressing the two protein domains separately, MMOR-Fd (containing the ferredoxin) and MMOR-FAD (containing the FAD). These domains were separately heterologously expressed in *Escherichia coli* and purified (Blazyk and Lippard, 2002). The NMR structure of the purified MMOR-Fd domain has similar structural characteristics to other [2Fe-2S] proteins. Modelling work on the interaction between the reductase and hydroxylase suggested that specificity for the electron transfer partner of SDIMO oxygenases could be linked to different conserved surface residues in different SDIMO subgroups (Müller *et al.*, 2002). The group working on purification of the FAD domain found that it could be resolved further into two domains, one which binds NADH and one which contains the FAD cofactor. The NADH binding domain contains alternating beta-strands and alpha-helices, forming a five-stranded parallel beta-sheet with two alpha-helices on either side, demonstrating a well-documented nucleotide binding fold (Chatwood *et al.*, 2004).

Rieske protein

Finally, the Rieske-type ferredoxin component is exclusive to the four-component SDIMOs. Rieske-type proteins contain a [2Fe-2S] cluster coordinated by two cysteine and two histidine ligands, rather than the four cysteine residues that coordinate traditional [2Fe-2S] clusters. The Rieske protein is involved in electron transfer between the reductase and the oxygenase.

Based on structural analysis of the oxygenase subunit of the toluene 4-monooxygenase from *Pseudomonas mendocina* KR1 and binding predictions for the toluene/*o*-xylene monooxygenase from *Pseudomonas stutzeri* OX1, the Rieske protein binds the hydroxylase in the same place as the coupling protein, which impacts the rate at which the reaction can occur (Figure 1.11) (Acheson *et al.*, 2014; Liang and Lippard, 2014).

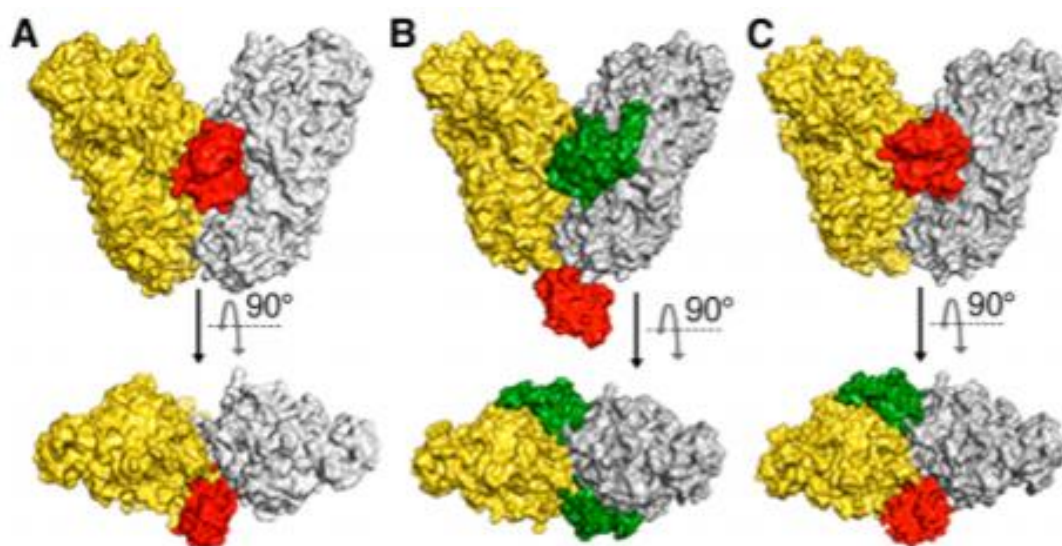


Figure 1.11: Predictions for binding between the oxygenase (yellow and grey) and the Rieske protein (red) and coupling protein (green). Image taken from Liang and Lippard, 2014. A) Rieske protein and oxygenase, B) in the presence of 2-fold excess of coupling protein and C) in the presence of the same amounts of Rieske protein and coupling protein.

1.4. Project Aims

This project aimed to characterise the isoprene monooxygenase from *Rhodococcus* sp. AD45 within the whole cell system. Whole cell and cell lysate assays needed to be developed in order to monitor activity on substrates, study the substrate range, inhibition

by alkynes and kinetics of the whole cell system, as this is most relevant in environmental studies of isoprene degradation by microbes.

Each of the three smaller components of the isoprene monooxygenase from *Rhodococcus* sp. AD45, the Rieske protein (IsoC), the coupling protein (IsoD) and the oxidoreductase (IsoF), were to be purified and characterised. The aim was to characterise the cofactor-containing subunits IsoC and IsoF spectroscopically using absorbance, circular dichroism and electron paramagnetic resonance techniques. Each of the three components were then to be assessed using various mass-spectrometry techniques. Liquid chromatography-mass spectrometry (LC-MS) was used to verify size, and inductively coupled plasma-mass spectrometry (ICP-MS) to quantify the level of [2Fe-2S] cluster incorporation in IsoC, in addition to accurate protein concentration determinations in order to calculate extinction coefficients.

The oxygenase component purification protocol was developed by Dr Colin Lockwood (Murrell Group, University of East Anglia). This was further characterised using the same techniques as for the smaller components for characterisation.

Purification of alternative reductases from the alkene monooxygenase of *Rhodococcus rhodochrous* B-276 and the toluene 4-monooxygenase from *Pseudomonas mendocina* KR1 was also an aim, as these are the most extensively characterised in the existing literature and could provide an interesting source of proteins for checking cross-reactivity between protein components of different SDIMOs.

Finally, reconstitution of the active complex using purified proteins was an ultimate goal. Overall, this project aimed to demonstrate the characteristics which define an isoprene monooxygenase within the wider protein family of soluble diiron monooxygenases.

2. Materials and Methods

2.1 Materials

Chemicals and media components were purchased from ThermoFisher Scientific, Formedium and Sigma-Aldrich. Gases were purchased from Sigma-Aldrich, Air Liquide, CK Special Gases or BOC. Custom oligonucleotides were synthesised by Invitrogen. Strains and plasmids were sourced from Merck Millipore, Sigma Aldrich and Invitrogen.

2.2 Buffers and antibiotic stock solutions

Buffers:

Tris-Borate-EDTA (TBE) buffer 10X: 108 g Trizma base, 55 g orthoboric acid, and 40 mL of an EDTA stock (0.5 M pH 8.0) were dissolved in 1 L total volume using deionised water.

SDS-PAGE running buffer: 30 g Trizma base, 144 g glycine and 10 g SDS were dissolved in 1 L total volume using deionised water.

Phosphate buffer (0.4M stock): 0.4 M solutions of each NaH_2PO_4 and K_2HPO_4 were prepared and mixed until the desired pH (7.0) was reached. The solution was sterilised by autoclaving.

Antibiotics:

Antibiotics were stored as 1000X stocks at $-20\text{ }^\circ\text{C}$ until use.

Chloramphenicol stock solutions were 35 mg mL^{-1} dissolved in ethanol.

Ampicillin stock solution was 100 mg mL^{-1} dissolved in de-ionised water and filter sterilised using a $0.2\text{ }\mu\text{m}$ filter (Sartorius, Germany).

2.3 Preparation of media and cultivation of bacterial strains

All media solutions were prepared using de-ionised water and autoclaved at 15 psi for 15 min at $121\text{ }^\circ\text{C}$ to sterilise. Solid medium was prepared by the addition of 1.5 % w/v Formedium agar. Solutions sensitive to autoclaving were sterilised filtering through a $0.2\text{ }\mu\text{m}$ filter (Sartorius, Germany) and added aseptically to cooled solutions.

Bacterial strains and plasmids used in this study are shown in Table 2.1.

Table 2.1: Bacterial strains and plasmids used in this study.

| Strain/Plasmid | Description | Reference/Source |
|---|--|---|
| Strains | | |
| <i>Escherichia coli</i> TOP10 | Strain used for cloning and plasmid maintenance | Invitrogen |
| <i>Escherichia coli</i> Rosetta 2 (pLysS) | Strain used for protein expression | Sigma Aldrich |
| <i>Rhodococcus</i> sp. AD45 | Wild-type strain | van Hylckama Vlieg <i>et al.</i> , 1998 |
| <i>Rhodococcus</i> sp. AD45-ID | <i>Rh.</i> sp. AD45 cured of megaplasmid | Crombie <i>et al.</i> , 2018 |
| <i>Xanthobacter</i> sp. Py2 | Wild-type strain | van Ginkel and de Bont, 1986 |
| <i>Variovorax</i> sp. WS11 | Wild-type strain | Larke-Mejía <i>et al.</i> , 2019 |
| Plasmids | | |
| pJET | Amp ^R cloning vector | ThermoFisher Scientific |
| pTipQC1 | ChI ^R cloning vector | Nakashima and Tamura, 2004 |
| pTipQC2 | ChI ^R cloning vector | Nakashima and Tamura, 2004 |
| pTipQC1: <i>isoABCDEF</i> | ChI ^R cloning vector containing <i>isoABCDEF</i> from <i>Rh.</i> sp. AD45 | Crombie, unpublished |
| pTipQC2S2: <i>isoABCDEF</i> | ChI ^R cloning vector containing <i>isoABCDEF</i> from <i>Rh.</i> sp. AD45 | Lockwood, unpublished |
| pTipQC1: <i>isoC</i> | ChI ^R cloning vector containing <i>isoC</i> from <i>Rh.</i> sp. AD45 | This study |
| pTipQC1: <i>isoD</i> | ChI ^R cloning vector containing <i>isoD</i> from <i>Rh.</i> sp. AD45 | This study |
| pTipQC1: <i>isoF</i> | ChI ^R cloning vector containing <i>isoF</i> from <i>Rh.</i> sp. AD45 | This study |
| pET51b | Amp ^R cloning vector | Novogen |
| pET51b: <i>isoD</i> | Amp ^R cloning vector containing <i>isoD</i> from <i>Rh.</i> sp. AD45 | This study |
| pET20MBP | Amp ^R cloning vector | Burton, unpublished |
| pET20MBP: <i>isoF</i> | Amp ^R cloning vector containing <i>isoF</i> from <i>Rh.</i> sp. AD45 | This study |

2.3.1 Growth of *Escherichia coli*

Luria-Bertani (LB) medium was used for routine cultivation of *Escherichia coli* strains at 37 °C. Liquid cultures were incubated with orbital shaking at 160 – 220 rpm.

LB medium was prepared by the addition of 10 g tryptone, 5 g yeast extract and 10 g NaCl to de-ionised water at a total volume of 1 L (Sambrook and Russell, 2001).

2.3.2 Preparation and transformation of chemically competent *Escherichia coli* strains

Escherichia coli TOP10

SOB medium was prepared by the addition of 20 g tryptone, 5 g yeast extract and 0.5 g NaCl to 900 mL de-ionised water. Following this, 2.5 mM KCl was added, 5 M NaOH was used to adjust the pH to 7.0 and the total volume was made up with water to 1 L and sterilised by autoclaving. Sterile 2 M MgCl₂ was added to make the final concentration 10 mM immediately before use.

CCMB80 buffer:

The following were dissolved in 800 mL de-ionised water: 11.8 g CaCl₂·2H₂O, 4.0 g MnCl₂·4H₂O, 2.0 g MgCl₂·6H₂O, 100 mL glycerol, 10 mL CH₃COOK (1 M stock, pH 7.0). The pH was adjusted down to 6.4 with 0.1 M HCl and the volume made up to 1 L with water. The solution was sterilised by filtration and stored at 4 °C.

All glassware used for preparation of *Escherichia coli* TOP10 competent cells was half filled with de-ionised water and autoclaved prior to use to remove any detergent residue.

Seed stocks were prepared by growing *Escherichia coli* TOP10 cells on solid SOB medium at room temperature for 36 hours. Single colonies were picked into 2 mL of liquid SOB medium and incubated overnight at room temperature with shaking. Glycerol was added to 15 % (v/v), and 1 mL samples were snap frozen in liquid nitrogen and stored at -80 °C.

To prepare chemically competent *Escherichia coli* TOP10 cells, a 2 L conical flask containing 250 mL SOB medium was inoculated with a seed stock vial and grown at 30 °C with shaking to an OD₅₄₀ of 0.3 - 0.4. The flask was cooled on ice for 10 min, and cells harvested by centrifugation at 2,000 x g for 10 min at 4 °C. The cell pellet was resuspended in 80 mL ice cold CCMB80 buffer and incubated on ice for 20 min before being centrifuged again, as

previously. The final cell pellet was resuspended in 10 mL ice cold CCMB80 buffer and the OD₅₄₀ adjusted to 5 – 7.5 using more CCMB80. Finally, competent cells were portioned into ice cold microcentrifuge tubes in 200 µL aliquots and snap-frozen in liquid nitrogen. The cells were stored at -80 °C until needed.

Escherichia coli Rosetta 2 (pLysS)

Chemically competent *E. coli* Rosetta 2 (pLysS) cells were prepared by inoculating a single colony into 5 mL of LB medium and incubating overnight at 37 °C. A 1 mL aliquot of this culture was used to inoculate 100 mL of LB medium in a 250 mL flask. This culture was incubated at 37 °C until it reached an OD₅₄₀ of 0.4 – 0.6. Cells were cold-shocked on ice for 10 min, followed by harvesting by centrifugation at 6,000 x g for 3 min. Pelleted cells were resuspended in 10 mL ice cold 0.1 M CaCl₂ and incubated on ice for 20 min. The cells were centrifuged as before and the cell pellet resuspended in 0.1 M CaCl and 15 % v/v glycerol.

Escherichia coli Rosetta 2 (pLysS) cells were frozen and stored in aliquots as for the *Escherichia coli* TOP10 cells.

Transformation of chemically competent *Escherichia coli* cells

To transform, the frozen tubes of chemically competent *Escherichia coli* cells were thawed on ice and split into 50 µL reactions in 1.5 mL microcentrifuge tubes. Between 1 – 100 ng plasmid DNA or ligation mix was added and gently mixed, followed by incubation on ice for 30 min. Cells were then subjected to heat shock at 42 °C for 60 sec and cooled on ice for 2 min. LB medium (250 µL) was added and cells were allowed to recover at 37 °C for one hour. For plasmid transformations, a 100 µL sample and appropriate dilutions were spread on LB plates containing the appropriate antibiotics. For ligation mixture transformations, cells were pelleted by centrifugation at 5,000 x g for 5 min and the pellet resuspended in 100 µL of the supernatant before plating onto LB agar plates containing the appropriate antibiotic.

2.3.3 Growth of *Rhodococcus* sp. AD45 and AD45-ID

For growth of *Rhodococcus* sp. AD45 and AD45-ID in liquid medium, a minimal medium based on a previous method for growth of *Ancylobacter* (van den Wijngaard *et al.*, 1993) was used with a modified trace elements solution, as referenced below.

Minimal medium for *Rhodococcus* sp. AD45:

Solution AD1 contained 5 g (NH₄)₂SO₄ per 100 mL de-ionised water. Solution AD2 contained 2 g MgSO₄·7H₂O per 100 mL de-ionised water. Solution AD3 contained 100 g L⁻¹ yeast extract in de-ionised water, without this *Rhodococcus* growth was poor, even with the addition of isoprene or succinate as a carbon source. A 3.4 % (w/v) FeEDTA solution was also prepared and all of these stocks were autoclaved to sterilise. The modified SL10 trace elements solution was prepared according to Crombie and Murrell (2011). To prepare the medium, 10 mL of each AD1, AD2 and AD3, 1 mL of trace elements and 0.1 mL of FeEDTA stock solution were added to de-ionised water to make a final volume of 1 L. The solution was autoclaved to sterilise. Na/K phosphate buffer was added immediately prior to use (50 mL of 0.4 M stock sterilised by autoclaving), as was 10 mM succinate where appropriate (10 mL from a 1 M stock sterilised by autoclaving).

For growth on plates, the same medium was used with the addition of 1.5 % (w/v) agar (Formedium).

Batch growth

All *Rhodococcus* sp. AD45 and AD45-ID batch cultures were grown at 30 °C and 180 rpm.

For batch growth on isoprene, *Rhodococcus* sp. AD45 cells were grown in 20 mL or 400 mL AD45 minimal medium in 120 mL vials or modified 2 L Duran bottles, respectively, sealed with rubber stoppers and aluminium crimp caps with the addition of 1% (v/v) gaseous isoprene (1.3 mM).

For batch growth on succinate, *Rhodococcus* sp. AD45 and AD45-ID were grown in 20 mL or 1 L AD45 minimal medium in 120 mL vials or 2 L conical flasks respectively. The container necks were blocked with cotton wool or foam bungs and covered with foil to prevent contamination.

Fermenter growth

For the fed-batch growth of *Rhodococcus* sp. AD45 a New Brunswick fermenter with a 4 L working volume was used. The fermenter was filled with AD45 minimal medium and inoculated with 400 mL of *Rhodococcus* sp. AD45 grown in batch culture on the appropriate carbon source. In the case of succinate-grown cells, 10 mM succinate was added to the fermenter and additional succinate was added when the dissolved oxygen level started increase. Cells were harvested when the OD₅₄₀ was 3.0 - 5.0 and the cells were still in exponential growth phase. In the case of isoprene-grown cells, isoprene was added through

the air inlet by bubbling gas through chilled liquid isoprene (Figure 2.1). The cells were harvested at an OD₅₄₀ below 2.4 as after this point, the isoprene monooxygenase activity of whole cell suspensions was noted to decrease. In both cases, harvesting of cells was performed by removing 3.5 L of culture. The fermenter was then refilled with 3.5 L of medium and the fermenter was restarted.

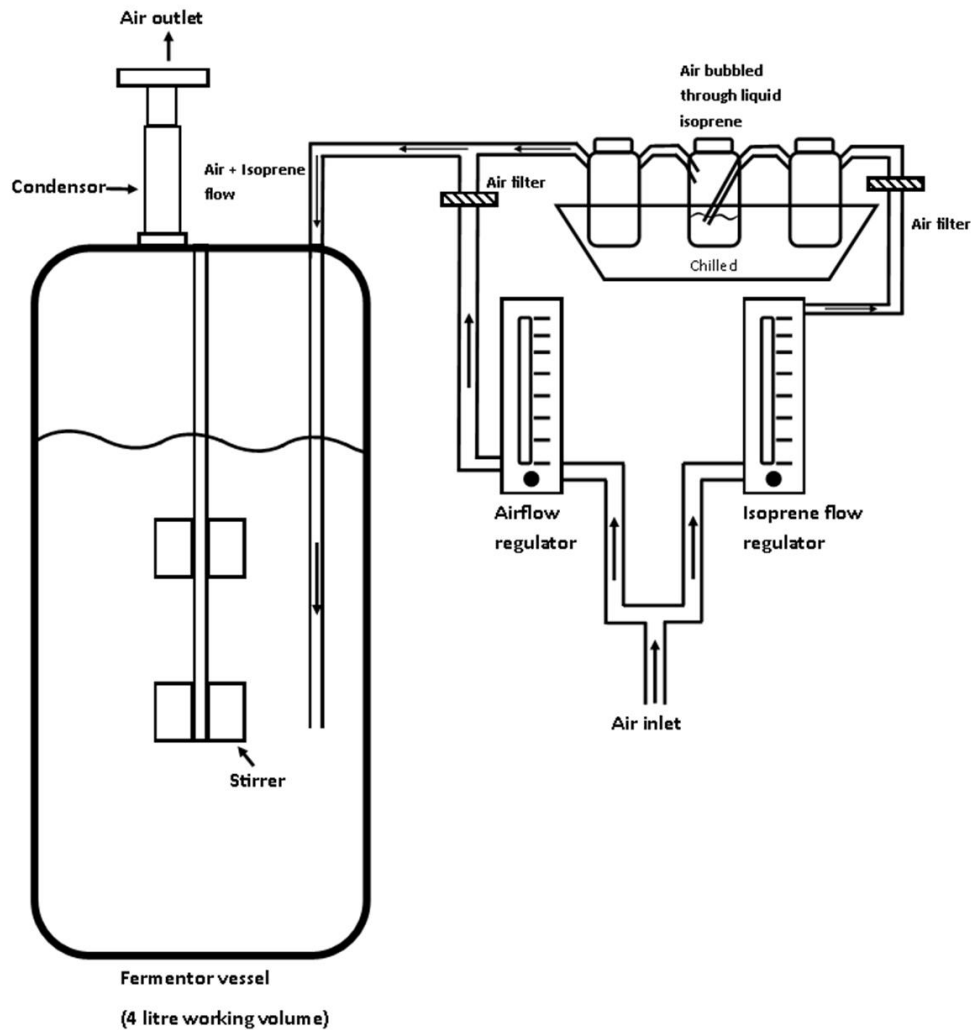


Figure 2.1: Diagram of fermenter growth of bacterial strains using gaseous isoprene as a carbon source. Image credit R. Dawson (Murrell group, University of East Anglia).

2.3.4 Preparation and transformation of electrocompetent *Rhodococcus* sp. AD45-ID

The methods outlined here were developed by Dr A. Crombie, Murrell group, University of East Anglia.

To prepare competent *Rhodococcus* sp. AD45-ID cells, a fresh single colony was inoculated into 5 mL minimal medium containing 10 mM succinate and grown for 24 hours. Subsequently, three 250 mL flasks containing 50 mL minimal medium with 10 mM succinate were inoculated with 0.25, 0.5 and 1 mL of culture and grown overnight. Once one of the cultures had reached an OD₅₄₀ of 0.6, typically the culture containing 0.5 mL of starter after 16 hours, it was cooled on ice for 15 min and the other two cultures were discarded. The cells were then harvested at 5,000 x g for 15 min at 4 °C. The supernatant was discarded and cells washed in 25 mL ice cold sterile de-ionised water followed by centrifugation as above. The cells were then washed in 10 mL ice cold, sterile 10 % (v/v) glycerol, centrifuged again and finally resuspended in 0.5 mL ice cold, sterile 10 % (v/v) glycerol.

For transformation, 100 µL of competent cells were transferred to a pre-chilled microcentrifuge tube and 1 – 50 ng in a volume of 4 µL or less of plasmid DNA added. The mixture was transferred to a cold 2 mm gap electroporation cuvette and pulsed at 2.5 kV, 25 µF and 600 Ω using a GenePulser Electroporation system (Bio-Rad, Hemel Hempstead, UK). Immediately 1 mL of minimal medium containing 10 mM succinate was then added and the cells allowed to recover at 30 °C for 4 h on an orbital shaker at 150 rpm. After recovery, 100 µL of the cells were plated on minimal medium plates containing 10 mM succinate and the appropriate antibiotic. The remaining cells were harvested by centrifugation at 2,500 x g for 6 min and the pellet resuspended in 50 µL of the supernatant. This cell suspension was plated on another minimal medium plate, and both plates were incubated at 30 °C.

2.3.5 Growth of *Xanthobacter* sp. Py2

Xanthobacter sp. Py2 was grown in batch culture in 20 mL or 400 mL AD45 minimal media in 120 mL or modified 2 L Duran bottles, respectively, sealed with rubber stoppers and aluminium crimp caps. Propylene gas was supplied as a carbon source at 10 % (v/v) in the headspace. Cultures were grown at 30 °C on an orbital shaker run at 180 rpm.

2.4 Extraction of nucleic acids

2.4.1 Plasmid extraction from *Escherichia coli* (mini- and midi-prep)

Plasmid extractions were performed on a small scale using 5 mL overnight *Escherichia coli* cultures using the GeneJET Plasmid Miniprep Kit (ThermoFisher Scientific) according to manufacturer's instructions.

On a larger scale for plasmid storage and sequencing, 50 mL overnight *Escherichia coli* cultures were used. For these DNA preparations the QIAGEN Plasmid Midi Kit was used, according to manufacturer's instructions.

2.4.2 Genomic DNA extraction from *Rhodococcus* sp. AD45

Genomic DNA from *Rhodococcus* sp. AD45 grown on isoprene as a carbon source was extracted by Dr A. Crombie (Murrell group, University of East Anglia) using the following protocol, based on Current Protocols in Molecular Biology, Unit 2.4.

Protocol components:

Resuspension buffer: 20 mM Tris, 2 mM EDTA, pH 8.0

CTAB/NaCl: 10 % (w/v) CTAB in 0.7 M NaCl

NaCl: 5.0 M stock solution

The following solutions were prepared in the resuspension buffer:

Lysozyme: 100 mg mL⁻¹

Proteinase K: 10 mg mL⁻¹

N-laurylsarcosine: 10 % w/v

The *Rhodococcus* sp. AD45 cell pellet was resuspended in 5 mL resuspension buffer, 60 µL of lysozyme was added and this was incubated for 60 min at 37 °C. Following this, 375 µL Proteinase K and 7 µL RNaseA (10 mg mL⁻¹) were added. This was incubated for a further 15 min at 37 °C. Next, 780 µL of sarcosine was added and a 60 min incubation at 60 °C was carried out. NaCl was then added from the stock solution to bring the concentration to 0.7 M, and 803 µL of the CTAB/NaCl stock was added, followed by a further 15 min incubation at 60 °C. An equal volume of phenol:ChI:IAA was added and the mixture was shaken followed by incubation at 60 °C for another 10 min. The mixture was centrifuged at 8,000 x g for 5 min, and the upper phase was transferred to a fresh microcentrifuge tube. The

protocol was repeated from the phenol chloroform addition without incubation twice more, each with a 5 min mixing time instead.

The DNA was then precipitated by the addition of 2 volumes chilled 100 % ethanol. This was incubated at -20 °C for 60 min and centrifuged at 13,000 $\times g$ (4 °C) to pellet the precipitated DNA. This was washed with 70 % ethanol followed by repetition of the centrifugation step. The DNA pellet was dried and resuspended in 400 μL of buffer (5 mM Tris pH 8.5). The resulting DNA sample was quantified by Qubit and 0.5 μL aliquots of a 1/100 dilution of the resulting genomic DNA were used as template in PCR reactions.

2.5 Nucleic acid manipulation techniques

2.5.1 Quantification of DNA

DNA concentrations were measured using the Qubit 3.0 fluorometer (ThermoFisher Scientific) with the dsDNA Broad Range reagents according to manufacturer's instructions.

2.5.2 Polymerase Chain Reaction (PCR)

Annealing was conducted at 5 °C less than the lower primer melting temperature of the PCR primer pair. Reactions without template were included in all cases as negative controls.

PCR for cloning

Polymerase chain reactions (PCR) for cloning were performed in 50 μL reactions using Q5 high fidelity DNA polymerase (New England Biolabs) according to manufacturer's instructions. Cycling conditions were typically: Initial denaturation at 95 °C, 3 min; 30 cycles of denaturation at 95 °C, 30 s; annealing (temperature depending on primers), 30 s; elongation at 72 °C (30 s – 1 min depending on product); final elongation at 72 °C, 10 min.

Colony PCR for checking transformants

Colony PCR for checking transformants was carried out in 25 μL reactions as above, but using either DreamTaq (ThermoFisher Scientific) or RedTaq (Sigma Aldrich) according to manufacturer's instructions. The typical cycle was as above, with an extended initial denaturation of 10 min.

2.5.3 Cloning of PCR products into pJETblunt1.2

PCR products were cleaned using the HighPure PCR Product Purification Kit (Roche) according to manufacturer's instructions. These cleaned PCR products were ligated into the pJETblunt1.2 plasmid using the CloneJET kit (ThermoFisher Scientific) according to manufacturer's instructions and used to transform *Escherichia coli* TOP10 cells.

2.5.4 DNA restriction digests

DNA was routinely digested using ThermoFisher Scientific FastDigest restriction enzymes according to manufacturer's instructions, at 37 °C for 1 h.

2.5.5 Dephosphorylation

Digested vector DNA was dephosphorylated by the addition of ThermoFisher Scientific FastAP Thermosensitive Alkaline Phosphatase and incubation according to manufacturer's instructions at 37 °C for 30 min.

2.5.6 DNA purification

For cloning, restriction enzyme digested DNA fragments were excised from TBE agarose gels and purified using the Nucleospin Extraction Kit (Macherey-Nagel, Duren, Germany).

2.5.7 DNA ligations

DNA vectors and inserts were quantified and the correct amount for a 3:1 molar ratio of insert to vector calculated using an online ligation calculator (http://www.insilico.uni-duesseldorf.de/Lig_Input.html). The ligation was carried out with these parameters and T4 DNA ligase (ThermoFisher Scientific) according to manufacturer's instructions.

2.5.8 Sequencing of DNA

Verification of clones was achieved by sending purified plasmid DNA for Sanger sequencing carried out at Eurofins Genomics (Ebersberg, Germany). For pET vector inserts, the M13 sequencing primers were provided by Eurofins Genomics. For pTip vectors, pTipF and pTipR primers were used (see the relevant chapters). For pJET vectors, the pJET primers provided in the CloneJET kit (ThermoFisher Scientific) were used.

2.5.9 Agarose gel electrophoresis

Agarose gel electrophoresis was performed using 1 % (w/v) agarose gels made with TBE buffer (section 2.2). Gels were run at 90 V for 20 – 40 min.

2.6 Harvesting of cells

Cells were harvested by centrifugation in a Beckman J-20 or J-26 centrifuge using a JLA 8.1000 or JLA 10.500 rotor (Beckman). *Escherichia coli* cells were harvested by centrifugation at 6,000 x *g* for 15 min at 4 °C followed by washing in 10 mL of 50 mM Na/K phosphate buffer (pH 7.0) per litre of culture, then centrifuged again using the same parameters as above. *Rhodococcus* sp. AD45 and AD45-ID cells were harvested by centrifugation at 8,000 x *g* for 20 min at 4 °C followed by washing as for *Escherichia coli* above. The resulting cell paste typically had an OD₅₄₀ of ~300. The cell paste was dropped into liquid nitrogen to snap freeze in pellets and stored at -80 °C until needed.

Xanthobacter sp. Py2 cells were harvested by centrifugation at 3,000 x *g* for 40 min and removal of the resulting supernatant. This was repeated 3 – 4 times and 50 mM phosphate buffer (pH 7.0) added to wash the cells. The resulting cell paste typically had an OD₅₄₀ of ~20. This cell paste was stored as for *Rhodococcus* sp. AD45

2.7 Preparation of cell extract

Small samples of *Escherichia coli* culture (1 mL) were sonicated on ice for 6 x 10 sec with at least 1 min rest between runs. The resulting mixture was centrifuged at 16,000 x *g* for 5 min to remove unbroken cells and cell debris before protein quantification.

Escherichia coli cell paste from larger scale growth were treated by sonication or French press. For sonicated samples, the cell paste was diluted 1:3 in buffer and subjected to 15 s of sonication followed by 45 s rest on ice over a total of 10 min. Cells broken by French press were subjected to three passes through a pre-chilled French pressure cell at 20,000 psi (137 MPa). In both cases, the mixture was then centrifuged at 16,000 x *g* for 30 min to remove unbroken cells and cell debris before protein quantification.

Rhodococcus sp. AD45 and AD45-ID cell pellets were diluted 1:2 in buffer and broken by passing three times through a pre-chilled French pressure cell at 20,000 psi (137 MPa). The mixture was centrifuged as above for preparation of *Escherichia coli* cell extracts.

2.7.1 Quantification of protein content

Protein concentrations were quantified using the BIO-Rad protein assay (Bio-Rad Laboratories Inc., Hercules, CA, USA) according to the manufacturer's instructions. Standards were prepared using bovine serum albumin (BSA).

2.7.2 SDS-PAGE

SDS-PAGE using an X-cell II Mini-Cell (Novex) was used to separate proteins. Gels were prepared with either a 12 % or 15 % (w/v) resolving gel and a 4 % (w/v) stacking gel. The layers were prepared as outlined below (Table 2.2) using premixed 40 % (w/v) acrylamide/bis (37.5:1). All volumes given are in mL.

Table 2.2: Components used to produce 12 % and 15 % SDS-PAGE resolving gels, and those used for the 4 % stacking gels.

| | 4 % stacking gel | 12 % resolving gel | 15 % resolving gel |
|--|------------------|--------------------|--------------------|
| 40 % (w/v) acrylamide/bis (37.5:1) | 1.25 | 6 | 7.5 |
| Tris-HCl 1 M pH 6.8 | 1.25 | 0 | 0 |
| Tris-HCl 1 M pH 8.8 | 0 | 3.6 | 3.6 |
| 10 % (w/v) SDS | 0.1 | 0.2 | 0.2 |
| 10 % (w/v) Ammonium persulfate, prepared fresh | 0.1 | 0.2 | 0.2 |
| TEMED (N,N,N',N'-tetramethylethane-1,2-diamine) | 0.01 | 0.02 | 0.02 |
| Water | 7.5 | 10 | 8.5 |

Samples for SDS-PAGE analysis were taken from soluble and insoluble fractions of cell-free extract, whole cells, chromatographic protein purification fractions or purified protein samples. Insoluble fractions of cell free extract were resuspended in the same volume of buffer as the corresponding soluble fraction and the same volume used to load onto the gel. Whole cells were resuspended in an equal volume of 2x loading dye (63 mM Tris-HCl (pH 6.8), 5 % (v/v) β -mercaptoethanol, 10 % (v/v) glycerol, 2 % (w/v) SDS, 0.00125 % (w/v) bromophenol blue), and other protein samples were prepared by the addition of 5x loading

dye to a final 1x concentration. All samples were heated for 10 min at 100 °C and then cooled on ice. Cell debris was removed from whole cell and insoluble samples by centrifugation at 16,000 x *g* for 5 min. Lanes were loaded with approximately 10 – 50 µg of protein from cell extract, and approximately 1 – 10 µg of purified proteins.

SDS-PAGE was run at 160 V for 60 min and gels were stained with InstantBlue protein stain (Expedeon). PageRuler Plus prestained protein ladder (ThermoFisher Scientific) was used as a marker of molecular mass.

2.8 Fast Isoprene Sensor

The Fast Isoprene Sensor (Hills Scientific, USA) was used to measure isoprene concentrations in the headspace of cultures and assay vials according to manufacturer's instructions. Headspace samples of 50 – 100 µL were applied to the system using a gas-tight syringe.

The Fast Isoprene Sensor (FIS) is a highly specialised instrument supplied by Hills Scientific to measure atmospheric isoprene concentrations. It is highly sensitive and has been used successfully to detect isoprene gas standards at levels of 0.5 ppbv (Exton *et al.*, 2010). It was modified by Dr A. Crombie (Murrell group, University of East Anglia) to be used in a similar way to a gas chromatograph, where samples of headspace could be injected and the isoprene present quantified. The FIS will also enable assay of other gaseous alkenes, as the reaction it quantifies is based on the carbon-carbon double bond reacting with ozone. This alkene-ozone reaction releases photons, which are quantified in a photomultiplier tube and can be seen as an output on the software. These data can be exported to QtiPlot where the peak areas of isoprene (or other short chain length alkene) can be calculated (Figure 2.2). These are compared to a standard curve produced by headspace samples of known concentrations, varying from approximately 70 to 500 ppmv.

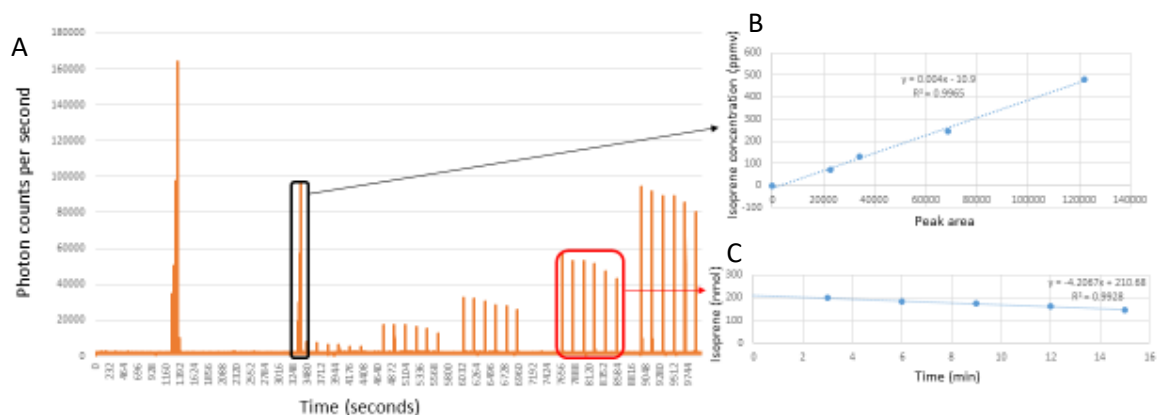


Figure 2.2: Output data from the Fast Isoprene Sensor (FIS) (A) and how peak areas are converted to isoprene concentrations (B) and degradation rates (C).

2.8.1 Quantification of gaseous substrates in the headspace using the Fast Isoprene Sensor

Isoprene standards

Standards were prepared by the addition of a known volume of liquid isoprene using a glass micro-syringe. Isoprene concentration in the vial was calculated from the molecular weight (68 g mol^{-1}) and density (0.68 g mL^{-1}). The standards were then diluted in further sealed 120 mL glass serum vials to yield concentrations between 70 and 500 ppmv isoprene. It should be noted that 1000 ppmv equates to 0.13 mM isoprene in the liquid phase, based on the Henry's Law constant (Sander, 2015).

Gaseous short chain alkene standards

Standards of gaseous short chain alkenes (ethylene, propylene, 1-butene and 1,3-butadiene) were prepared by preparing a vial containing 1 % (v/v) alkene and diluting into further sealed vials to yield concentrations in the same range as for the isoprene standards (above).

Quantifying headspace isoprene

Concentration of headspace alkenes was quantified by injecting 50 μL of headspace gas from sealed glass vials into the Fast Isoprene Sensor. The data were exported into QTIPlot, which was used to calculate the peak area of the photon count and a standard curve produced. The peak area of samples was compared to those of the 0 – 500 ppmv standards to determine alkene concentration.

2.8.2 Whole-cell assay for alkene degradation by *Rhodococcus* sp. AD45 using the Fast Isoprene Sensor

Frozen *Rhodococcus* sp. AD45 cell paste from fermenter batches grown on isoprene or succinate (as a negative control) was thawed on ice and the optical density measured. Cell suspension containing 0.25 mg dw cells in 1 mL 50 mM phosphate buffer (pH 7.0) based on OD₅₄₀ (assuming 1 mL cells at OD₅₄₀ = 1 is equivalent to 0.25 mg dry weight cells) was sealed in a 25 mL glass vial and slowly warmed to 30 °C in a rotary shaking water bath. After 3 min equilibrating in the water bath, 0.5 mL 1 % (v/v) alkene was injected and the vial returned to the shaking water bath for the remainder of the assay.

Headspace samples were taken every 3 min as outlined above for a total reaction time of 18 min. The photon count peaks were quantified and rates of alkene degradation calculated in nmol min⁻¹ mg dw cells⁻¹.

2.8.3 *Rhodococcus* sp. AD45 cell lysate assay for alkene degradation

The protein content of cell extract from *Rhodococcus* sp. AD45 grown on isoprene in a fermenter was quantified and diluted in 50 mM phosphate buffer (pH 7.0) to 10 mg mL⁻¹. A 1 mL sample of the cell extract was added to a 25 mL glass vial, 5 mM dithiothreitol (DTT) was added and sealed followed by injection of 0.5 mL 1 % (v/v) alkene. The vial was then incubated at 30 °C in a rotary shaking waterbath as above for 3 min.

After 3 min, NADH was added from a 1 M stock to a final concentration of 1 mM and headspace measurements of isoprene were immediately initiated. The assay was performed and analysed as for the whole-cell assay, which rates of alkene degradation calculated in nmol min⁻¹ mg protein⁻¹.

2.8.4 Calculating the kinetic constants K_S and V_{max} for isoprene degradation by whole cells of *Rhodococcus* sp. AD45 containing isoprene monooxygenase

Whole-cell assays of *Rhodococcus* sp. AD45 and *Xanthobacter* sp. Py2 were performed as outlined above with varying concentrations of isoprene. The Henry's Law Constant 1.3 x 10⁻² M atm⁻¹ was used to calculate the concentration of isoprene in the solution based on the headspace measurement.

The resulting rates of isoprene depletion in whole-cell assays and concentrations of isoprene were analysed using the nonlinear regression function of the Microsoft Excel add-on Solver to calculate the K_s and V_{max} for isoprene in the *Rhodococcus* sp. AD45 whole-cell system.

The results from Solver were verified by plotting the data in Eadie-Hofstee, Hanes-Woolf and Lineweaver-Burk plots to ensure that the Solver-calculated values of K_s and V_{max} were consistent.

2.9 Oxygen electrode

To monitor a change in oxygen consumption caused by isoprene monooxygenase activity, a Clark-type oxygen electrode was used (Clark *et al.*, 1953). This technique was used exclusively for whole-cell assays. Endogenous and substrate-induced oxygen depletion was calculated according to the published method (Green and Hill, 1984). The addition of substrate resulted in oxygen consumption by isoprene monooxygenase to form epoxides from the alkene bonds in the substrate. This led to an increased rate of oxygen consumption when in the presence of a substrate which was not recorded for compounds tested which were not substrates.

2.9.1 Preparation of alkenes and aromatics for substrate specificity assays

Saturated solutions of liquid alkenes and aromatic compounds were prepared by adding an excess of substrate to 5 mL deionised water in a 25 mL vial at room temperature, followed by sealing and shaking, 5 - 150 μ L of these saturated solutions were added to the oxygen electrode to yield 100 μ M substrate in the final 3 mL volume. Amounts to add were calculated using Henry's Law Constants for gaseous compounds and solubility values for liquid compounds (Appendix I).

2.9.2 Oxygen electrode based whole-cell assay to determine substrate specificity of isoprene monooxygenase from *Rhodococcus* sp. AD45

Frozen cell paste was thawed on ice and the optical density quantified. Cell suspension containing 1.5 mg dw cells based on OD_{540} (assuming 1 mL cells at $OD_{540} = 1$ is equivalent to 0.25 mg dw cells) was added to the oxygen electrode instrument cell in a total of 3 mL of

oxygenated 50 mM phosphate buffer (pH 7.0) and prewarmed to 30 °C by a circulating water bath (Rank Brothers Ltd., Cambridge, UK). After the endogenous oxygen depletion rate had stabilised (typically 2-5 min), this baseline was allowed to continue for 100 s. Substrate was added from a saturated solution using a Hamilton micro-syringe to a final concentration of 100 µM unless otherwise stated. The substrate-stimulate oxygen consumption rate was allowed to stabilise and then the substrate-induced rate of oxygen consumption calculated over 100 s. The overall rate given for a substrate was calculated by subtracting the endogenous rate from the substrate-induced rate of oxygen depletion.

2.10 Gas chromatography

Gas chromatography analysis of isoprene headspace concentration was performed using a 7890A or 7820A gas chromatograph (Agilent Technologies). The 7890A gas chromatograph was fitted with an HP-Plot/Q-column (30 m, 40 µm film 530 µm bore). The oven temperature at analysis was 175 °C, the injector was 250 °C and the flame ionization detector (FID) was 300 °C. A 1:5 split ratio was used, as was a He carrier gas (4 mL min⁻¹). The isoprene retention time was approximately 6.5 min (method taken from Crombie *et al.*, 2015), and this technique was used for isoprene concentrations above 10 ppmv, below which level readings became unreliable. The 7820A gas chromatograph was fitted with a Porapak Q column (Supelco) coupled to a FID. The injector, column and detector temperatures were 150 °C, 125 °C and 200 °C, respectively. The retention time for isoprene was approximately 4 min. In all cases 50 µL samples of headspace were analysed using these techniques.

2.10.1 Preparation of alkynes for inhibition assays

Gaseous alkynes (C₂ - C₄) were added directly to assay vials using a gas-tight syringe. Higher chain length alkynes (C₆ - C₈) were dissolved to a known concentration in DMSO and added as a liquid to the specified concentrations in the appropriate section. The concentration of gaseous alkynes in the liquid phase of assays was calculated using Henry's law.

2.11 Chromatographic Purification

All protein purification was carried out at 4 °C using an AKTApure chromatography system with sample pump and fraction collector (GE Life Sciences) in a cold cabinet. The AKTApure

chromatography system was controlled using the UNICORN™ 7 software. In all cases, the columns were equilibrated in the appropriate binding buffer until the UV absorbance (280 nm) and conductivity were stable (minimum two column volumes). The sample was then applied using the sample pump or a capillary loop and the column washed in 2 – 10 column volumes of binding buffer until the UV absorbance (280 nm) and conductivity were stable. Elution of proteins were then carried out in either linear gradients or steps of increasing elution buffer. Columns were washed with 2 – 5 column volumes of elution buffer to ensure all protein was removed, regenerated where appropriate and stored according to manufacturer's instructions.

2.11.1 Affinity chromatography

Affinity chromatography was used for the purification of proteins expressed with an affinity tag or as a fusion protein. For proteins expressed with a 6-Histidine tag, the GE life sciences 1 mL and 5 mL HisTrap Immobilised Metal Affinity Chromatography (IMAC) columns were used. The binding buffer used contained 50 mM Tris-HCl, 300 mM NaCl and 30 mM imidazole at pH 7.4 and the elution buffer was the same except for the imidazole concentration, which was 500 mM. Where noted, buffers also contained 10 % (v/v) glycerol.

For StrepII-tagged proteins, the 5 mL Strep-Tactin XT (IBA LifeSciences) column was used with a binding buffer containing 100 mM Tris-HCl, 150 mM NaCl, and 1 mM EDTA at pH 8.0, the elution buffer was as for the binding but with the addition of 50 mM biotin.

Maltose binding protein fusions were purified with the MBPTrap 5 mL column (GE Life Sciences). Unless otherwise stated, the binding buffer contained 20 mM Tris-HCl and 200 mM NaCl at pH 7.4, with 10 mM maltose being added to the elution buffer.

2.11.2 Anion exchange chromatography

Anion exchange chromatography was used to separate proteins by surface charge using a Q-Sepharose or DEAE-Sepharose matrix. The Q-Sepharose columns utilised were 1 mL (prepacked) and 130 mL, and the DEAE-Sepharose columns were 1 mL (prepacked) and 150 mL. All columns and column matrices were obtained from GE Life Sciences. Unless otherwise stated, the binding buffers for anion exchange protocols contained 50 mM Tris-

HCl and 50 mM NaCl at pH 7.4, whereas the elution buffer contained 50 mM Tris-HCl and 1.0 M NaCl at pH 7.4.

2.11.3 Hydrophobic interaction chromatography

Hydrophobic interaction chromatography (HIC) was used to separate protein based on the hydrophobicity of their surface using a 30 ml Phenyl Sepharose column. The binding buffer for this column contained 50 mM MOPS, 15 % (v/v) glycerol and 1.5 M $(\text{NH}_4)_2\text{SO}_4$ at pH 7.2. The elution buffer was as for the binding buffer without the ammonium sulfate. The buffers were based on the methods used for purification of the alkene monooxygenase of *Xanthobacter* sp. Py2 (Small and Ensign, 1997).

2.11.4 Size exclusion chromatography

Size exclusion chromatography was used to separate proteins based on their size. The columns used were the Superdex 200 10/300 GL 30 mL column and the Superdex HiLoad 26/600 200 µg column (GE Life Sciences). Samples were loaded in less than 1 mL via capillary loop. For all size exclusion columns, the buffer contained 50 mM sodium phosphate, 150 mM NaCl (pH 7.0) unless otherwise stated.

2.11.5 Concentration and buffer exchange of protein solutions

Proteins were concentrated using spin columns with an appropriate molecular weight cut off able to concentrate 14 mL or 1 mL of sample (Centricon). Where small volumes of protein were to be exchanged (<2 mL) into a different buffer, the same 14 mL concentration columns were used, whereas larger volumes of protein preparation were exchanged into a new buffer using dialysis tubing over at least two changes in a 200-fold excess of buffer.

2.12 Spectroscopic techniques

2.12.1 Absorbance spectroscopy

Absorbance spectroscopy to monitor cell density, identify the UV-visible spectra of purified proteins and perform colorimetric assays was performed using a UV-1800 spectrophotometer (Shimadzu, Milton Keynes, UK). UV-visible spectra and colorimetric

assays were performed using quartz cuvettes and UVprobe software (Shimadzu, Milton Keynes, UK).

2.12.2 Electron Paramagnetic Resonance (EPR) Spectroscopy

EPR spectroscopy was performed by Dr D. Svistunenko (University of Essex, UK). EPR measurements were made using an X-band Bruker EMX EPR spectrometer equipped with a helium flow cryostat (Oxford Instruments). EPR spectra were measured at 10 K at the following instrumental settings: microwave frequency, 9.471 GHz; microwave power, 3.18 mW; modulation frequency, 100 kHz; modulation amplitude, 5 G; time constant, 82 ms; scan rate, 22.6 G s⁻¹; single scan per spectrum. Protein samples for EPR spectroscopy were prepared in an anaerobic glovebox. The protein was reduced by the addition of an excess of sodium dithionite, and samples were snap frozen in liquid nitrogen.

2.12.3 Circular Dichroism spectroscopy

A JASCO model J810 circular dichrograph was used to measure CD spectra for the wavelength range 250 – 800 nm. Protein samples were prepared as for EPR spectroscopy, without the snap freezing step as this was performed on-site.

2.13 Mass spectrometry techniques

2.13.1 Liquid chromatography-mass spectrometry (LC-MS) analysis

LC-MS was conducted using a Bruker microQToF-QIII electrospray ionisation time of flight (TOF) mass spectrometer with guidance from Dr L Jenner (University of East Anglia). The instrument was calibrated in the m/z range 300–2000 using ESI-L Low Concentration Tuning Mix (Agilent Technologies). Samples were prepared by ten-fold dilution of 50 µM protein solution with 0.1 % (v/v) formic acid and 2 % (v/v) acetonitrile to 500 µL. An autosampler using an UltiMate 3000 HPLC system (Dionex) was used to load samples into the LC-MS. A 20 µL sample of the protein was applied to a ProSwift reversed phase RP-1S column (Dionex) at 25 °C. The elution was performed over a gradient using solvents, line A contained 0.1 % formic acid, and line B contained acetonitrile and 0.1 % formic acid, and was performed at 200 mL min⁻¹. An isocratic wash (2 % B, 0 - 2 min) was performed, followed by a linear gradient from 2 – 100 % B (2 - 12 min), an isocratic wash (100 % B, 12 - 14 min) and column re-equilibration (2 % B, 14 - 15 min). Mass spectra were acquired

throughout using the following parameters: dry gas flow 8 L min⁻¹, nebuliser gas pressure 0.8 bar, dry gas 240 °C, capillary voltage 4500 V, offset 500 V, collision RF 650 Vpp. Mass spectra from elution volumes manually selected for their proximity to the predicted protein mass were averaged and deconvoluted using a deconvolution algorithm in Compass DataAnalysis version 4.1 (Bruker Daltonik).

2.13.2 Inductively coupled plasma mass spectrometry (ICP-MS)

ICP-MS analysis was performed by Dr L. Jenner (Le Brun group, University of East Anglia, UK). Samples were prepared by pipetting purified protein samples (1 – 20 μM, 500 μL) into clean microcentrifuge tubes. To the protein samples, 200 μL of ultra-pure nitric acid was added, followed by 200 μL of ultra-pure hydrogen peroxide. These were then sealed and heated at 30 – 40 °C overnight. These samples were then centrifuged (13,000 x g, 10 min) to remove any undissolved protein sample. Following this, 500 μL of digested sample was transferred to a 10 mL Falcon tube, and both 500 μL of ¹⁰³Rh internal standard and 4 mL ultra-pure Milli-Q water was added. These samples were then applied to the instrument using an associated autosampler. Accuracy was verified by the ¹⁰³Rh measurement, and data was only collected where this was recorded as at 80 – 100 % of the expected amount.

2.14 Cyclic voltammetry

Cyclic voltammetry was used to identify the midpoint potential of the [2Fe-2S] cluster containing IsoC component. A graphite electrode was prepared by three cycles of polishing with sodium bicarbonate followed by washing in ultra-pure milli-Q water. A 4 μL aliquot of 1 mg L⁻¹ poly-L-lysine solution was applied to the electrode and left to adsorb for 5 min before excess was removed. The electrode was then covered with a thin layer of prepared protein, which was again left to adsorb for 5 min before excess was removed. This was transferred to an anaerobic glovebox and placed into an electrochemical cell containing 4 mL of buffer (50 mM HEPES, 50 mM NaCl). A scan rate of 10 mV s⁻¹ was used and the potential cycled between -0.5 and 0.1 V. The resulting data were analysed using the Nova software, and the oxidative and reductive peaks calculated by subtracting the baseline. The midpoint potential was then calculated as the mean of these two peaks.

3. Characterisation of isoprene monooxygenase in whole cells of *Rhodococcus* sp. AD45

3.1. Introduction

In this chapter, results from characterisation of isoprene monooxygenase from whole cells of *Rhodococcus* sp. AD45 will be presented. These include optimisation of an isoprene degradation assay, studies into the substrate specificity of isoprene monooxygenase, its kinetics for both isoprene and propylene and comparison to those of the closely related alkene monooxygenase in *Xanthobacter* sp. Py2, and inhibition by terminal alkynes of different carbon chain lengths.

The development of an isoprene degradation assay was vital for quantifying and comparing the ability of various *Rhodococcus* sp. AD45 cultures to degrade isoprene and to draw appropriate conclusions about the isoprene monooxygenase. Cultures examined included a wild-type *Rhodococcus* sp. AD45 grown on either isoprene or succinate as a carbon source, a strain designated *Rhodococcus* sp. AD45-ID which does not contain the isoprene monooxygenase-containing megaplasmid (Crombie *et al.*, 2018), and this *Rhodococcus* sp. AD45-ID strain which contained an expression vector to homologously express the isoprene monooxygenase genes.

The whole-cell kinetic parameters for both isoprene and propylene degradation were examined for both *Rhodococcus* sp. AD45 and *Xanthobacter* sp. Py2. The affinity of the enzymes for isoprene was compared to environmentally-relevant concentrations of isoprene. *Xanthobacter* sp. Py2 was used as a comparison due to the extensive whole-cell characterisation already carried out with respect to propylene degradation, providing a base to verify methods developed here. In addition, the alkene monooxygenase of *Xanthobacter* sp. Py2 is highly similar to the isoprene monooxygenase of *Rhodococcus* sp. AD45, with the active site-containing subunits sharing a 70 % amino acid identity (Crombie *et al.*, 2015).

The substrate specificity of isoprene monooxygenase in whole-cell systems of *Rhodococcus* sp. AD45 was also investigated and compared to that of a Gram-negative isoprene degrading bacterium, *Variovorax* sp. WS11 (Dawson *et al.*, 2020) to establish the substrate specificity of the enzyme and to investigate if any biotechnologically relevant reactions could be catalysed. This was important as soluble diiron monooxygenases are well-established as promiscuous enzymes with broad substrate specificity and biocatalytic

potential. The related soluble methane monooxygenase has been found to be capable of catalysing the oxidation of over 50 substrates (Smith and Dalton, 2004; Jiang *et al.*, 2010).

Finally, alkyne inhibition of isoprene monooxygenase activity in *Rhodococcus* sp. AD45 was assessed. Isoprene can be co-oxidised by other soluble diiron monooxygenase-containing bacteria, for example the soluble methane monooxygenase-containing *Methylobacterium* sp. strain CRL-26 (Patel *et al.*, 1982), making distinction between isoprene oxidation by these bacteria and degradation by true isoprene degraders such as *Rhodococcus* sp. AD45 in environmental samples an issue. Here, the aim was to identify an alkyne inhibitor which could differentiate between the sources of oxidation and enhance understanding of microbial isoprene degradation as a whole.

3.2. Expression of isoprene monooxygenase in *Rhodococcus* sp. AD45 during growth on isoprene and succinate

3.2.1. Development of an assay to quantify degradation of isoprene by whole-cell suspensions of *Rhodococcus* sp. AD45

First, an assay for isoprene degradation needed to be optimised. A gas chromatography-based assay for isoprene degradation by whole cells of *Rhodococcus* sp. AD45 has been previously described (Crombie *et al.*, 2018), though not optimised. All *Rhodococcus* sp. AD45 cells for optimisation were grown on isoprene as a sole carbon source in 400 mL batch-cultures as outlined in section 2.3.3. Gas chromatography assays were performed on an Agilent 7890 gas chromatograph as described in section 2.10.

Initially, the concentration of cell suspension used in the 200 μ L aliquots was optimised for isoprene uptake assays. In the original assay, approximately 2.5 mg dry weight (dw) cells was used in each assay (Crombie *et al.*, 2018). By decreasing the amount of cells used, the rate of isoprene degradation per mg dw cells increased (Table 3.1). This could have been due to enhanced gas-exchange in the less concentrated cell suspensions, as molecular oxygen is needed by the isoprene monooxygenase. With this accounted for, the size of the vials and amount of cell suspension present could be altered to enhance this further.

Table 3.1: Effect of cell suspension concentration on isoprene degradation rate of *Rhodococcus* sp. AD45 grown on isoprene in 2 mL vials. n=1

| Cells (mg dry weight) | Isoprene uptake (nmol min⁻¹ mg dry weight cells⁻¹) |
|----------------------------------|---|
| 0.05 | 4.66 |
| 0.10 | 4.16 |
| 0.30 | 1.69 |
| 0.45 | 1.64 |
| 0.90 | 0.93 |

Next, in order to optimise the gas exchange, the size of the vials was changed to 30 mL. The amount of cell suspension added was also altered to 1 mL, and the concentration of cell suspension was also altered again (Table 3.2).

Table 3.2: Effect of cell suspension concentration on isoprene degradation rate of *Rhodococcus* sp. AD45 grown on isoprene in 30 mL vials. n=3

| Cells (mg dry weight) | Isoprene uptake (nmol min⁻¹ mg dry weight cells⁻¹ ± SD) |
|----------------------------------|--|
| 0.25 | 8.39 ± 1.26 |
| 0.50 | 6.73 ± 0.64 |
| 1.00 | 2.13 ± 0.75 |

Comparing results in Tables 3.1 and 3.2, it was clear that the rate of isoprene degradation could be further enhanced through use in the assay of the larger serum vials. The highest rate was achieved using 0.25 mg dw cells, which was the equivalent concentration of cell suspension to 0.05 mg in the 2 mL vials outlined above. Halving again the concentration of cell suspension did not alter the rate of isoprene uptake (data not shown), suggesting that the gas exchange had been optimised. Thereafter, 0.25 mg dw cells in 1 mL of cell suspension in a 30 mL vial was used for all assays unless stated otherwise.

Given that *Rhodococcus* sp. AD45 demonstrated optimum growth at 30 °C, isoprene degradation activity was checked at 22, 30 and 37 °C (Table 3.3). The optimum temperature for isoprene degradation in whole-cell suspensions of *Rhodococcus* sp. AD45 grown on isoprene was found to be 30 °C, so this was used in all subsequent assays.

Table 3.3: Effect of temperature on isoprene degradation rate of *Rhodococcus* sp. AD45 grown on isoprene. n=3 (22/30 °C), n=1 (37 °C)

| Temperature (°C) | Isoprene uptake (nmol min ⁻¹ mg dry weight cells ⁻¹ ± SD) |
|------------------|---|
| 22 | 4.46 ± 0.99 |
| 30 | 8.39 ± 1.26 |
| 37 | 3.60 |

All assays were performed in 50 mM phosphate buffer, pH 7.0. This is the same buffer as in the minimal medium used for growth of *Rhodococcus*, although at a slightly higher concentration (section 2.2). This buffer was selected for isoprene degradation assays as it clearly does not inhibit growth of *Rhodococcus* sp. AD45 on isoprene and has been used in whole-cell studies on other soluble diiron monooxygenases (Furuhashi *et al.*, 1986; Ensign *et al.*, 1992; van Hylckama Vlieg *et al.*, 1998).

Growth of *Rhodococcus* sp. AD45 cultures on isoprene as a carbon and energy source in batch or fed-batch also had an effect on the rate of isoprene degradation in whole cell assays. By growing *Rhodococcus* sp. AD45 in a fermenter using a fed-batch technique (section 2.3.3), larger quantities of cells could be grown over a shorter time. This technique was limited, however, by the inverse relationship between OD₅₄₀ at harvest and the rate of isoprene degradation above an OD₅₄₀ of approximately 2.0. Therefore, the 4 L fermenter culture was supplemented with additional isoprene every day and 3.5 L of cells were harvested every second day at an OD₅₄₀ between 1.5 and 2.2 to strike a balance between increased biomass and high isoprene degradation rate.

3.2.2. The effect of growth substrate on expression of the isoprene monooxygenase in *Rhodococcus* sp. AD45.

Rhodococcus sp. AD45 grows on a range of carbon sources, including 3-methyl-1-butene, ethanol, glucose and isoprene (van Hylckama Vlieg *et al.*, 1998). Further research demonstrated that the growth of *Rhodococcus* sp. AD45 on isoprene induced expression of isoprene monooxygenase, whereas the enzyme was not produced when the bacterium was grown on succinate (Crombie *et al.*, 2015). This was demonstrated by the presence of isoprene monooxygenase peptide bands in an SDS-PAGE gel (Figure 3.1)

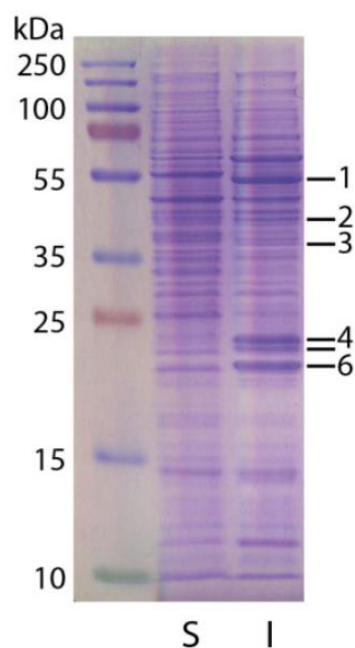


Figure 3.1: SDS-PAGE gel showing polypeptide profile of *Rhodococcus* sp. AD45 grown on succinate (S) or isoprene (I). Highlighted bands were confirmed by extraction and analysis by mass spectrometry. Band 1=IsoA, 2=IsoB, 3=IsoF, 4=IsoJ, 5=IsoI, 6=IsoH. Taken from Crombie *et al.*, 2015.

After growing *Rhodococcus* sp. AD45 on either isoprene or succinate in 400 mL batch culture as outlined in section 2.3.3, the extent of isoprene monooxygenase production was quantified using the whole-cell GC assay outlined in Crombie *et al.*, 2018 (Table 3.4).

Table 3.4: Different levels of isoprene degradation by different *Rhodococcus* sp AD45 or AD45-ID grown on isoprene (iso) or succinate (succ) against a buffer control. n=1

| Sample | Rate of isoprene degradation (nmol min ⁻¹ mg dw cells ⁻¹) |
|--------------|---|
| Buffer | 0.08 |
| AD45 iso | 0.56 |
| AD45 succ | 0.11 |
| AD45-ID succ | 0.09 |

3.2.3. Homologous expression of isoprene monooxygenase in *Rhodococcus* sp.

AD45-ID

Rhodococcus sp. AD45 has been cured of the megaplasmid containing the isoprene degradation cluster, including the genes *isoABCDEF* which encode the isoprene monooxygenase. This new strain, designated AD45-ID, was incapable of growth on isoprene as a carbon source (Crombie *et al.*, 2018). The isoprene degradation activity of this AD45-ID strain could be partially complemented by the addition of a pTipQC series plasmid encoding an isoprene monooxygenase sequence recovered from metagenomics data (Crombie *et al.*, 2018). The pTip series of expression vectors were developed for use in *Rhodococcus erythropolis* to allow expression of proteins which formed inclusion bodies in *Escherichia coli* at temperatures down to 4 °C (Nakashima and Tamura, 2004a). A pTipQC series vector containing the *isoABCDEF* gene cluster from *Rhodococcus* sp. AD45 had also been produced. This homologous expression system could partially complement the capacity for isoprene degradation in *Rhodococcus* sp. AD45-ID, but did not restore the ability of the strain to grow on isoprene as a carbon source (Crombie, unpublished).

In order to monitor the expression of isoprene monooxygenase using this homologous expression system, three *Rhodococcus* cultures were grown in batch culture (section 2.3.3). *Rhodococcus* sp. AD45 was grown on isoprene, whereas AD45-ID was grown on succinate as a carbon source. The cultures of AD45-ID contained either the empty pTipQC1 vector (MT) or the *isoABCDEF* expression vector (pTipQC1:IsoEx). Cell lysate of these cultures were prepared according to section 2.7 and their polypeptide profiles were assessed by running cell-free extract on an SDS-PAGE gel (as described in section 2.7.4) (Figure 3.2).

Although not all of the isoprene monooxygenase polypeptides were visible, the subunit of the oxygenase containing the active site (IsoA, indicated by a red arrow) is clearly visible. This is important as the oxygenase components of soluble diiron monooxygenases have often failed to expressed, or expressed in an insoluble form, when heterologous expression has been attempted using *Escherichia coli* (West *et al.*, 1992; Chan Kwo Chion *et al.*, 2005; Furuya *et al.*, 2013), making the soluble expression demonstrated here promising for future purification.

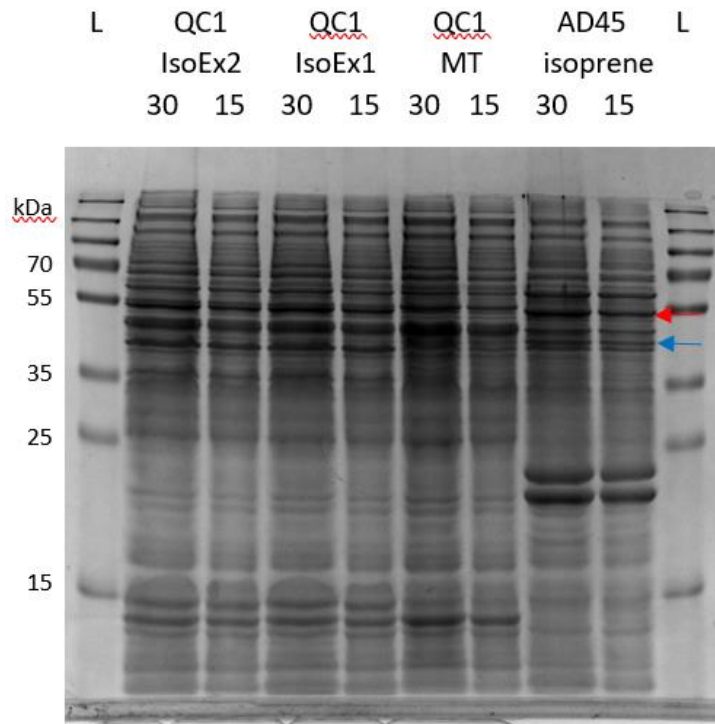


Figure 3.2: Polypeptide profiles of different *Rhodococcus* sp. AD45 and AD45-ID cultures as determined by SDS-PAGE gel electrophoresis. AD45-ID cells contained pTipQC1 plasmid as either an empty vector (MT) or *isoABCDEF* expression vector (IsoEx). IsoA and IsoE peptides are highlighted by red and blue arrows respectively.

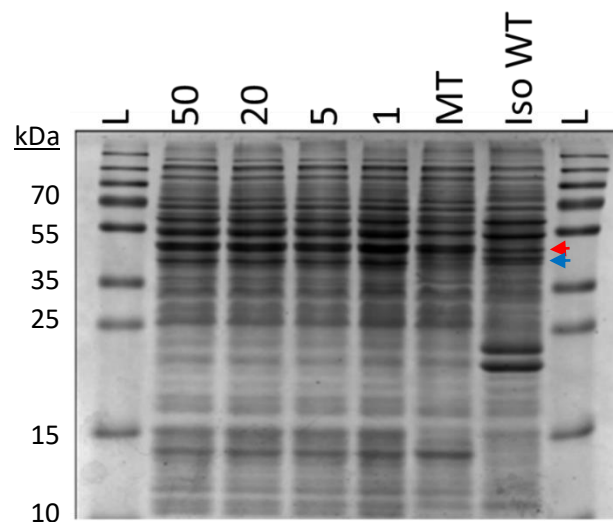


Figure 3.3: The effect of thioestrepton concentration (1 - 50 $\mu\text{g ml}^{-1}$) on induction of protein expression from the pTipQC1 IsoEx plasmid. IsoWT shows the polypeptide profile of cell-free extract from *Rhodococcus* sp. AD45 grown on isoprene. MT shows the profile of cell-free extract from *Rhodococcus* sp. AD45-ID containing the empty pTipQC1 vector. IsoA and IsoE bands are highlighted with red and blue arrows respectively.

Subsequently, optimisation of protein expression was attempted by altering the concentration of the inducer, thioestrepton. The *Rhodococcus* sp. AD45-ID expressing pTipQC1:IsoEx were grown as above, with 1 $\mu\text{g mL}^{-1}$ thioestrepton being used for a standard induction as in previous work. Concentrations of thioestrepton between 1 and 50 $\mu\text{g mL}^{-1}$ were tested, however none of the higher concentrations were found to increase expression of the isoprene monooxygenase components (Figure 3.3).

Optimisation of isoprene monooxygenase production was then attempted by altering the OD_{540} at induction of cultures. The standard protocol outlined in the previous section involved inducing the cultures at an OD_{540} of 0.6. Altering this OD_{540} at the time of induction to between 0.2 and 0.8 did not result in any significant change in expression of the isoprene monooxygenase subunits IsoA or IsoE based on polypeptide profiles (Figure 3.4). After the optimisation attempts were unsuccessful, a thioestrepton concentration of 1 $\mu\text{g mL}^{-1}$ and induction at an OD_{540} of 0.6 was carried forward.

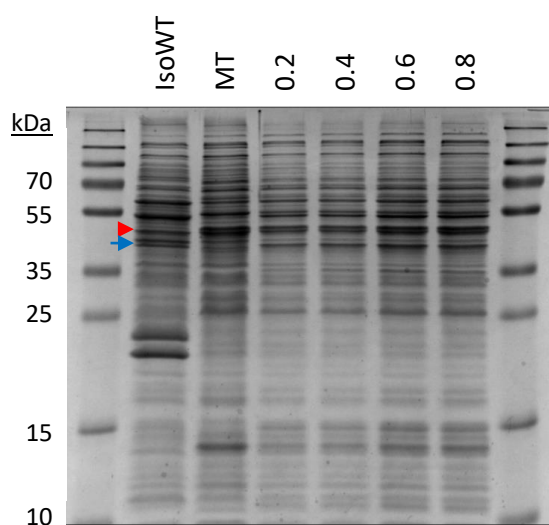


Figure 3.4: The effect of OD_{540} at induction (numbered samples) on protein expression from the pTipQC1 IsoEx plasmid. IsoWT = polypeptide profile of cell-free extract of *Rhodococcus* sp. AD45 grown on isoprene. MT = profile of cell free extract of *Rhodococcus* sp. AD45-ID containing the empty pTipQC1 vector. IsoA and IsoE bands are highlighted with red and blue arrows respectively.

3.2.4. Quantification of isoprene degradation by *Rhodococcus* sp. AD45 and AD45-ID expressing pTipQC1:IsoEx.

Using the isoprene degradation assay protocol outlined in section 3.2.1, the difference in isoprene monooxygenase expression between the wild-type *Rhodococcus* sp. AD45 grown

in batch culture on isoprene as a carbon source (section 2.3.3) and the AD45-ID strain containing both the empty pTipQC1 vector (MT) and the vector containing *isoABCDEF* from *Rhodococcus* sp. AD45 (IsoEx) was assessed using gas chromatography (Table 3.5).

The rate isoprene is removed by the *Rhodococcus* sp. AD45-ID system complemented with the pTipQC1:IsoEx expression vector was not the same as *Rhodococcus* sp. AD45 grown on isoprene, suggesting that less of the isoprene monooxygenase was being expressed, or some of the subunits were less active. However, the fact that an isoprene degradation rate was observable suggested that this protocol could be used to purify active protein expressed in AD45-ID using the homologous protein expression system, which will be utilised and presented in later results chapters.

Table 3.5: Difference in rate of isoprene degradation between whole cell suspensions of *Rhodococcus* sp. AD45 grown on isoprene (AD45iso), AD45-ID expressing the pTipQC1 empty expression vector (QC1 MT), the same vector expressing the *isoABCDEF* gene cluster from *Rhodococcus* sp. AD45 (QC1 IsoEx) and a buffer control. n=1

| Sample | Rate of isoprene degradation (nmol min ⁻¹ mg dw cells ⁻¹) |
|-------------------|---|
| Buffer | 0.06 |
| AD45 iso | 0.44 |
| AD45-ID QC1 MT | 0.06 |
| AD45-ID QC1 IsoEx | 0.12 |

3.2.5. Quantifying *Rhodococcus* sp. AD45 isoprene monooxygenase activity using the Fast Isoprene Sensor and an oxygen electrode

In addition to the use of gas chromatography to quantify isoprene levels, a Fast Isoprene Sensor and oxygen electrode were also available for monitoring isoprene monooxygenase activity.

The Fast Isoprene Sensor (FIS) is a highly specialised instrument supplied by Hills Scientific to measure atmospheric isoprene concentrations using headspace measurements, though it can also be used to measure concentrations of other gaseous alkenes (see Section 2.8). Conversely, the Clark-type oxygen electrode can be used to indirectly monitor monooxygenase activity by monitoring oxygen consumption. When cells are added to the oxygen electrode chamber, oxygen is slowly depleted by cells respiring residual substrate,

known as the endogenous rate. When a substrate for the isoprene monooxygenase is added, this leads to more rapid oxygen depletion, referred to as the induced rate. The endogenous rate is subtracted from the induced rate, resulting in the substrate-induced rate of oxygen depletion, which should be directly proportional to the rate of isoprene monooxygenase activity (Figure 3.5).

Different approaches for estimating isoprene oxidation are used throughout the rest of this thesis. In general, when lower isoprene concentrations were used, such as in kinetics studies, the Fast Isoprene Sensor was used due to the high sensitivity of the instrument, which has been demonstrated to detect isoprene down to 0.5 ppbv in a gaseous standard (Exton *et al.*, 2010). When a wide range of substrates was to be tested, the oxygen electrode was used. In the case of alkyne inhibition experiments with isoprene monooxygenase, the gas chromatograph was used as this is not impaired by the presence of alkynes or DMSO (section 2.10.1).

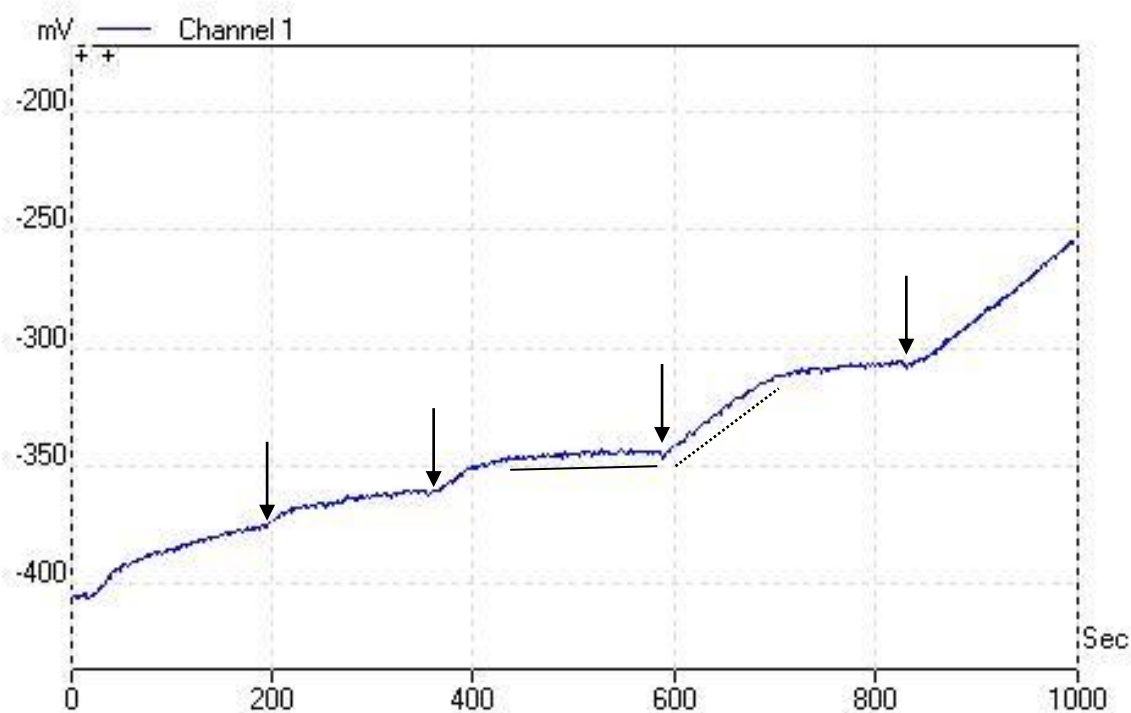


Figure 3.5: Output of the Clark-type electrode (blue line) and where endogenous rates (black solid line) and induced rates (black dotted line) are calculated after addition of potential substrates (black arrows).

3.3. Whole cell kinetics of isoprene and propylene degradation by *Rhodococcus* sp. AD45 and *Xanthobacter* sp. Py2

3.3.1. Development of Fast Isoprene Sensor assays for whole-cell enzyme kinetics of isoprene and propylene degradation

The Fast Isoprene Sensor was utilised to study whole-cell kinetics for both isoprene and propylene oxidation by *Rhodococcus* sp. AD45 and *Xanthobacter* sp. Py2. *Rhodococcus* sp. AD45 was grown on isoprene as a carbon source in a fed-batch system (section 2.3.3) to ensure it was expressing isoprene monooxygenase, whereas *Xanthobacter* sp. Py2 was grown on propylene in batch culture (section 2.3.5) to ensure the bacterium was producing alkene monooxygenase. The Fast Isoprene Sensor was the only technique available to monitor isoprene and propylene depletion at the required concentrations. The assays were performed according to the optimised protocol outlined in section 3.2.1. The headspace concentration of isoprene was monitored every 3 minutes with the Fast Isoprene Sensor to calculate the rate of isoprene consumption. The isoprene concentration was calculated from the first Fast Isoprene Sensor reading to ensure accurate recording of concentration due to the variability introduced by injecting 0.2 – 1.0 ml of gaseous isoprene stocks of concentrations between 1 % and 10 % (v/v).

The FIS data were analysed using QtiPlot to calculate the areas of isoprene peaks, and the rates calculated using Microsoft Excel. The kinetics were calculated by fitting the data to the Michaelis-Menten equation using the Microsoft Excel add-in Solver under the least squares fitting parameters.

3.3.2. Whole-cell kinetics for isoprene and propylene degradation by *Rhodococcus* sp. AD45 expressing isoprene monooxygenase

In this section, the results of whole cell kinetics experiments of *Rhodococcus* sp. AD45 cells in the presence of isoprene or propylene will be presented. Concentrations of isoprene between 0.9 and 54.0 μM were used to determine whole-cell kinetics of *Rhodococcus* sp. AD45 for isoprene using the Fast Isoprene Sensor (Figure 3.6).

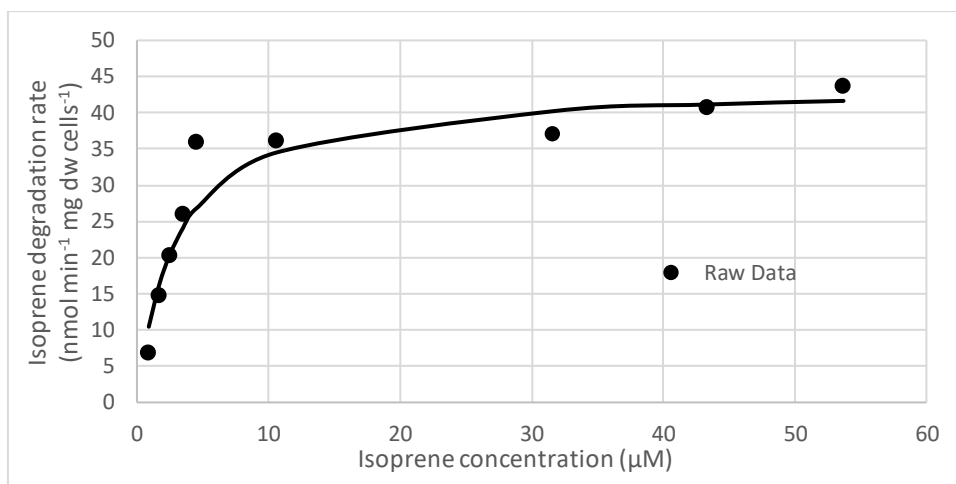


Figure 3.6: Whole-cell kinetics of isoprene degradation by *Rhodococcus* sp. AD45 expressing isoprene monooxygenase. Filled circles show the raw data, and the line shows the data fitted to the Michaelis-Menten equation.

Based on the kinetic analysis of *Rhodococcus* sp. AD45 oxidising isoprene, the apparent K_M for isoprene was $2.88 \mu\text{M}$ and the V_{max} was $43.9 \text{ nmol min}^{-1} \text{ mg dw cells}^{-1}$. This showed a lower affinity and maximum rate than the data obtained in previous work, where the apparent K_M for *Rhodococcus* sp. AD45 grown on isoprene was $0.8 \mu\text{M}$ and the V_{max} was $76 \text{ nmol min}^{-1} \text{ mg cells}^{-1}$ (van Hylckama Vlieg *et al.*, 1998). This could be due to the continuous culture methods used by this group, which were not used here.

In an environmental setting, concentrations of isoprene leading to a rate of reaction approaching V_{max} of either trial are highly unlikely. The affinity of the enzyme is reasonably similar between the two studies. In order for liquid to contain $2.9 \mu\text{M}$ (the apparent K_M estimated in this study), 200 ppmv isoprene would need to be present in the atmosphere. Whilst not impossible, this is a very high isoprene concentration, particularly considering the bacterium was isolated from freshwater sediment and not directly from the leaves of a high isoprene emitting tree. The higher affinity found by van Hylckama Vlieg *et al.* (1998) would only require approximately 70 ppmv, which is more realistic but still very high.

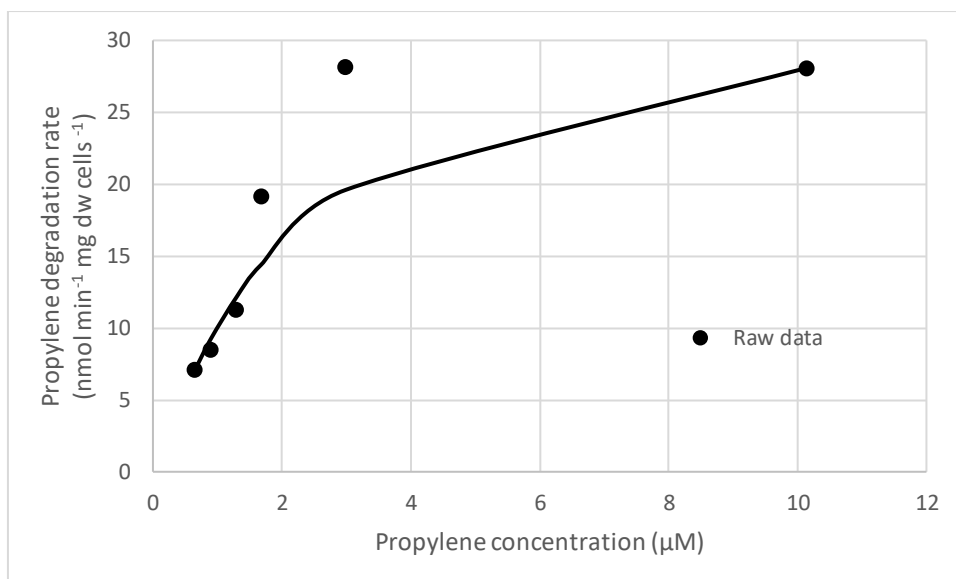


Figure 3.7: Whole-cell kinetics of propylene degradation by *Rhodococcus* sp. AD45 expressing isoprene monooxygenase. Filled circles show the raw data, and empty circles show the data fitted to the Michaelis-Menten equation.

For propylene, the concentrations used in whole cell kinetics experiments were between 0.5 and 12.0 µM (Figure 3.7). In this case, it appeared that the affinity is almost identical, and the V_{\max} very similar, to that for isoprene in *Rhodococcus* sp. AD45. By again fitting the data to the Michaelis-Menten equation using Excel Solver the apparent K_M was found to be 2.32 µM and the V_{\max} was found to be 34.51 nmol min⁻¹ mg dw cells⁻¹. This will be interesting to compare to the alkene monooxygenase of *Xanthobacter* sp. Py2 due to the extensive characterisation of the whole cell system (van Ginkel and de Bont, 1986; van Ginkel *et al.*, 1986; Ensign *et al.*, 1992; Reij *et al.*, 1995; Zhou *et al.*, 1999) and the high homology between the active-site containing alpha subunits, as the amino acid identity between IsoA and XamoA is 70% (Crombie *et al.*, 2015), which is higher than to any other characterised soluble diiron monooxygenase.

3.3.3. Whole-cell kinetics for isoprene and propylene degradation by *Xanthobacter* sp. Py2 expressing alkene monooxygenase

In this section, the results of kinetics experiments with whole-cell suspensions of *Xanthobacter* sp. Py2 will be presented. The concentrations of alkene used and method are the same as in section 3.3.2. This experiment was done to determine the reliability of the Fast Isoprene Sensor as a method for quantifying kinetic parameters and to compare the

isoprene monooxygenase of *Rhodococcus* sp. AD45 and the alkene monooxygenase of *Xanthobacter* sp. Py2.

The apparent K_M for isoprene in whole cells of *Xanthobacter* sp. Py2 was found to be 16.31 μM (Figure 3.8). This suggests a slightly lower affinity for isoprene than *Rhodococcus* sp. AD45, however the difference is small as they both lie within the low micromolar range. Surprisingly, the V_{max} appears to be higher than *Rhodococcus* sp. AD45, at $75.76 \text{ nmol min}^{-1} \text{ mg dw cells}^{-1}$.

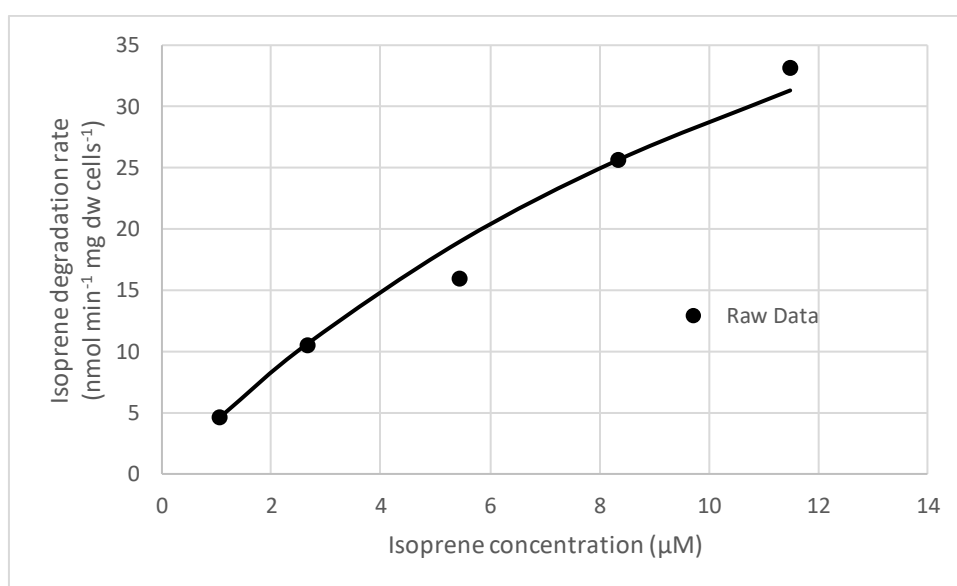


Figure 3.8: Whole-cell kinetics of isoprene degradation by *Xanthobacter* sp. Py2 cells expressing alkene monooxygenase. Filled circles show the raw data, and the line shows the data fitted to the Michaelis-Menten equation.

For propylene degradation by *Xanthobacter* sp. Py2 cells, the apparent K_M was $5.25 \mu\text{M}$ and the V_{max} was $94.57 \text{ nmol min}^{-1} \text{ mg dw cells}^{-1}$ (Figure 3.9). This slightly higher affinity and rate was expected as the preferential substrate for *Xanthobacter* sp. Py2 growth is propylene (van Ginkel *et al.*, 1986).

The whole-cell analysis of *Xanthobacter* sp. Py2 kinetic parameters have been researched previously in two separate studies, both of which utilised gas chromatography to quantify headspace concentrations. One study found that the apparent K_M for propylene was $0.62 \mu\text{M}$ (Reij *et al.*, 1995), whereas the other determined it to be $1.34 \mu\text{M}$ (van Ginkel and de Bont, 1986). As these were both in the low micromolar range, they are similar to the results presented here. The V_{max} recorded for propylene why these two studies are consistent

between the two, however possibly vary compared to the results presented here. One study found the V_{\max} to be $75 \text{ nmol min}^{-1} \text{ mg protein}^{-1}$ (Reij *et al.*, 1995), and the other found it to be $70 \text{ nmol min}^{-1} \text{ mg protein}^{-1}$ (van Ginkel and de Bont, 1986). This could be due to their calculations using protein concentrations rather than cell dry weight, which has been utilised here.

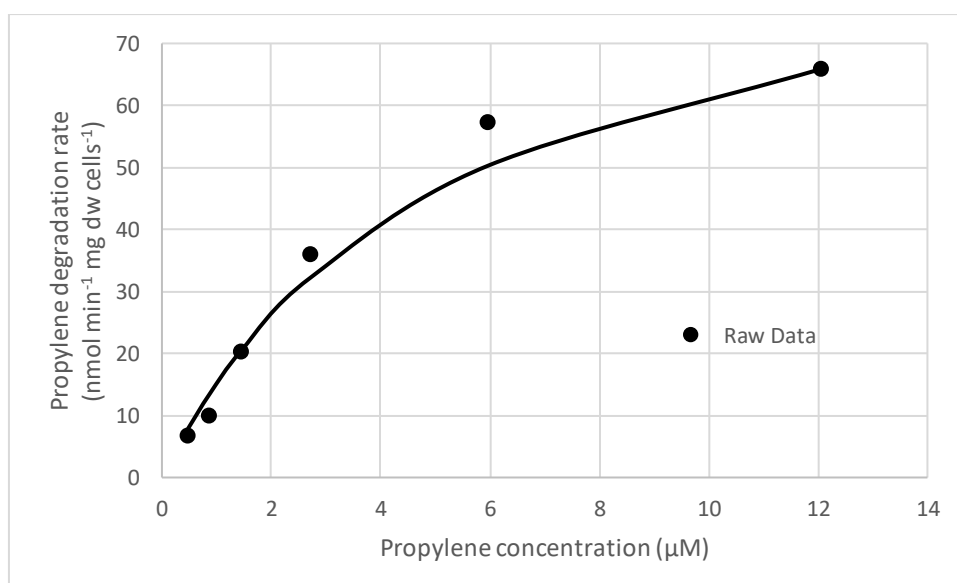


Figure 3.9: Whole-cell kinetics of propylene degradation by *Xanthobacter* sp. Py2 expressing alkene monooxygenase. Filled circles show the raw data, and the line shows the data fitted to the Michaelis-Menten equation.

3.3.4. Comparison of isoprene degradation by *Rhodococcus* sp. AD45 with other isoprene monooxygenases

There are limited data on whole cell kinetics for isoprene degradation, as microbial isoprene consumption is understudied. Isoprene degradation by the isoprene monooxygenase-containing *Variovorax* sp. WS11 has also been characterised in whole-cells by Robin Dawson (unpublished). The kinetic parameters for isoprene degradation were determined to be an apparent K_M of $2.15 \mu\text{M}$ and a V_{\max} of $21.73 \text{ nmol min}^{-1} \text{ mg}^{-1}$, which is similar to the values presented here for *Rhodococcus* sp. AD45. The isoprene monooxygenases in both bacteria are highly similar, and the two active-site containing alpha subunits of their oxygenases (IsoA) have 71 % amino acid identity, which is very similar to the homology between the isoprene monooxygenase of *Rhodococcus* sp. AD45 and the alkene monooxygenase from *Xanthobacter* sp. Py2 (70 %).

A range of bacteria capable of degrading isoprene and their kinetic parameters have been characterised recently (Singh *et al.*, 2019). The bacteria were taxonomically diverse, with the eight isolates of the six genera *Pseudomonas*, *Arthrobacter*, *Bacillus*, *Sphingobacterium*, *Sphingobium* and *Pantoea*. The K_s values obtained for isoprene were between 1.47 and 3.70 mM, demonstrating a lower affinity for isoprene than *Rhodococcus* sp. AD45 as presented here. The V_{max} values calculated, however, lie between 35.35 and 104.17 nmol min⁻¹ mg protein⁻¹. The value for *Rhodococcus* sp. AD45 found in this study would lie within the upper end of this range based on half of the dry weight of a cell being protein.

3.3.5. Comparison of isoprene degradation by *Rhodococcus* sp. AD45 with other soluble diiron monooxygenases

Kinetic studies of soluble diiron monooxygenases have been performed using a range of techniques. The most extensive study has been carried out on the soluble methane monooxygenase using a Clark-type electrode and purified protein. The substrates tested included a range of alkanes and alkenes of different chain lengths (Green and Dalton, 1986). This study found that the affinity of the purified sMMO for methane was almost identical to the apparent K_M value presented here for *Rhodococcus* sp. AD45 and isoprene, at 3 μ M, and a V_{max} recorded at 56.0 nmol min⁻¹ mg purified protein⁻¹. The sMMO had a lower affinity for all of the longer chain-length alkanes tested, with the K_M value ranging from 12.5 μ M for propane, and 500 μ M for butane. However, there was no obvious link between carbon chain length and affinity. For sMMO, the K_M for propylene was 0.94 μ M, suggesting a slightly higher affinity for this compound (Green and Dalton, 1986). This could simply be due to the highly reactive nature of the alkene bond, which would be easier to break than the highly stable C-H bonds of methane and other alkanes.

Studies on the toluene monooxygenases have also focussed on purified proteins. One study assessed the affinity of toluene-2-monooxygenase from *Burkholderia cepacia* to the groundwater contaminant TCE by quantifying the K_M as 12 μ M (Newman and Wackett, 1997). Another study explored kinetics of the studied the toluene 4-monooxygenase from *Pseudomonas mendocina* KR1 and its K_M for toluene, which was found to be 5 μ M which is highly similar to the apparent K_M results presented here for both *Rhodococcus* sp. AD45 and *Xanthobacter* sp. Py2 for isoprene and propylene (their preferred substrates) respectively (Pikus *et al.*, 2000).

In addition to studying the affinity of alkene monooxygenase of *Xanthobacter* sp. Py2 for propylene, one study also investigated the apparent K_M for whole cell suspensions of other environmental isolates capable of growth on propylene, including *Mycobacterium* sp. Py1 and *Xanthobacter* sp. Py10. The *Mycobacterium* sp. Py1 isolate had a higher affinity for propylene (apparent K_M 0.5 μM), but a lower rate of oxidation (V_{max} 15 $\text{nmol min}^{-1} \text{mg protein}^{-1}$), whereas *Xanthobacter* sp. Py10 had a both a similar affinity (apparent K_M 1.10 μM) and rate of oxidation (V_{max} 65 $\text{nmol min}^{-1} \text{mg protein}^{-1}$) in comparison to the aforementioned *Xanthobacter* sp. Py2 (van Ginkel and de Bont, 1986).

3.4. Substrate specificity of isoprene monooxygenase from *Rhodococcus* sp. AD45

3.4.1. Assay parameters to determine substrate specificity of isoprene monooxygenase from *Rhodococcus* sp. AD45

To determine substrate specificity, the Clark-type electrode was used because all of the potential substrates could be screened without issues with varying retention times on the gas chromatograph of gaseous substrates, and non-gaseous substrates could still be identified.

All potential substrates were added as saturated solutions in water, with the Henry's Law Coefficient being used to calculate the concentration of solutions of gaseous substrates (Appendix I). The concentrations based on solubility of non-gaseous substrates were calculated using data obtained from <http://www.chemspider.com/> (Appendix I). Substrates listed as "insoluble" were added as 200 μL of the saturated solution in order to minimise the effect of additional volume on the reaction.

Where possible, 100 μM of each substrate was used in a final volume of 3 mL, as this is considerably higher than the apparent K_M of 2.88 μM (presented in section 3.3.2). Where this would require more than 200 μL of saturated solution, only 200 μL was added, though this is only relevant to terminal alkenes with a chain length above seven carbons. This did not appear to reduce the activity on these longer chain and less-soluble alkenes.

3.4.2. Oxidation of terminal alkenes by isoprene monooxygenase in whole cells of *Rhodococcus* sp. AD45

The activity of SDIMOs with terminal alkenes has been extensively studied. Stereospecific epoxidation reactions are important in industry, and a considerable amount of research has gone into epoxidation of propylene, the three carbon alkene, using a variety of SDIMOs.

In this section, oxidation of terminal alkene substrates ranging from C₂ – C₁₈ will be presented and the rates compared to that of isoprene. *Rhodococcus* sp. AD45 was grown on isoprene in a fed-batch culture for all experiments. The rate of substrate-induced oxygen uptake rate was quantified using a Clark-type oxygen electrode (section 2.9). As a negative control, *Rhodococcus* sp. AD45 grown in fed-batch culture on succinate was used as it did not express isoprene monooxygenase (section 3.2.2).

There was no clear relationship between the length of the alkene and the rate of substrate-induced oxygen uptake, nor was the rate linked to how similar in chain length the terminal alkenes were to isoprene (Figure 3.10). The most notable result is that of octene, where succinate-grown cells also have a high substrate-induced rate. Other enzymes which can oxidise 1-octene include the ubiquitous cytochrome P450 enzymes. One study on alkene epoxidation of cytochrome P450 enzymes was focussed on directional evolution, and suggests that the cytochrome P450 enzymes work not only on 1-octene but also 1-hexene (Lindsay Smith and Sleath, 1982), which did not produce an increased rate of oxygen uptake in the succinate grown *Rhodococcus* sp. AD45 cells. There is a cytochrome P450 present in the *Rhodococcus* sp. AD45 genome, with the accession number WP_045070969.1.

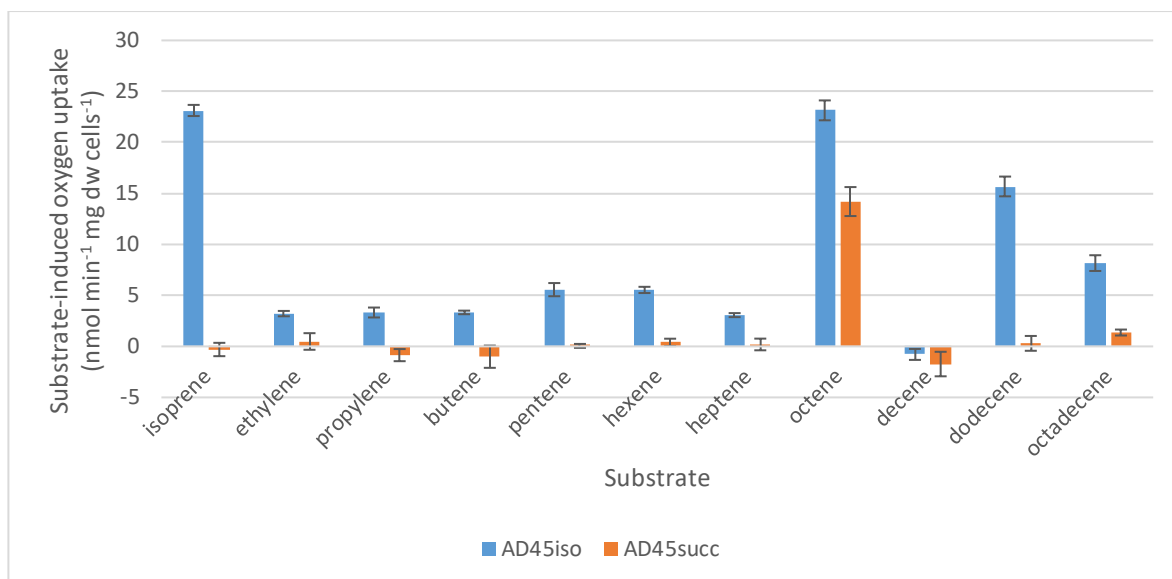


Figure 3.10: The rate of terminal alkene-induced oxygen uptake of whole-cell suspensions of *Rhodococcus* sp. AD45 grown on either isoprene (AD45iso, blue bars) or succinate (AD45succ, orange bars) \pm SEM (n=3). AD45iso cells contain isoprene monooxygenase, whereas AD45succ cells do not and are used as a negative control. All substrates were added at 100 μ M.

3.4.3. Activity of isoprene monooxygenase in whole-cell suspensions of *Rhodococcus* sp. AD45 with cyclic alkenes, dienes and aromatic compounds

In this section, the results of the more unusual hydrocarbon substrates including cyclic alkenes, dienes and aromatics will be presented and the rates of substrate-induced oxygen uptake compared to that of isoprene (Figure 3.11). *Rhodococcus* sp. AD45 grown on either isoprene or succinate in a fed-batch system were used, as outlined in the previous section.

The greatest similarity to the rate of isoprene-induced oxygen uptake was observed with 1,3-butadiene. This is not surprising as it has the most similar structure to isoprene of all of the tested compounds, and was the only alkene tested which *Rhodococcus* sp. AD45 can use as a carbon source (unpublished data). Isoprene monooxygenase was capable of oxidising cyclohexene and a range of dienes and aromatic compounds. The only compounds which were not substrates for the isoprene monooxygenase were methylcyclohexene and propylbenzene.

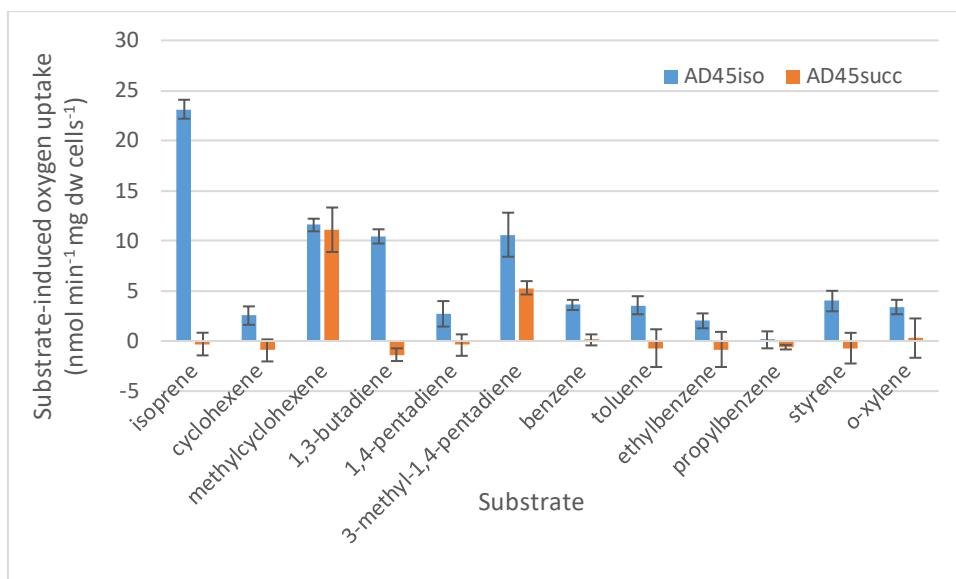


Figure 3.11: The rate of substrate-induced oxygen uptake of whole-cell suspensions of *Rhodococcus* sp. AD45 grown on either isoprene (AD45iso, blue bars) or succinate (AD45succ, orange bars) \pm SEM (n=3). AD45iso cells contain isoprene monooxygenase, whereas AD45succ cells do not and are used as a negative control. Substrates tested are dienes, cyclic alkenes and aromatic compounds, all of which were added at a concentration of 100 μ M.

The high rates of substrate induced oxidation of both methylcyclohexene and 3-methyl-1,4-pentadiene suggests that *Rhodococcus* sp. AD45 may be producing another enzyme which can oxidise these compounds. Again, the cytochrome P450 outlined above could be responsible, as papers have demonstrated the ability of these enzymes to oxidise alkenes in general (Farinas *et al.*, 2004; Funhoff *et al.*, 2007), and more specifically methylcyclohexene (Roiban *et al.*, 2013). In contrast, some of these studies have established that both 1-hexene, styrene and cyclohexene can be utilised by these enzymes (Lindsay Smith and Sleath, 1982), which has not been demonstrated as a capacity the succinate-grown *Rhodococcus* sp. AD45 cells possess here. Methylcyclohexene oxidation could be catalysed by a benzene 1,2-dioxygenase, of which there is an alpha subunit annotated in the *Rhodococcus* sp. AD45 genome under the accession number KJF2944.1. While benzene 1,2-dioxygenase from *Pseudomonas putida* can oxidise 1-methylcyclohexene (Swift *et al.*, 2001), again these enzymes would be expected to work on aromatic compounds, whereas none of those tested here showed significant substrate-induced rate of oxygen uptake in the presence of succinate-grown AD45 cells.

3.4.4. Comparison of *Rhodococcus* sp. AD45 isoprene monooxygenase substrate specificity with that of other isoprene monooxygenases

Using the same techniques used here, the substrate specificity of isoprene monooxygenase in *Variovorax* sp. WS11 has also been characterised (Dawson *et al.*, 2020). In this section, the similarities and differences between the two systems will be presented, as to date these are the only isoprene monooxygenases studied for their substrate specificity. The results are presented as a comparison below (Figure 3.12), with the rates obtained from the succinate-grown cells subtracted from the rates obtained from the isoprene-grown cells in order to directly compare isoprene monooxygenase activity, and rates expressed as a percentage of that the cell suspensions demonstrate for activity on isoprene.

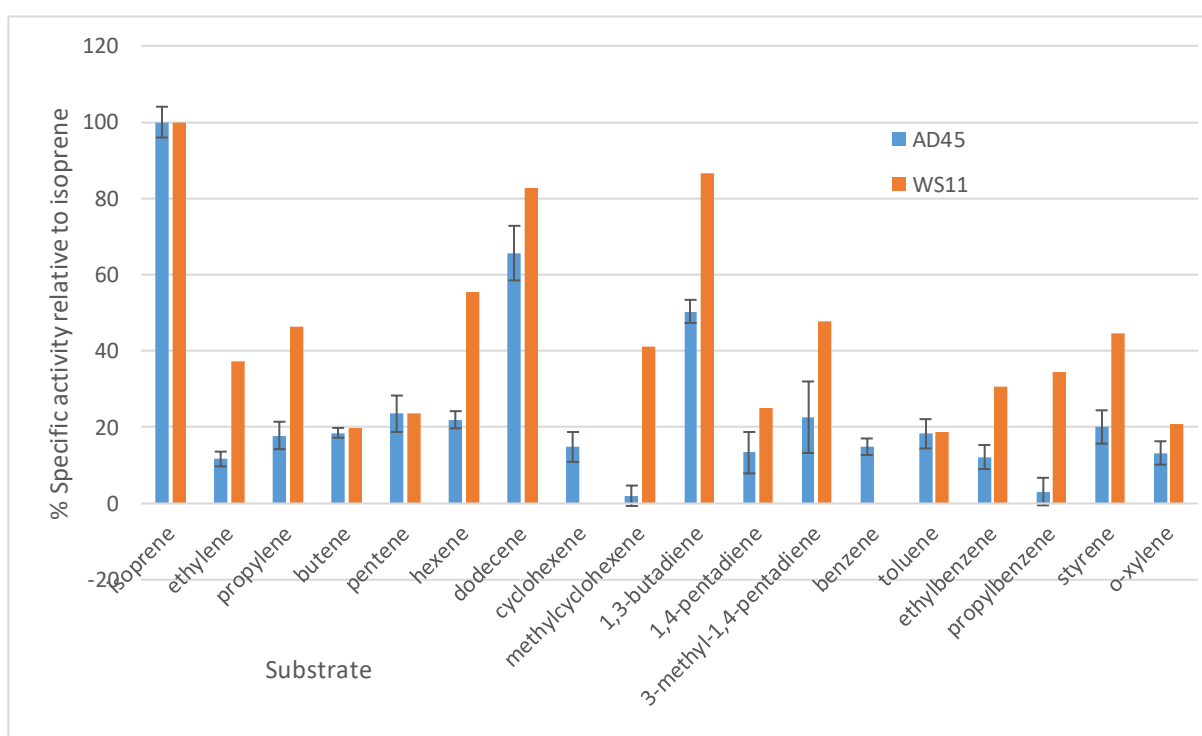


Figure 3.12: Comparison of whole-cell substrate specificity of the isoprene monooxygenase from *Rhodococcus* sp. AD45 and *Variovorax* sp. WS11 (WS11 data provided by R. Dawson, University of East Anglia), shown as a % activity in comparison to the specific activity of the enzymes for isoprene \pm SEM (n=3). Specific activity for *Rhodococcus* sp. AD45 was 23.13 $\text{nmol min}^{-1} \text{mg dw cells}^{-1}$, whereas for *Variovorax* sp. WS11 it was 31.52 $\text{nmol min}^{-1} \text{mg dw cells}^{-1}$.

Whilst the general substrate profile of these two enzymes were similar, there are some key differences. The whole cell suspensions of *Variovorax* did not respond to cyclohexene or benzene as a substrate, whereas *Rhodococcus* sp. AD45 did. The opposite was true for

methylcyclohexene and propylbenzene. In general, it appears that isoprene monooxygenases are capable of oxidising terminal alkenes up to high carbon chain lengths, a range of dienes, cyclic alkenes and aromatics, many of which have important industrial roles.

3.4.5. Comparison of substrate specificity of isoprene monooxygenase in whole-cells of *Rhodococcus* sp. AD45 to that of other SDIMOs

The methods used to study the substrate specificity of other soluble diiron monooxygenases have been diverse, and each method used will be stated when referenced. In general, studies of soluble methane monooxygenase (sMMO) were performed using soluble cell extracts for the assays, as the presence of both soluble and particulate methane monooxygenase in most methanotrophs complicates the use of whole-cells. The rate of isoprene degradation in soluble extract of *Rhodococcus* sp. AD45 is too low for this approach to have been used here, as the low rates would not lend themselves to identifying oxidations of the weaker substrates such as benzene, which may have been completely undetectable in soluble extract assays (more work on the development of isoprene degradation assays using *Rhodococcus* sp. AD45 soluble extract will be presented in Chapter 7). Many studies have been performed on purified proteins, as this clears up any ambiguity over which enzymes could be performing the reactions. Finally, some assays, as here, have been performed with whole cells.

As the most extensively characterised SDIMO, over 50 substrates have been identified for the sMMO from both *Methylococcus capsulatus* (Bath) and *Methylosinus trichosporium* OB3b (reviewed in Jiang *et al.*, 2010, Smith and Dalton, 2004). The original study into sMMO substrate specificity found that the sMMO can oxidise C₁-C₈ alkanes, C₂-C₄ alkenes, dimethyl & diethyl ether, cyclohexane, and a range of aromatic compounds including styrene and toluene using soluble extract and headspace measurements analysed by gas chromatography (Colby *et al.*, 1977). In contrast, the results presented here suggested that the isoprene monooxygenase was capable of oxidising higher chain length alkenes, although it is not capable of oxidising highly stable alkanes.

One study into the microbial oxidation of hydrocarbons demonstrated that the sMMO of *Methylobacterium* sp. strain CRL-26 is capable of oxidising isoprene. Isoprene degradation by soluble extract was approximately one third of that on methane, at 38 nmol min⁻¹ mg protein⁻¹ (Patel *et al.*, 1982), which is still high when compared to the data obtained for the

isoprene monooxygenases in section 3.4.4. This raises an interesting issue in research of microbial degradation of isoprene, as co-oxidation by sMMOs may complicate environmental studies of the level of microbial isoprene oxidation and attributing the effects to different enzyme systems.

The alkene monooxygenase of *Rhodococcus rhodochrous* B-276 was studied using whole cells and found to be capable of utilising C₂ – C₁₈ terminal alkenes as substrates, although N-hexadecane had to be added as a solvent for C₆ – C₉ 1-alkenes (Furuhashi *et al.*, 1986), which was not used here, although the rate is still clearly apparent. The alkene monooxygenase enzyme was also capable of oxidising styrene, as was the isoprene monooxygenases from both *Rhodococcus* sp. AD45 in this study and *Variovorax* sp. WS11 (Dawson *et al.*, 2020).

The substrates of the toluene monooxygenases have also been studied. The toluene 2-monooxygenase of *Burkholderia cepacia* G4 and the toluene 4-monooxygenase of *Pseudomonas mendocina* KR1 were capable of oxidizing 1,3-butadiene, 2-butene, 1-pentene, 2-pentene, 2-chloropropene and 2,3-chloropropene (McClay *et al.*, 2000). The 1,3-butadiene is structurally very similar to isoprene, suggesting that other bacteria may be capable of environmental isoprene oxidation. The oxidation of chlorinated alkenes in the study of toluene monooxygenases was focussed on applications in bioremediation. In this thesis the oxidation of chloroalkenes by *Rhodococcus* sp. AD45 has not been investigated, as this has been done in detail previously (van Hylckama Vlieg *et al.*, 1998). However, it should be noted that these previous studies found that isoprene monooxygenase oxidised a range of chlorinated alkenes including trichloroethylene, a widespread groundwater contaminant.

As the most similar to isoprene monooxygenase in terms of amino acid sequence, it would be expected that the alkene monooxygenase of *Xanthobacter* sp. Py2 would demonstrate a substrate range most similar to isoprene monooxygenase. Research into the whole cell system identified degradation of a range of chlorinated alkenes (Ensign *et al.*, 1992), the relevance of which has been previously mentioned. Characterisation of other isolates, *Xanthobacter* sp. Py2 and *Xanthobacter* sp. Py10, using gas chromatography identified their preferential oxidation of propylene. *Xanthobacter* sp. Py2 also oxidised 1,3-butadiene, 1-pentene, 1-hexene and isoprene (van Ginkel *et al.*, 1986), all of which have now been shown to be substrates for the isoprene monooxygenases from both *Rhodococcus* sp. AD45 (this study) and *Variovorax* sp. WS11 (Dawson *et al.*, 2020). Conversely, *Xanthobacter* sp.

Py10 was only capable of oxidising ethylene, butene and 1,3-butadiene (van Ginkel *et al.*, 1986), which shows variation both from the results presented here and the results for alkene monooxygenase in *Xanthobacter* sp. Py2. A soluble diiron monooxygenase from *Xanthobacter* sp. Py10 has not been identified, so comparisons of homology between the proteins are not possible.

There has not been extensive characterisation of substrate specificities of SDIMOs to compare these results to. The most similar system appears to be *Xanthobacter* sp. Py2 in terms of both which compounds are substrates and the rates of reaction. This is somewhat unsurprising due to the close homology between the active-site containing alpha subunits of alkene monooxygenase and isoprene monooxygenase. The number of substrates tested in other systems has generally been limited, or at least poor or non-substrates have not been published, making comparison difficult.

3.5. Inhibition of isoprene monooxygenase in *Rhodococcus* sp. AD45 by alkynes

3.5.1. Development of an assay to quantify isoprene monooxygenase inhibition by alkynes

The study of SDIMO inhibitors is often used to place their environmental relevance. In the case of isoprene monooxygenase, it may be useful in distinguishing isoprene degraders from opportunistic isoprene co-oxidisers. As previously mentioned, SDIMOs are promiscuous enzymes with wide substrate ranges, particularly sMMOs as these can break the highly stable C-H bonds in methane and many other hydrocarbons, making them one of the most powerful oxidants in nature (Rosenzweig, 2015).

Previously, isoprene degradation by soil samples has been suggested to be due to the presence of methanotrophs, with isoprene depletion attributed to the known co-oxidation by their methane monooxygenases (Patel *et al.*, 1982). Both soluble and particulate methane monooxygenases are inhibited completely by low concentrations of acetylene, which acts as a suicide substrate, irreversibly binding to the active site to incapacitate the enzyme (Prior and Dalton, 1985). The ability to distinguish between these two degradation reactions would allow valuable insight into microbial isoprene consumption.

For the results presented here, alkyne stocks were prepared in a variety of different ways. Terminal alkynes with a carbon chain length between two and four are gaseous, and

various headspace concentrations were prepared in sealed serum vials to be injected into the headspace of the assay vials. Terminal alkynes containing six to eight carbons, however, had to be diluted in DMSO to known concentrations as they are liquid at room temperature. Pentynes could not be assessed as they had the same retention time as isoprene when assaying by gas chromatography. Altering the oven temperature could not rectify this issue so inhibition by pentynes has not been quantified. Previous work on assay optimisation was performed on an Agilent 7890 GC, however this work had to be performed on the 7820 model (section 2.10) as the DMSO is known to interfere with the column fitted to the Agilent 7890.

Initially, the volume of DMSO added to reactions needed to be minimised in order to prevent any inhibition by its addition. The longer-chain alkynes were thus diluted to an adequate concentration where no more than 10 μL of DMSO (equivalent to 0.14 mM) would need to be used. This did not significantly inhibit isoprene monooxygenase activity (Figure 3.13).

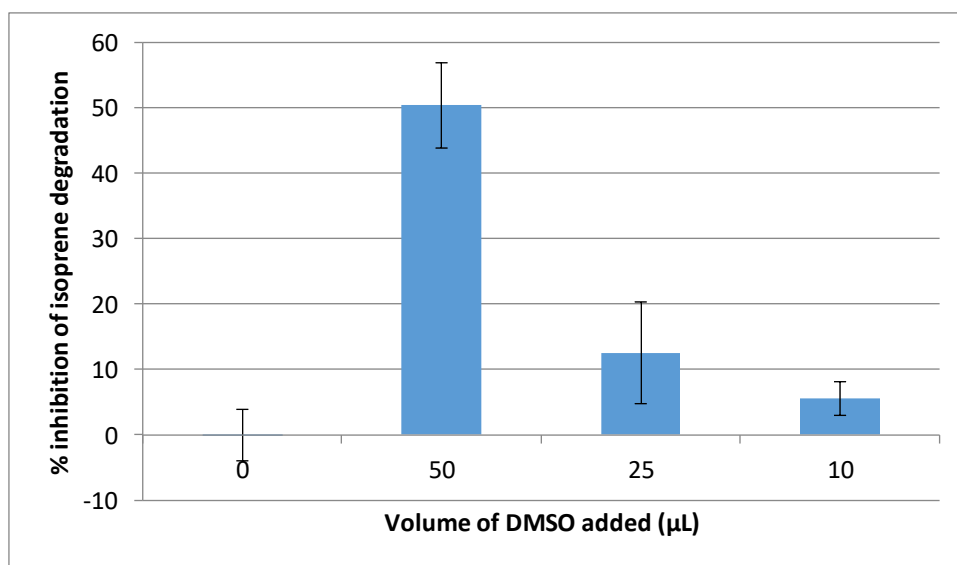


Figure 3.13: Inhibition of isoprene degradation by *Rhodococcus* sp. AD45 by the addition of DMSO \pm SEM (n=3). Volumes of DMSO added are equivalent to the following concentrations: 50 μL = 0.70 mM, 25 μL = 0.35 mM, 10 μL = 0.14 mM.

3.5.2. Inhibition of isoprene monooxygenase in whole cells of *Rhodococcus* sp. AD45 by terminal C₂-C₈ alkynes

Alkyne inhibition of isoprene monooxygenase by a range of terminal alkynes was assessed using gas chromatography (section 2.10). The isoprene degradation protocol outlined previously (section 3.2.1) was used, and alkyne stocks (section 2.10.1) were used to apply

inhibitor after five samples were taken. The following sample was discounted, and a further four samples were taken and analysed. The percentage of inhibition was calculated by comparing the rate after the addition of alkyne to the already isoprene-degrading cell suspension to the rate before it, and normalised to a control where no alkyne was added. The amount of isoprene added was approximately 5 μM , and between 10 and 200 μM of alkyne were used in the inhibition assays, meaning that in all cases, the potential inhibitor was in excess of the substrate (Figure 3.14).

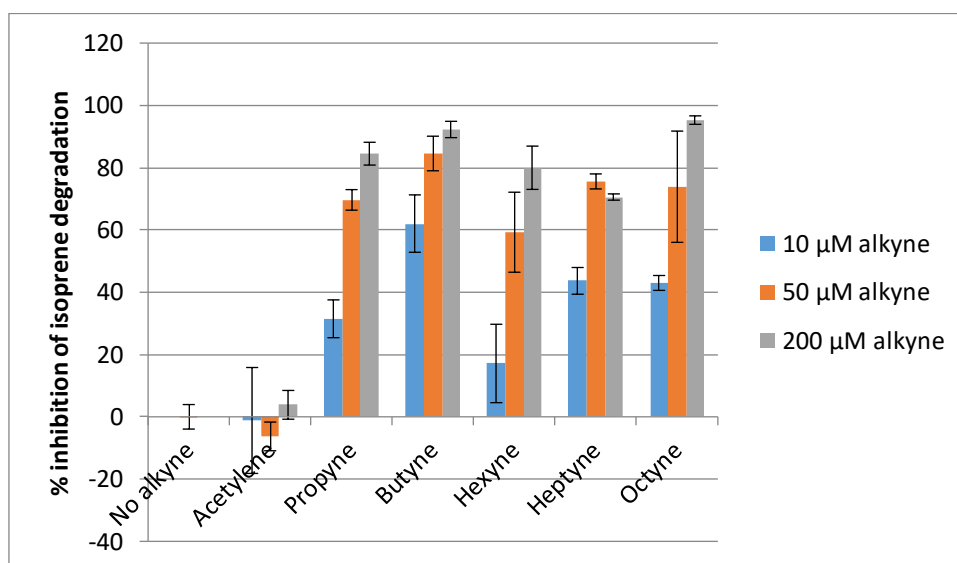


Figure 3.14: Inhibition by alkynes of isoprene degradation by *Rhodococcus* sp. AD45 grown on isoprene (\pm SEM, $n=3$).

Even in the presence of a large molar excess of acetylene, no inhibition of isoprene monooxygenase is observed. All of the other tested alkynes lead to inhibition of the isoprene monooxygenase, however none completely inhibit the enzyme even at the highest concentrations tested, suggesting that they are unlikely to be acting as suicide substrates as acetylene is for sMMO.

3.5.3. Inhibition by alkynes of alkene epoxidation by isoprene monooxygenase in *Rhodococcus* sp. AD45

It is plausible that the level of inhibition by alkynes and rate of epoxidation of alkenes by the isoprene monooxygenase is due to the structure of the active site. Therefore, these rates from sections 3.5.2 and 3.4.2 respectively have been compared in Figure 3.15.

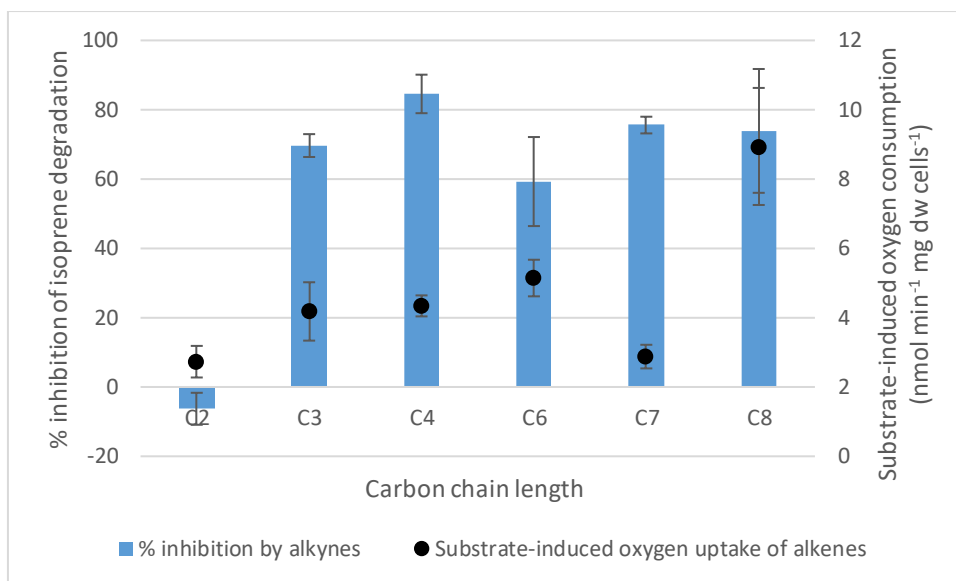


Figure 3.15: Comparison of inhibition of isoprene degradation by whole cells of *Rhodococcus* sp. AD45 grown on isoprene by alkynes against the terminal alkene-induced rate of oxygen consumption of the same cell type (\pm SEM, $n=3$).

There was no observable relationship between inhibition of isoprene monooxygenase of *Rhodococcus* sp. AD45 by alkynes and oxidation rate of alkenes of the same carbon chain length. Of the compounds tested, butene is the closest related to isoprene structurally. Whilst butyne was an effective inhibitor in comparison to the other alkynes tested, butene was not as good a substrate for the enzyme as hexene or octene.

3.5.4. The alkyne inhibition profile of *Rhodococcus* sp. AD45 isoprene monooxygenase compared to other isoprene monooxygenases

As explained in section 3.4.4, the only other partially characterised isoprene monooxygenase is from *Variovorax* sp. WS11 (Dawson *et al.*, 2020). The work on this bacterium was performed by Robin Dawson (Murrell Lab, UEA), as was the comparison to the sMMO-expressing *Methylococcus capsulatus* (Bath) which are presented in comparison to the *Rhodococcus* sp. AD45 data in Figure 3.16. These experiments were all performed in the presence of 50 μ M alkyne, according to the protocol in section 3.5.2.

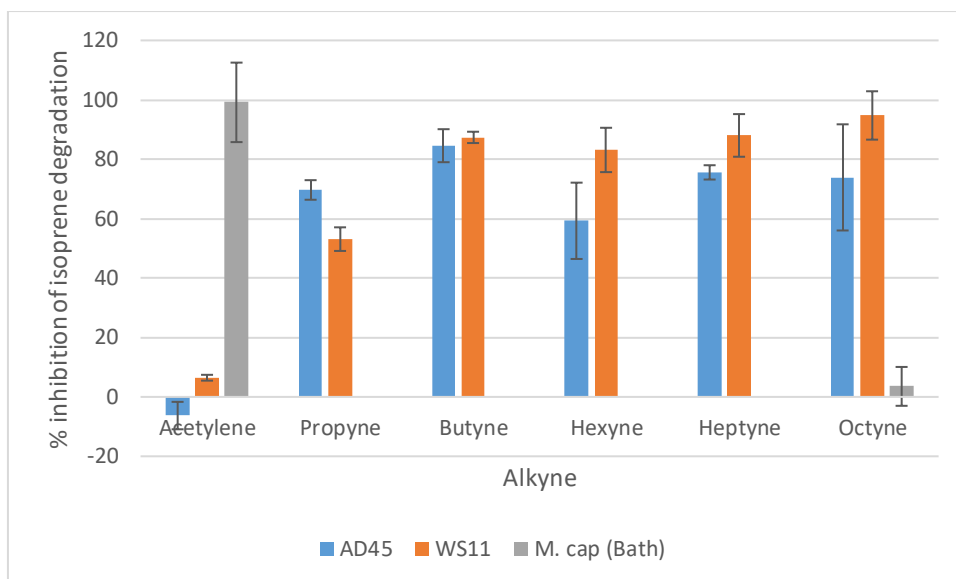


Figure 3.16: Comparison of inhibition of isoprene degradation by whole cells of *Rhodococcus* sp. AD45 and *Variovorax* sp. WS11 (\pm SEM, $n=3$). WS11 and *M. cap* (Bath) data provided by R. Dawson (University of East Anglia).

Generally, inhibition of isoprene monooxygenase in both *Rhodococcus* sp. AD45 and *Variovorax* sp. WS11 was consistent according to the length of terminal alkyne tested. Both showed poor inhibition by acetylene, whereas the sMMO-containing *Methylococcus capsulatus* (Bath) showed complete inhibition of isoprene degradation activity by acetylene. In comparison, a high level of isoprene monooxygenase inhibition for both strains was reported for the addition of octyne, whereas the sMMO was not inhibited by this compound. The potential for inhibitor-based determination of isoprene monooxygenase activity in environmental samples will be explored in the following section.

3.5.5. Inhibition of isoprene monooxygenase by terminal alkynes and comparison with studies on other SDIMOs

Triple-bonded compounds used in metalloenzyme inhibition studies include acetylene, longer chain alkynes and cyanide. Acetylene can inhibit multiple microbial processes, including N_2 fixation, denitrification, nitrification, methanotrophy, methanogenesis, nitrate assimilation and dihydrogen metabolism, which are catalysed by a range of metalloenzymes. These include nitrogenase, which contains both [4Fe-4S] clusters and a FeMo cofactor; hydrogenase, which contains Fe-S clusters and Ni; the copper-containing ammonium monooxygenase, particulate methane monooxygenase and N_2O reductase, the

FeMo containing assimilatory nitrate reductase, and finally the most characterised SDIMO soluble methane monooxygenase (reviewed in Hyman and Arp, 1988).

The inhibition of sMMO by alkynes has been studied on cell lysate systems, as the presence of particulate methane monooxygenase (pMMO) can complicate matters in whole-cell studies. Acetylene inhibits both sMMO and pMMO and acts as a suicide substrate. Acetylene acts as both a substrate and inhibitor (Anthony, 1986), and longer-chain alkynes such as propyne and butyne have been demonstrated to be less potent inhibitors (Dalton and Whittenbury, 1976; Stirling and Dalton, 1977). Where sMMO can catalyse the epoxidations of terminal alkenes, ethylene has been used as a competitive inhibitor of sMMO, which has been used in environmental studies rather than acetylene (Bu *et al.*, 2019). However, whole cells were used over long time periods, so the shorter-term inhibition by acetylene in the growth experiments may be due to its ability to covalently bond with the sMMO. Therefore, as the surviving cells multiplied, the acetylene concentration would decrease and methane oxidation could recover.

The alkene monooxygenase of *Rhodococcus rhodochrous* B276 has also been extensively characterised. In growth experiments with a 5-fold molar excess of propene over the inhibiting alkyne, propyne and butyne were shown to be better inhibitors than acetylene (Fosdike *et al.*, 2005). In studies with partially purified proteins, the presence of 50 % headspace acetylene did not result in any inhibition, whereas 50 % propyne in the headspace caused 70% inhibition (Gallagher *et al.*, 1997), which is a more similar inhibition profile to isoprene monooxygenase from both *Rhodococcus* sp. AD45 and *Variovorax* sp. WS11. Acetylene was found to inhibit alkene monooxygenase activity by 20 % in crude cell extracts of *Rhodococcus rhodochrous* B276 (Miura and Dalton, 1995). Subsequently, in assays containing purified alkene monooxygenase, and preincubated with 5 % v/v acetylene or propyne and NADH, an 80 % inhibition of the alkene monooxygenase from *Rhodococcus rhodochrous* B276 was observed, which was found to be irreversible (Fosdike *et al.*, 2005). This pre-incubation method was not utilised here for the isoprene monooxygenase, which suggests that it may be beneficial to repeat these experiments using preincubation to confirm that the acetylene is not an inhibitor.

Alkynes have also been used to differentiate between mechanisms of toluene oxidation, using various inhibitors at 20 μ M and 30 μ L toluene. For toluene 4-monooxygenase (which is closely related to isoprene monooxygenase) aromatic alkynes with terminal acetylene groups were found to be the most effective inhibitors (Keener *et al.*, 2001). Aromatic

alkynes have not been tested as inhibitors of isoprene monooxygenase, which could make interesting future work to identify more effective inhibitors. It has also been demonstrated that 1-pentyne inhibited growth of *Burkholderia cepacia* G4 (producing toluene 2-monooxygenase) and *Burkholderia pickettii* PKO1 (producing toluene 3-monooxygenase), whereas phenylacetylene was a potent inhibitor of growth of *Pseudomonas mendocina* KR1 (producing toluene 4-monooxygenase). Whole-cell growth studies were used to distinguish between the toluene degradation pathways in environmental samples where it was found that toluene monooxygenase catalysed the initial step in toluene metabolism (Keener *et al.*, 2001).

Alkyne inhibition of toluene 2-monooxygenase in *Burkholderia cepacia* G4 by alkynes has also been studied in the whole-cell system using an oxygen electrode. Only 25 % of toluene oxidation activity was found to be retained after treating with acetylene, and less activity was retained when cells were treated with butyne or 1-2- or 3-hexyne. In growth experiments, high concentrations of acetylene (10 - 50 % v/v) were required to inhibit growth on toluene, however only 1 % v/v headspace concentrations of both propyne and butyne completely halted growth on toluene. Longer chain alkynes were also found to be potent inhibitors, and non-terminal alkynes were more efficient inhibitors than the 1-alkyne counterparts (Yeager *et al.*, 1999). In contrast, isoprene monooxygenase in both *Rhodococcus* sp. AD45 and *Variovorax* sp. WS11 have been effectively inhibited by all tested alkynes except for acetylene and there is no clear link between carbon chain length and level of inhibition. Non-terminal alkynes have not been tested, but may offer a potential for suicide substrate discovery to aid in differentiation of SDIMO and isoprene monooxygenase activity in environmental samples.

Limited inhibition studies have been carried out on other SDIMOs. Most notably, the alkene monooxygenase from *Mycobacterium* has been shown to be inhibited by over 85 % the presence of 5 % v/v acetylene in cell free extract assays, however other alkynes were not studied (Hartmans *et al.*, 1991). Conversely, the alkene monooxygenase from *Xanthobacter* sp. Py2 is not inhibited by acetylene, and propyne was used as an effective inhibitor instead, though the level of inhibition was not quantified and other alkynes were not tested (Ensign *et al.*, 1992).

Overall, whilst addition of acetylene to environmental samples may be able to eliminate co-oxidation of isoprene by sMMO and pMMO, in addition to some other SDIMOs such as the alkene monooxygenase from *Mycobacterium*, many other SDIMOs are not inhibited by

acetylene yet can still co-oxidise isoprene. To date, a single selective suicide substrate of isoprene monooxygenase has not been found, however future work testing the purified enzyme when pre-incubated with potential inhibitors, and looking into aromatic alkynes, non-terminal alkynes or methylated alkynes may be fruitful.

3.6. Conclusions

In this chapter, the development of an optimised assay for isoprene degradation by cell suspensions of *Rhodococcus* sp. AD45 has been outlined. Whole-cell kinetics of the enzyme have been presented and discussed, and compared to those calculated for the closely related alkene monooxygenase enzyme found in *Xanthobacter* sp. Py2. Isoprene monooxygenase has been demonstrated as capable of oxidising a range of substrates, including terminal alkenes, dienes, aromatics and cyclohexene. Whilst no specific alkyne inhibitor has been identified, the ability to exclude the contribution of sMMO co-oxidation of isoprene in environmental studies using acetylene has been established.

In the following chapters, the focus will move to purifying and characterising the components of isoprene monooxygenase, starting with the Rieske-type ferredoxin.

4. Purification and characterisation of IsoC: The Rieske protein component of isoprene monooxygenase from *Rhodococcus* sp. AD45

4.1. Introduction

In this chapter, results of the purification and characterisation of the 12.8 kDa Rieske protein component of isoprene monooxygenase from *Rhodococcus* sp. AD45, termed IsoC, are presented. The Rieske protein is the additional component found in four-component soluble diiron monooxygenases as opposed to three-component systems. This Rieske-protein component is used to shuttle electrons from the reductase to the oxygenase via the [2Fe-2S] Rieske-type cluster cofactor.

The 345 base pair gene encoding IsoC was cloned into a vector for N-terminally His-tagged IsoC production in the homologous expression strain *Rhodococcus* sp. AD45-ID. The expression vector used was pTipQC1, developed to allow expression of proteins which often form inclusion bodies in *Escherichia coli* to be expressed in a soluble form in *Rhodococcus erythropolis* (Nakashima and Tamura, 2004a). IsoC was also purified from *Rhodococcus* sp. AD45-ID containing the pTipQC2S2:*IsoEx* expression vector which produces the full isoprene monooxygenase system with a StreptII-tagged IsoA, the alpha subunit of the oxygenase component.

The purified His-tagged IsoC protein was characterised by a range of spectroscopic and mass spectrometric techniques to establish the presence of the predicated cofactor. The cofactor was also examined to determine whether the redox cycling capability was maintained, to establish the midpoint potential and compare this to existing studies of soluble diiron monooxygenase Rieske components.

Finally, this midpoint potential was compared between the tagged and untagged IsoC preparations in order to establish whether the tag would impact the ability of IsoC to perform the electron transfer role it would be required for in reconstitution experiments.

4.2. Cloning *isoC* from *Rhodococcus* sp. AD45 into the pTipQC1 plasmid for expression in *Rhodococcus* sp. AD45-ID

The *isoC* gene was amplified from *Rhodococcus* sp. AD45 genomic DNA using PCR with a Q5 high-fidelity DNA polymerase (section 2.5.2). The *Rhodococcus* sp. AD45 genomic DNA was a gift from Andrew Crombie (Murrell group, University of East Anglia). The primers used for polymerase chain reaction amplification of *isoC* are outlined in Table 4.1. All cloning was performed in *Escherichia coli* TOP10 cells.

Table 4.1: Primer sequences used for polymerase chain reaction amplification of *isoC* from *Rhodococcus* sp. AD45 genomic DNA and cloning into expression vectors.

| Primer Name | Sequence | Restriction Site | Orientation |
|-------------|---------------------------------|------------------|-------------|
| isoCF | ATATATCATATGGCTGACGGTCAGGACA | <i>NdeI</i> | Forward |
| isoCR | ATATATGGATCCTACTTTCAGTGTTGCGCCT | <i>BamHI</i> | Reverse |

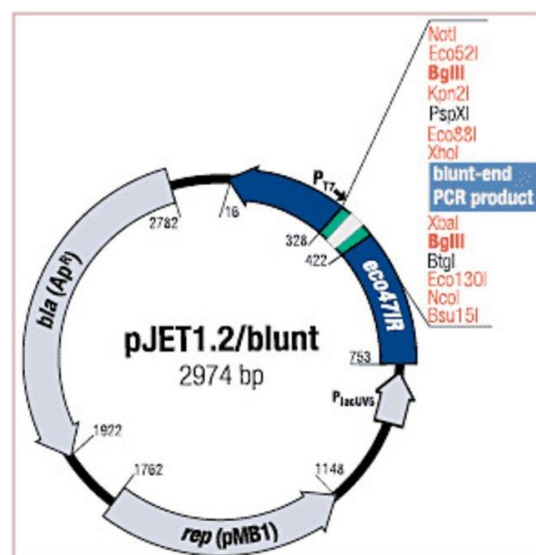


Figure 4.1: pJET1.2/blunt cloning system (image taken from <https://www.thermofisher.com/order/catalog/product/K1231#/K1231>, ThermoFisher Scientific).

The PCR product was cleaned according to section 2.5.3 in order to remove any remaining primers and unused nucleotides. The prepared PCR product was then cloned into pJET1.2/blunt (section 2.5.3) (Figure 4.1) and used to transform *Escherichia coli* TOP10 chemically competent cells (section 2.3.2). Colony PCR was performed (section 2.5.2) on colonies which grew on an LB agar plate containing ampicillin (section 2.3) using the same primers used for cloning (Table 2.1) (section 2.5.2) to determine the presence of the *isoC* insertion. The corresponding successful transformants were used to prepare plasmid stocks, designated pJET1.2:*isoC* (section 2.4.1). The *isoC* gene was removed from the pJET1.2:*isoC* construct by restriction digest with *Nde*I and *Bam*HI, and the pTipQC1 vector was linearized by restriction enzyme digest with the same restriction enzymes (section 2.5.4). The linearized vector was dephosphorylated (section 2.5.5), and both digested vector and insert were run using agarose gel electrophoresis (section 2.5.9). These were then extracted using the Macherey-Nagel gel extraction kit (section 2.5.6), followed by ligation with T4 DNA ligase (section 2.5.7). The ligation mixture was used to transform *Escherichia coli* TOP10 cells (section 2.3.2), which were plated on LB agar plates containing ampicillin (section 2.3)

The pTipQC1 expression system used was developed for protein expression in *Rhodococcus erythropolis* to minimise issues with insolubility in heterologous protein expression (Nakashima and Tamura, 2004a). The pTip series of expression vectors all contain thiostrepton and chloramphenicol resistance genes for *Rhodococcus*, and an ampicillin resistance gene for vector preparation in *Escherichia coli*. The promoter used is *tipA*, so protein production is induced by the addition of thiostrepton (Figure 4.2A). By cloning *isoC* into the *Nde*I and *Bam*HI sites of the multiple cloning site (MCS) of pTipQC1, an N-terminal 6-Histidine tag was introduced. The stop codon was maintained directly before the *Bam*HI site, so no C-terminal 6-Histidine tag was introduced (Figure 4.2B).

The full pTipQC1:*isoC* expression plasmid (Figure 4.3) was extracted from *Escherichia coli* TOP10 cells according to section 2.4.1, followed by ratification of the construct by sequencing (section 2.5.8). Electrocompetent *Rhodococcus* sp. AD45-ID cells were prepared, and the verified construct was used to transform them by electroporation (section 2.3.4), followed by plating on AD45 minimal media agar plates (section 2.3.3) containing 10 mM succinate and chloramphenicol.

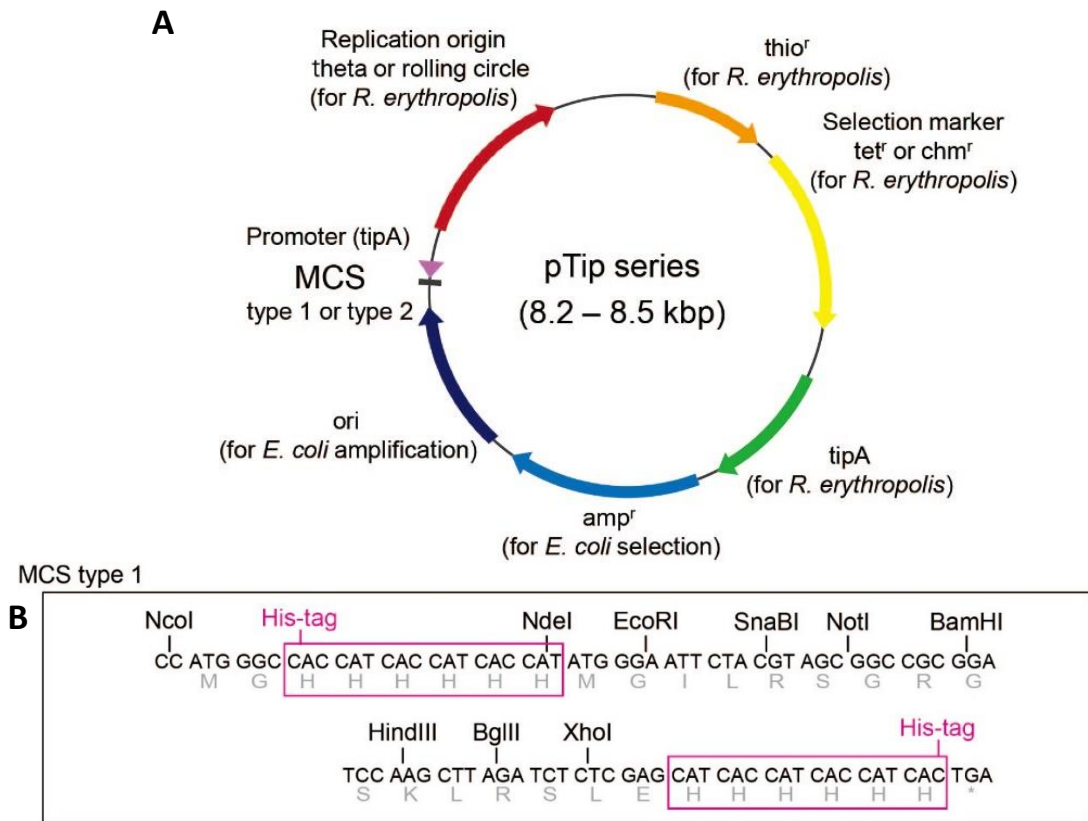


Figure 4.2: pTip expression system for protein production in *Rhodococcus* sp. AD45-ID. A) pTip series vector map. B) Multiple cloning site of Type 1 pTip vectors. (Images taken from https://www.hssnet.co.jp/e/2/2_7_22.html).

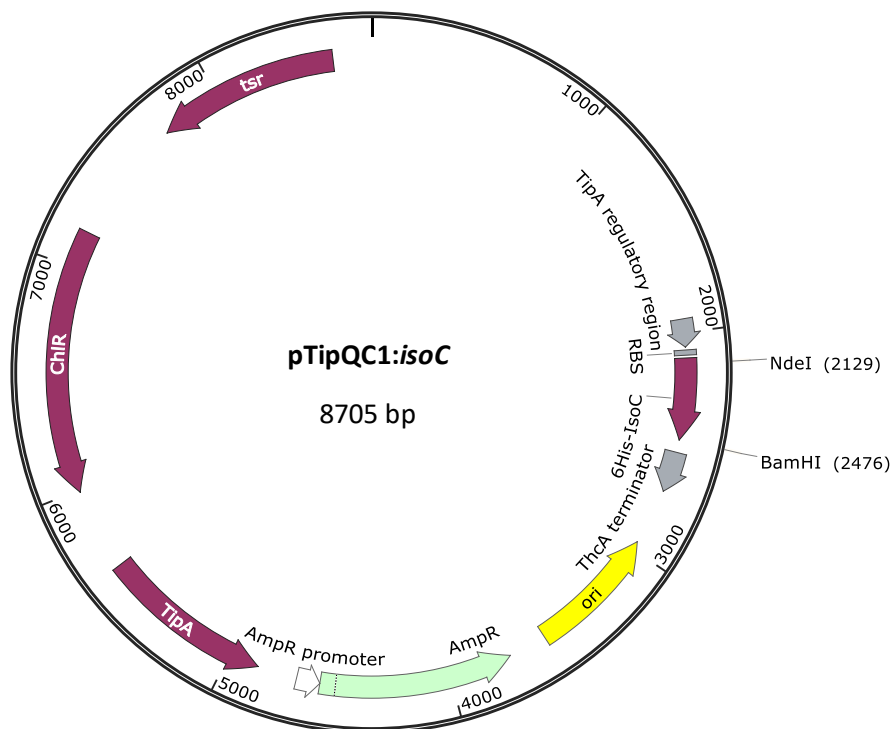


Figure 4.3: pTipQC1:isoC vector map.

4.3. Production of IsoC in the *Rhodococcus* sp. AD45-ID homologous expression system

Rhodococcus sp. AD45-ID cells containing the pTipQC1:*isoC* plasmid were grown in batch culture (section 2.3.3) to check whether the IsoC protein was being produced. The culture was grown until the OD₅₄₀ reached ~0.6, followed by induction with 1 µg mL⁻¹ thiostrepton. The cultures were then incubated at 25 °C overnight, harvested the following morning (section 2.6), and the cell lysate prepared (section 2.7). The His-tagged IsoC protein was predicted to be 13.78 kDa, however SDS-PAGE analysis of cell lysate demonstrated that a peptide band associated with induction with thiostrepton was apparently slightly larger than the 15 kDa protein ladder marker (Figure 4.4). This anomalous migration has been recorded during purification of the Rieske protein component of toluene 4-monooxygenase, termed T4moC (Whited and Gibson, 1991; Yen *et al.*, 1991; Pikus *et al.*, 1996), and the Rieske protein component of alkene monooxygenase from *Xanthobacter* sp. Py2, termed XamoC (Champreda *et al.*, 2004).

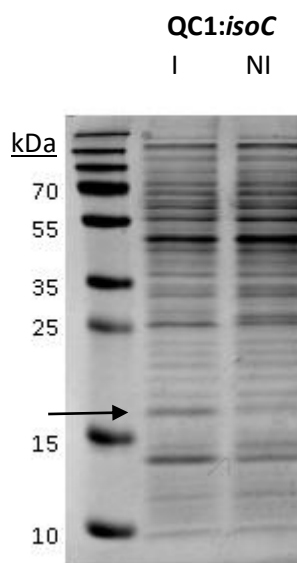


Figure 4.4: Polypeptide profiles of *Rhodococcus* sp. AD45-ID expressing pTipQC1:*isoC* as determined by SDS-PAGE gel electrophoresis. AD45-ID cultures were either non-induced (NI) or induced with 1 µg mL⁻¹ thiostrepton (I) to produce the IsoC protein, which has been indicated with an arrow.

To check whether this band was the His-tagged IsoC, the soluble extract from a 50 mL grow-up (section 2.7) was passed down a HisTrap spin-column (GE Life Sciences) according to manufacturer's instructions. SDS-PAGE analysis of the cell lysate, flow through, wash and

elution steps of the spin-column purification proved that the expected band was present in the elution (Figure 4.5), suggesting that it was the correct protein and could be carried forwards.

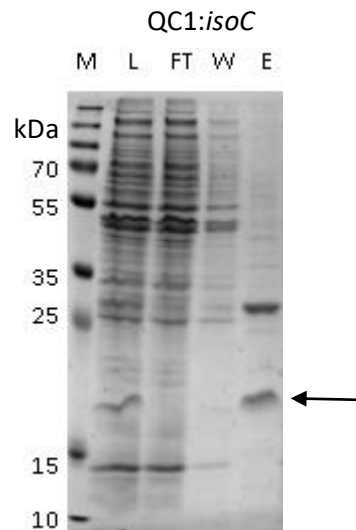


Figure 4.5: Polypeptide profiles of IsoC purification by 1 ml HisTrap spin-columns. CL is cell lysate, FT is the flow through, W is the wash and E is the elution. The IsoC bands have been highlighted by an arrow.

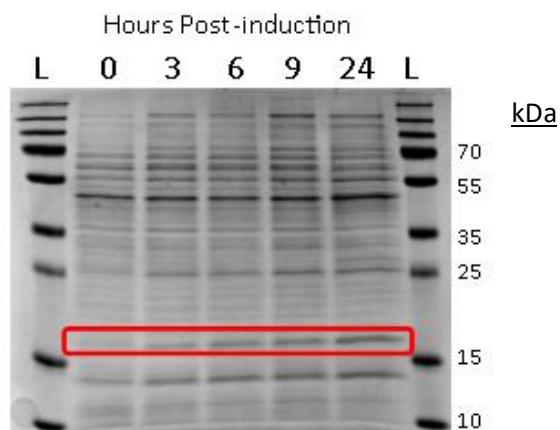


Figure 4.6: Polypeptide profiles of *Rhodococcus* sp. AD45-ID expressing pTipQC1:isoC as determined by SDS-PAGE gel electrophoresis. The number of hours after induction with $1 \mu\text{g ml}^{-1}$ thioestrepton has been labelled and the band corresponding to the IsoC polypeptide has been highlighted with a box.

Production of IsoC after induction of the expression strain (as outlined above) was monitored over 24 hours (Figure 4.6). The protein was not produced in higher amounts after being left for a full 24 hours, suggesting that the low amount of protein observed in

the SDS-PAGE gels was not due to the protein being produced and then degraded within the cells over this time frame. Due to this, subsequent expression was maintained with cell harvest after 16 h incubation with $1 \mu\text{g mL}^{-1}$ thiostrepton.

In order to optimise [2Fe-2S] cluster incorporation, supplementation with additional iron and sulfur with or without cold-shock was tested. Once the cultures had reached an OD_{540} of ~ 0.6 , they were placed on ice for 20 min. After this, they were supplemented with $100 \mu\text{M}$ ferric ammonium citrate, $25 \mu\text{M}$ L-methionine and $25 \mu\text{M}$ L-cysteine, followed by incubation at 25°C overnight before harvesting (section 2.6) and preparing soluble extract (section 2.7). After running the soluble extract through the HisTrap spin-columns (as outlined above), the absorbance spectra were measured (section 2.12.1) (Figure 4.7), and the ratio between A_{280} and A_{454} compared. The A_{280} measurement measures protein concentration whereas A_{454} measures the presence of the [2Fe-2S] cluster, and has been used in characterisation of the Rieske protein from the alkene monooxygenase of *Xanthobacter* sp. Py2 (Small and Ensign, 1997).

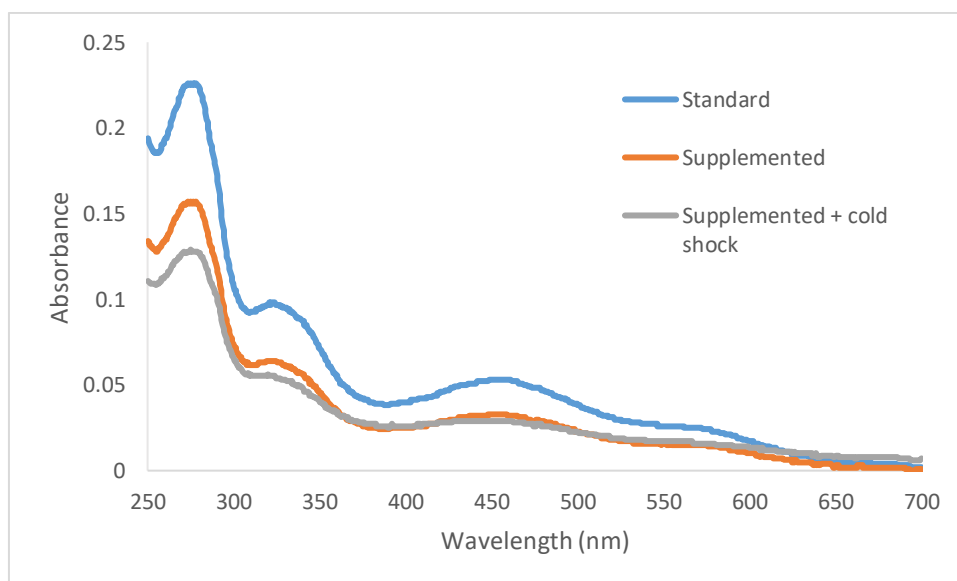


Figure 4.7: Absorbance spectroscopy of partially purified IsoC from *Rhodococcus* sp. AD45-ID expressing pTipQC1:isoC. The blue line shows the spectrum of the sample where the culture was grown and induced as normal. The culture producing sample 2 (orange line) was supplemented with additional iron and sulfur, and the culture producing sample 3 (grey line) was both supplemented as for culture 2 and exposed to a 20 minute cold shock on ice.

The ratio of $A_{280}:A_{454}$ for IsoC prepared using the standard expression protocol was 0.24. The addition of exogenous iron in the form of ferric ammonium citrate and sulfur in the

form of L-methionine slightly reduced the ratio of cluster-loaded protein ($A_{280}:A_{454} = 0.21$), and supplementation with the cold-shock step did not considerably increase cluster incorporation ($A_{280}:A_{454} = 0.25$). This ratio is similar to other characterised Rieske cluster-containing proteins, including that from *Thermus thermophilus* (Fee *et al.*, 1984), the Rieske component of toluene/*o*-xylene monooxygenase (Cafaro *et al.*, 2002) and that of toluene 4-monooxygenase (Xia *et al.*, 1999). Having optimised the protein production, batches of 6 x 1 L cultures of *Rhodococcus* sp. AD45-ID containing the pTipQC1:*isoC* expression vector were grown according to section 4.3 for purification of larger volumes of protein for characterisation.

4.4. Purification of IsoC from *Rhodococcus* sp. AD45-ID containing pTipQC1:*isoC*

The purification protocol for IsoC from *Rhodococcus* sp. AD45-ID containing pTipQC1:*isoC* was developed with both benchtop and HPLC purification using an AKTApure. Purification protocols were developed both for the His-tagged and untagged proteins, with the untagged protein being expressed in the *Rhodococcus* sp. AD45-ID homologous system but utilising the pTipQC2S2 expression system. The protocol for purification of the untagged IsoC was developed by Colin Lockwood (Murrell group, University of East Anglia) and will be outlined in section 4.7.2.

4.4.1. Partial purification of IsoC by immobilised metal affinity chromatography

The first step of his-tagged IsoC purification utilised a 5 ml immobilised metal affinity chromatography (IMAC) column; a Nickel containing column sold under the HisTrap brand by GE Life Sciences.

In all cases the same purification buffers were used. The binding buffer for the IMAC column was 50 mM sodium phosphate and 40 mM imidazole at pH 7.4, and the elution buffer contained 50 mM sodium phosphate and 500 mM imidazole at pH 7.4.

Initial purification attempts utilised benchtop methods with a Luer syringe and varying concentrations of imidazole by altering the ratio of binding and elution buffers in a stepped elution (Figure 4.8).

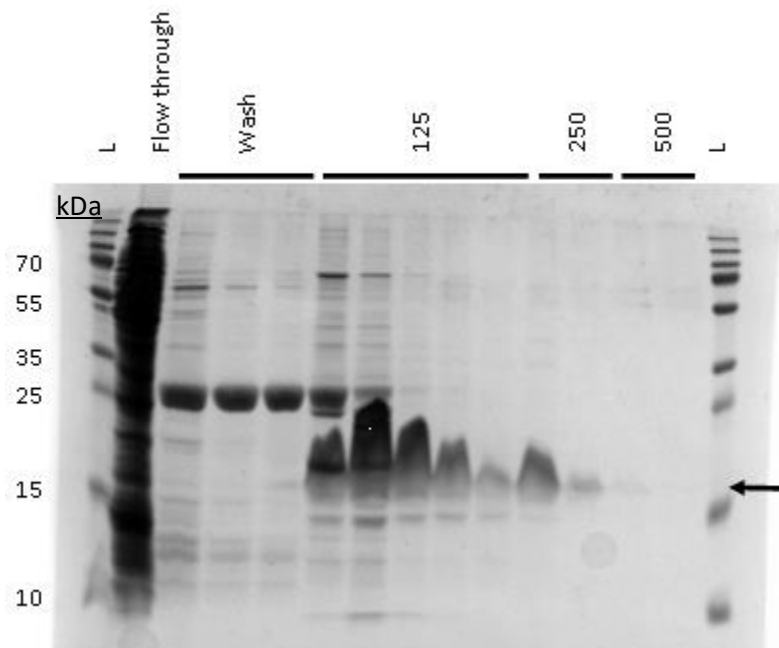


Figure 4.8: Purification of IsoC using a 5 ml HisTrap column and a stepped benchtop elution as demonstrated by SDS-PAGE gel electrophoresis. The concentration of imidazole used in each elution step is presented above the relevant lanes and given as mM concentrations. Polypeptide bands corresponding to IsoC have been highlighted by an arrow.

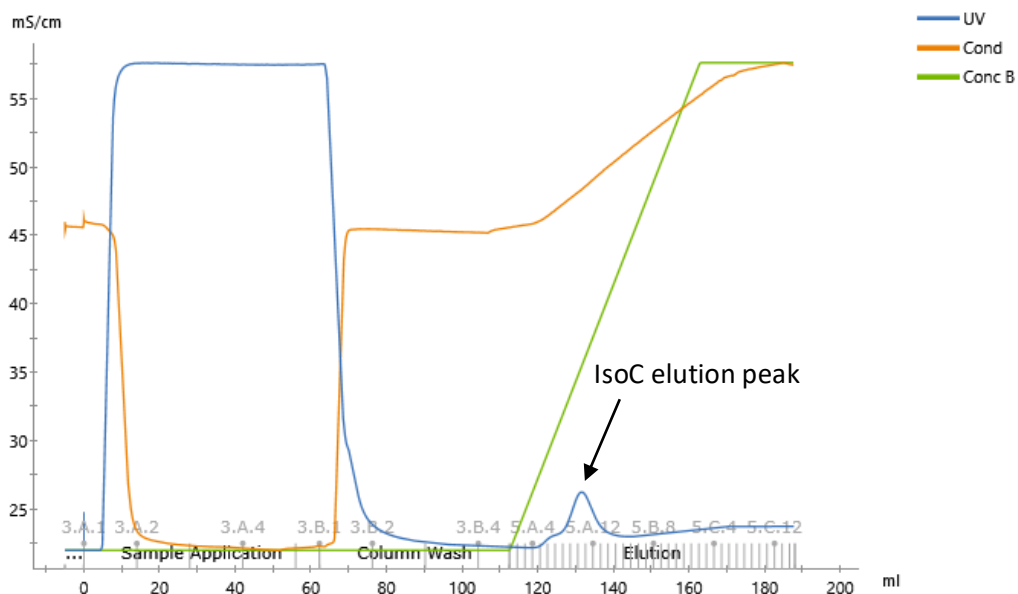


Figure 4.9: HPLC trace of a gradient elution of IsoC on a 5 mL HisTrap column using an AKTApure HPLC system. The concentration of the imidazole in the elution buffer (green line) varies from 40 – 500 mM (0 – 100 % buffer B) over the gradient.

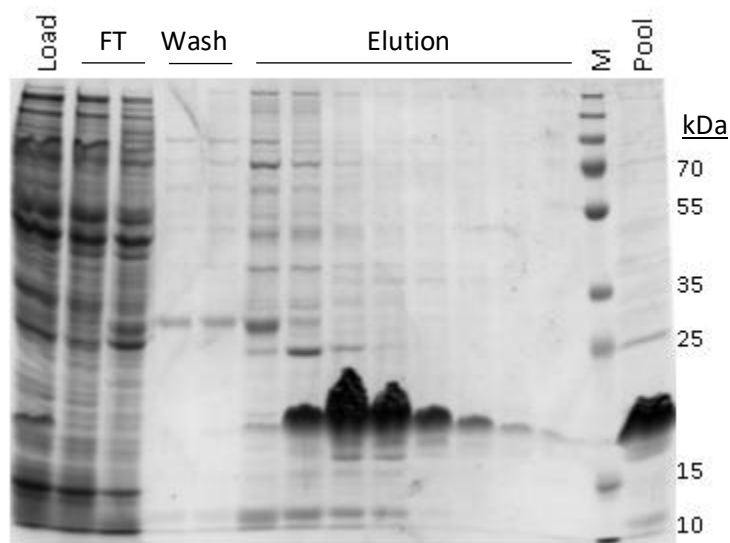


Figure 4.10: Purification of IsoC using a 5 mL HisTrap column and a gradient elution from 40 – 500 mM imidazole over 50 mL using an AKTApure HPLC system. Polypeptide profiles of fractions from the purification process were visualised using SDS-PAGE gel electrophoresis and InstantBlue staining.

A purification protocol was also developed using the AKTApure HPLC system using UNICORN™ 7 software. This protocol used the same binding and elution buffers, however the elution was performed using a linear gradient over 50 mL (10 column volumes). The elution profile is shown in Figure 4.9. This purification of IsoC was assessed by SDS-PAGE and demonstrated that the single IMAC column resulted in mostly pure protein (Figure 4.10). The most concentrated fractions were pooled and concentrated to 2 mL. These fractions were brown due to the presence of the [2Fe-2S] Rieske-type cluster, which made identification and pooling of samples clearer.

4.4.2. Purification of IsoC from *Rhodococcus* sp. AD45 by gel filtration chromatography

The pooled IsoC samples from the IMAC purification protocol were concentrated to 2 mL and dialysed overnight into the gel filtration buffer, which contained 150 mM sodium phosphate and 300 mM NaCl. The concentrated protein sample was applied to an equilibrated Superdex 26/600 200 µg column supplied by GE life sciences and run at 1.5 mL min⁻¹. The AKTA trace is shown in Figure 4.11.

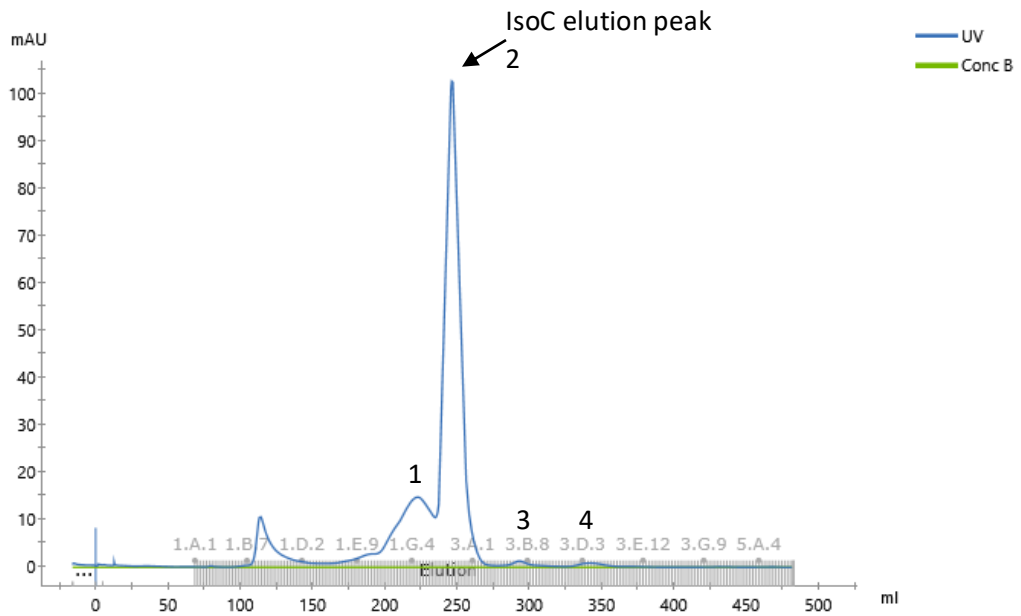


Figure 4.11: Trace from AKTApure HPLC system showing IsoC purification using gel filtration chromatography. The peak which corresponds to IsoC has been highlighted with an arrow. Elution peaks checked by SDS-PAGE gel are numbered 1-4.

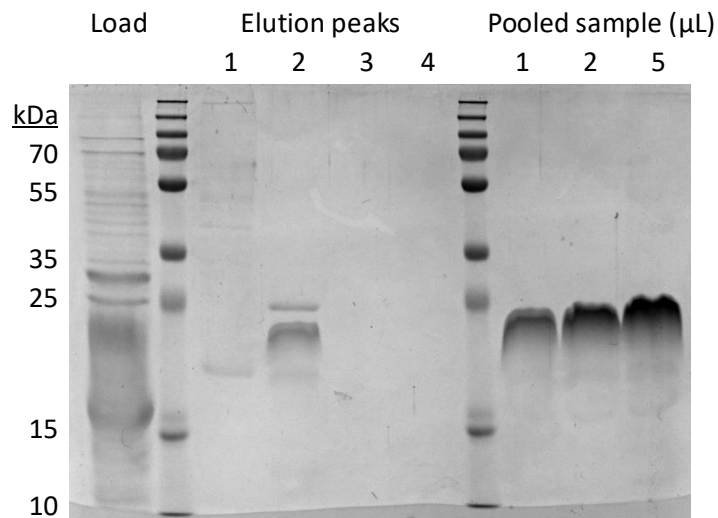


Figure 4.12: Polypeptide profiles of fractions from the final gel filtration purification step to obtain pure IsoC. The three lanes on the far-right show fully purified and concentrated IsoC samples.

Samples from the peaks highlighted by arrows in the AKTA trace in Figure 4.11 were examined by SDS-PAGE analysis, which showed that the largest peak contained a large amount of IsoC, which ran as a smear on the gel due to the high concentration. The brown fractions corresponding to the fractions in the high peak of the gel filtration AKTA trace

were pooled and concentrated to 1.25 ml, and measured to be 2 mg mL⁻¹ using a Bradford assay (section 2.7.1), suggesting a concentration of 145 µM. Varying amounts of the protein were run on the SDS-PAGE gel to demonstrate that the resulting IsoC sample was pure. The protein stock was then flash-frozen in 150 µL aliquots using liquid nitrogen.

4.5. Spectroscopic characterisation of purified IsoC from *Rhodococcus* sp. AD45

Various methods were available to examine the spectroscopic characteristics of the purified IsoC protein samples, including absorbance, circular dichroism and electron paramagnetic resonance spectroscopy. All of these techniques can assess the presence of protein cofactors, such as the Rieske-type [2Fe-2S] cluster predicted to be present in IsoC.

4.5.1. Absorbance spectra of oxidised and reduced IsoC from *Rhodococcus* sp. AD45

The absorbance spectrum of IsoC was recorded aerobically (section 2.12.1). The sample was assessed by diluting in a 2 mL quartz cuvette and measuring the absorbance of the sample over wavelengths between 300 and 700 nm. The sample was then reduced by the addition of sodium dithionite, and the spectrum analysed again (Figure 4.13).

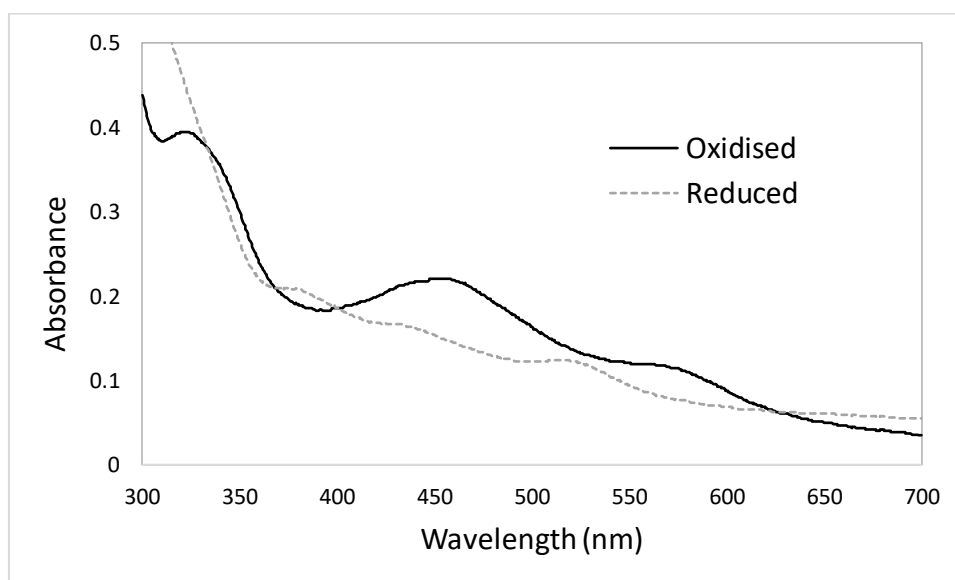


Figure 4.13: Absorbance spectra of purified N-terminally 6His-Tagged IsoC as purified (oxidised, black solid line) and reduced by an excess of sodium dithionite (grey dotted line) between 300 and 700 nm.

The absorbance spectrum of the protein showed maxima at 323 and 454 nm, with a shoulder at 575 nm. The reduced form of the protein had a profile with absorbance maxima at 382, 431 and 515 nm. These characteristics suggested that the protein contained a Rieske-type [2Fe-2S] cluster. After being exposed to air for approximately 10 minutes, the absorbance spectrum was further assessed and had returned to the oxidised spectrum, and could also be reduced by further addition of sodium dithionite (results not shown). This demonstrates that the cluster is highly stable in an aerobic environment and the His-tag has not impacted the ability of the protein to redox cycle.

The absorbance of a purified toluene 4-monooxygenase Rieske protein at 328 and 456 nm was demonstrated to reduce by 50 % after reduction with dithionite (Pikus *et al.*, 1996). The difference between oxidised and reduced IsoC was not so severe, only accounting for approximately a 30 % drop in absorbance at 454 nm, and a slight increase in absorbance at 323 nm, though this is likely to be due to the high absorbance associated with the excess of dithionite. The absorbance spectrum of both oxidised and reduced IsoC was highly similar to that of other Rieske proteins, including from the four-component SDIMOs alkene monooxygenase from *Xanthobacter* sp. Py2 (XamoC) (Small and Ensign, 1997), toluene 4-monooxygenase from *Pseudomonas mendocina* KR1 (T4moC) (Pikus *et al.*, 1996), and toluene/*o*-xylene monooxygenase from *Pseudomonas stutzeri* OX1 (TomoC) (Cafaro *et al.*, 2002). More generally, the presence of maxima at around 460 and 575 nm with a shoulder at around 315 nm in the oxidised spectra and maxima at 380, 420 and 515 in the reduced spectra have been found to be characteristic of Rieske proteins (Rieske *et al.*, 1964). Spectroscopically characterised proteins containing Rieske-type [2Fe-2S] clusters which show this characteristic spectrum include the *bc*₁ complex from bovine heart mitochondria, benzene dioxygenase from *Pseudomonas putida* ML2 (Link *et al.*, 1996), phthalate oxygenase from *Pseudomonas cepacia* (Batie *et al.*, 1987) and sulredoxin from the archaeon *Sulfobolus* sp. strain 7 (Iwasaki *et al.*, 1995).

4.5.2. Circular dichroism spectroscopy of purified IsoC from *Rhodococcus* sp. AD45
The circular dichroism spectroscopic analysis of IsoC was performed anaerobically. The sample was prepared in an anaerobic glovebox by purging with nitrogen followed by dilution with nitrogen-purged buffer to approximately 30 µM. The reduced spectrum was measured using a JASCO model J810 circular dichrograph, and the sample was then

oxidised by the addition of an excess of potassium ferricyanide in the anaerobic glovebox. The CD spectrum of the oxidised sample was then recorded (Figure 4.14A).

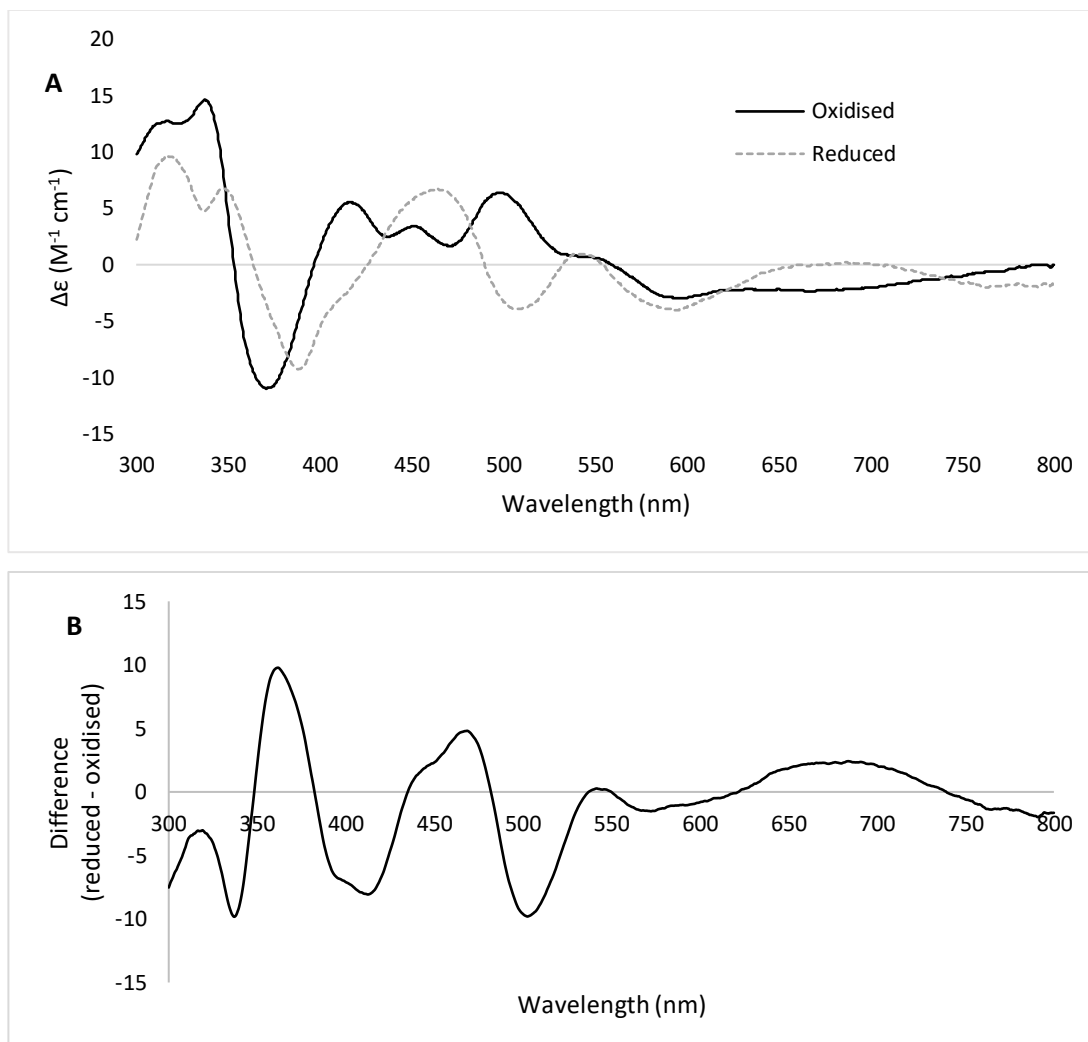


Figure 4.14: A: Circular dichroism spectra of oxidised (black solid line) and reduced (grey dotted line) purified IsoC with an N-terminal 6His-tag. B: The difference between the CD spectra of oxidised and reduced IsoC.

The sample was also re-reduced by the addition of an excess of sodium dithionite (results not shown), demonstrating further stability of the protein and cofactor in anaerobic conditions. The oxidised IsoC sample showed maxima at 315, 337, 416, 451 and 498 nm, and minima at 370, 436, 471 and 595 nm; whereas the reduced IsoC sample had maxima at 318, 347, 464, 542 and 680 nm, and minima at 336, 389, 509 and 594 nm. These CD spectra profiles of oxidised and reduced IsoC showed similar characteristics to the Rieske protein of alkene monooxygenase from *Xanthobacter* sp. Py2 (Small and Ensign, 1997), as well as

other Rieske cluster containing proteins such as the phthalate oxygenase from *Pseudomonas cepacia* (Batie et al., 1987), the sulredoxin from the archaeon *Sulfolobus* sp. strain 7 (Iwasaki et al., 1995), the Rieske protein from *Thermus thermophilus*, and the bc_1 complex from bovine heart mitochondria and benzene dioxygenase from *Pseudomonas putida* ML2 (Link et al., 1996). The most noted characteristic of Rieske cluster containing proteins is the appearance of a strong negative band which appears at 500 nm upon reduction. The similarities between Rieske proteins in CD spectroscopy have been described as most obvious in the reduced-oxidised difference spectra, where minima were observed at 340, 390-410 and 500 nm, whereas a maximum was present at 365-370 nm (Link et al., 1996), which were all apparent in the IsoC difference spectrum (Figure 4.14B).

4.5.3. Electron paramagnetic resonance spectroscopy of IsoC from *Rhodococcus* sp. AD45

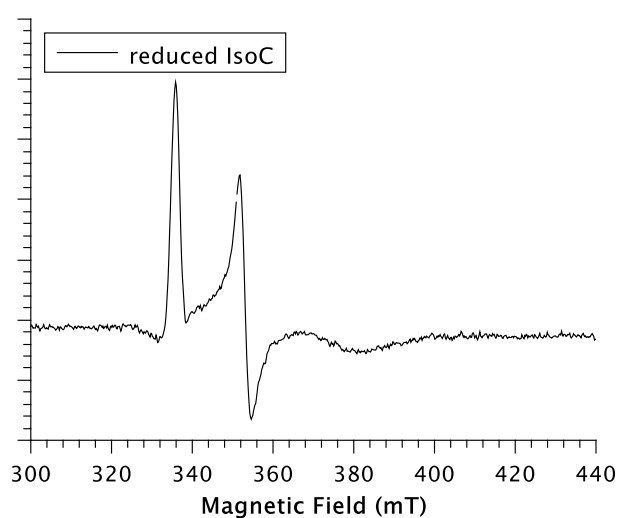


Figure 4.15: EPR spectrum of reduced IsoC.

During preparation of samples for CD spectroscopy, samples of IsoC were removed and snap-frozen in liquid nitrogen for EPR analysis by Dr Dimitri Svistunenko (University of Essex). The oxidised IsoC sample did not have an EPR spectrum, whereas the reduced form had a spectrum consistent with a Rieske-type [2Fe-2S] cluster, as shown in Figure 4.15. The g -values were calculated to be 2.01, 1.91 and 1.77. These confirmed the predicted presence of a Rieske-type [2Fe-2S] cluster, which is consistent with the Rieske protein

components of the other four component soluble diiron monooxygenases, including toluene 4-monooxygenase from *Pseudomonas mendocina* sp. KR1 (Pikus *et al.*, 1996) and alkene monooxygenase from *Xanthobacter* sp. Py2 (Small and Ensign, 1997). These EPR features were also consistent with those of other Rieske cluster containing proteins, including the Rieske component of the (reduced coenzyme Q)-cytochrome *c* reductase complex from bovine heart mitochondria (Rieske *et al.*, 1964), a component of the respiratory chain isolated from *Thermus thermophilus* (Fee *et al.*, 1984), and the phthalate oxygenase purified from *Pseudomonas cepacia* (Batie *et al.*, 1987).

4.6. Characterisation of IsoC from *Rhodococcus* sp. AD45 by mass spectrometry

Various types of mass spectrometric analysis were used to analyse the purified IsoC sample. These experiments were used to determine the size, purity, amount of protein containing the predicted [2Fe-2S] cofactor and true concentration.

4.6.1. LC-MS analysis of IsoC from *Rhodococcus* sp. AD45

The predicted mass for IsoC with the N-terminal His tag was 13,782 Da. LC-MS analysis of an approximately 30 μ M 40 μ L sample of IsoC showed a single peak with a molecular mass of 13,650 Da, suggesting a highly pure protein (Figure 4.16). This is 132 Da smaller than the expected mass, which suggests removal of the N-terminal methionine. This is common in His-tagged proteins expressed in *Escherichia coli* and does not tend to affect enzyme activity, however expression in *Rhodococcus* has not been well studied.

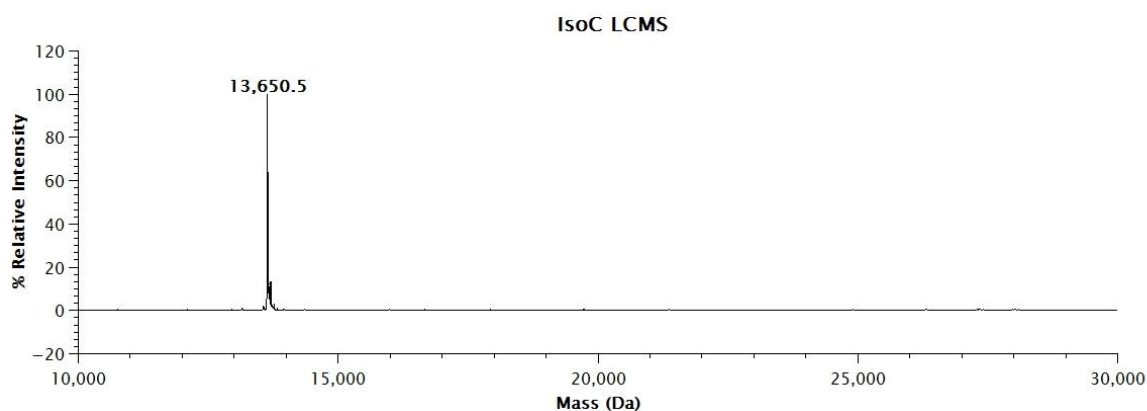


Figure 4.16: LC-MS analysis of purified N-terminally 6His-tagged IsoC. Expected mass 13,782 Da.

LC-MS analysis of the Rieske protein component of alkene monooxygenase from *Xanthobacter* sp. Py2 demonstrated that the protein exists in both 12,852 and 13,335 Da forms, suggesting a truncation. This was suggested to facilitate the protein binding as a dimer, as suggested from gel filtration analysis (Small and Ensign, 1997).

4.6.2. ICP-MS analysis of IsoC from *Rhodococcus* sp. AD45

ICP-MS analysis was used to determine the true concentration of IsoC, as colorimetric assays such as Bradfords can be inaccurate, particularly in small proteins such as IsoC (reviewed in Sapan *et al*, 1999). Also, ICP-MS was used to quantify the percentage of IsoC containing a [2Fe-2S] cluster cofactor, and check for the presence of other metals commonly found as enzyme cofactors.

IsoC samples for ICP-MS analysis were prepared aerobically by dilution to 29 μM based on a Bradford assay in 500 μL total volume using the same buffer as for gel filtration chromatography (section 4.4.2), and prepared for ICP-MS analysis according to section 2.13.3. Results are presented in Table 4.2.

The results of ICP-MS analysis demonstrated that the true concentration of the IsoC sample was 27.63 μM based on sulfur concentration within the sample and a predicted 8 sulfurs per monomer of protein, including the two in the Rieske-type [2Fe-2S] cluster. Comparing this with the absorbance spectroscopy, the extinction coefficient of oxidised IsoC at 280 nm was calculated to be 29,461 $\text{M}^{-1} \text{cm}^{-1}$. The amount of protein containing the [2Fe-2S] cluster cofactor was calculated to be over 90 % based on the total 1.85 iron molecules per IsoC monomer, suggesting that the homologous expression system allowed efficient production of correctly folded and cluster-containing proteins. This allowed calculation of the extinction coefficient for the cluster at A_{460} as 7,926 $\text{M}^{-1} \text{cm}^{-1}$. These calculated extinction coefficients are similar to those previously identified for XamoC from *Xanthobacter autotrophicus* sp. Py2, which have been recorded at 26,863 $\text{M}^{-1} \text{cm}^{-1}$ at 280 nm, and 7,230 $\text{M}^{-1} \text{cm}^{-1}$ at 460 nm (Small and Ensign, 1997). Finally, the ICP-MS results demonstrated that no other common elements involved in enzymatic metal-based cofactors were present. The elements tested for were magnesium, manganese, cobalt, nickel, copper, zinc and molybdenum (Table 4.2).

Table 4.2: Results of ICP-MS analysis of purified N-terminally 6His-tagged IsoC, showing the number of equivalents of each element per monomer of protein.

| Protein | Concentration (μM) | Moles of element per mole of protein | | | | | | | |
|---------|------------------------------------|--------------------------------------|------|------|------|------|------|------|------|
| | | Fe | Mg | Mn | Co | Ni | Cu | Zn | Mo |
| IsoC | 27.63 | 1.85 | 0.02 | 0.00 | 0.00 | 0.02 | 0.12 | 0.00 | 0.00 |

4.7. Electrochemical characterisation of IsoC from *Rhodococcus* sp. AD45 using cyclic voltammetry

The electrochemical characterisation of IsoC was performed using cyclic voltammetry in order to assess the midpoint potential of the protein and compare this value to other known SDIMO subunits and Rieske cluster-containing proteins.

4.7.1. Determination of the midpoint potential of IsoC from *Rhodococcus* sp. AD45

The purified His-tagged IsoC sample was purged with nitrogen to make it anaerobic and cyclic voltammetry was used to determine the midpoint potential of the protein inside an anaerobic glovebox. The IsoC sample was added to the electrode as a protein film before the electrode potential was cycled at a 20 ms scan rate. A signal was only obtained by the addition of a coadsorbant, in this case poly-lysine, before the protein film was laid (Figure 4.17).

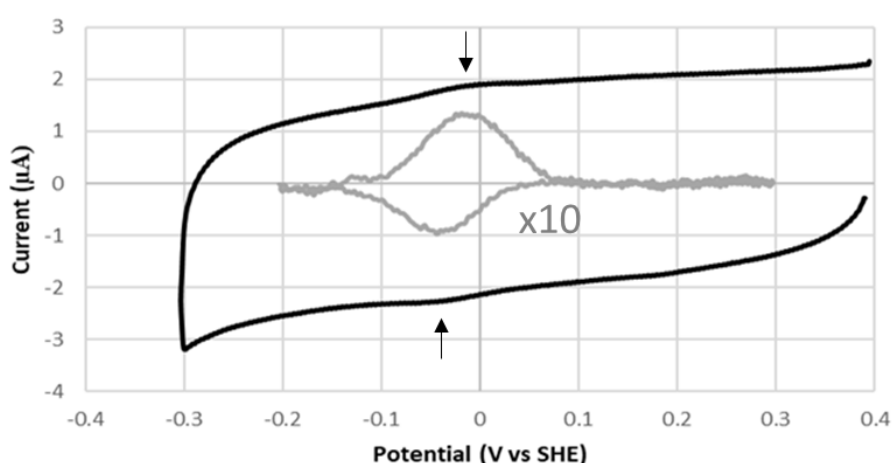


Figure 4.17: Cyclic voltammetry analysis of purified N-terminally 6His-tagged IsoC with poly-lysine as a co-adsorbant (black line). Baseline subtracted from oxidative and reductive peaks multiplied (x10, grey line). Peaks are highlighted by arrows. Grey line data manipulation credit Dr C. Lockwood (University of East Anglia).

The midpoint potential was calculated to be -26 ± 10 mV vs SHE, which is high in comparison to the recorded midpoint potentials of other Rieske proteins from soluble diiron monooxygenases. The midpoint potential of IsoC was most similar to that found for the Rieske protein of alkene monooxygenase from *Xanthobacter* sp. Py2 (-49 ± 10 mV vs SHE) (Small and Ensign, 1997), which is unsurprising as this enzyme is the closest characterised SDIMO to isoprene monooxygenase. With regard to other SDIMOs, the Rieske component of toluene/*o*-xylene monooxygenase from *Pseudomonas stutzeri* OX1 was found to have a midpoint potential of -130 mV vs SHE (Liang and Lippard, 2014), and the Rieske component of toluene 4-monooxygenase from *Pseudomonas mendocina* KR1 had a midpoint potential of -173 mV vs SHE (Elsen *et al.*, 2007). Whilst the midpoint potential of IsoC has been identified to be considerably lower than this, it still lies within the range identified for Rieske cluster containing proteins. These were found to be between -155 ± 5 mV to $+312 \pm 5$ mV vs SHE in the benzene dioxygenase of *Pseudomonas cepacia* and the *bc*₁ complex of bovine heart mitochondria respectively (Link *et al.*, 1996). The midpoint potential of the hydroxylase in the three-component SDIMO soluble methane monooxygenase has been identified as $+48$ mV vs SHE, whereas this dropped to -84 mV vs SHE in the presence of the coupling protein, which has been suggested to occur after reduction of the diiron centre to aid in oxygen reduction (Paulsen *et al.*, 1994). However, the Rieske protein and coupling protein have been demonstrated to bind at the same site of the oxygenase in toluene 4-monooxygenase of *Pseudomonas mendocina* KR1 (Liang and Lippard, 2014), suggesting that this may not be the case in four-component SDIMOs. Interestingly, the four component systems are incapable of oxidising methane and other alkanes, so identifying interactions between the Rieske protein, coupling protein and the hydroxylase, in addition to the effect these have on the midpoint potential, may enhance understanding of the difference between three- and four-component systems and how methane hydroxylation capability is achieved enzymatically.

4.7.2. Comparison of N-terminally His tagged and untagged IsoC from *Rhodococcus* sp. AD45

An alternative purified source of untagged IsoC was prepared by Dr C. Lockwood (Murrell Group, University of East Anglia), using the pTipQC2S2:IsoEx expression vector which will be presented in Chapter 7 for purification of the oxygenase component. After the initial step in oxygenase purification using a StrepTactin-XT affinity chromatography column (section 7.2.2), the flow through was found to contain IsoC. This flow through was diluted

with 50 mM HEPES (pH 7.0) to reduce the NaCl concentration to 50 mM. This was applied to a ~130 mL Q-Sepharose anion exchange column (section 2.11.2) equilibrated with a binding buffer containing 50 mM HEPES and 50 mM NaCl (pH 7.0) using an AKTApure sample pump and UNICORN™ 7 software. The column was washed with 2 column volumes of the binding buffer followed by a gradient elution from 50 mM to 1 M NaCl over 1.5 column volumes. The fractions eluting at approximately 300 mM NaCl were brown in colour and confirmed to contain IsoC by SDS-PAGE analysis and absorbance spectroscopy, based on the data collected from the purified His-tagged IsoC.

This partially purified IsoC was concentrated to 2 mL (section 2.11.5) and exchanged into buffer containing 50 mM HEPES, 1 M ammonium sulfate pH 7.0 using dialysis tubing and two exchanges of 500 mL buffer. This was then centrifuged at 16,000 x *g* for 30 min to remove precipitated protein and applied to a ~20 mL Phenyl Sepharose hydrophobic interaction column (section 2.11.3), where IsoC was collected in the flow through. Finally, this flow through was concentrated to 2 mL and applied to an equilibrated Superdex HiLoad 26/600 200 µg gel filtration chromatography column (section 2.11.4), where it eluted pure according to SDS-PAGE analysis (Figure 4.19).

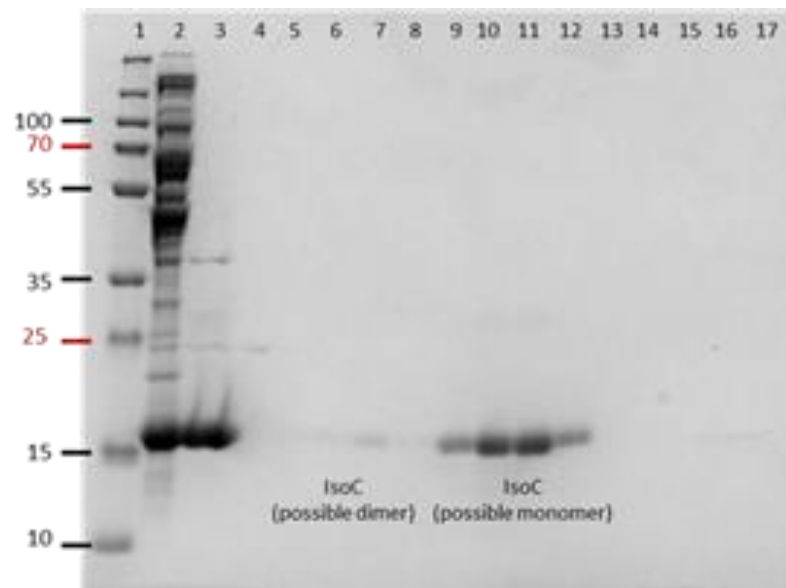


Figure 4.18: Gel filtration step of untagged IsoC purification. Sample 2 is *Rhodococcus* sp. AD45-ID (pTipQC2S2:IsoEx) cell lysate. Sample 3 is the load for the gel filtration column. Samples 4 – 17 are elution fractions from the column. Image credit: Dr Lockwood, Murrell Group, University of East Anglia.

The purified untagged IsoC was analysed by both absorbance spectroscopy (Figure 4.19) and cyclic voltammetry (Figure 4.20), as in sections 4.5.1 and 4.7.1, respectively. These were both consistent with the findings for the His-tagged IsoC, including a similar $A_{280}:A_{454}$ ratio, which suggested a comparable incorporation of the [2Fe-2S] cluster. The midpoint potential of the untagged IsoC was found to be -25 mV vs SHE, which proved that the presence of the His-tag did not significantly affect the redox cycling capability of IsoC, and the easier to purify His-tagged version could be used going forwards.

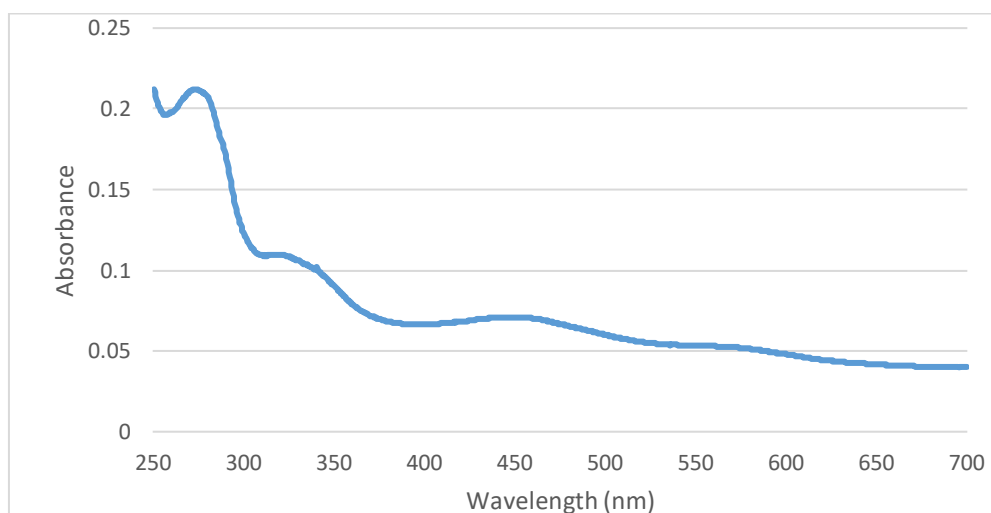


Figure 4.19: Absorbance spectrum of purified untagged IsoC as purified between 300 and 700 nm.

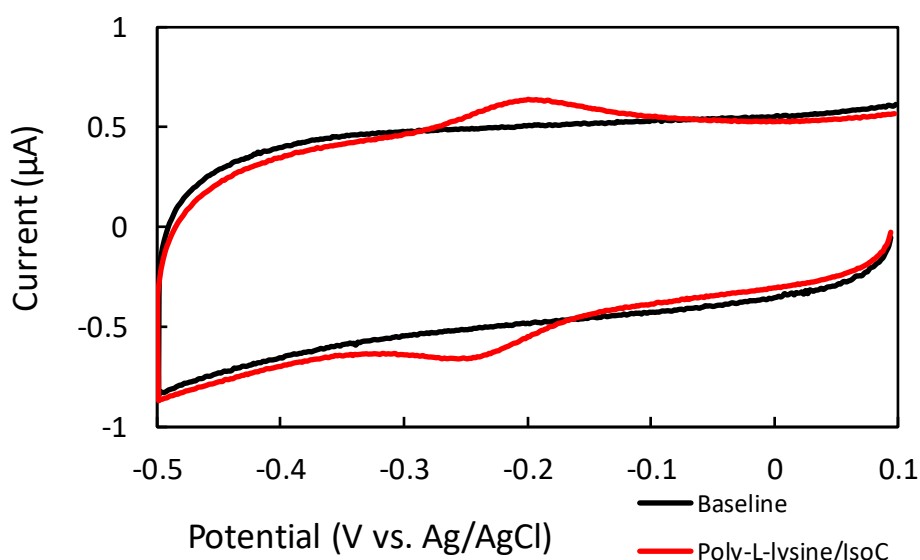


Figure 4.20: Cyclic voltammetry analysis of purified untagged IsoC with poly-lysine as a co-adsorbant. Image credit: Dr Lockwood, Murrell Group, University of East Anglia.

4.8. Conclusions

In this chapter, results of the purification and characterisation of the Rieske component of isoprene monooxygenase have been presented. IsoC was expressed as an N-terminally His6-tagged protein using the homologous expression system *Rhodococcus* sp. AD45-ID and the pTip expression vector series. The His-tagged protein was purified by immobilised metal affinity chromatography followed by gel filtration chromatography on an AKTApure HPLC system.

Purified IsoC was characterised by a variety of spectroscopic and mass spectrometric techniques. Absorbance, circular dichroism and electron paramagnetic resonance spectroscopy were used to prove the presence of a Rieske-type [2Fe-2S] cluster and the ability of the protein to redox cycle, and proved the stability of IsoC and the cluster it contains.

LC-MS was used to demonstrate the size and purity of the purified IsoC sample, and ICP-MS demonstrated that over 90 % of purified IsoC contained the Rieske cluster cofactor. Cyclic voltammetry was utilised to determine the midpoint potential of both His-tagged and untagged IsoC, and demonstrated that the difference between the two was negligible, suggesting that the tag does not inhibit the electron transfer capability of the protein.

In the next chapter, results of purification and characterization of the isoprene monooxygenase coupling protein (IsoD), which is the other small subunit of the complex, will be presented.

5. Purification and characterisation of IsoD: The coupling protein component of isoprene monooxygenase from *Rhodococcus* sp. AD45

5.1. Introduction

In this chapter the results of work on the coupling protein component of the isoprene monooxygenase from *Rhodococcus* sp. AD45, termed IsoD, will be presented. The coupling protein is a small component that interacts with the hydroxylase to alter substrate specificity, and regioselectivity (Froland *et al.*, 1992), and rate of reaction (Pikus *et al.*, 1996; Mitchell *et al.*, 2002) in SDIMO systems. Purification of recombinant IsoD utilising both a homologous expression system in the *Rhodococcus* sp. AD45-ID strain and heterologous expression in *Escherichia coli* was attempted. The homologous system was used to produce an N-terminally His-tagged protein, and the heterologous system was used to produce an N-terminally StrepII-tagged protein. The homologous expression system was the same as utilised in Chapter 4, the pTip vectors designed for protein production in *Rhodococcus erythropolis*.

The purified recombinant IsoD protein from *Escherichia coli* was characterised by absorption spectroscopy and mass spectrometric techniques. These were used to determine whether any cofactors were present.

5.2. Cloning *isoD* from *Rhodococcus* sp. AD45 into the pTipQC1 expression plasmid for expression in *Rhodococcus* sp. AD45-ID

Initially, the cloning of *isoD* for purification of the coupling protein component of the isoprene monooxygenase from *Rhodococcus* sp. AD45 was attempted using the same homologous expression system utilised for IsoC purification in Chapter 4. *Escherichia coli* heterologous expression of soluble methane monooxygenase coupling proteins from *Methylococcus capsulatus* (Bath) has resulted in production of a truncated form of the protein which was inactive (Lloyd *et al.*, 1997). Much of the initial research into purification and characterisation of coupling proteins from soluble methane monooxygenases (Green and Dalton, 1986; Fox *et al.*, 1989; Nakajima *et al.*, 1992), alkene monooxygenases (Miura and Dalton, 1995; Small and Ensign, 1997), and toluene monooxygenases (Whited and Gibson, 1991; Newman and Wackett, 1995) utilised proteins purified from the native

system. This made the use of a homologous expression system attractive in the first instance, as it should combine the ease of affinity chromatography for purification and the reliability of expression in the native organism.

5.2.1. Amplification of *isoD* from *Rhodococcus* sp. AD45 genomic DNA

PCR with a Q5 high-fidelity DNA polymerase (section 2.5.2) was used to amplify the *isoD* gene from *Rhodococcus* sp. AD45 genomic DNA, which was a gift from Dr A. Crombie (Murrell group, University of East Anglia). The primers used for this step are given in Table 5.1, and all cloning steps were performed using *Escherichia coli* TOP10 cells. The expression vector was assembled following the same steps as described in section 4.2 for the production of the pTipQC1:*isoC* expression vector.

The pTipQC1:*isoD* construct for production of IsoD in the homologous expression strain *Rhodococcus* sp. AD45-ID was prepared to yield an N-terminally 6-Histidine tagged protein for quick IMAC purification (Figure 5.1). The DNA sequence of the expression vector was ratified by sequencing at MWG eurofins (section 2.5.8). His-tags had successfully been utilised in coupling protein expression and purification previously. N-terminally His-tagged coupling proteins of the alkene monooxygenase from *Xanthobacter* sp. Py2 were demonstrated to retain 80 % of activity in comparison to the untagged protein, though this was expressed in *Escherichia coli* (Champreda *et al.*, 2004). This same study also demonstrated that a GST fusion was less effective than a His-tagged variant, however both were found to be active, even without removal of the tag or fusion protein. The untagged recombinant alkene monooxygenase coupling protein was degraded and inactive, suggesting that the tags afforded some protection from degradation.

Table 5.1: Primer sequences used for polymerase chain reaction amplification of *isoD* from *Rhodococcus* sp. AD45 genomic DNA and subsequent cloning into expression vectors.

| Primer Name | Sequence | Restriction Site | Orientation |
|-------------|----------------------------------|------------------|-------------|
| isoDF | ATATATCATATGGCCATTGTTCGATATGGATC | <i>NdeI</i> | Forward |
| isoDR | ATATATGGATCCAGGTCTTGAGACCGCG | <i>BamHI</i> | Reverse |

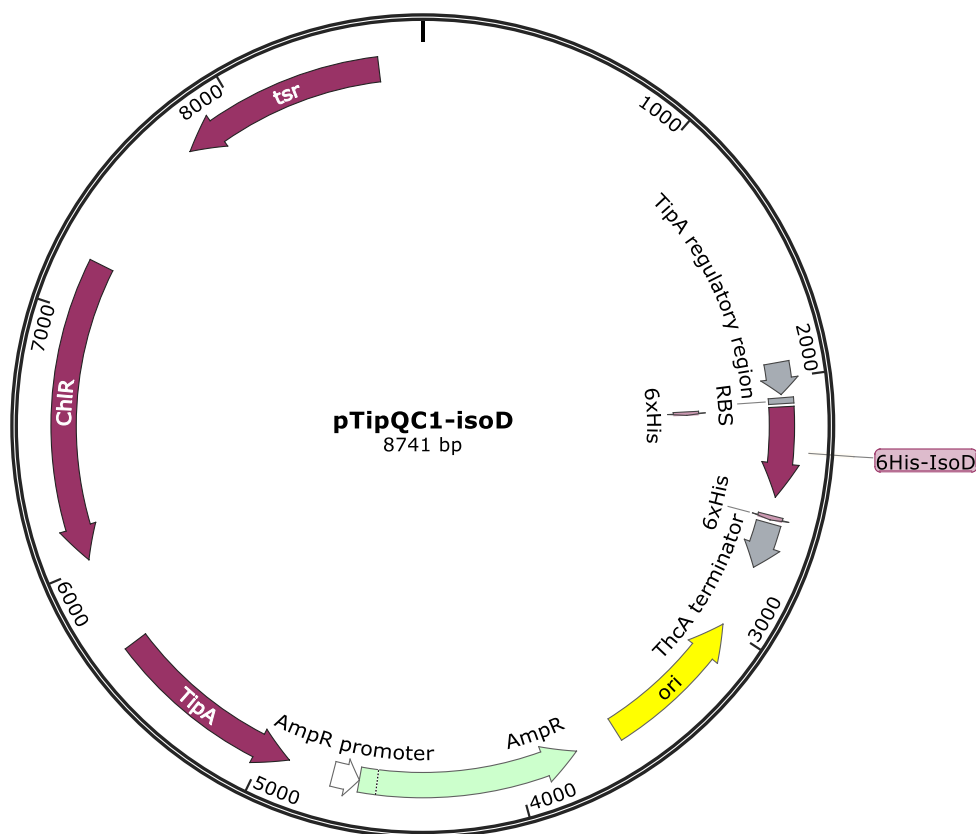


Figure 5.1: pTipQC1:*isoD* vector map for expression of *isoD* from *Rhodococcus* sp. AD45 in *Rhodococcus* sp. AD45-ID.

5.2.2. Production of IsoD in the *Rhodococcus* sp. AD45-ID homologous expression system

Rhodococcus sp. AD45-ID cells were transformed by electroporation (section 2.3.4) with the pTipQC1:*isoD* plasmid and plated onto minimal medium plates containing 10 mM succinate as a carbon source and 35 $\mu\text{g mL}^{-1}$ chloramphenicol. Transformants were grown in batch culture (section 4.3) to ascertain whether the IsoD protein was being produced. The N-terminally His-tagged IsoD protein was predicted to be 13.3 kDa, and the protein band associated with induction by the addition of 1 $\mu\text{g mL}^{-1}$ thiostrepton ran somewhere between 15 and 25 kDa (Figure 5.2). Anomalous migration during SDS-PAGE analysis of the coupling protein of alkene monooxygenase from *Xanthobacter* sp. Py2 has been previously recorded (Champreda *et al.*, 2004), so this was not deemed to be an issue.

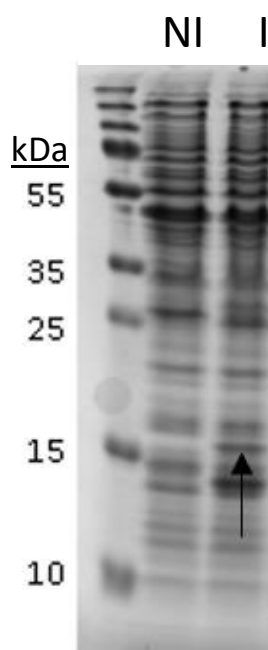


Figure 5.2: Polypeptide profiles of *Rhodococcus* sp. AD45-ID expressing pTipQC1:*isoD* as determined by SDS-PAGE gel electrophoresis. AD45-ID cultures were either non-induced (NI) or induced with $1 \mu\text{g mL}^{-1}$ thiostrepton (I) to produce the IsoD protein, which has been indicated with an arrow.

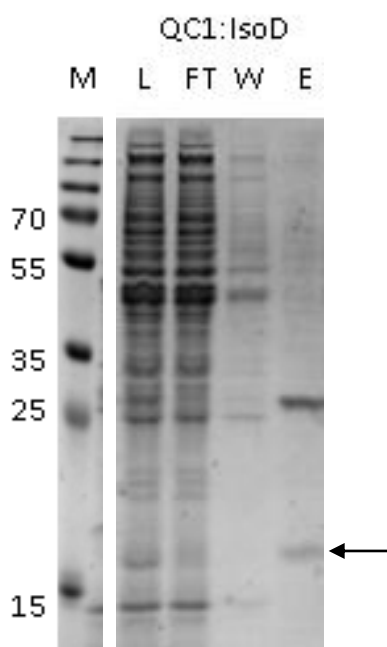


Figure 5.3: Polypeptide profiles of IsoD purification by 1 mL HisTrap spin-columns as determined by SDS-PAGE. L is cell lysate, FT is the flow through, W is the wash and E is the elution. The band predicted to correspond to IsoD has been highlighted by an arrow.

Some gels used in assessing expression trials showed IsoD running as more of a smear (data not shown). As the polypeptide appeared to run variably and with an abnormal molecular mass, spin-column His-trap purification was utilised in order to establish whether the bands and smears present after induction with thioestrepton were IsoD (Figure 5.3). A faint band of approximately the correct size was observed, suggesting that IsoD was being produced, though at very low quantities in comparison to the expression trials with IsoC outlined in Chapter 4, section 4.3.

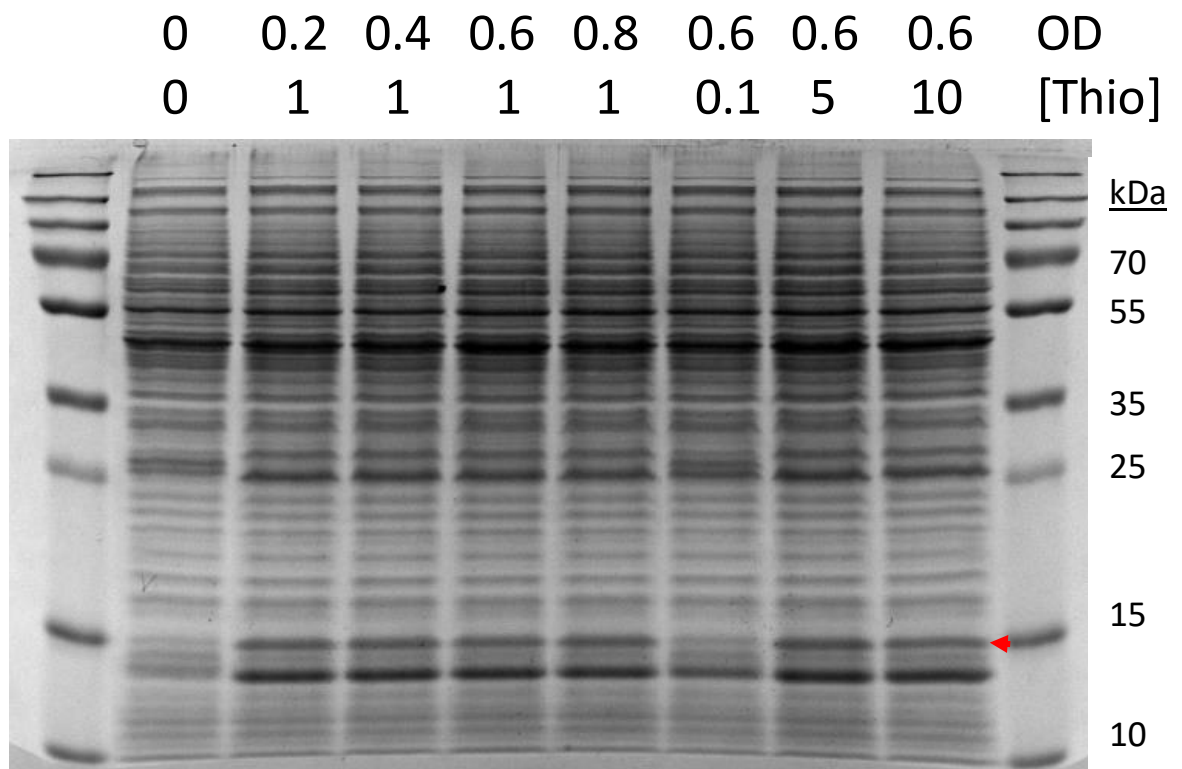


Figure 5.4: Polypeptide profiles of *Rhodococcus* sp. AD45-ID expressing pTipQC1:*isoD* as determined by SDS-PAGE. The OD₅₄₀ at induction and concentration of thioestrepton used to induce ($\mu\text{g mL}^{-1}$) are labelled for each profile and the band predicted to correspond to the IsoD polypeptide has been highlighted with an arrow.

Optimisation of IsoD production was attempted by altering the OD₅₄₀ and thioestrepton concentration at induction in 50 mL cultures in 100 mL flasks grown according to section 2.3.3. After induction, the cultures were grown at 30 °C overnight to allow protein production, and harvested by centrifugation (section 2.6). The cell pellet was resuspended in 4 mL of 50 mM phosphate buffer (pH 7.0) and the cells were broken by three passes through a French pressure cell at 20,000 psi (137 MPa). Unbroken cells and cell debris were

removed by centrifugation at 16,000 x *g* for 30 min at 4 °C, followed by analysis of the polypeptide profiles using SDS-PAGE (Figure 5.4). The soluble extract of the cells induced in these varying stages of growth and with varying amounts of thiostrepton showed no significant difference in the amount of IsoD protein being produced, so the standard induction protocol was used (section 4.3).

5.2.3. Attempted purification of IsoD from *Rhodococcus* sp. AD45-ID containing pTipQC1:*isoD* using immobilised metal chromatography

All IsoD purification was carried out using an AKTApure HPLC system with UNICORN™ 7 software. The buffers used for purification attempts with a 5 mL HisTrap column were the same as those described in section 4.1.1. The cell pellet of harvested *Rhodococcus* sp. AD45-ID cells expressing the pTipQC1:*isoD* plasmid was resuspended in the IMAC binding buffer and applied to the 5 mL HisTrap column at 1 mL min⁻¹. The column was then washed with 50 mL (10 column volumes) of binding buffer, followed by a linear elution from 40 mM to 500 mM of imidazole (0 – 100 % elution buffer) over another 50 mL, followed by a 25 mL column wash with 100 % elution buffer to clear any remaining protein from the column. The trace of the AKTA program used to purify IsoD is shown in Figure 5.5. IsoD was not obviously present in the elution profile, with only one slight bump in the absorbance (highlighted with an arrow) suggesting that any protein may have been eluted. A selection of fractions from the column flow through, wash and elution were examined using SDS-PAGE (section 2.7.4), the results of which are presented in Figure 5.6.

The SDS-PAGE analysis of the IMAC purification of IsoD from the *Rhodococcus* sp. AD45-ID homologous expression system suggested that IsoD was present (Figure 5.6A). The elution “peak” fractions were pooled and spin-concentrated from 8 mL to 1.5 mL. The resulting concentrated sample was again analysed by SDS-PAGE gel (Figure 5.6B). The large smear present on the gel implied that the protein may have degraded. Degradation of the coupling protein of alkene monooxygenase from *Rhodococcus rhodochrous* B-276 over longer purification protocols has been documented previously, however this was resolved by the use of affinity tags to speed up purification (Smith *et al.*, 1999), such as the His tag utilised here.

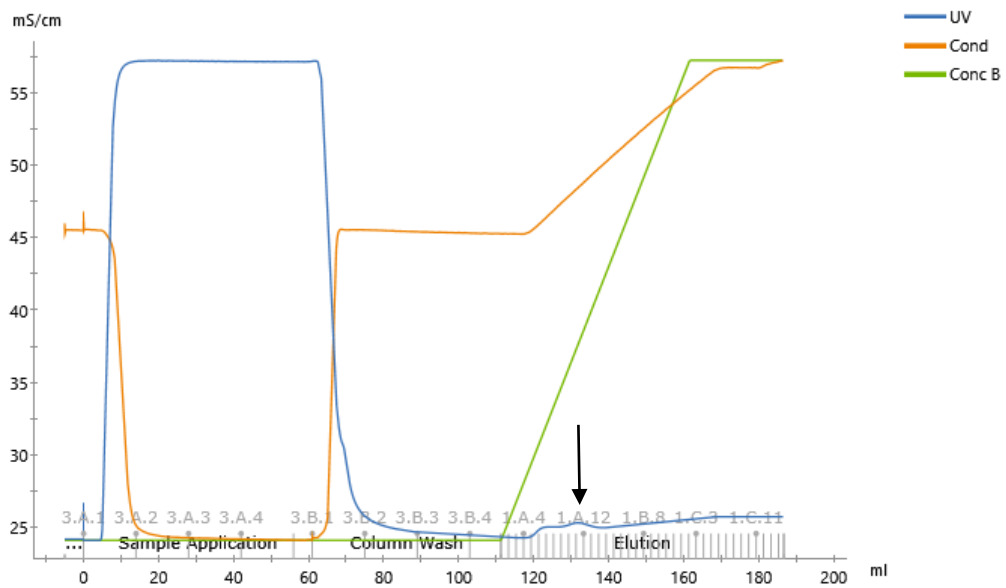


Figure 5.5: HPLC trace of a gradient elution of IsoD on a 5 mL HisTrap column using an AKTApure HPLC system. The concentration of imidazole in the elution buffer (green line) varied from 40 – 500 mM (0 – 100 % buffer B) over the gradient.

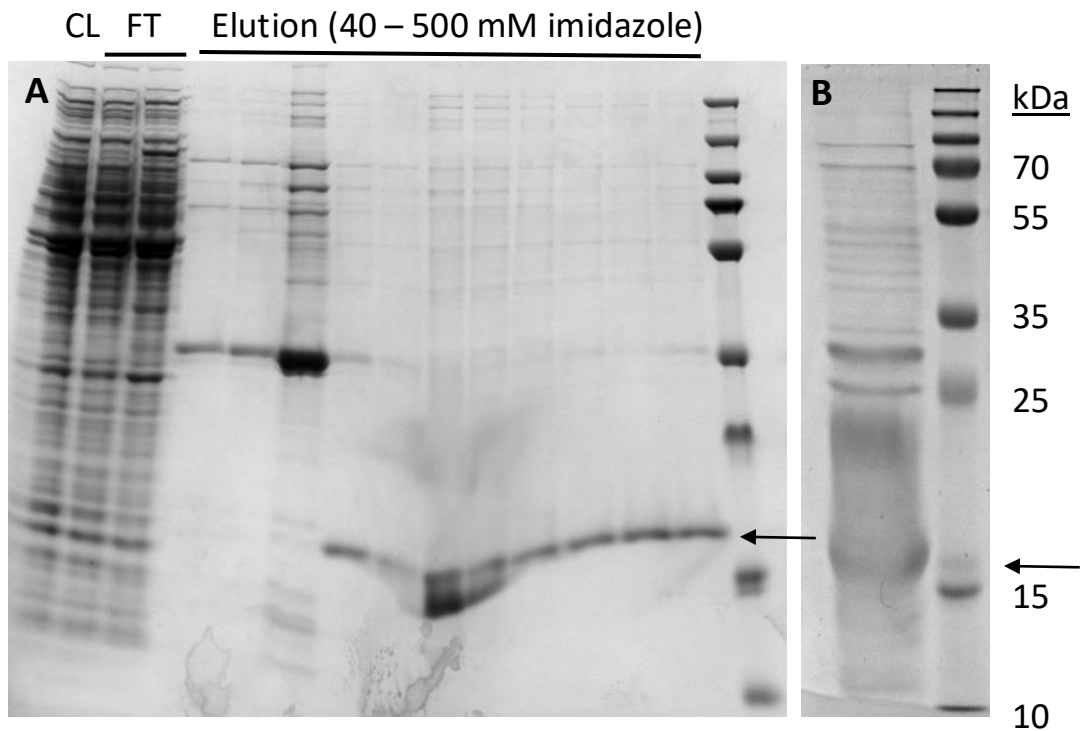


Figure 5.6: A: Purification of IsoD using a 5 mL HisTrap column and a linear gradient elution from 40 – 500 mM imidazole over 50 mL using an AKTApure HPLC system. Polypeptide profiles of fractions were visualised using SDS-PAGE and InstantBlue staining. **B:** The pooled fractions highlighted in A after spin-concentrating as visualised by SDS-PAGE.

The process of IsoD purification was attempted again with less time between purification and concentration. However, this time the SDS-PAGE gel of the IMAC purification step showed no protein just above the 15 kDa protein marker (Figure 5.7). This may have been due to the plasmid or protein being unstable in *Rhodococcus* sp. AD45-ID, although this should have been unlikely as the plasmid worked well for IsoC expression. Also the AD45-ID strain was selected as a homologous host so was least likely to encounter problems with protein production.

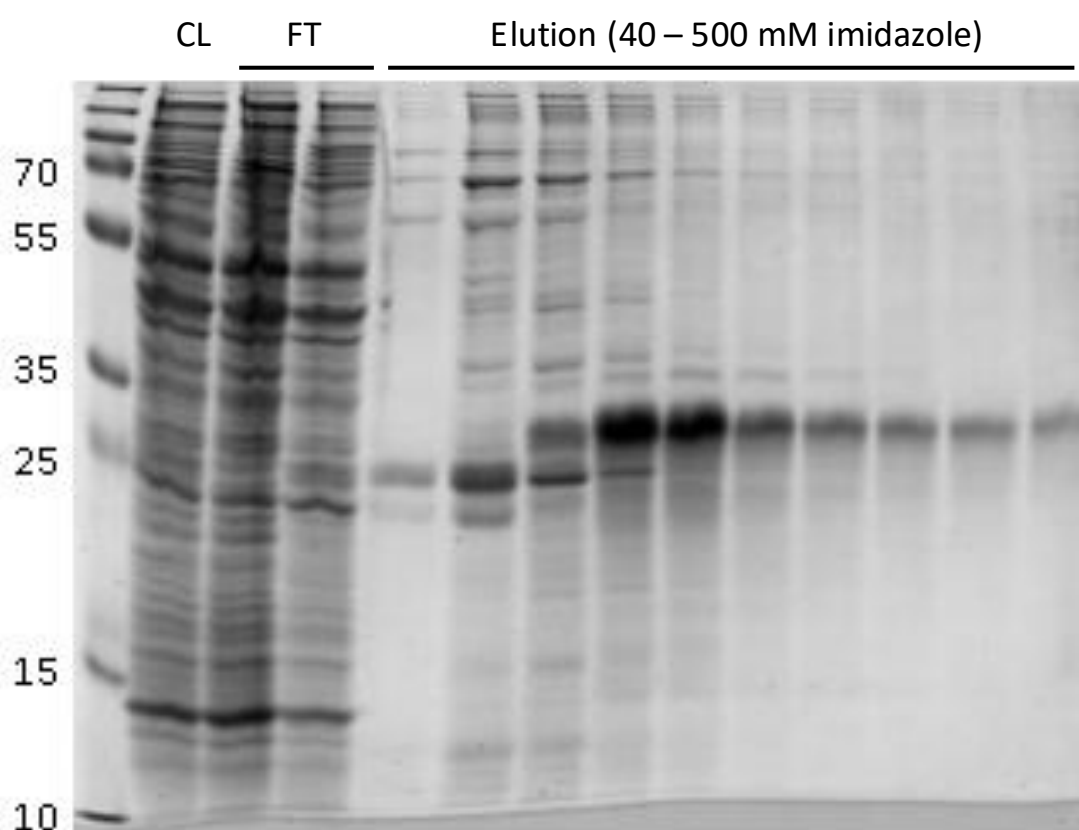


Figure 5.7: Attempted purification of IsoD using a 5 mL HisTrap column and a gradient elution from 40 – 500 mM imidazole over 50 mL using an AKTApure HPLC system. Polypeptide profiles of fractions were visualised using SDS-PAGE.

Many other research groups had successfully produced SDIMO coupling proteins in *Escherichia coli* to study interactions of coupling proteins and their associated hydroxylases. This has been accomplished for soluble methane monooxygenases (West *et al.*, 1992; DeWitt *et al.*, 1995; Lloyd *et al.*, 1997; Gallagher *et al.*, 1999; Walters *et al.*, 1999), alkene monooxygenases (Smith *et al.*, 1999; Champreda *et al.*, 2004) and toluene 4-monooxygenases (Yen *et al.*, 1991; Pikus *et al.*, 1996; Studts and Fox, 1999; Lountos *et al.*,

2005). As mentioned previously, some researchers had encountered issues with expression in *Escherichia coli* resulting in the production of truncated and inactive coupling proteins (Lloyd *et al.*, 1997; Champreda *et al.*, 2004); an issue which needed to be considered. Despite this, the coupling protein of the characterized SDIMO most closely related to isoprene monooxygenase of *Rhodococcus* sp. AD45, alkene monooxygenase from *Xanthobacter* sp. Py2, had been successfully expressed in *Escherichia coli*. IsoD itself was purified and utilised in a cross-reactivity test where it was found to partially complement the alkene monooxygenase system from *Xanthobacter* sp. Py2 (Champreda *et al.*, 2006). With this accounted for, plasmids for the expression of tagged IsoD in *Escherichia coli* were constructed.

5.3. Cloning *isoD* from *Rhodococcus* sp. AD45 into the pET51b plasmid for expression in *Escherichia coli*

The pET expression system is commonly used for the high-yield production of recombinant proteins in *Escherichia coli*. The pET51b plasmid used here was chosen due to the ability to produce an N-terminally StrepII tagged recombinant protein. This tag was chosen as a highly specific sequence designed to allow single-step purification of proteins (Schmidt and Skerra, 2007), which could eliminate the degradation issues highlighted previously.

5.3.1. Amplification of *isoD* from *Rhodococcus* sp. AD45 genomic DNA

The same protocol for cloning *isoD* into the pTipQC1:*isoD* expression vector was also used for cloning *isoD* into the pET51b vector (Figure 5.8), as outlined in section 5.2.1. The only difference was the PCR primers utilised, which are outlined in Table 5.2, and the restriction enzymes used, which were *Bam*HI and *Hind*III. The vector map of the expression plasmid, termed pET51b:*isoD*, is presented in Figure 5.9. The sequence of the expression plasmid was ratified by sequencing by MWG Eurofins.

Table 5.2: Primer sequences used for polymerase chain reaction amplification of *isoD* from *Rhodococcus* sp. AD45 genomic DNA and cloning into the pET51b expression vector.

| Primer Name | Sequence | Restriction Site | Orientation |
|-------------|---------------------------------------|------------------|-------------|
| 51bisODF | TATATAGGATCCGATGGCCATTGTTCGATATGGATGC | <i>Bam</i> HI | Forward |
| 51bisODR | TATATAAAGCTTTCATGACTTCTCCTGTCCAGGGT | <i>Hind</i> III | Reverse |

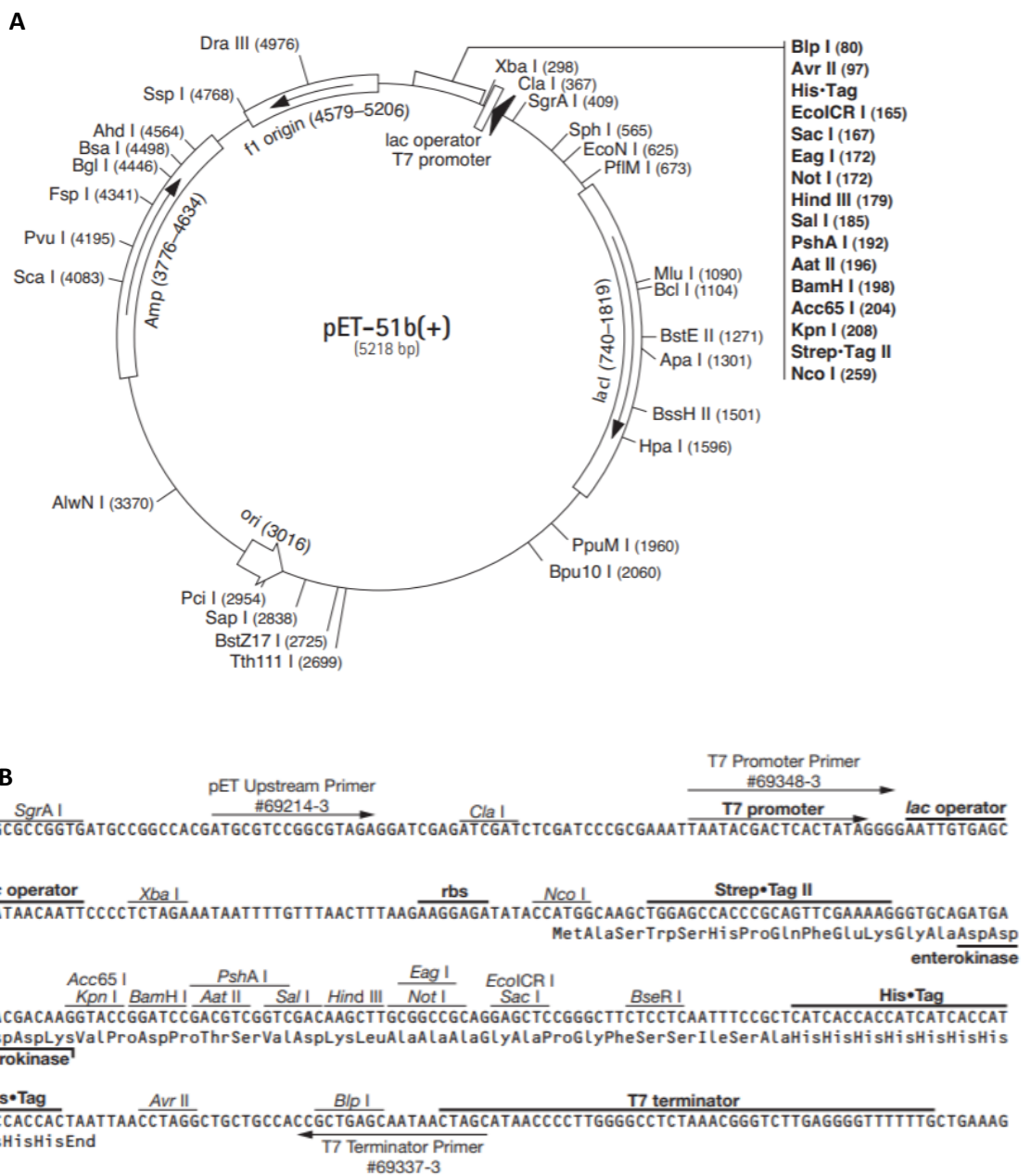


Figure 5.8: pET51b expression system for recombinant protein expression in *Escherichia coli*. A) pET51b vector map. B) Multiple cloning site for the pET51b vector. Images from https://www.merckmillipore.com/GB/en/product/pET-51b+-DNA-Novagen,EMD_BIO-71553#anchor_VMAP

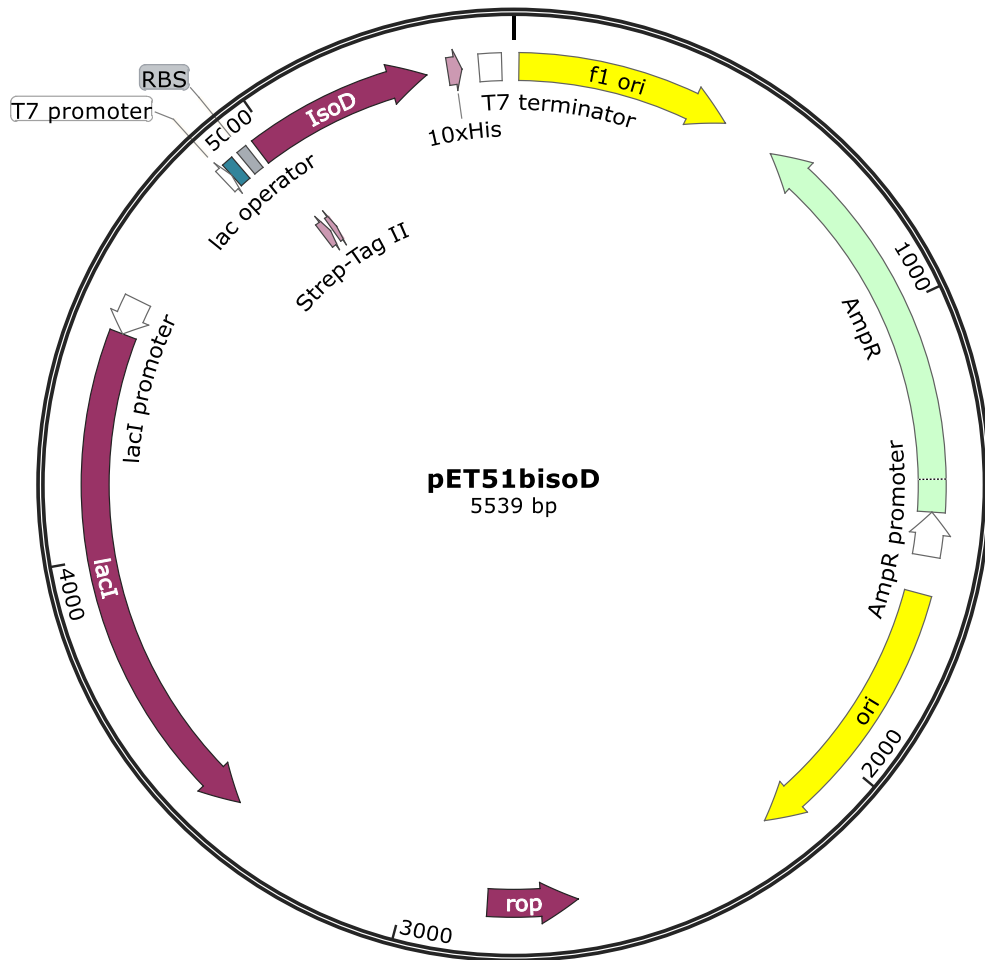


Figure 5.9: pET51b:*isoD* vector map for expression of *isoD* from *Rhodococcus* sp. AD45 in *Escherichia coli*.

5.3.2. Production of IsoD in the *Escherichia coli* heterologous expression system

For production of recombinant proteins, the ratified pET51b:*isoD* vector was used to transform chemically competent *Escherichia coli* cells of either strain BL21 (DE3) or Rosetta 2 (pLysS) using heat shock (section 2.3.2). To check whether the *Escherichia coli* BL21 (DE3) (pET51b:*isoD*) cells could produce soluble recombinant IsoD, the cultures were grown in 100 mL conical flasks culture (section 2.3.1) to an OD₅₄₀ of 0.6-0.8. At this point, the recombinant protein production was induced by the addition of 50 μM IPTG, followed by a further 3 h of growth at 37 °C, then cell harvest by centrifugation (section 2.6). SDS-PAGE analysis of the soluble extract from a 10 mL culture (section 2.7) demonstrated that the protein present in the induced culture ran as an indistinct smear (Figure 5.10).

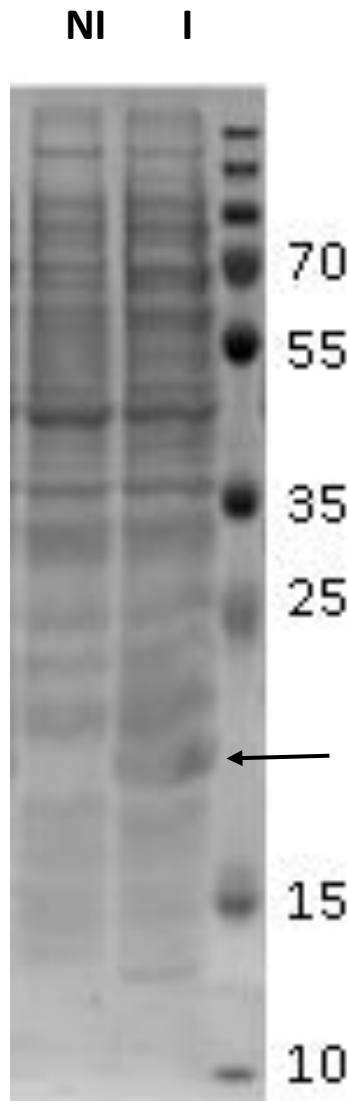


Figure 5.10: Polypeptide profiles of *Escherichia coli* BL21 (DE3) expressing pET51b:*isoD* as determined by SDS-PAGE. BL21 (DE3) cultures were either non-induced (NI) or induced (I) with 50 μ M IPTG to produce the IsoD protein, which has been indicated with an arrow.

To check whether this smear was simply how the recombinant protein ran or if there was an issue with the expression strain, the same experiment was carried out with *Escherichia coli* Rosetta 2 (pLysS) cells. Analysis of protein production by this strain showed a clearer band at the expected molecular mass without the smearing, and demonstrated clear overexpression of the recombinant protein (Figure 5.11). As a result of this analysis, subsequent work with heterologous protein expression in *Escherichia coli* solely utilised the Rosetta 2 (pLysS) strain.

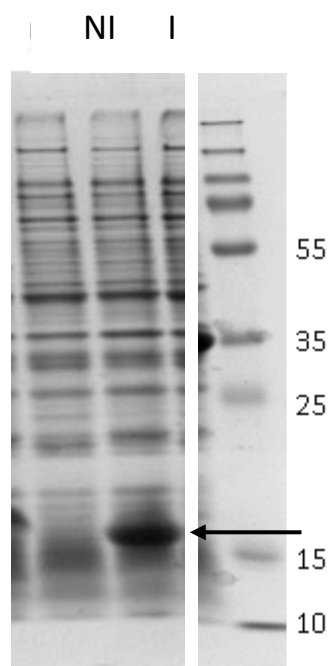


Figure 5.11: Polypeptide profiles of *Escherichia coli* Rosetta 2 (pLysS) cells expressing pET51b:*isoD* as determined by SDS-PAGE. Rosetta 2 (pLysS) cultures were either non-induced (NI) or induced (I) with 50 μ M IPTG to produce the IsoD protein, which has been indicated with an arrow.

5.4. Purification of IsoD from *Escherichia coli* Rosetta 2 cells containing pET51b:*isoD*

As with previous attempts to purify IsoD from *Rhodococcus* sp. AD45 (section 5.2.3), an AKTApure HPLC system was used with UNICORN™ 7 software. In contrast to the previous work, cell pellets from *Escherichia coli* cultures expressing the recombinant IsoD were broken by sonication (section 2.7) rather than a French pressure cell. Cell lysate was subjected to a further ultracentrifugation step (42,000 \times *g*, 45 min, 4 °C) to remove the membrane fraction as well as any unbroken cells and debris that had not been removed with the previous lower speed centrifugation step.

5.4.1. Affinity chromatography and anion exchange partial purification of IsoD

The affinity column used for the purification of StrepII-tagged IsoD from *Escherichia coli* cells was the StrepTactin-XT 5 mL column. The buffers used for purification are listed in section 2.11.1. In brief, the elution buffer contained 10 mM D-biotin for removal of bound protein from the column. Cultures of *Escherichia coli* Rosetta 2 (pLysS) containing the

pET51b:*isoD* plasmid, totalling 2 L, were grown in 4 x 2 L flasks in LB media (section 2.3.1) and *isoD* expression was induced by the addition of 50 μ M IPTG. After induction at 37 °C for 3 h, cells were harvested by centrifugation and stored at -80 °C until use. The frozen cell pellet was thawed and resuspended in 20 mL of the column binding buffer and placed on ice. The cells were broken by sonication (section 2.7) and the cell debris removed by centrifugation at 16,000 x *g* for 30 min. The supernatant was then subjected to ultracentrifugation at 42,000 x *g* for 60 min to remove any membrane proteins. The clarified cell lysate was applied to the StrepTactin-XT column, using the AKTApure HPLC system and UNICORN™ 7 software, at a flow rate of 1 mL min⁻¹. The column was washed with 25 mL of binding buffer, followed by elution with 25 mL of elution buffer. The AKTA trace is shown in Figure 5.12, and suggested that the yield was considerably higher than the *Rhodococcus* sp. AD45-ID expression system, although lower than anticipated. Samples of the purification run were analysed by SDS-PAGE (section 2.7.4), and resulted in visualisation of a large protein smear at a higher than expected molecular mass of well over 15 kDa based on the protein marker (Figure 5.13). Due to the high specificity of the StrepII tag in protein purification, this was carried forwards to determine what the issue could be.

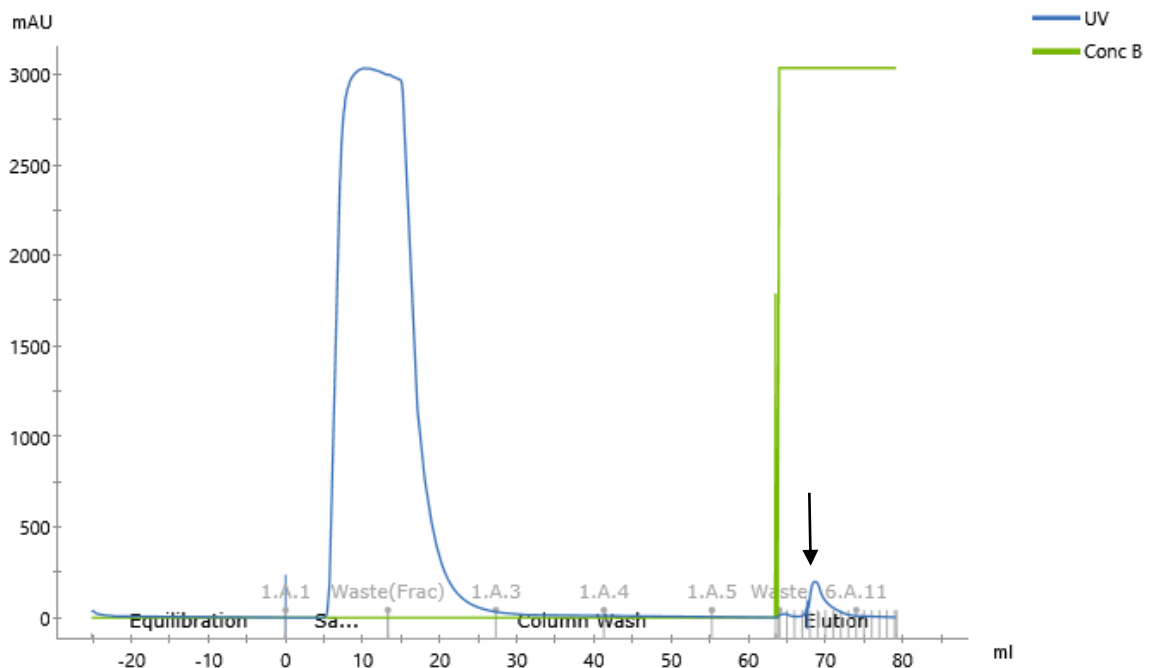


Figure 5.12: HPLC trace of a single-step elution of IsoD on a 5 mL StrepTactin-XT column with 10 mM biotin using an AKTApure HPLC system.

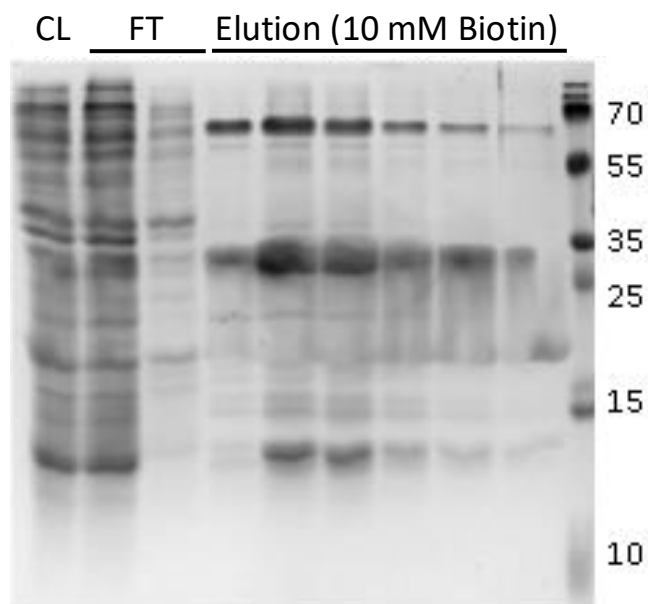


Figure 5.13: SDS-PAGE analysis of fractions from HPLC purification of IsoD using a 5 mL StrepTactin-XT column in a single step elution with 10 mM Biotin using an AKTApure HPLC system.

Further purification of IsoD was attempted using a Q-Sepharose column for anion exchange chromatography using binding and elution buffers described in section 2.11.2, which contained between 0 and 1 M NaCl. The fractions containing the predicted peak of IsoD elution on the AKTA trace were pooled and concentrated down from 8 mL to 2 mL using spin-concentrators, followed by dialysis into the Q-Sepharose binding buffer. This sample was applied to a 1 mL Q-Sepharose column at 1 mL min⁻¹, followed by a 10 mL wash and elution by a linear gradient of 0 – 1 M NaCl (0 – 100 % elution buffer) over 15 mL. The AKTA trace is presented in Figure 5.14 and showed two clear elution peaks. SDS-PAGE analysis of the first elution peak showed a clear band at around 15 kDa (Figure 5.15), as observed for the HisTrap spin-columns utilised in trials of the *Rhodococcus* sp. AD45-ID homologous expression system in described in section 5.2.2. The second peak did not contain any clear protein bands not present in the first elution peak, suggesting that this was mostly DNA.

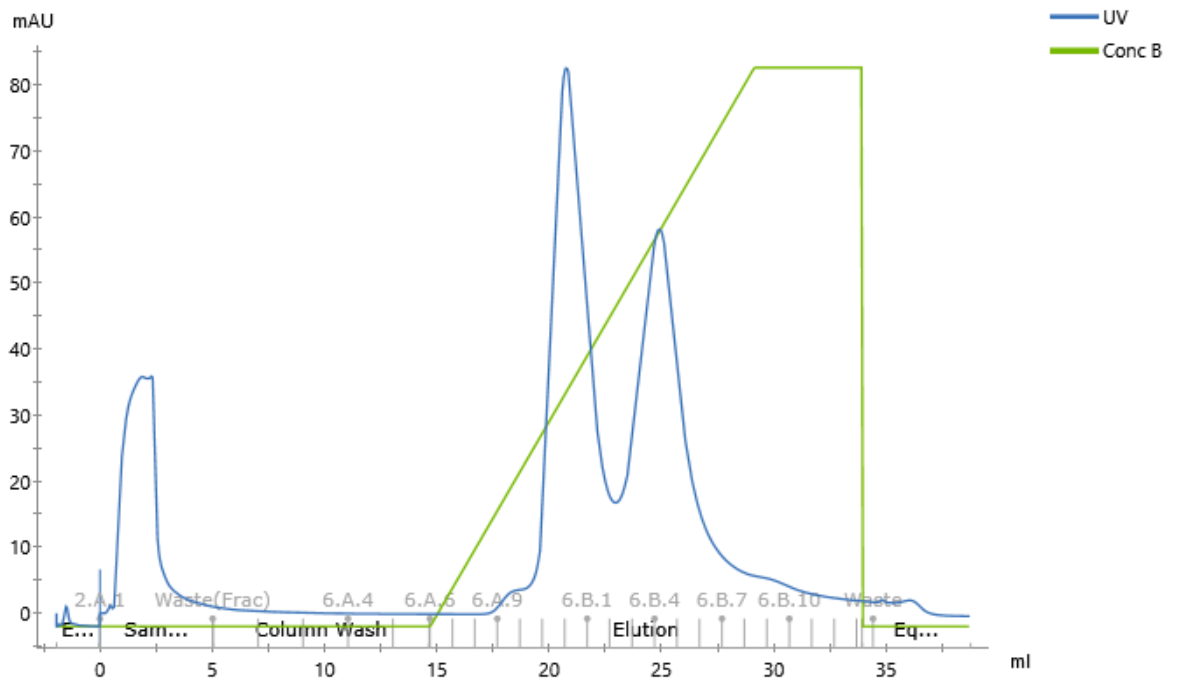


Figure 5.14: HPLC trace of purification of IsoD using a 1 mL Q-Sepharose column using an AKTApure system. The concentration of NaCl in the elution buffer (green line) varied from 0 – 1 M (0 – 100 % buffer B) over the gradient.

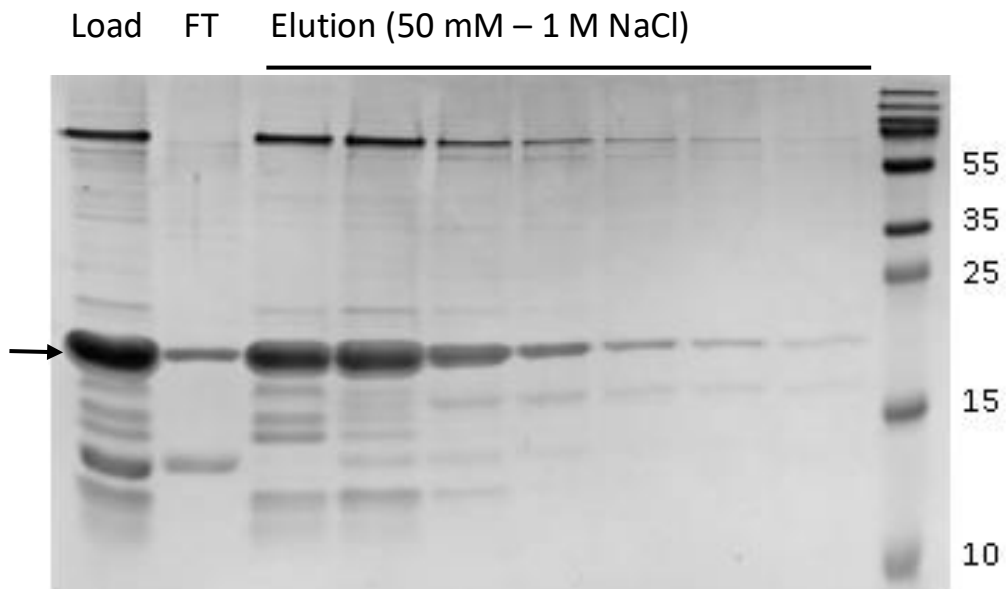


Figure 5.15: SDS-PAGE analysis of fractions from HPLC purification of IsoD using a 1 mL Q-Sepharose column. The band corresponding to IsoD has been indicated with an arrow.

Very few of the contaminating protein bands were removed by this anion exchange step. Consequently, the anion exchange step was omitted in subsequent purification protocols and gel filtration was then utilised in an attempt to clean up the preparation of IsoD.

5.4.2. Purification of IsoD by gel filtration chromatography

Fractions corresponding to the peak of IsoD from the Q- Sepharose column were pooled and spin concentrated to 2 mL as outlined in the previous section. This sample was applied at 0.5 mL min⁻¹ to a Superdex 200 10/300 gel filtration column equilibrated with buffer containing 50 mM sodium phosphate and 150 mM NaCl (pH 7.4). Two column volumes of buffer were passed through the column at 1 mL min⁻¹ (AKTA trace presented in Figure 5.16), and samples of the fractions were run on an SDS-PAGE gel (section 2.7.4). This analysis (Figure 5.17) showed that the dominant protein band had shifted to a higher position on the gel. Repeating the whole process did not give an obvious reason for what was happening, since the band size varied regardless of which buffer the protein sample was in, which column it had been eluted from, and whether the polyacrylamide gel utilised for analysis of fractions was premade or not (results not shown). Whilst anomalous migration on polyacrylamide gels of the coupling protein has been mentioned in the SDIMO literature (Champreda *et al.*, 2004), none of the coupling proteins previously examined have been reported to run as multiple bands on SDS-PAGE gels.

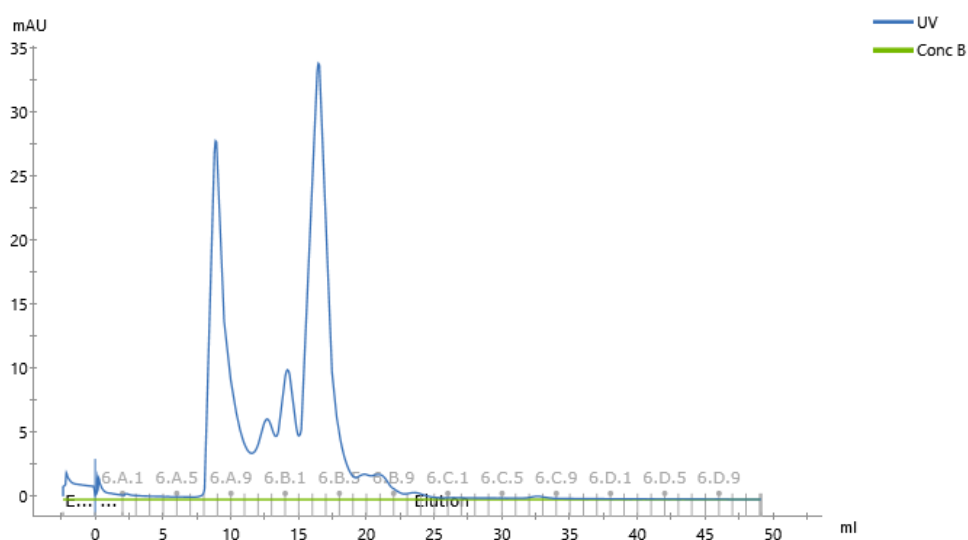


Figure 5.16: HPLC trace of purification of IsoD using a Superdex 200 pg 10/300 gel filtration column using an AKTApure system.

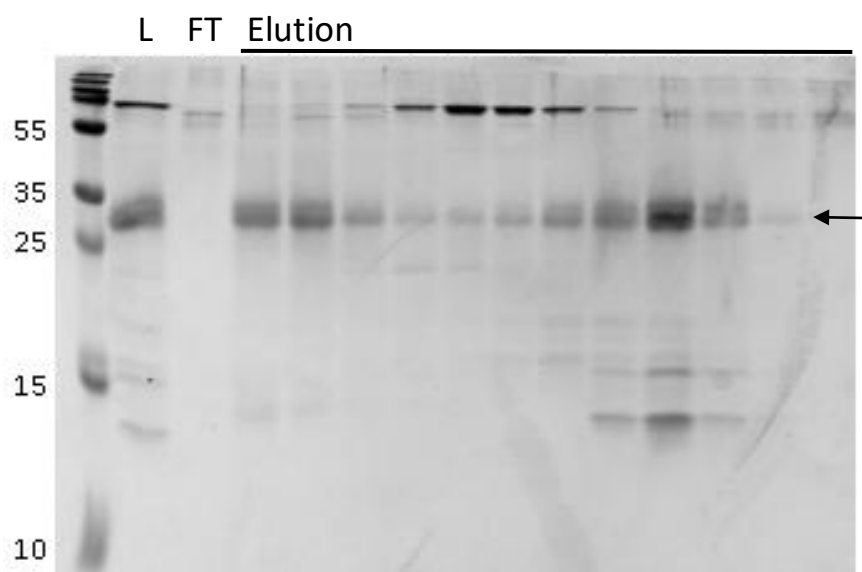


Figure 5.17: SDS-PAGE analysis of fractions from HPLC purification of IsoD using a Superdex 200 pg 10/300 gel filtration column. The band corresponding to IsoD has been indicated with an arrow.

Whilst the gel filtration appeared to have enhanced the purity of the sample by removing many of the larger contaminating proteins, some issues still remained. Some of the predicted IsoD protein eluted at the beginning of the elution profile, suggesting that some of the IsoD could be aggregating. This has been reported previously, where the coupling protein from soluble methane monooxygenase was found to aggregate in concentrated solutions (Chang *et al.*, 1999). In addition, there were some lower molecular mass contaminants present which had still not been removed. This was a concern as a number of coupling proteins from soluble methane monooxygenase systems have been found to truncate, particularly when expressed in *Escherichia coli*, which resulted in inactivation of the coupling protein (Lloyd *et al.*, 1997; Shinohara *et al.*, 1998). In order to attempt to remove these proteins, hydrophobic interaction chromatography was used.

5.4.3. Hydrophobic interaction chromatography purification of IsoD

Hydrophobic interaction chromatography was chosen as it has successfully been used to purify the coupling protein of the alkene monooxygenase from *Xanthobacter* sp. Py2 (Small and Ensign, 1997). For application of the IsoD sample to a 15 mL Phenyl Sepharose column, the fractions corresponding to predicted non-aggregated IsoD from the gel filtration

column (Figure 5.17) was stirred at 4 °C while ammonium sulfate was slowly added to 2 M. The binding and elution buffers for Phenyl Sepharose chromatography are detailed in section 2.11.3.

The sample was centrifuged at 16,000 x *g* and the supernatant filtered to ensure that no precipitated protein was added to the column. The load, column flow through and precipitated protein resuspended in 50 mM phosphate buffer were analysed by SDS-PAGE gel (Figure 5.18), and showed that both the protein of interest and contaminants were partially precipitated at the high ammonium sulfate concentration (2 M). Due to this, it was possible that removal of the StrepII tag and re-applying to the StrepTactin column may be the only way to remove these contaminants, which was attempted next.

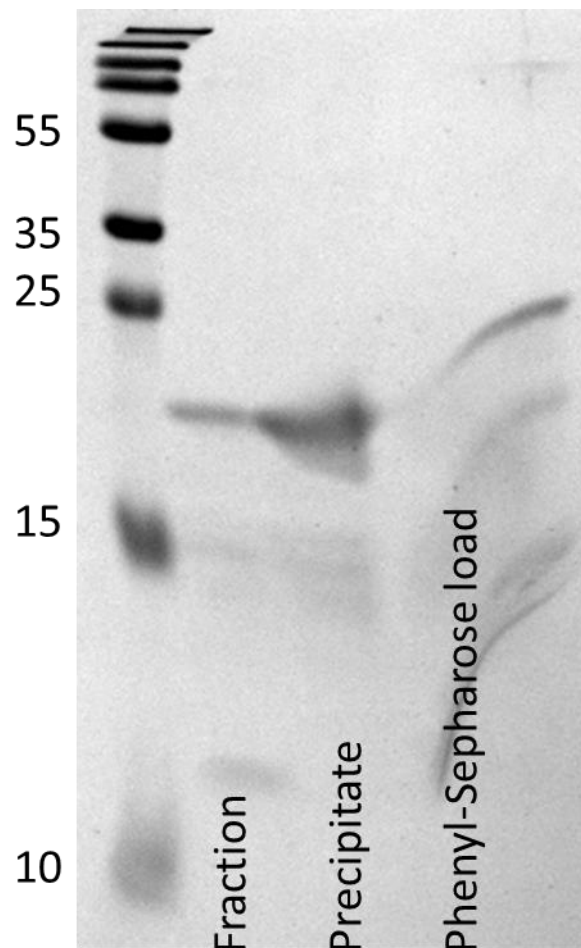


Figure 5.18: SDS-PAGE analysis of IsoD sample before and after addition of 2 M ammonium sulfate. The sample with ammonium sulfate added was centrifuged and both the pellet (Precipitate) and supernatant (Phenyl Sepharose load) were analysed.

5.4.4. Enterokinase cleavage of the N-terminal Strep-II Tag from recombinant IsoD
After the failed attempt at a cleaning step with Phenyl Sepharose, the full process was repeated again with a fresh transformation of *Escherichia coli* Rosetta 2 (pLysS) with pET51b:*isoD* being grown in 1500 mL of batch culture split into three 2 L flasks (section 2.3.1). The harvest and initial steps of purification were carried out as above with omission of the Q-Sepharose column anion exchange step as this did not seem to considerably improve the sample purity.

The same fractions from the gel filtration elution were concentrated to 5 mL (as described previously), followed by dialysis into the buffer for enterokinase cleavage (20 mM Tris-HCl, 50 mM NaCl, 2 mM CaCl₂, pH 8.0). The total protein content of the sample was estimated at 7 mg based on a Bradford protein assay (section 2.7.1). Enterokinase (New England Biolabs Inc., 2.5 µL/mg protein) was added to the IsoD sample and incubated at 20 °C for 16 h to cleave the N-terminal StrepII tag from IsoD, as per manufacturer's instructions. The resulting protein sample was applied to the StrepTactin-XT 5 mL column at 0.5 mL min⁻¹ and the same program as outlined in section 5.4.1 was used. The AKTA trace from this HPLC run is presented in Figure 5.19. This demonstrated that some of the cleaved IsoD appears to be present in the flow through. Samples of the flow-through and elution were analysed using SDS-PAGE (section 2.7.4), the results of which are shown in Figure 5.20. The SDS-PAGE analysis demonstrated that much of the IsoD remained uncleaved and in the elution.

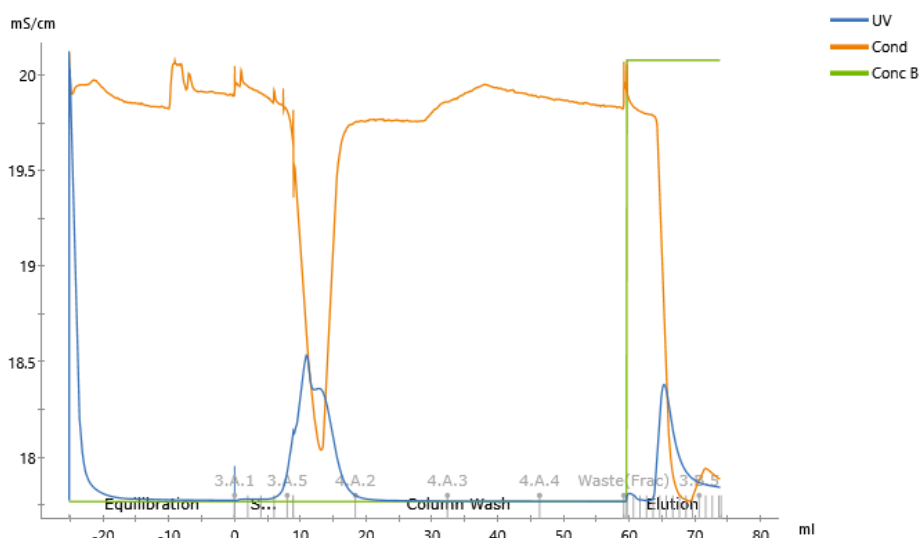


Figure 5.19: HPLC trace of IsoD purification after StrepII-tag removal using a 5 mL StrepTactin-XT column.

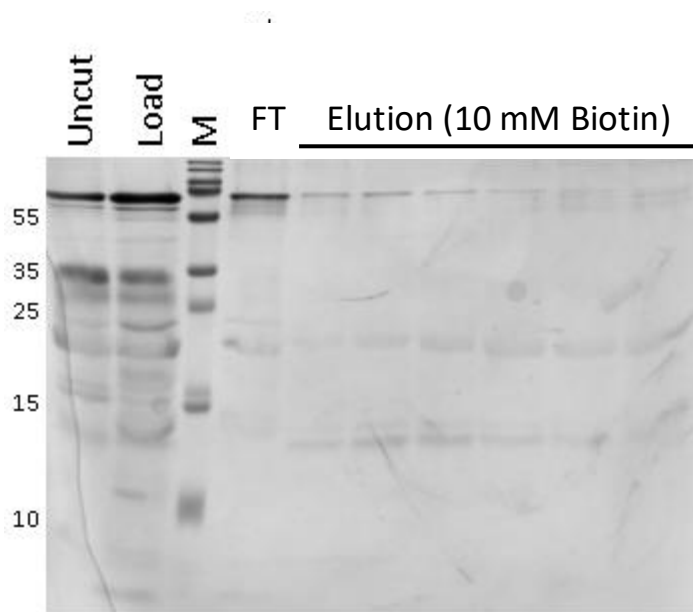


Figure 5.20: SDS-PAGE analysis of fractions from HPLC purification of IsoD after StrepII tag removal using a 5 mL StrepTactin-XT column.

While some of the IsoD had cleaved and been recovered in the flow through, the yield was very low at less than 1 mg total protein as quantified by the Bradford assay (section 2.7.1). This was unexpected as SDIMO coupling proteins have been well documented to contain N-terminal unstructured tails (Brandstetter *et al.*, 1999; Chang *et al.*, 1999; Walters *et al.*, 1999; Hemmi *et al.*, 2001; Lountos *et al.*, 2005; Lee *et al.*, 2013; Acheson *et al.*, 2017), which should have made the tag easily accessible for the protease. The poor cleavage and low yield suggested that enterokinase cleavage may not be practical for IsoD purification. Intact fusion and tagged coupling proteins from the sMMO of *Methylococcus capsulatus* (Bath), alkene monooxygenase from *Xanthobacter* sp. Py2 and toluene 4-monooxygenase from *Pseudomonas mendocina* sp. KR1 have been documented as functional in the past (Brandstetter *et al.*, 1999; Champreda *et al.*, 2004; Moe *et al.*, 2006), which suggested that reconstitution may occur even without the removal of the tag. Indeed, one study found that cleaving the GST fusion protein from the alkene monooxygenase coupling protein from *Rhodococcus rhodochrous* B-276 removed all activity (Smith *et al.*, 1999), so research into IsoD continued with the StrepII tag still in place. The purity and anomalous gel migration of the IsoD samples was became the next issue to be tackled.

5.4.5. Preventing anomalous migration of IsoD in SDS-PAGE analysis

By diluting IsoD samples from the gel filtration step into varying concentrations of Tris-HCl buffer and NaCl, and attempting to freeze a small sample it was found that none of these had an effect on how the protein ran on the SDS-PAGE gels (Figure 5.21). Use of higher and lower concentrations of protein (labelled as dilution factor) also seemed to have no effect.

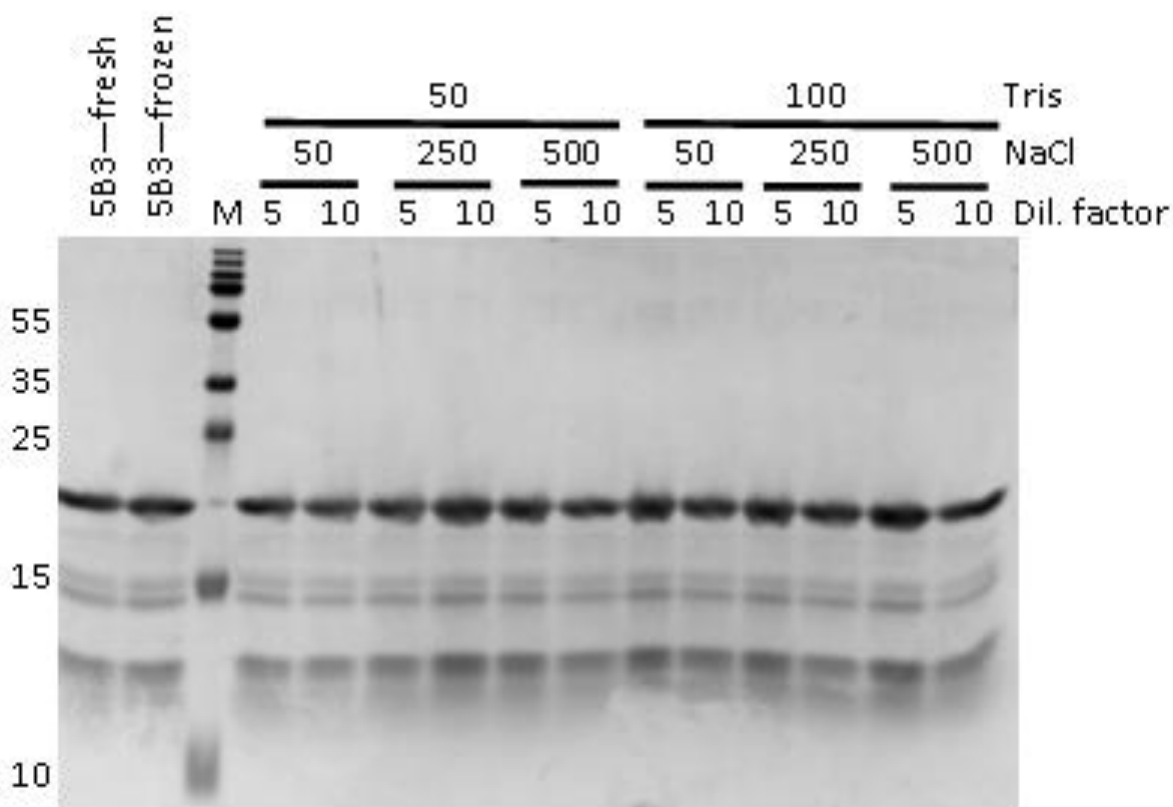


Figure 5.21: SDS-PAGE analysis of the purified IsoD sample under different buffer and salt conditions and after freezing.

As a result of the above experiment, subsequent purification of IsoD was performed in two steps, using the StrepTactin-XT affinity and gel filtration chromatography columns. Comparison of the two gel filtration attempts in Figure 5.22 showed that the shorter purification time achieved by using only two columns resulted in a higher proportion of IsoD being present in the second elution peak, suggesting that less of the protein had aggregated. The use of more rapid purification protocols with coupling proteins from SDIMOs has been advised previously, with the purification of the coupling protein from

soluble methane monooxygenase being adjusted to affinity chromatography to minimise inactivation of the component (Lloyd *et al.*, 1997; Smith *et al.*, 1999).

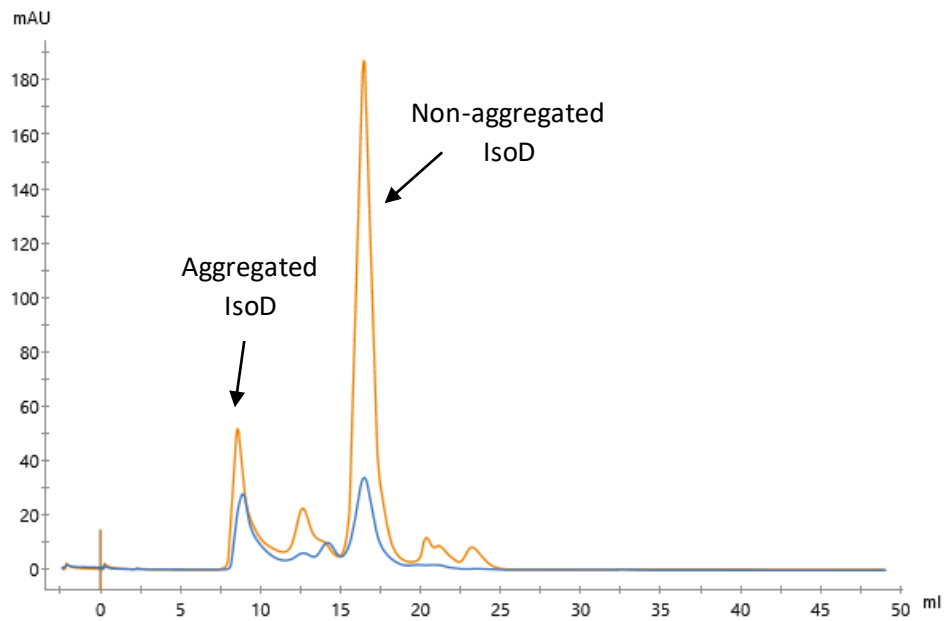


Figure 5.22: Comparison of IsoD purification by gel filtration one (orange line) or three (blue line) days after cell breakage. The peaks associated with standard and aggregated IsoD have been labelled with arrows.

5.5. Absorbance spectrum of IsoD from *Rhodococcus* sp. AD45

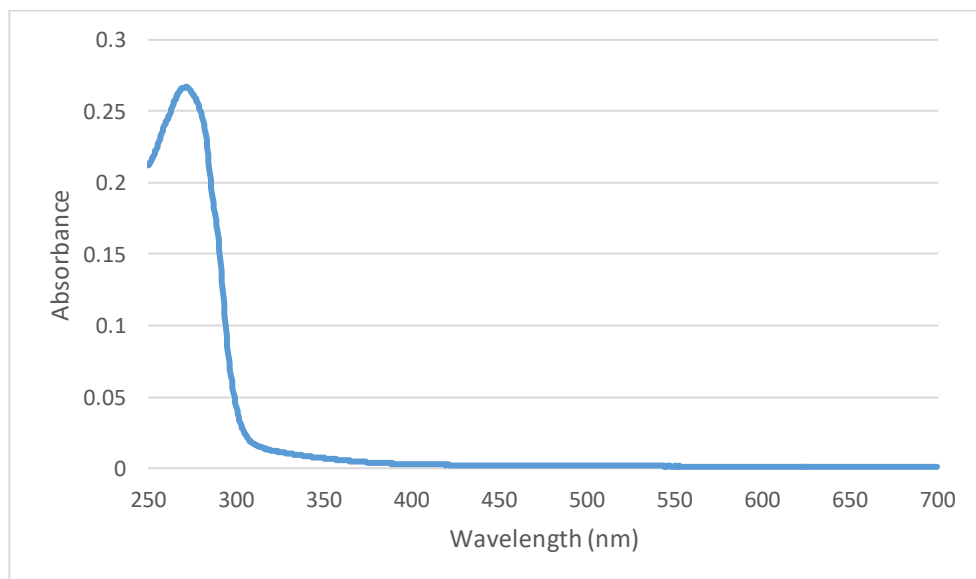


Figure 5.23: Absorption profile of IsoD.

In order to establish whether any cofactors with spectroscopic features were present in IsoD, absorbance spectroscopy was performed. No absorbance peaks were observed between 300 and 800 nm (Figure 5.23), indicating a lack of optically active cofactors. This was expected, as has been shown for a number of other purified coupling proteins, including those of alkene monooxygenase from *Xanthobacter* sp. Py2 (Small and Ensign, 1997) and soluble methane monooxygenase from *Methylosinus trichosporium* OB3b (Fox *et al.*, 1989).

5.6. LC-MS analysis of IsoD from *Rhodococcus* sp. AD45

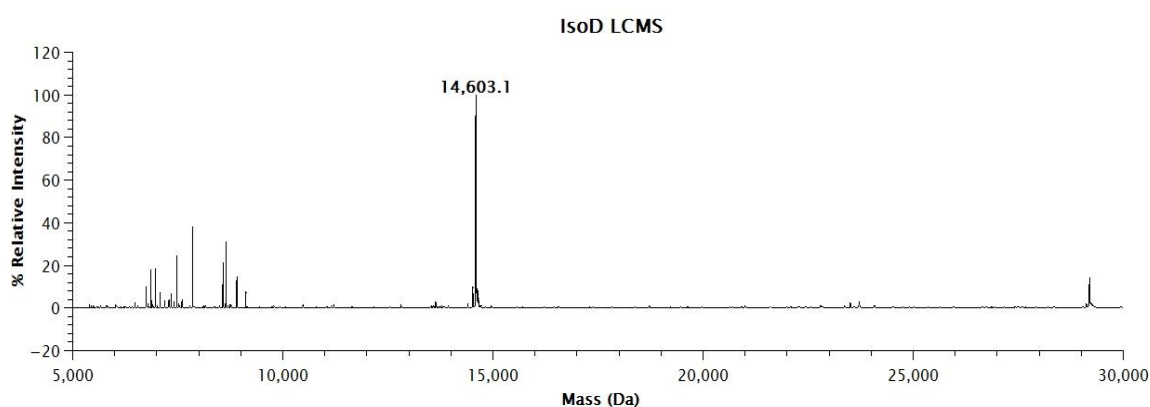


Figure 5.24: LC-MS analysis of purified N-terminally StrepII-tagged IsoD. Expected mass 14,735 Da.

The LC-MS analysis of purified IsoD showed that the main constituent of the sample was a protein of 14,603 Da (Figure 5.24). This suggested that StrepII-tagged IsoD was the protein most dominant in the sample and that the N-terminal methionine had been cleaved from the protein, as the tagged protein had a predicted molecular mass of 14,735 Da. There was a range of lower molecular mass contaminants around 6,000 – 9,000 Da. These explained the less intense smears lower on the SDS-PAGE gel, however these also appeared to migrate at a higher apparent molecular mass than they were observed on the gel (Figure 5.21). There is no clear single protein in the deconvoluted LC-MS data which would suggest a truncation, such as that observed for the methane monooxygenase. The methane monooxygenase coupling protein truncates between Met12 and Gly13, which was alleviated by a Gly – Gln modification without compromising reconstituted monooxygenase

activity (Lloyd *et al.*, 1997). The IsoD amino acid sequence does not contain this site, resulting in purified IsoD running as a single band rather than doublet during SDS-PAGE. This characteristic is shared with the four-component monooxygenases alkene monooxygenase from *Xanthobacter* sp. Py2 (Small and Ensign, 1997) and toluene 4-monooxygenase from *Pseudomonas mendocina* sp. KR1 (Pikus *et al.*, 1996).

5.7. Conclusions

In this chapter, results of the purification and characterisation of the coupling protein component of isoprene monooxygenase from *Rhodococcus* sp. AD45 have been presented. IsoD was heterologously expressed as an N-terminally StrepII-tagged protein in *Escherichia coli*, after the homologous expression system used in Chapter 4 resulted in low yield which could not be tracked by SDS-PAGE analysis due to anomalous migration. The StrepII-tagged IsoD was purified using a combination of affinity, anion exchange and gel filtration chromatography, and the faster these steps were performed the less IsoD was found to aggregate before the final gel filtration chromatography step.

The absorbance spectrum of purified IsoD showed no optically active cofactors were present, as expected. Subsequent LC-MS analysis of the purified protein demonstrated that the N-terminal methionine was cleaved, and that no truncations which could affect activity were occurring, unlike in some other SDIMOs.

In the next chapter, results will be presented of purification and characterisation of a range of SDIMO reductases, including IsoF. These transfer electrons from NADH to the Rieske protein, and are the final SDIMO subunit which does not form part of the oxygenase.

6. Purification and characterisation of IsoF: The reductase component of isoprene monooxygenase from *Rhodococcus* sp. AD45

6.1. Introduction

In this chapter the results of work on the reductase component of the isoprene monooxygenase from *Rhodococcus* sp. AD45, termed IsoF, will be presented. The reductase component of SDIMOs enables the shuttling of electrons from NADH through the FAD and [2Fe-2S] cluster cofactors. The electron shuttled either goes straight to the hydroxylase in three-component systems (Lund *et al.*, 1985), or through the Rieske protein in the four-component systems (Cafaro *et al.*, 2002). The reductase component of SDIMOs has historically been the most troublesome to purify and characterise, with recombinant systems often leading to formation of inclusion bodies (Pikus *et al.*, 1996; Cafaro *et al.*, 2002; Champreda *et al.*, 2004; Bailey, Elsen, *et al.*, 2008; Oppenheimer *et al.*, 2010). Compounding this problem of purification, often the natively purified protein would rapidly lose activity (Miura and Dalton, 1995; Small and Ensign, 1997). This chapter will illustrate that IsoF is no different, with production of recombinant protein being attempted in both *Rhodococcus* sp. AD45-ID and *Escherichia coli*, using a variety of protein tags and fusions.

A recombinant IsoF protein fused to maltose binding protein (MBP) was successfully expressed in *Escherichia coli*. Purification and cleavage of the MBP tag yielded a single polypeptide which was checked for NADH inducible potassium ferricyanide reductase activity, absorption spectrum characteristics and the molecular mass based on LC-MS.

Finally, GST fusions of the reductases from soluble methane monooxygenase of *Methylococcus capsulatus* (Bath), alkene monooxygenase of *Rhodococcus rhodochrous* sp. B-276 (as controls), isoprene monooxygenase from *Rhodococcus* sp. AD45, and an MBP fusion of toluene 4-monooxygenase reductase were expressed in *Escherichia coli*, purified using affinity chromatography and compared in terms of absorption spectroscopy and activity in both fusion and cleaved proteins.

6.2. Cloning *isoD* from *Rhodococcus* sp. AD45 into the pTipQC1 expression plasmid for expression in *Rhodococcus* sp. AD45-ID

Originally, the cloning of *isoF* for purification of the reductase component of isoprene monooxygenase from *Rhodococcus* sp. AD45 was attempted using the same homologous expression system utilised for IsoC purification (Chapter 4). This is because the majority of work on reductases, particularly those of the soluble methane monooxygenases, has been performed on those purified from the native producer rather than recombinant proteins (Colby and Dalton, 1979; Hartmans *et al.*, 1991; Nakajima *et al.*, 1992; Miura and Dalton, 1995; Newman and Wackett, 1995; Kopp *et al.*, 2001). Many attempts to express recombinant SDIMO reductases in *Escherichia coli* resulted in the formation of inclusion bodies or inactive protein (Cafaro *et al.*, 2002; Champreda *et al.*, 2004; Oppenheimer *et al.*, 2010). This suggested that a homologous expression system may be a promising start, and the pTip system for expression of His-tagged proteins in *Rhodococcus* sp. AD45 could aid in the fast purification of IsoF, minimising the risk of activity loss during long purifications, which has also been reported as an issue (Whited and Gibson, 1991; Miura and Dalton, 1995; Small and Ensign, 1997).

6.2.1. Amplification of *isoF* from *Rhodococcus* sp. AD45 genomic DNA

The *isoF* gene was amplified from *Rhodococcus* sp. AD45 genomic DNA, a gift from Andrew Crombie (Murrell lab, University of East Anglia). The PCR used to accomplish this utilised the high-fidelity Q5 DNA polymerase and was described in section 2.5.2, and the primers used are presented in Table 6.1. All cloning steps were performed using *Escherichia coli* TOP10 cells. The expression vector was constructed following the same steps as described in section 4.2 for the production of the pTipQC1:*isoC* expression vector. The expression vector, designated pTipQC1:*isoF* (Figure 6.1), was designed to produce IsoF in the homologous expression strain *Rhodococcus* sp. AD45-ID, yielding an N-terminally 6-histidine tagged protein for fast purification using IMAC. The vector was ratified by DNA sequencing at MWG Eurofins (section 2.5.8).

Table 6.1: Primer sequences used for polymerase chain reaction amplification of *isoF* from *Rhodococcus* sp. AD45 genomic DNA and cloning into expression vectors.

| Primer Name | Sequence (5' – 3') | Restriction Site | Orientation |
|-------------|-------------------------------------|------------------|-------------|
| isoFF | ATATATCATATGACTGTCACAGTGAATTTCAATGG | <i>Nde</i> I | Forward |
| isoFR | ATATATGGATCCGGATTCGGGGGTAGT | <i>Bam</i> HI | Reverse |

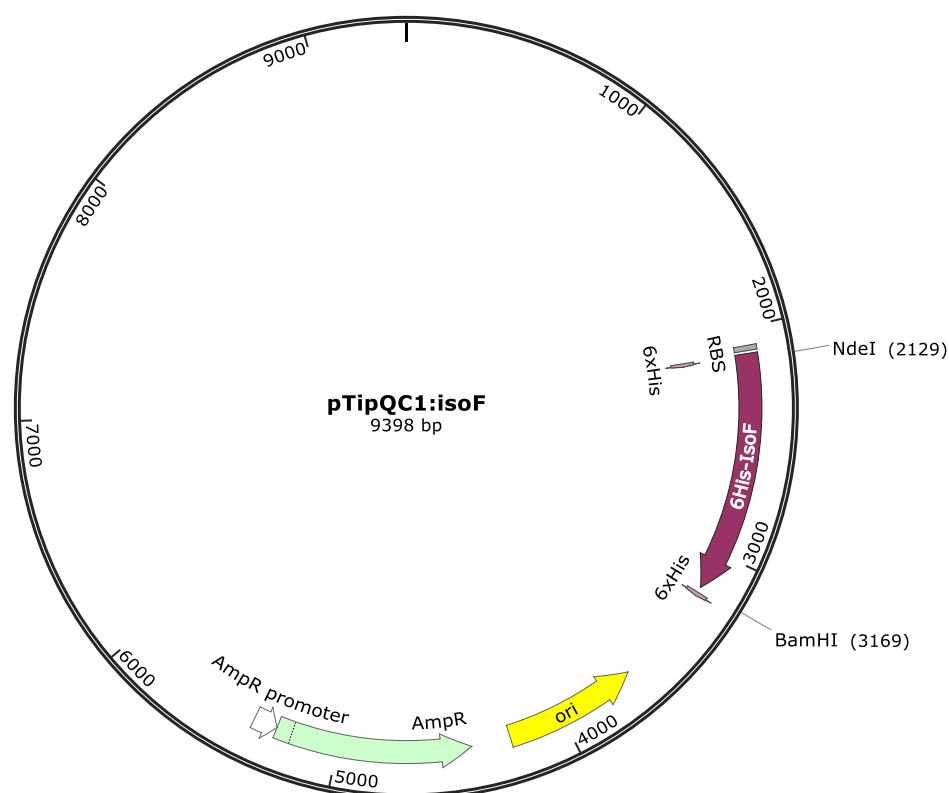


Figure 6.1: pTipQC1:*isoF* vector map for expression of *isoF* from *Rhodococcus* sp AD45 in *Rhodococcus* sp. AD45-ID.

6.2.2. Production of IsoF in the *Rhodococcus* sp. AD45-ID homologous expression system

The pTipQC1:*isoF* plasmid was used to transform *Rhodococcus* sp. AD45-ID cells by electroporation (section 2.3.4). The cells were then plated onto minimal medium plates containing 10 mM succinate as a carbon source and chloramphenicol to select for successful transformants. Successful transformants were grown in batch culture (section

2.3.3) using the same liquid minimal medium as the base for the agar plates. The His-tagged IsoF protein was predicted to have a molecular mass of 39.8 kDa, and a polypeptide band of approximately the correct molecular mass could be visualised by SDS-PAGE analysis of soluble cell extract from induced cultures (Figure 6.2).

To verify that the faint band was the His-tagged IsoF as anticipated, the cell lysate of the *Rhodococcus* sp. AD45-ID transformants (section 2.7) was applied to 1 mL HisTrap spin-columns (GE Life Sciences), according to manufacturer's instructions. SDS-PAGE analysis of the cell lysate, flow through, wash and elution steps of the partial purification yielded a faint band of the expected size (Figure 6.3). The amount of IsoF present was low, as found with the IsoD expression trials (section 5.2.2), in contrast to the expression of the Rieske protein, IsoC, using the same pTipQC1 vector base (section 4.3). As optimisation of protein production using the homologous expression system had been unsuccessful for both expression of IsoC (section 4.3) and IsoD (section 5.2.2), it was not attempted for IsoF.

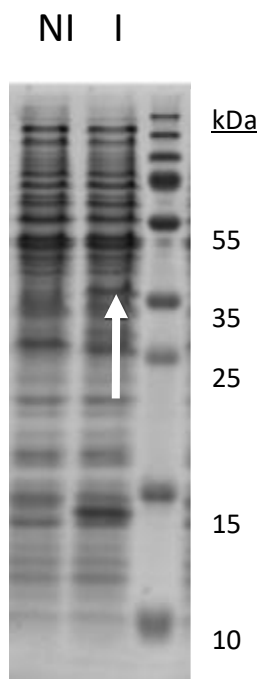


Figure 6.2: Polypeptide profiles of *Rhodococcus* sp. AD45 expressing pTipQC1:*isoF* as determined by SDS-PAGE. AD45-ID cultures were either non-induced (N) or induced with $1 \mu\text{g ml}^{-1}$ thiostrepton (I) to produce a His-tagged IsoF protein, which has been indicated with an arrow.

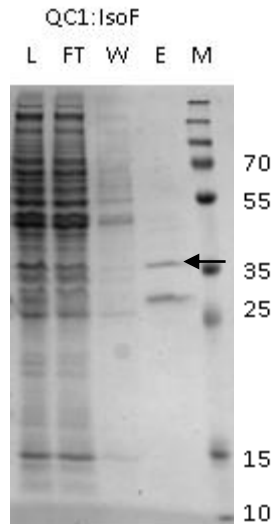


Figure 6.3: Polypeptide profiles of IsoF partial purification by 1 mL HisTrap spin-columns as determined by SDS-PAGE. CL is cell lysate, FT is flow through, W is wash and E is elution. The band predicted to correspond to IsoF has been indicated with an arrow.

6.2.3. Attempted purification of IsoF from *Rhodococcus* sp. AD45-ID containing pTipQC1:*isoF*

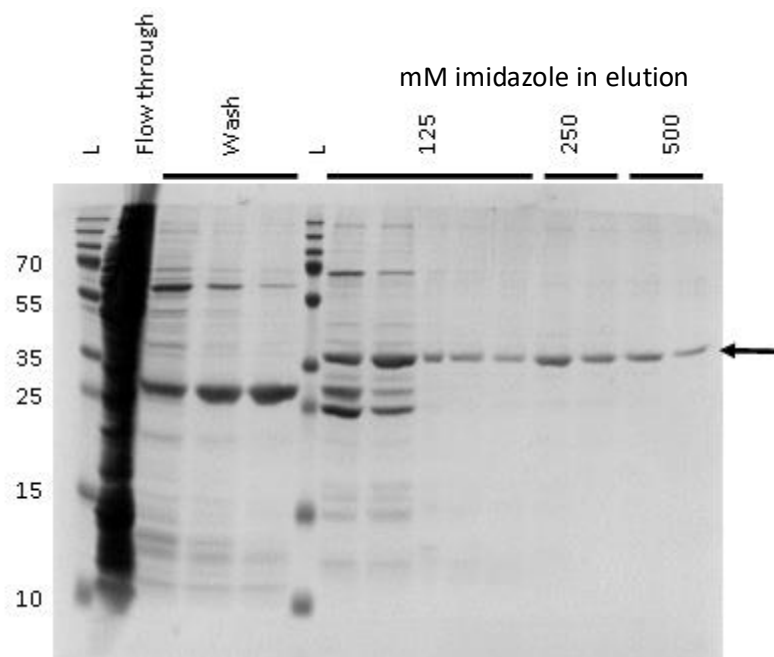


Figure 6.4: Attempted purification of IsoF from *Rhodococcus* sp. AD45 (pTipQC1:*isoF*) using a 5 mL HisTrap column and stepped elution with 125 – 500 mM imidazole. Polypeptide profiles of fractions were visualised using SDS-PAGE and InstantBlue staining.

The initial attempt to purify IsoF was performed on the bench with a Luer syringe and 5 mL HisTrap IMAC column using the cell lysate from 2 L batch growth of *Rhodococcus* sp. AD45-ID (pTipQC1:*isoF*). Concentrations of imidazole were varied between 40 and 500 mM by altering the ratio of binding and elution buffers (section 2.11.1) in a stepped elution. IsoF eluted from the column across a wide range of imidazole concentrations (Figure 6.4), suggesting an issue with the His tag interaction with the column. The eluent was always colourless and showed no spectroscopic characteristics (section 2.12.1) of either the predicted FAD or [2Fe-2S] clusters (Figure 6.5), suggesting that they had either not been correctly incorporated into the recombinant protein or they were being stripped during the IMAC purification process.

The use of ammonium sulfate precipitation had been used successfully in the purification of recombinant toluene 4-monooxygenase reductase (T4moF) of *Pseudomonas mendocina* KR1 (Pikus *et al.*, 1996), so this became the next strategy for IsoF purification. This would theoretically allow determination of whether the protein was not being produced properly or whether the IMAC purification step was the issue.

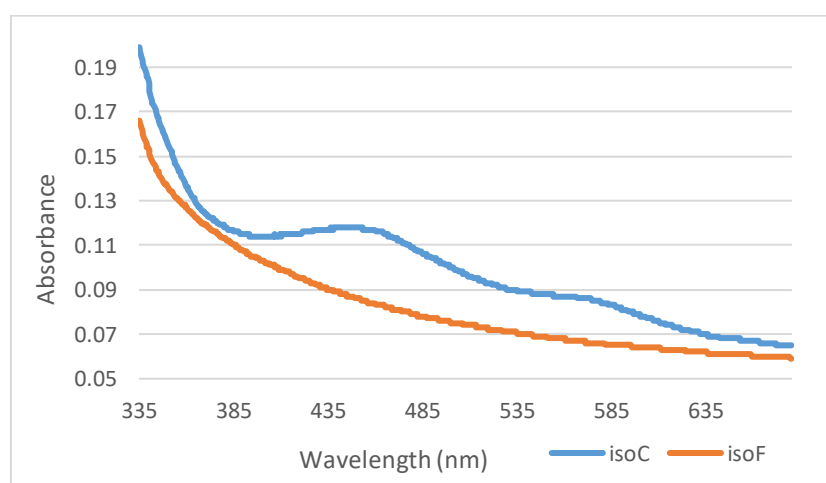


Figure 6.5: Absorbance spectrum of IsoF partially purified by HisTrap column in comparison to the equivalent purification of IsoC.

Ammonium sulfate was added slowly at 4 °C up to 45 % w/v to a stirred cell lysate made from 6 x 1 L batch cultures of *Rhodococcus* sp. AD45-ID (pTipQC1:*isoF*). SDS-PAGE analysis of polypeptide profiles of the cell lysate at several intervals after centrifugation to remove precipitated proteins resulted in no clear precipitation of any individual polypeptide bands at any concentration of ammonium sulfate, suggesting that this technique was not working to successfully precipitate IsoF (Figure 6.6). At the final concentration of ammonium sulfate

(45 % w/v) most proteins had been precipitated out. This was unexpected, and led to attempted IsoF purification by applying cell lysate from the same sized culture to an anion exchange column.

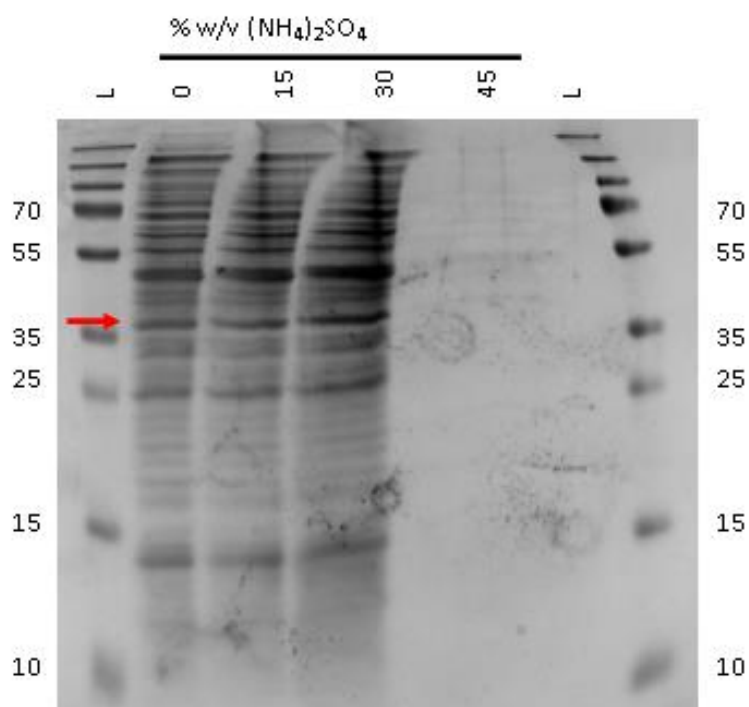


Figure 6.6: Ammonium sulfate precipitation of proteins in *Rhodococcus* sp. AD45-ID (pTipQC1:*isoF*) cell lysate. Each lane represents the non-precipitated proteins of that trial.

Anion exchange has been used as an initial step in purification of numerous SDIMO reductases from their native producers (Whited and Gibson, 1991; Nakajima *et al.*, 1992; Miura and Dalton, 1995; Newman and Wackett, 1995; Small and Ensign, 1997; Grosse *et al.*, 1999; Pessione *et al.*, 1999). The Q-Sepharose column utilised here and the purification performed used an AKTApure HPLC system with UNICORN™ 7 software. The binding and elution buffers are outlined in section 2.11.2. The cell pellet was resuspended in binding buffer and the lysate prepared. The cell lysate was filtered and applied to the ~130 mL Q-Sepharose column. The column was washed in 130 mL of binding buffer followed by a linear gradient elution from 0 – 1 M NaCl over 260 mL. The HPLC trace of this purification is shown in Figure 6.7. Samples from the cell lysate, flow through and two of the elution fractions with a clear yellow-brown colour (1C3 and 2C2) indicative of the predicted cofactors were subjected to HisTrap spin-column purification (GE Life Sciences) according to manufacturer's instructions. Results of the elution of each of these spin-columns were

assessed by SDS-PAGE, and suggested that the IsoF had not been expressed as it was not present in any of the samples (Figure 6.8).

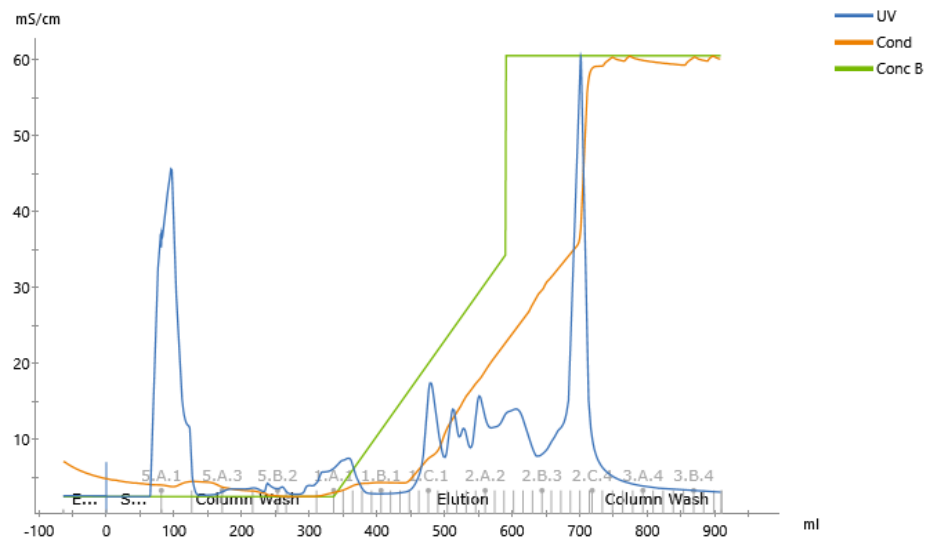


Figure 6.7: HPLC trace of a gradient elution of IsoF on a 130 mL Q-Sepharose column on an AKTApure system. The concentration of NaCl in the elution buffer (green line) varied from 0 – 550 mM (0 – 55 % buffer B) in a 260 mL gradient, followed by a 1 M step of the same volume.

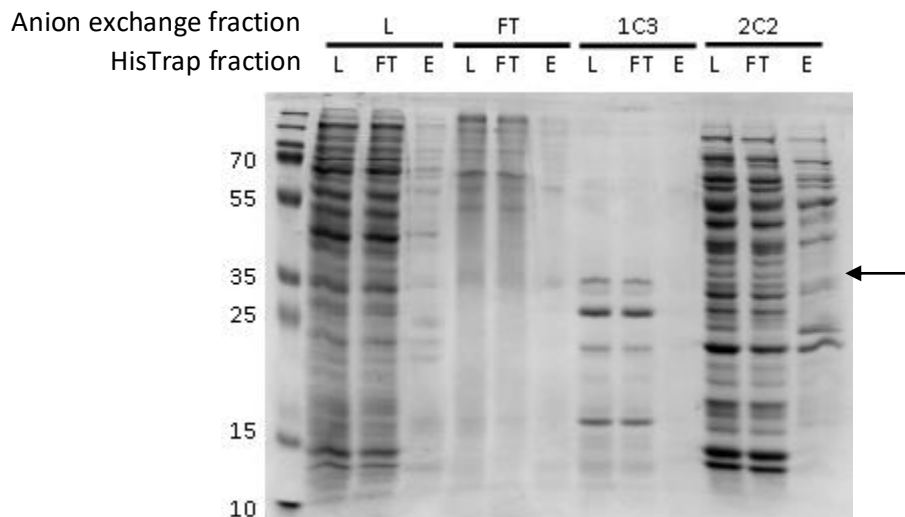


Figure 6.8: Attempted identification of fractions containing His-tagged IsoF from the anion exchange purification step using 1 mL HisTrap spin columns. L is load, FT is flow through, E is elution. Arrow indicates predicted size of IsoF

As outlined in section 5.2.3, there had been issues with poor expression in the *Rhodococcus* sp. AD45-ID homologous expression system. Because of this, the potential

for expression of IsoF in *Escherichia coli* was explored. There have been many reports of inclusion bodies forming in production of recombinant reductase in *Escherichia coli*, research groups have successfully used this method for production of some SDIMO reductases, including soluble methane monooxygenase (West *et al.*, 1992; Gassner and Lippard, 1999; Kopp *et al.*, 2001), toluene 2-monooxygenase (Newman and Wackett, 1995) and toluene/*o*-xylene monooxygenase (Tinberg *et al.*, 2011).

6.3. Cloning *isoF* from *Rhodococcus* sp. AD45 into the pET21a plasmid for expression in *Escherichia coli*

6.3.1. Production of the pET21a:*isoF* plasmid

The pJET plasmid containing the *isoF* gene used to subclone the gene into pTipQC1 was also used to subclone *isoF* into pET21a using the same restriction enzymes as in section 6.2.1. The pET21a was selected as a plasmid to enable expression of *isoF* in *Escherichia coli* Rosetta 2 (pLysS) with no tag, in case this and the interaction with the IMAC column was the cause of the aforementioned issues with purification of cofactor-containing proteins. The construction of the pET21a:*isoF* plasmid (Figure 6.9) was ratified by sequencing at MWG Eurofins (section 2.5.8).

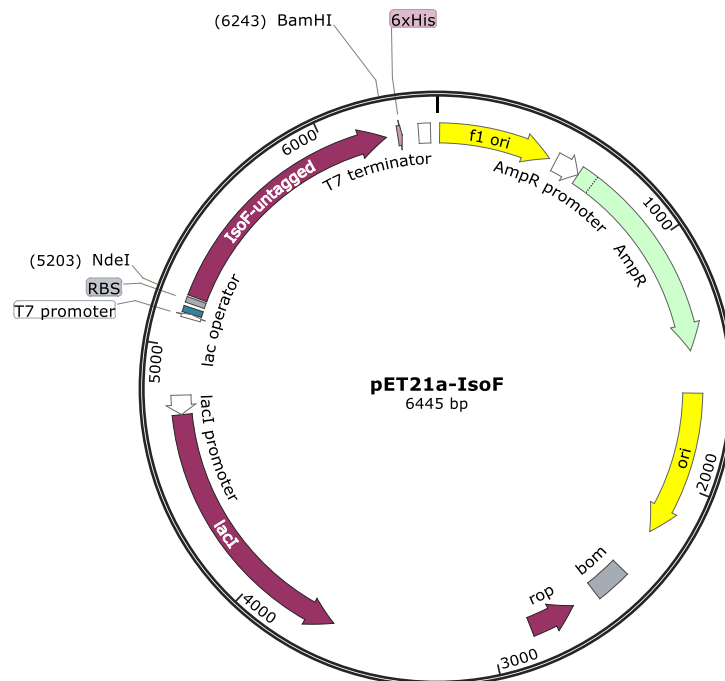


Figure 6.9: pET21a:*isoF* vector map for expression of *isoF* from *Rhodococcus* sp. AD45 in *Escherichia coli* Rosetta 2 (pLysS).

6.3.2. Production of IsoF in the *Escherichia coli* Rosetta 2 (pLysS) heterologous expression system

For the production of recombinant IsoF protein, the ratified pET21a:*isoF* vector was used to transform chemically-competent *Escherichia coli* Rosetta 2 (pLysS) cells (section 2.3.2). The standard protocol for expression of recombinant proteins (section 5.3.2) was used to test for IsoF production in 10 mL cultures of successful transformants. The cells were harvested by centrifugation (section 2.6), and broken by boiling in SDS-PAGE loading buffer. SDS-PAGE analysis of the whole-cell suspension suggested that a polypeptide of the predicted size (37.3 kDa) was being produced (Figure 6.10), however this did not determine whether this was soluble or insoluble, which has been an issue previously reported in heterologous expression in *Escherichia coli* strains of SDIMO reductase proteins. This issue has been reported for the toluene/*o*-xylene monooxygenase (Cafaro *et al.*, 2002), tetrahydrofuran monooxygenase (Oppenheimer *et al.*, 2010) and alkene monooxygenase (Champreda *et al.*, 2004) reductases.

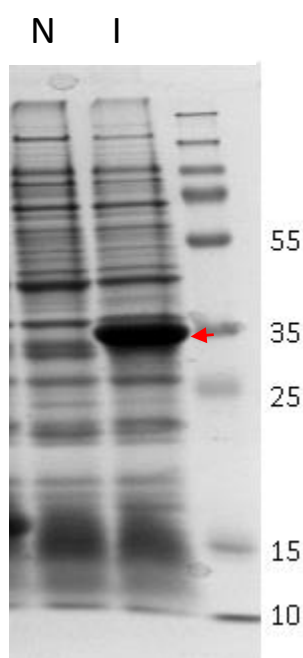


Figure 6.10: Polypeptide profiles of whole cells of *Escherichia coli* Rosetta 2 (pLysS) expressing pET21a:*isoF* as determined by SDS-PAGE. *Escherichia coli* Rosetta 2 cultures were either non-induced (N) or induced with 100 μ M IPTG (I) to produce untagged IsoF protein, which has been indicated with an arrow.

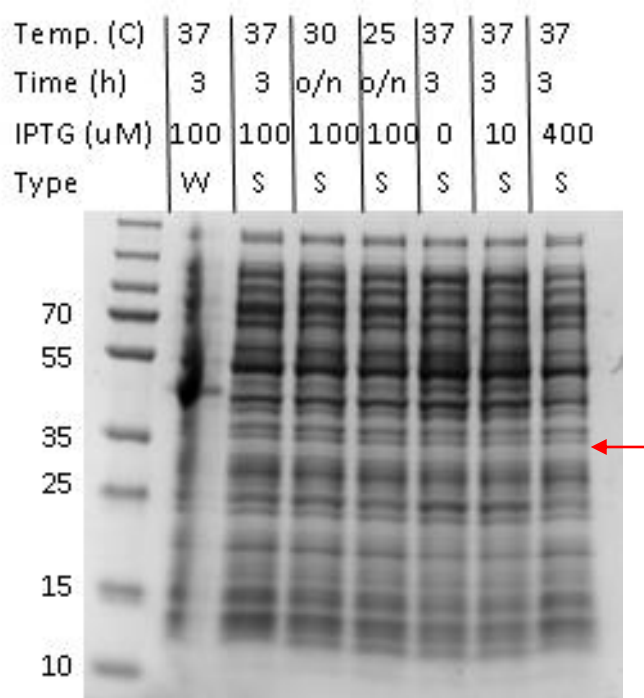


Figure 6.11: Polypeptide profiles of *Escherichia coli* Rosetta 2 (pLysS) expressing pET21a:*isoF* as determined by SDS-PAGE. The temperature at induction (°C), time of induction (h) and IPTG concentration (µM) were altered in an attempt to optimise soluble IsoF production. W samples were from whole cells, whereas S samples were soluble extract only. Predicted IsoF position is highlighted with an arrow

Subsequently, the soluble cell lysate was extracted by sonication and centrifugation (section 2.7) to check whether IsoF was forming inclusion bodies. The protocol was altered to allow expression at lower temperatures and lower concentrations of IPTG. Expression trials conducted at 25 °C or 30 °C were incubated overnight, whereas the standard 37 °C expression was only continued for three hours. Based on SDS-PAGE analysis of both soluble extract and whole-cells, IsoF was not present in the soluble fractions obtained after expression using any of the tested parameters (Figure 6.11).

Next, expression was monitored by removing samples from expression cultures over time. The induction was carried out by cold-shocking the culture on ice for 18 minutes, followed by induction with 100 µM IPTG and supplementation with 200 µM ferric ammonium iron citrate, 25 µM L-methionine, 25 µM L-cysteine and 10 µM riboflavin. This strategy was based on the protocols developed previously to enhance soluble expression of SDIMO reductases complete with their cofactors in *Escherichia coli* from the toluene 4-monooxygenase (Pikus *et al.*, 1996; Bailey, Elsen, *et al.*, 2008), alkene monooxygenase (Champreda *et al.*, 2004), soluble methane monooxygenase (Blazyk and Lippard, 2002) and

tetrahydrofuran monooxygenase systems (Oppenheimer *et al.*, 2010). The culture was then incubated at 25 °C and samples were taken after 1, 2, 3, 5 and 16 hours. These samples were subjected to sonication and centrifugation, and the soluble fraction was removed. The insoluble fraction was resuspended in a volume of phosphate buffer equal to the soluble fraction, and both were boiled with SDS-PAGE loading dye in preparation for analysis. The SDS-PAGE analysis suggested that IsoF was being produced but was insoluble within 1 hour of induction (Figure 6.12).

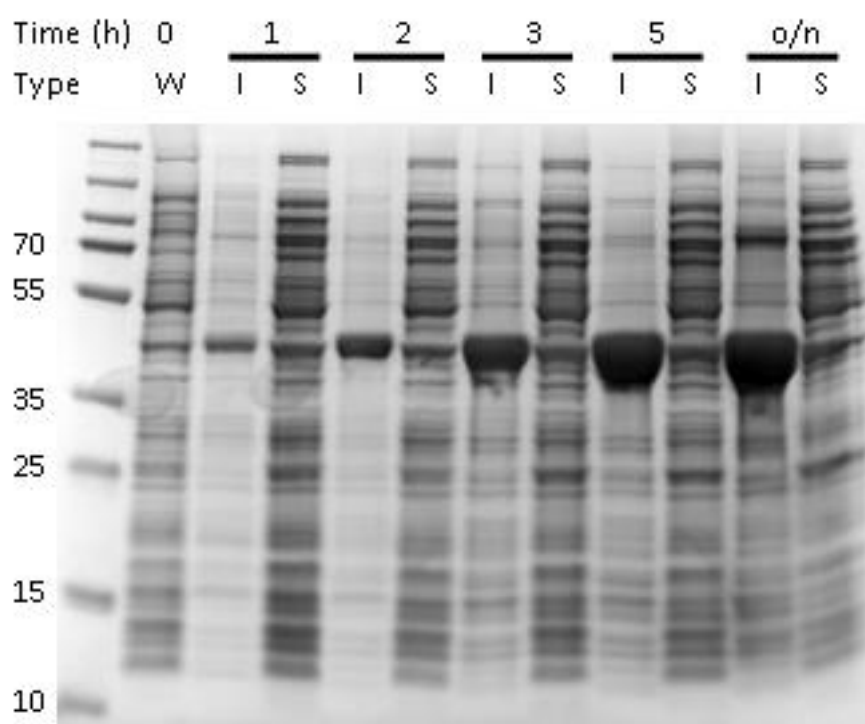


Figure 6.12: Polypeptide profile of *Escherichia coli* Rosetta 2 (pLysS) expressing pET21a:isoF as determined by SDS-PAGE. The time after induction (h) is indicated at the top. W samples were whole cells, I samples were insoluble fractions of cell extract, S samples were soluble fractions of cell extract. The culture was induced with 100 μ M IPTG at 25 °C.

Following this, the timecourse experiment outlined above was repeated using lower concentrations of IPTG (25 and 50 μ M) and a lower expression temperature (18 °C). This resulted in lower amounts of IsoF production, and it remained entirely insoluble (Figure 6.13). While the toluene/*o*-xylene monooxygenase reductase from *Pseudomonas stutzeri* OX1 has been successfully reconstituted from inclusion bodies previously (Cafaro *et al.*, 2002), this avenue was not pursued for IsoF. More recent research had suggested that the

use of maltose binding protein fusions could be used to enhance the solubility of target recombinant proteins (Raran-Kurussi and Waugh, 2012; Waugh, 2016). This technique had also been successfully used to produce recombinant tetrahydrofuran monooxygenase reductase from *Pseudonocardia* sp. K1 (Oppenheimer *et al.*, 2010) and toluene 4-monooxygenase from *Pseudomonas mendocina* sp. KR1 (Acheson *et al.*, 2015) in *Escherichia coli*. These recombinant proteins were successfully purified to a high concentration in active form, and made possible x-ray crystallographic structural analysis of toluene 4-monooxygenase reductase (Acheson *et al.*, 2015); the first reported case of this technique being used on an SDIMO reductase. Due to these promising reports, this was the next avenue of investigation for IsoF purification and characterisation.

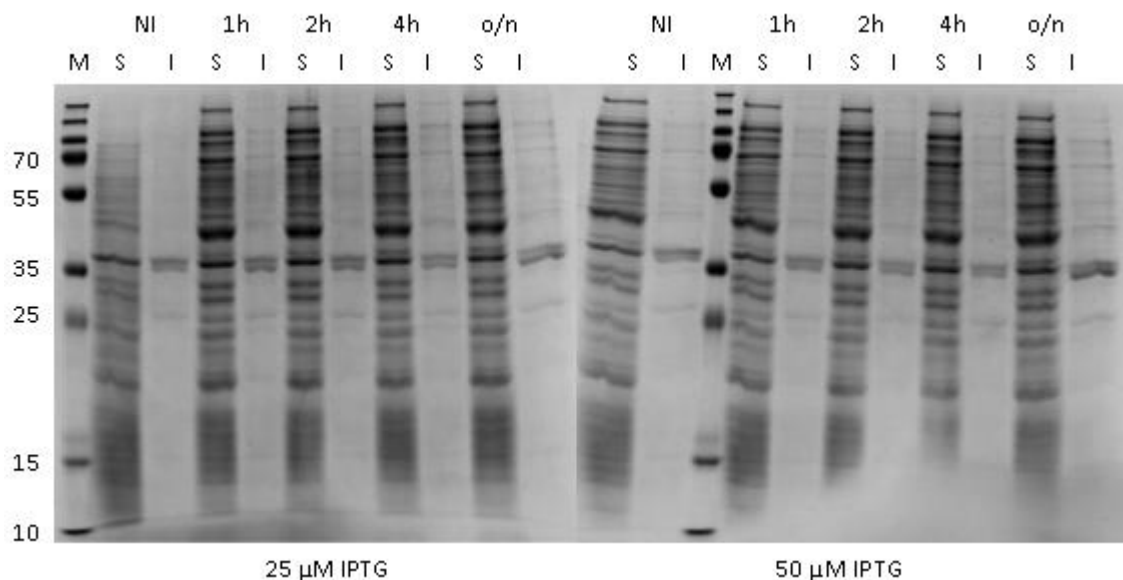


Figure 6.13: Polypeptide profile of *Escherichia coli* Rosetta 2 (pLysS) expressing pET21a:*isoF* as determined by SDS-PAGE. The time after induction (h) is indicated at the top. W samples were whole cells, I samples were insoluble fractions of cell extract, S samples were soluble fractions of cell extract. The culture was induced with 25 (left) or 50 (right) μM IPTG at 18 $^{\circ}\text{C}$.

6.4. Cloning *isoF* from *Rhodococcus* sp. AD45 into the pET20MBP plasmid for expression in *Escherichia coli* as a maltose binding protein fusion

6.4.1. Production of the pET20MBP:*isoF* expression plasmid

The pJET plasmid containing the *isoF* gene used to subclone the gene into pTipQC1 was also used to subclone *isoF* into pET20MBP using the same restriction enzymes as in section

6.2.1. The pET20MBP source plasmid was a gift from Dr N. Burton (Inspiralis, UK). The vector map of the expression plasmid, designated pET20MBP:*isoF* is presented in Figure 6.14. This expression system was designed to produce a recombinant IsoF protein in *Escherichia coli* which had an N-terminal maltose binding protein fusion which was cleavable using tobacco etch virus (TEV) protease. The sequence of the expression plasmid was ratified by sequencing at MWG Eurofins (section 2.5.8).

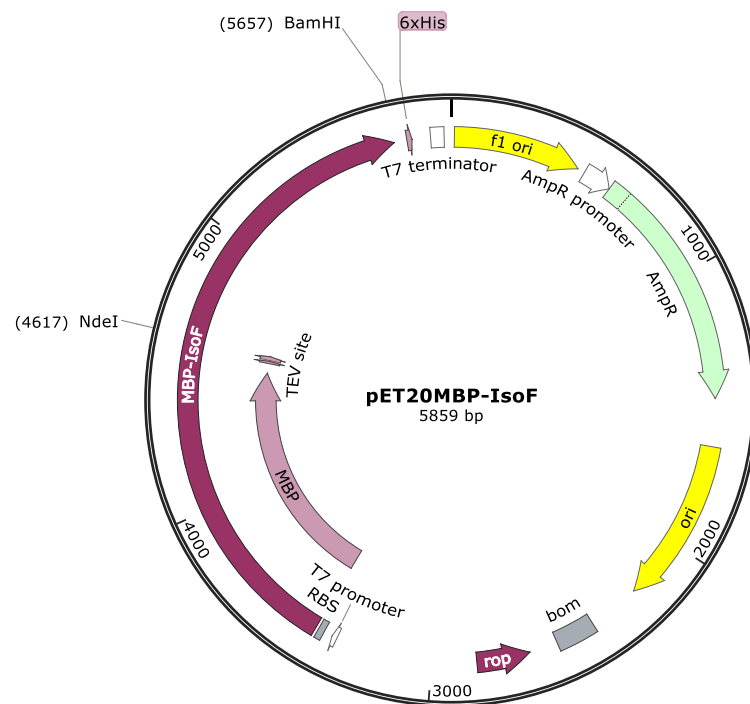


Figure 6.14: pET20MBP:*isoF* vector map for production of IsoF from *Rhodococcus* sp. AD45 as an MBP fusion in *Escherichia coli* Rosetta 2 (pLysS).

6.4.2. Production of MBP-IsoF fusion in the *Escherichia coli* heterologous expression system

The ratified pET20MBP:*isoF* vector was used to transform chemically competent *Escherichia coli* Rosetta 2 (pLysS) cells (section 2.3.2). The expression of *isoF* was induced by addition of 100 μ M IPTG using the same cold-shock and supplementation protocol outlined in section 4.3, and the production of IsoF proceeded during culture incubation at 30 °C. Again, both the soluble and insoluble protein fractions were checked after multiple time points, however in this case, SDS-PAGE analysis suggested that a polypeptide of the

predicted molecular mass (80.8 kDa) was being produced in a soluble form (Figure 6.15), so this expression protocol was used to produce larger volumes of bacterial cultures in preparation for IsoF purification.

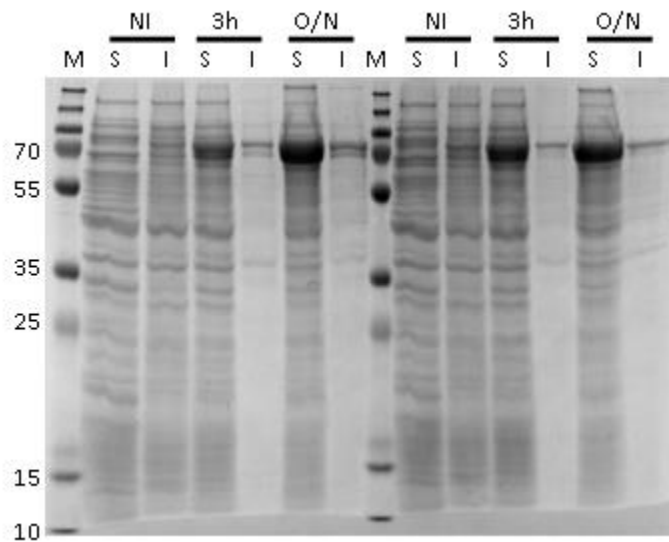


Figure 6.15: Polypeptide profile of *Escherichia coli* Rosetta 2 (pLysS) expressing pET20MBP:*isoF* as determined by SDS-PAGE. The time after induction (h) is indicated at the top. W samples were whole cells, I samples were insoluble fractions of cell extract, S samples were soluble fractions of cell extract. NI samples were non-induced, I samples were induced with 100 μ M IPTG at 30 $^{\circ}$ C.

6.5. Attempted purification of MBP-IsoF from *Escherichia coli* Rosetta 2 cells
Purification of the MBP-IsoF fusion protein was attempted using a variety of columns. All of these utilised the AKTApure HPLC system with UNICORN™ 7 software. All purification steps were carried out at 4 $^{\circ}$ C, and *Escherichia coli* cell lysate was prepared by sonication (section 2.7).

6.5.1. Affinity chromatography purification of MBP-IsoF

The affinity column used for the initial attempt at MBP-IsoF purification from *Escherichia coli* Rosetta 2 (pLysS) cells was the 5 mL MBPTrap column, the buffers for which are described in section 2.11.1. The elution buffer contained 10 mM maltose for removal of bound fusion protein from the column. The *Escherichia coli* cells for expression of MBP-IsoF was grown in batch culture, and initially 1 L of culture was used. The cells harvested by centrifugation and were washed in two volumes of binding buffer, followed by

resuspension in binding buffer to a total volume of 20 mL. The cell lysate was prepared (section 2.7), and applied to the column at 1 mL min⁻¹. The column was washed with 25 mL of binding buffer, followed by a single step elution with the elution buffer. The AKTA trace is presented in Figure 6.16 and showed a clear elution peak.

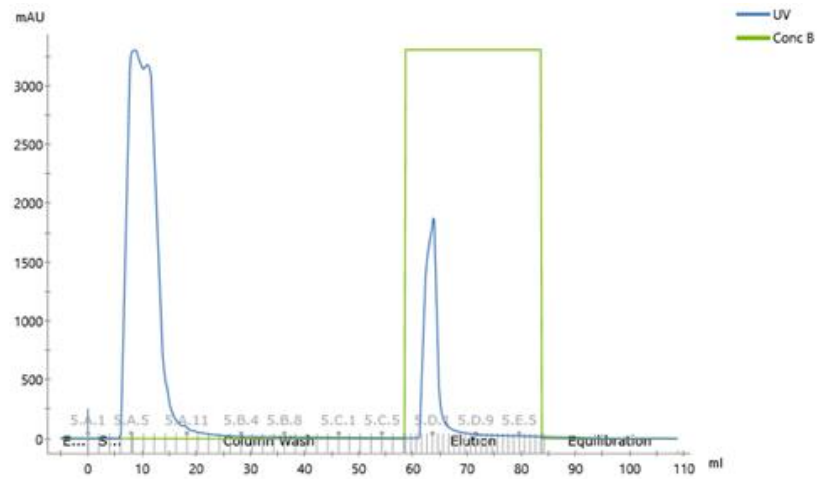


Figure 6.16: HPLC trace of a step elution of MBP-IsoF on a 5 mL MBPTrap column using an AKTApure system. The elution buffer contained 10 mM maltose.

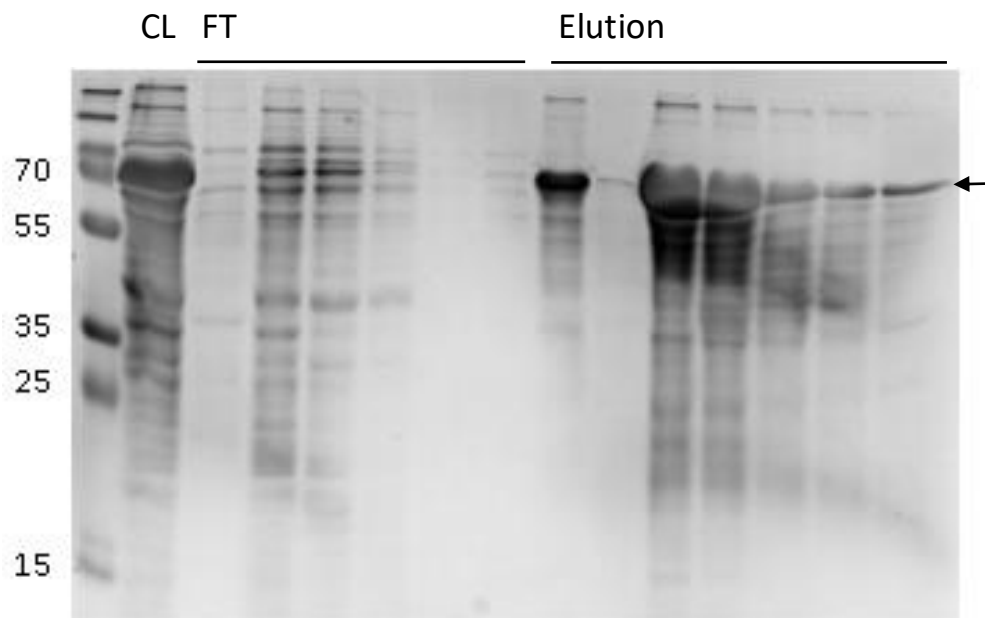


Figure 6.17: Purification of MBP-IsoF using a 5 mL MBPTrap column and step elution with 10 mM maltose using an AKTApure HPLC system. Polypeptide profiles of fractions were visualised using SDS-PAGE and InstantBlue staining.

The polypeptide profile of the flow-through and elution fractions were assessed by SDS-PAGE (Figure 6.17). This analysis suggested that the affinity column removed a lower number of contaminants than expected. The most concentrated fraction (indicated with an arrow in Figure 6.17) was subjected to absorbance spectroscopy (section 2.12.1, Figure 6.18). This showed a large amount of scattering due to the precipitation of the partially purified protein, possibly due to the high concentration. One absorbance maximum was present at approximately 420 nm, which suggested that the predicted [2Fe-2S] cluster was present, if only in low amounts, which was an improvement on the protein produced previously using the homologous expression system (section 6.2.3). By centrifuging the protein sample, a small amount of brown precipitate was present in the bottom of the microcentrifuge tube. However, the resulting supernatant still contained precipitated protein and showed absorbance characteristics similar to the original sample (Figure 6.18). The pellet could not be redissolved by addition of buffer.

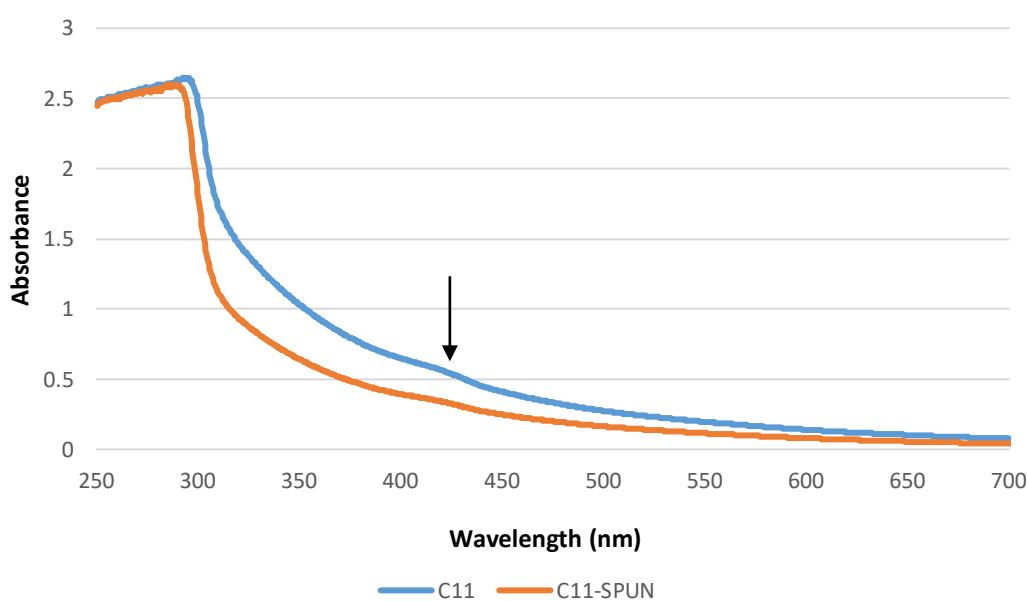


Figure 6.18: Absorbance spectrum of the most concentrated fraction from an MBPTrap purification of MBP-IsoF both before (C11) and after (C11-SPUN) centrifugation to remove precipitated protein. The 420 nm absorbance spectrum feature has been highlighted with an arrow.

A variety of approaches were attempted using 500 mL *Escherichia coli* Rosetta 2 (pLysS) (pET21MBP:*isoF*) cultures to try and reduce this occurrence of protein precipitation upon elution from the MBPTrap column. These included halving the amount of cell pellet used in the purification to reduce the protein concentration, the addition of glycerol, which was

suggested to stabilise the reductase component from alkene monooxygenase of *Rhodococcus rhodochrous* B-276 (Miura and Dalton, 1995), and altering the buffer characteristics to those successfully used in the purification and crystallisation of the reductase from toluene 4-monooxygenase of *Pseudomonas mendocina* KR1 (Acheson *et al.*, 2015), which also used an MBP-fusion expressed in *Escherichia coli*. Despite the reduced amount of material, addition of stabilising agent and alteration of buffer components, the fusion protein continued to precipitate upon elution (results not shown). Continuing from this, the use of anion exchange as a first step was attempted, as this has successfully been used for other MBP-reductase protein fusions of the tetrahydrofuran monooxygenase and toluene 4-monooxygenase systems (Oppenheimer *et al.*, 2010; Acheson *et al.*, 2015).

6.5.2. Anion exchange chromatography purification of MBP-IsoF

The anion exchange column utilised for partial purification of MBP-IsoF was a ~130 mL Q-Sepharose column (GE Life Sciences) and the standard anion exchange buffers (section 2.11.2). The clarified cell lysate from a 1 L culture of *Escherichia coli* Rosetta 2 (pLysS) (pET20MBP:*isoF*) was prepared as in section 2.7, and applied to the Q-Sepharose column. The column was washed with 1.5 column volumes of binding buffer and the proteins bound to the column were eluted over a 2 column volume linear gradient of elution buffer ranging from 0 to 550 mM NaCl followed by an elution step at 1 M NaCl (HPLC trace can be seen in Figure 6.19). Samples of the resulting fractions corresponding to elution peaks on the AKTA trace were subjected to SDS-PAGE analysis. This identified that the polypeptide corresponding to MBP-IsoF was not bound to the column, and instead eluted in the flow through (Figure 6.20). The flow through fractions were assessed by absorbance spectroscopy, which suggested again the presence of the [2Fe-2S] cluster, based on an absorbance maximum at 420 nm (Miura and Dalton, 1995; Newman and Wackett, 1995; Small and Ensign, 1997; Oppenheimer *et al.*, 2010) (Figure 6.21). In contrast, the maximum at around 450 nm associated with the predicted FAD cofactor (Nakajima *et al.*, 1992; Newman and Wackett, 1995; Small and Ensign, 1997; Pessione *et al.*, 1999; Cafaro *et al.*, 2002; Oppenheimer *et al.*, 2010) was not present. This suggested that exogenous FAD may need to be supplied in order to confer activity, which has been successfully used for reductases from the toluene 4- and toluene 2-monooxygenase SDIMO systems (Whited and Gibson, 1991; Newman and Wackett, 1995). There was considerably less scatter than in the previous trial, suggesting that the MBP-IsoF in the Q-Sepharose eluent may be less prone to

precipitation, though it was unclear whether this was simply due to the lower protein concentration of the sample.

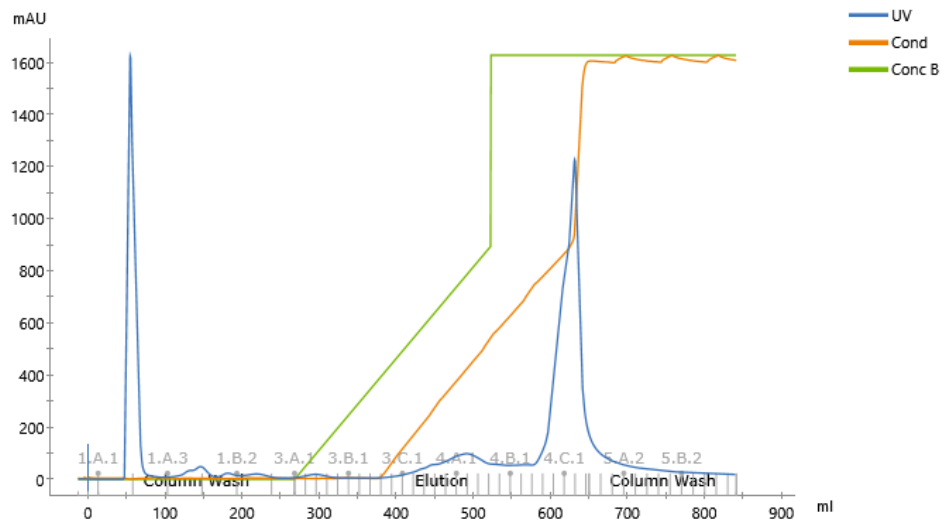


Figure 6.19: HPLC trace of a gradient elution of MBP-IsoF on a 130 mL Q-Sepharose column using an AKTApure HPLC system. The concentration of NaCl was varied from 0 – 550 mM over a 260 mL gradient, followed by a step of the same volume at 1 M.

L FT Elution (0 – 550 mM NaCl)

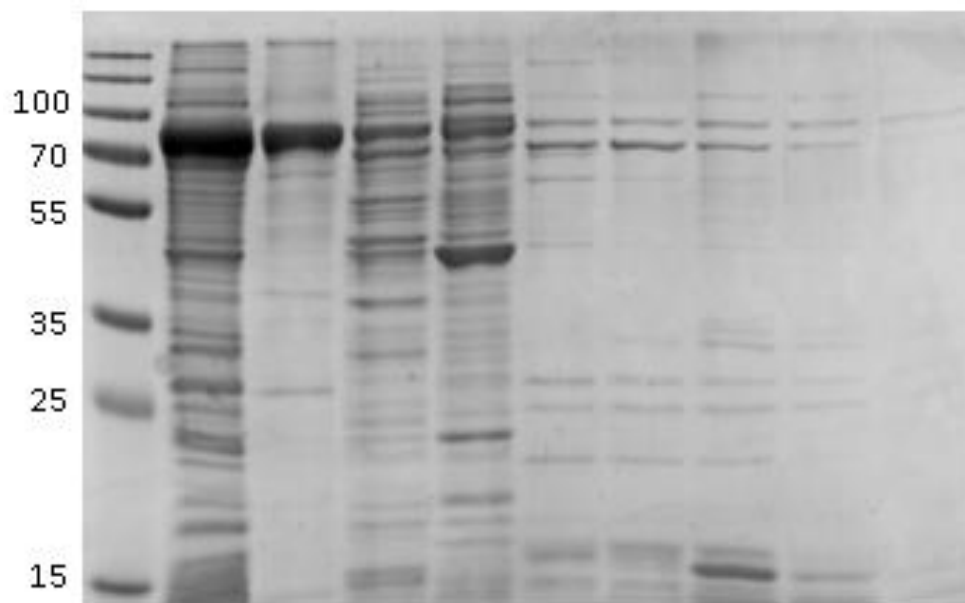


Figure 6.20: Purification of MBP-IsoF using a 130 mL Q-Sepharose column using an AKTApure HPLC system. Polypeptide profiles of fractions were visualised using SDS-PAGE and InstantBlue staining. L is the load and FT is the flow through.

The 90 mL of flow-through from the Q-Sepharose column was combined and split into three samples. The first sample was concentrated using spin-columns (section 2.11.5). The reduction in volume from 30 mL to 5 mL resulted in precipitation of the protein (Figure 6.22), suggesting that this was being caused by the protein concentration rather than the interaction with the MBPTrap column. The second third of the flow through was applied to a 5 mL MBPTrap column according to the same protocol outlined in section 6.5.1. The protein in the resulting eluent precipitated shortly after elution, suggesting that the contaminants removed by the anion exchange step did not successfully reduce the protein concentration by enough to prevent precipitation.

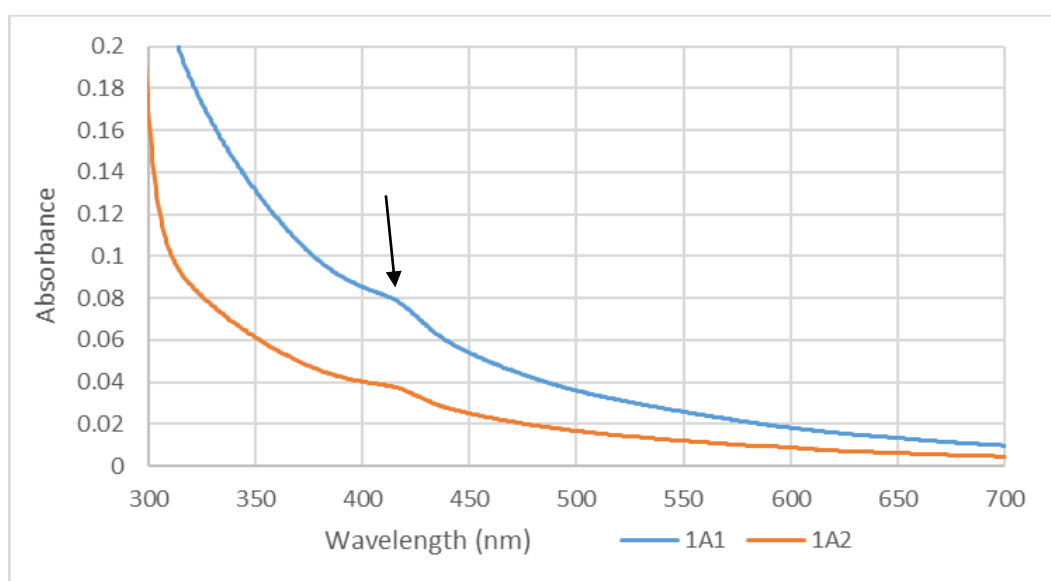


Figure 6.21: Absorbance spectra of the two flow through fractions from the 130 mL Q-Sepharose anion exchange column (1A1 and 1A2) used to partially purify MBP-IsoF. The maximum at 420 nm indicative of the presence of an iron-sulfur cluster has been indicated with an arrow.

The final third of the Q-Sepharose flow through was maintained at the lower concentration in order to prevent protein precipitation. This was applied to a 1 mL HiTrap Blue Sepharose column, which should bind to the NADH-binding pocket of IsoF. Blue Sepharose had previously been used in purification of sMMO reductase from *Methylocystis* sp. strain WI 14 (Grosse *et al.*, 1999). Additionally, another column matrix which binds to NADH-binding sites, Reactive Green, has been successfully used in purification the alkene monooxygenase reductase from *Xanthobacter autotrophicus* sp. Py2 (Small and Ensign, 1997) and the toluene 2-monooxygenase reductase from *Burkholderia cepacia* sp. G4 (Newman and

Wackett, 1995). The HPLC trace of this attempted purification step is presented in Figure 6.23, and the SDS-PAGE analysis of the resulting fractions clearly showed that the MBP-IsoF did not bind to the column and was present in the flow through (Figure 6.24).

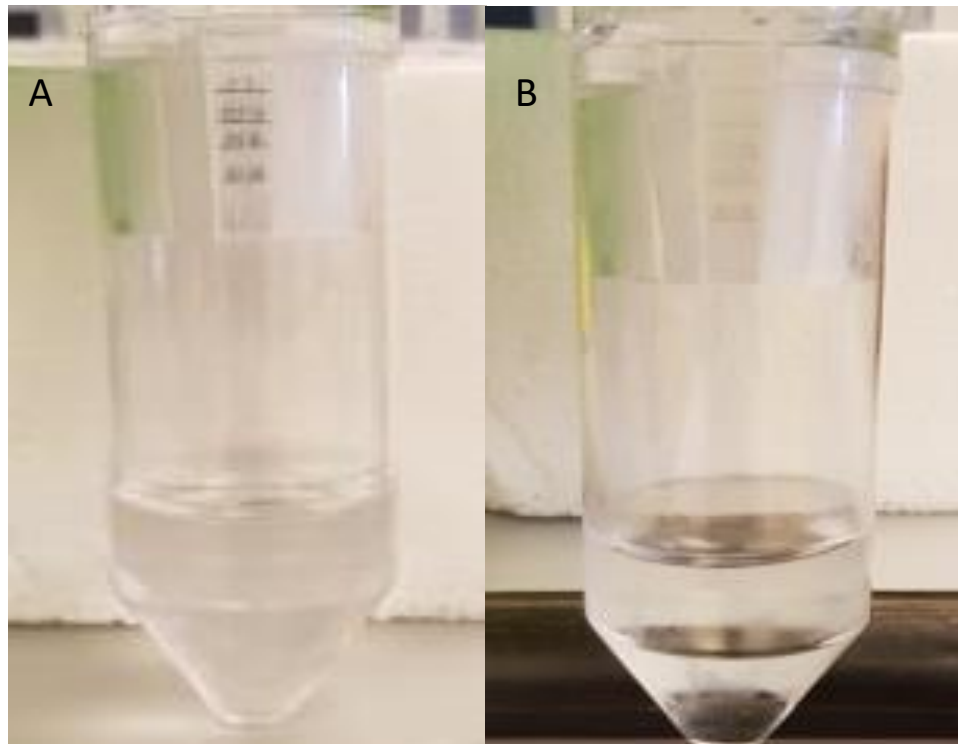


Figure 6.22: Spin concentration columns containing the A – flow through and B – concentrated flow through of the Q-Sepharose anion exchange column used to partially purify MBP-IsoF. The level of precipitation after concentration can be clearly seen in the increased opacity of B.

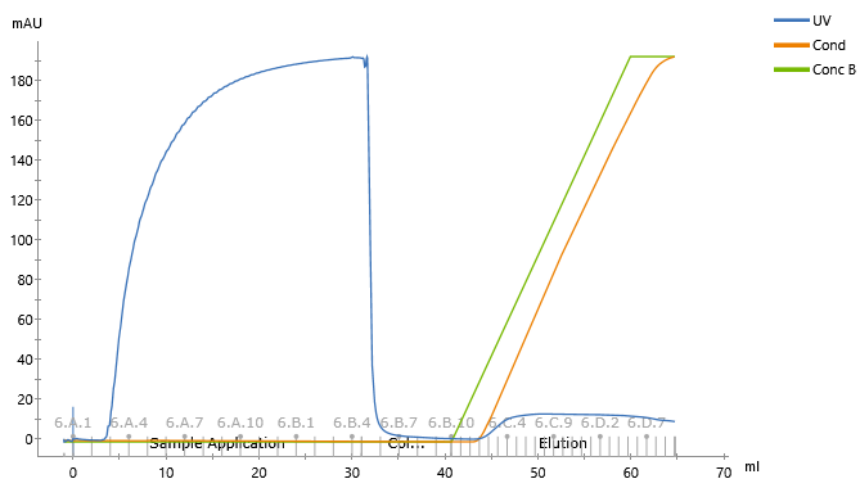


Figure 6.23: HPLC trace of attempted purification of MBP-IsoF using a 1 mL Blue Sepharose column using an AKTApure HPLC system. The concentration of NaCl in the elution buffer (green line) varied from 0 – 1 M over the 20 mL gradient.

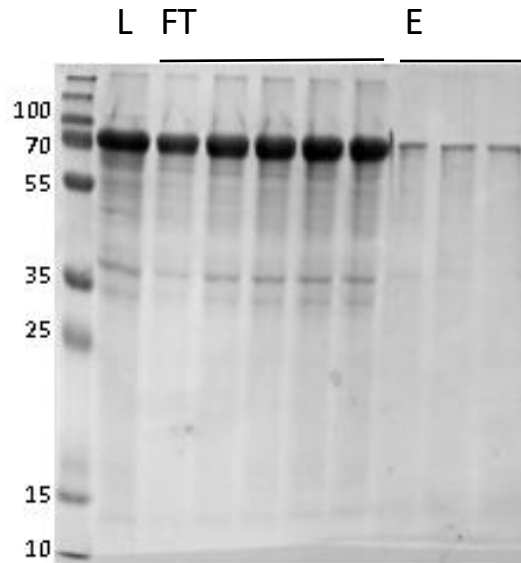


Figure 6.24: Attempted purification of MBP-IsoF using a 1 mL Blue Sepharose column and a linear gradient elution from 0 – 1 M NaCl over a 20 mL gradient using an AKTApure HPLC system. Polypeptide profiles of fractions were visualised using SDS-PAGE and InstantBlue staining. L is the load, FT is the flow through and E is the elution.

6.5.3 Removal of MBP from the IsoF fusion protein with Tobacco Etch Virus protease

The flow-through from the Blue Sepharose column was concentrated back to 30 mL using a spin-column (section 2.11.5) and exchanged into buffer containing 50 mM Tris-HCl, 0.5 mM EDTA, 1mM DTT, pH 8.0. This sample was subjected to proteolytic cleavage with Tobacco Etch Virus (TEV) protease, which was a gift from Dr. S. Bennett (Le Brun group, University of East Anglia). The fusion protein was cleaved by the addition of TEV protease to a concentration 100x lower than that of the target protein, based on Bradford assay. This mixture was incubated overnight at 4 °C, as suggested by the published protocol (Raran-Kurussi *et al.*, 2017). The resulting cleaved protein was applied to the MBPTrap column to remove any uncut protein and cleaved MBP. The flow through from this column was subsequently applied to a 5 mL HisTrap column to remove the His-tagged TEV protease. The flow through from this column was spin-concentrated and samples from all stages of the purification were analysed by SDS-PAGE gel. This analysis suggested that the TEV protease had successfully cleaved some of the MBP-IsoF, but not all of it. Very little of the protein sample was retained after application to the MBPTrap column, though the TEV protease was clearly bound to, and eluted from the HisTrap column. In the HisTrap elution,

there was a faint band suggesting the presence of a polypeptide of approximately the correct size to be IsoF (37.5 kDa) (Figure 6.25). Although the yield appeared to be low and there was a chance that some of the cleaved protein had remained bound to the MBPTrap column or precipitated out during the TEV protease cleavage step, this sample was carried forward to assess the protein characteristics and to determine whether this was in fact IsoF.

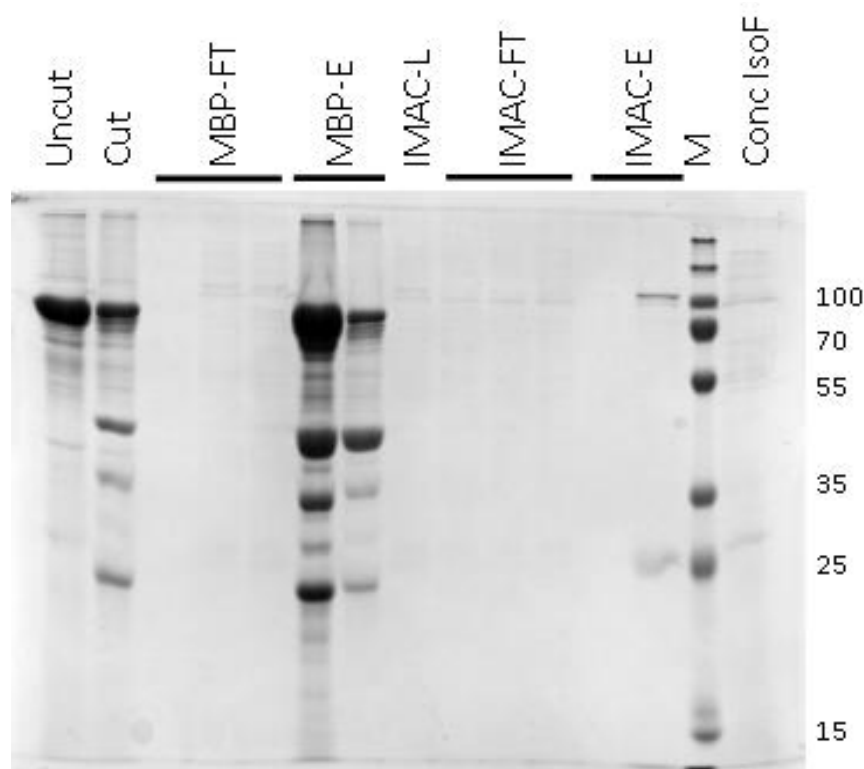


Figure 6.25: Polypeptide profiles of the MBP-IsoF before (uncut) and after (cut) cleavage of the fusion protein with TEV protease. The resulting sample was applied to two affinity chromatography columns using an AKTApure HPLC system: a 5 mL MBPTrap (MBP) and 5 mL HisTrap (IMAC) column. The flow through from MBP was the load for IMAC, and the load (L), flow through (FT) and elution (E) are presented. The flow through from the IMAC column was concentrated (Conc IsoF). All samples were visualised by SDS-PAGE.

6.6. Characterisation of the purified protein

6.6.1. Absorbance spectrum of the purified protein

The absorbance spectrum of this purified protein (Figure 6.26) still showed the presence of an absorbance maximum at 420 nm (sections 6.2.1 and 6.5.2), suggesting the present of an iron-sulfur cluster (Miura and Dalton, 1995; Newman and Wackett, 1995; Small and Ensign, 1997; Oppenheimer *et al.*, 2010). Again, the absorbance maxima associated with the predicted FAD cofactor, identified as multiple features around 450 nm in multiple other

SDIMO reductase characterizations (Nakajima *et al.*, 1992; Miura and Dalton, 1995; Newman and Wackett, 1995; Small and Ensign, 1997; Pessione *et al.*, 1999; Cafaro *et al.*, 2002; Oppenheimer *et al.*, 2010), were absent. The FAD was identified as lacking in many of the reductases purified from heterologous hosts such as *Escherichia coli*, and this problem has previously been overcome by the addition of exogenous FAD during the reconstitution process (Whited and Gibson, 1991; Newman and Wackett, 1995).

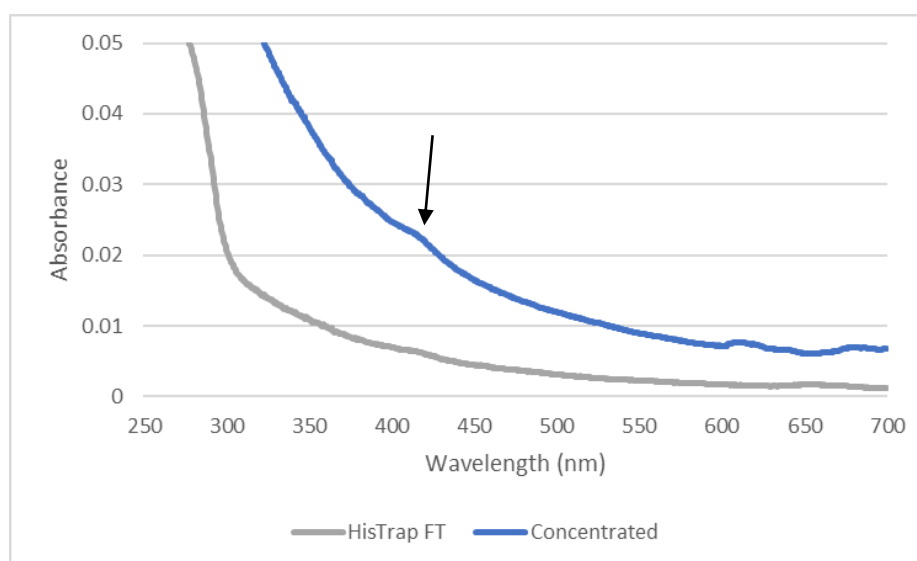


Figure 6.26: Absorbance spectra of the resulting protein sample from the attempted IsoF purification (HisTrapFT) and the concentrated sample (Concentrated). The maximum at 420 nm indicating the presence of an iron sulfur cluster has been indicated with an arrow.

6.6.2. NADH:ferricyanide reductase activity of the purified protein

To test the activity of the cleaved and uncleaved purified protein, a potassium ferricyanide assay was utilised. This is due to it being extensively used to characterise SDIMO reductases in previous research (Lund *et al.*, 1985; Hartmans *et al.*, 1991; Nakajima *et al.*, 1992; Miura and Dalton, 1995; Small and Ensign, 1997; Blazyk and Lippard, 2004). For the assay, 0.5 mM potassium ferricyanide, varying amounts of reductase and 1 mM NADH were prepared in a quartz cuvette, and the change in absorbance at 420 nm was monitored. This resulted in a clear change in absorbance in the presence of NADH and ferricyanide, which was not observed in the absence of either of these components (Figure 6.27). This implied that the purified protein could act as an NADH-dependent ferricyanide reductase, like in the reductases of other SDIMOs. The specific activity of the reductase in this reaction was calculated using $\epsilon_{420} = 1,020 \text{ M}^{-1} \text{ cm}^{-1}$, which is in agreement with previous reductase

research (Lund *et al.*, 1985; Miura and Dalton, 1995; Blazyk and Lippard, 2004). The specific activity on potassium ferricyanide was found to be $13.32 \mu\text{mol min}^{-1} \text{mg}^{-1}$. The level of specific activity of other SDIMO reductases on ferricyanide was highly variable. An activity of $9.8 \mu\text{mol min}^{-1} \text{mg}^{-1}$, $28.1 \mu\text{mol min}^{-1} \text{mg}^{-1}$ and $0.4 \mu\text{mol min}^{-1} \text{mg}^{-1}$ has been recorded for the sMMO reductase from *Methylococcus capsulatus* (Bath) (Blazyk and Lippard, 2004), *Methylocystis* sp. M (Nakajima *et al.*, 1992) and alkene monooxygenase reductase purified from *Rhodococcus rhodochrous* sp. B-276 (Miura and Dalton, 1995) respectively. It should be noted that all of these are natively purified proteins, as the specific activity of recombinant proteins is often based on reconstitution assays, which was not possible here. Though this activity was observed, it was unexpected due to the apparent absence of the FAD cofactor, as noted in section 6.6.1.

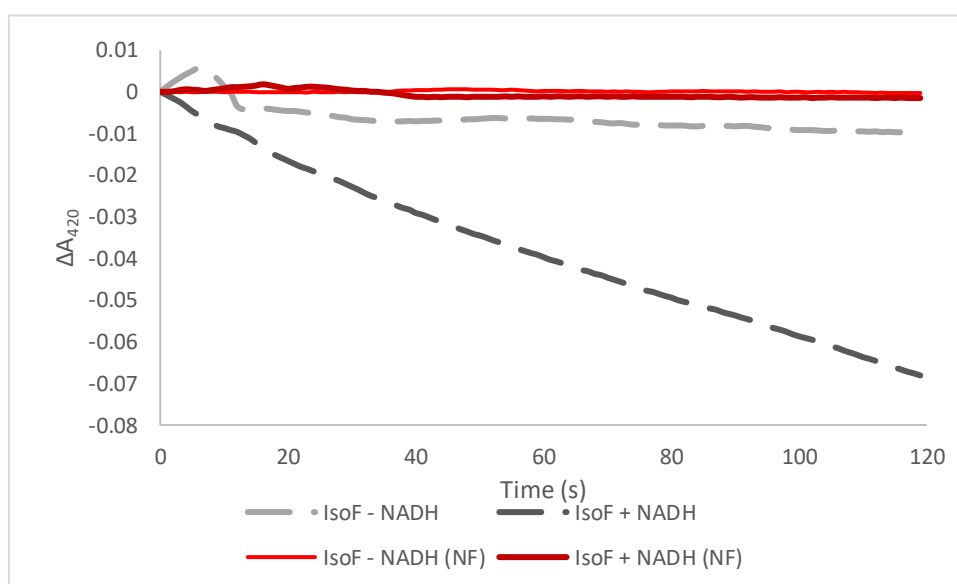


Figure 6.27: Ferricyanide reductase activity of the protein sample believed to be IsoF in the presence and absence (+/-) of NADH. Control reactions not containing ferricyanide are indicated by (NF).

6.6.3. LC-MS analysis of the purified protein

To verify whether the purified protein was in fact IsoF, the purified sample was subjected to LC-MS analysis (section 2.13.1). The cleaved protein product from MBP-IsoF was predicted to have a molecular mass of 37,512 Da, whereas the LC-MS analysis suggested that the actual weight of the protein was 31,546 Da (Figure 6.28). This was 5,966 Da lower than predicted, and no cleavage site(s) could be identified which would result in this mass

+/- 2 Da, which would be within the accuracy range of the instrument. Due to this, it was theorised that the cleaved IsoF may have remained bound to the MBPTrap column after cleavage with TEV protease, as this step seemed to have low specificity in which proteins bound to the matrix. Resending the pET20MBP:*isoF* plasmid for sequencing verified that the protein produced should be the predicted size, and that the issue was not with the vector sequence.

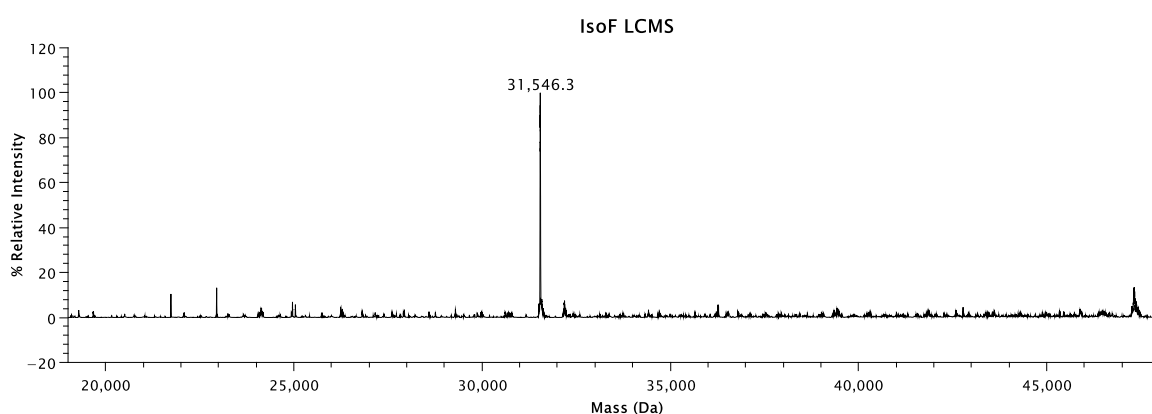


Figure 6.28: LC-MS analysis of the protein product of attempted IsoF purification from an MBP fusion produced in *Escherichia coli* Rosetta 2 (pLysS). Expected mass 37,512.42 Da.

6.7. Purification of the reductases from soluble methane monooxygenase of *Methylosinus trichosporium* OB3b, alkene monooxygenase of *Rhodococcus rhodochrous* sp. B-276 and isoprene monooxygenase of *Rhodococcus* sp. AD45 as GST-fusions

The use of alternative SDIMO reductases within reconstitution experiments has been previously reported (Yen and Karl, 1992; Lloyd *et al.*, 1999; Champreda *et al.*, 2004). These experiments have mostly been carried out to explore how these altered interactions affect the stereoselectivity of SDIMO reactions. However, this approach was also successfully used during research into the alkene monooxygenase reductase from *Xanthobacter autotrophicus* sp. Py2, as the reductase proved impossible to purify from the *Escherichia coli* expression system so an alternative protein was required (Champreda *et al.*, 2004). To minimise the risk of using a potentially incorrect protein, this approach was subsequently utilised to investigate the differences in expression and purification of three different SDIMO proteins and a smaller characterisation of each. These have all been produced as N-terminal GST fusions, an approach which was successfully used to produce soluble, recombinant reductase from the alkene monooxygenase of *Rhodococcus rhodochrous* sp.

B-276 in *Escherichia coli* (Smith *et al.*, 1999), the plasmid for which was a gift from Professor T. Smith (Sheffield Hallam University).

6.7.1. Construction of the pGEX-*isoF* plasmid for expression of GST-IsoF in *Escherichia coli*

Table 6.2: Primer sequences used for polymerase chain reaction amplification of *isoF* from *Rhodococcus* sp. AD45 genomic DNA and cloning into the pGEX-2T expression vector.

| Primer Name | Sequence (5'-3') | Restriction Site | Orientation |
|-------------|--|------------------|-------------|
| GEXisoFF | ATATATGGATCCATGACTGTCACAGTGAATTTCAATGG | BamHI | Forward |
| GEXisoFR | ATATATGGATCCGGATTCGGGGGTAGT | BamHI | Reverse |
| GEXcheck | ATGTCCCCTATACTAGGTTATTGG | N/A | Forward |

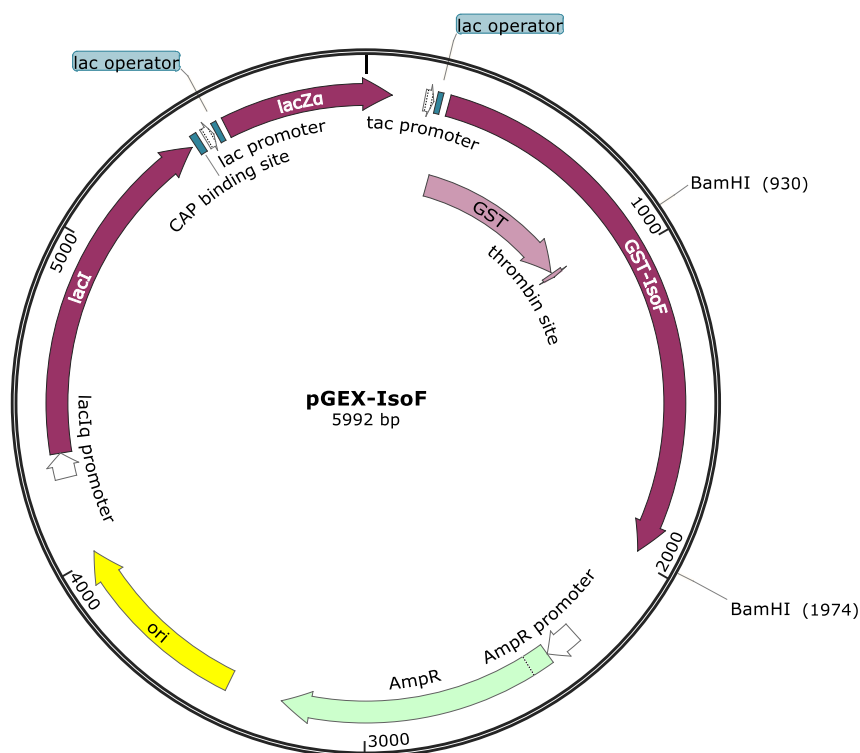


Figure 6.29: Vector map of pGEX-IsoF for expression of the isoprene monooxygenase from *Rhodococcus* sp. AD45 as a GST fusion in *Escherichia coli* Rosetta 2 (pLysS).

In order to directly compare the expression of several different SDIMO reductases, the sMMO reductase from *Methylosinus trichosporium* OB3b and the alkene monooxygenase reductase from *Rhodococcus rhodochrous* B-276 were generously gifted by Professor T. Smith (Sheffield Hallam University) in the plasmids pGEX-MMOC and pTJS103 respectively. The pGEX-AMOD vector was prepared by Colin Lockwood (Murrell Group, University of East Anglia) using the protocol previously reported (Smith *et al.*, 1999) with the pTJS103 plasmid as a DNA template, and the pGEX-MMOC as a vector backbone. This technique was also used for cloning *isoF*, where the pGEX-MMOC vector was cut with the restriction enzyme *Bam*HI and the *isoF* gene amplified from *Rhodococcus* sp. AD45 using the same techniques detailed in section 6.2.1. The primers utilised are detailed in Table 6.2, and the resulting PCR product was cloned into the interim vector pJETblunt1.2 as detailed in section 4.2. The *isoF* gene was cut from this plasmid using *Bam*HI and subcloned into the linearized pGEX-AMOD (sections 2.5.4 – 2.5.7). The resulting pGEX-*isoF* plasmid (Figure 6.29) was ratified by sequencing at MWG Eurofins (section 2.5.8) and was designed to produce a GST-IsoF fusion protein.

6.7.2. Production of GST-MmoC, GST-AmoD and GST-IsoF in the *Escherichia coli* heterologous expression system

Chemically competent *Escherichia coli* Rosetta 2 (pLysS) cells (section 2.3.2) were transformed with either pGEX-MMOC, pGEX-AMOD or pGEX-*isoF*. The resulting transformants were grown in 10 mL of LB to test expression of the GST-reductase fusions. The expression protocol developed in section 6.3.2, with the cold shock and supplementation was utilised to increase the chance of cofactor incorporation. The cells were harvested by centrifugation (section 2.6) and washed in 50 mM phosphate buffer (pH 7.0). The resulting cell pellets were resuspended in 200 μ L of the same buffer, and both the soluble and insoluble fractions were prepared for SDS-PAGE analysis as outlined in section 6.3.2. The subsequent analysis demonstrated a clear difference in soluble protein expression between different SDIMO reductases from the same pGEX-2T backbone (Figure 6.30). The alkene monooxygenase reductase (AmoD) from *Rhodococcus rhodochrous* sp. B-276 was clearly the most soluble of the proteins, with most of the polypeptide the same mass as the predicted GST-AmoD fusion being visualised in the soluble fraction. The soluble methane monooxygenase reductase (MmoC) from *Methylosinus trichosporium* OB3b was

less soluble, with apparent low expression of the appropriately sized polypeptide in the soluble fraction, and some being present in the insoluble fraction. Finally, IsoF was clearly poorly expressed in the soluble fraction, though the insoluble sample was contaminated with the soluble, making it impossible to determine whether any of this sample had formed inclusion bodies.

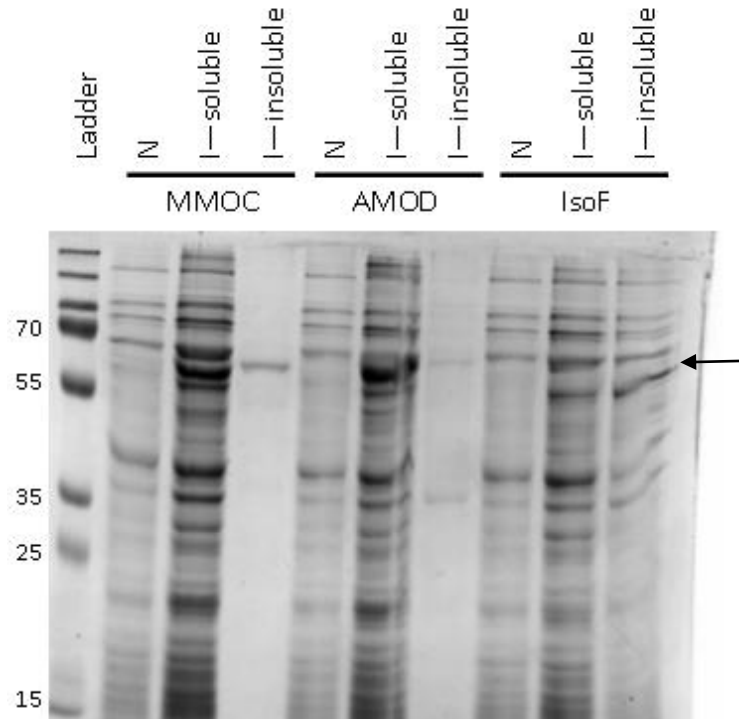


Figure 6.30: Polypeptide profiles of *Escherichia coli* Rosetta 2 (pLysS) expressing pGEX-MMOC, pGEX-AMOD or pGEX-IsoF as determined by SDS-PAGE. Cultures were wither non-induced (N) or induced with 100 μ M IPTG at 30 $^{\circ}$ C to produce the GST fusion proteins. Soluble refers to the soluble fraction of the cell extract, whereas the insoluble is the insoluble fraction of the cell extract. “N” samples were the soluble fraction. The size of expected GST-reductase fusions has been indicated with an arrow.

Next, the expression parameters were altered to try and alter the level of soluble GST-reductase expression. The amount of IPTG used to induce the protein production was altered to 50 μ M or 100 μ M, and the temperature at expression reduced to 30 $^{\circ}$ C. The cells were grown in 100 mL cultures and samples were taken both 3 h and 20 h after induction. SDS-PAGE analysis of the soluble extract from these samples suggested that the IPTG concentration made little difference, but incubating the cultures for 20 h after induction did increase the amount of soluble GST-reductase in all cases, though the yield was still very low in both the MmoC and IsoF trials (Figure 6.31). This suggested that these two

reductases may simply be poorly expressed in a soluble form in *Escherichia coli*, and this could be an intrinsic property of certain SDIMO reductases.

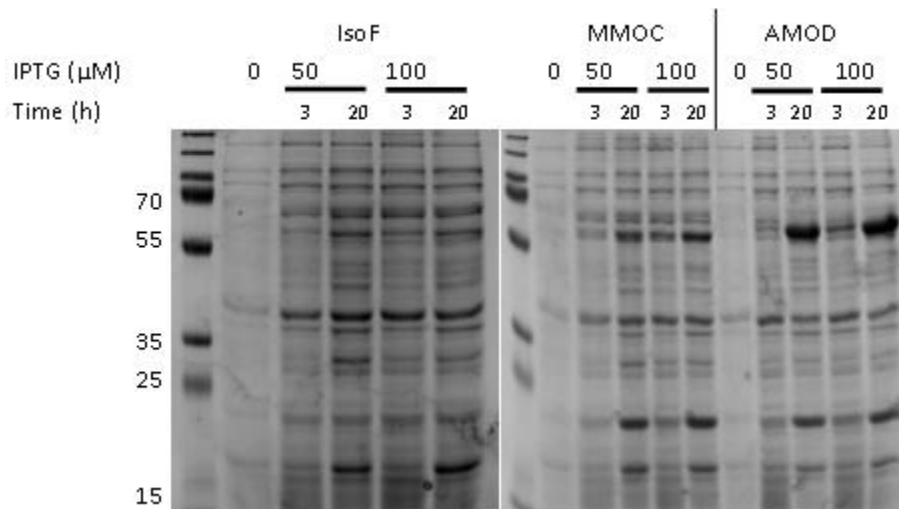


Figure 6.31: Polypeptide profiles of *Escherichia coli* Rosetta 2 (pLysS) expressing pGEX-IsoF, pGEX-MMOC or pGEX-AMOD as determined by SDS-PAGE. The IPTG concentration used to induce gene expression (μM) and time after induction at 30 °C (h) are indicated. All samples were soluble extract from the cells.

The cells from the remaining 80 mL from the previous expression trials with 100 μM IPTG after 20 h incubation were harvested by centrifugation and washed in the binding buffer for GSTrap affinity columns (section 2.11.1). The cell pellets were resuspended in 10 mL of the same buffer and the clarified cell lysate prepared (section 2.7). The cell lysates were applied individually to a 5 mL GSTrap column using an AKTApure HPLC system with UNICORN™ 7 software. The columns were washed with 5 column volumes of binding buffer, followed by a single step elution with 100 % elution buffer. Samples of the cell lysate, flow through and elution were analysed by SDS-PAGE (section 2.7.2), and the polypeptide profiles demonstrated further the high yield of GST-AmoD in comparison to GST-MmoC and GST-IsoF (Figure 6.32). This further suggested that the latter two reductases may share characteristics which make them more difficult to obtain a high yield of soluble protein in *Escherichia coli*. The polypeptides visualised in the GST-IsoF expression trial were also similar to the contaminating proteins in the other two reductase trials, making it unclear whether IsoF was produced at all.

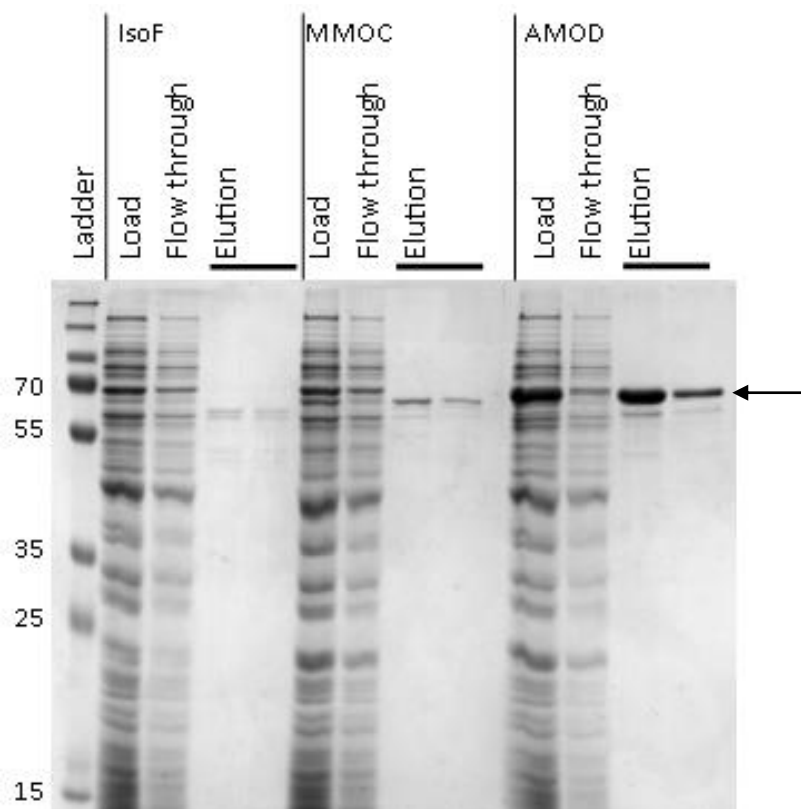


Figure 6.32: Polypeptide profiles of GST fusions of IsoF, MmoC and AmoD by 5 mL GSTrap columns using an AKTApure HPLC system, as determined by SDS-PAGE. The size of the expected GST-reductase fusions has been indicated by an arrow.

The absorbance spectra of the resulting samples of GST-IsoF, GST-MmoC and GST-AmoD were analysed (section 2.12.1). Their absorbance spectra are shown in Figure 6.33 and Figure 6.34 respectively. These demonstrated the presence of both FAD and [2Fe-2S] cofactors in GST-AmoD, based on the observed maxima at around 420 nm, and the large absorbance between 340 and 520 nm, which was also recorded in the sMMO reductase from *Methylococcus capsulatus* (Bath) (Lund and Dalton, 1985). Conversely, only the maximum at around 420 nm was present in the GST-MmoC and GST-IsoF samples, suggesting that these only contained the [2Fe-2S] cofactor which has been mentioned in attempted recombinant IsoF production previously (sections 6.5.1, 6.5.2 and 6.6.1).

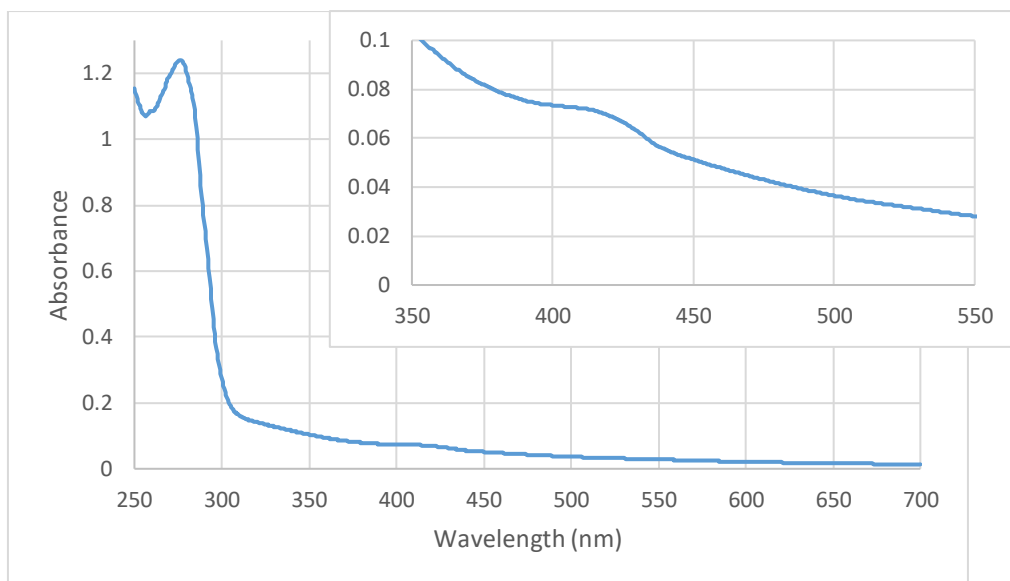


Figure 6.33: Absorbance spectrum of GST-IsoF fusion partially purified by GSTrap column. Inset is zoomed in to show spectroscopic feature at 420 nm.

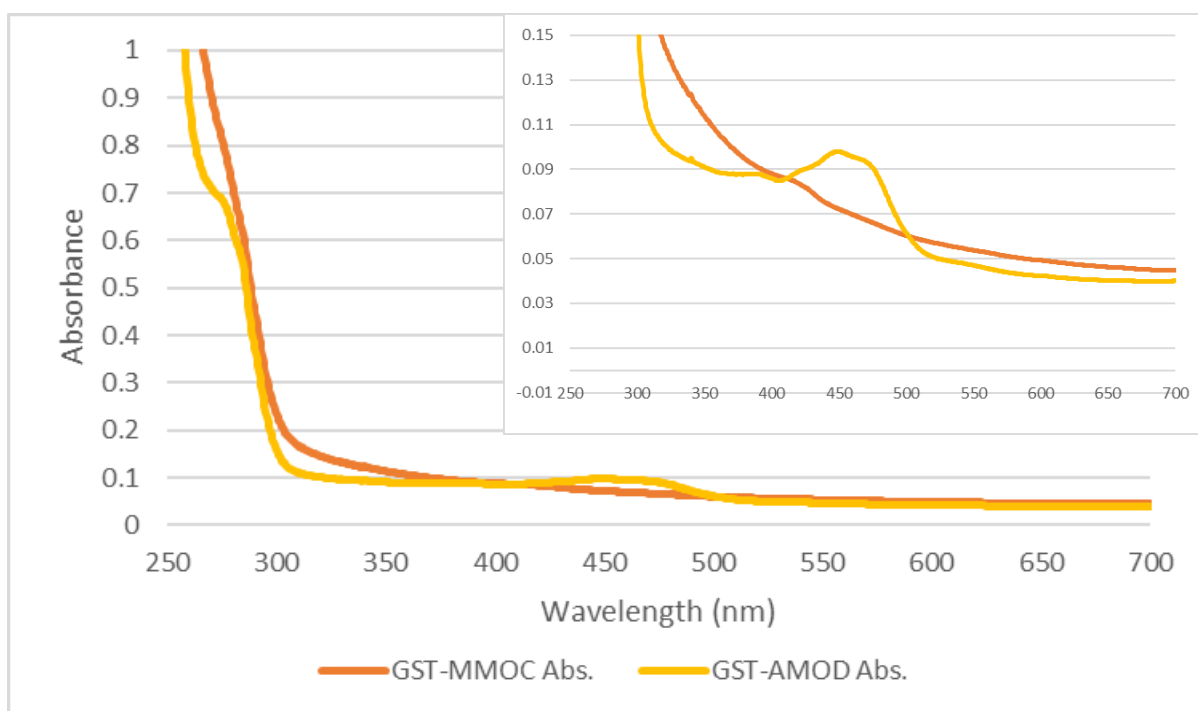


Figure 6.34: Absorbance spectra of purified GST fusions of both MmoC (orange line) and AmoD (yellow line). Inset is zoomed in to show the spectroscopic features after the A_{280} peak of protein more clearly.

All three of the GST-reductase samples were treated with thrombin (SigmaAldrich), according to manufacturer's instructions. Briefly, the samples were incubated with 1 Unit of thrombin per 100 μ g of target fusion protein overnight at room temperature. The GST-

IsoF samples were analysed by SDS-PAGE to check whether the thrombin cleavage had been successful, and whether the room temperature incubation of the sample negatively impacted the protein (Figure 6.35). The results suggested that the cleavage had been successful due to a clear change in the polypeptide profile of the sample, and that this was not due to the room temperature incubation of the protein. No band was present in at the expected size of cleaved IsoF (37.5 kDa), suggesting that it had either degraded or simply did not stain well. This was also visible in analysis of the thrombin cleavage of both GST-AmoD and GST-MmoC (Figure 6.36). Due to the higher concentration of GST-AmoD, a sample of this was re-applied to the GSTrap affinity column in order to remove the cleaved GST. Samples of this were analysed at the same time as the thrombin cleavage by SDS-PAGE (Figure 6.36). The cleaved AmoD and thrombin should have been apparent in the flow-through from the second GSTrap column, however no polypeptide band of the corresponding mass could be seen, suggesting that reductases may not stain well at low concentrations and rely on the presence of the fusion proteins to monitor by SDS-PAGE.

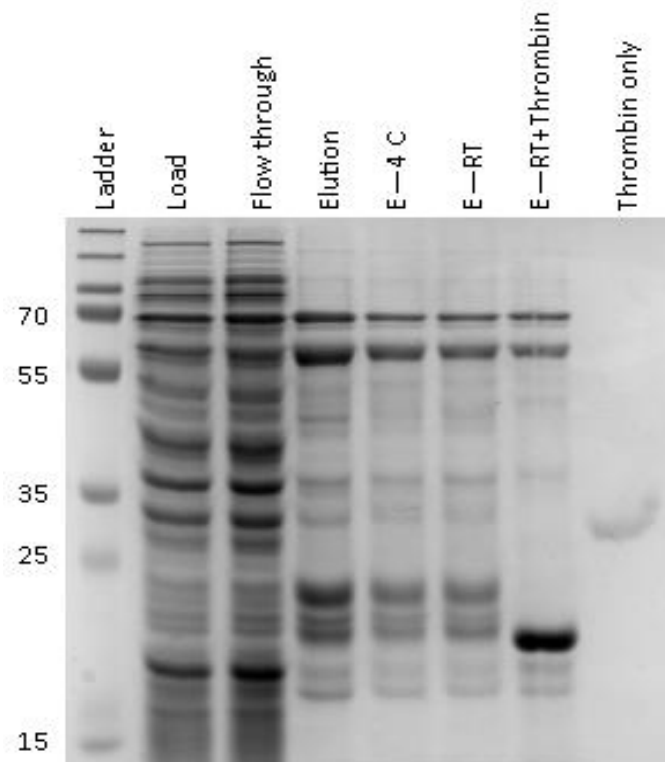


Figure 6.35: Polypeptide profiles of the partial purification of GST-IsoF using a 5 mL GSTrap column and an AKTApure HPLC (Load, Flow through and Elution) as determined by SDS-PAGE. Samples of the elution fraction were incubated overnight at 4 °C (E-4C), room temperature (E-RT) and room temperature in the presence of thrombin to cleave the GST (E-RT+Thrombin). The thrombin alone is also present to show where this polypeptide band lies.

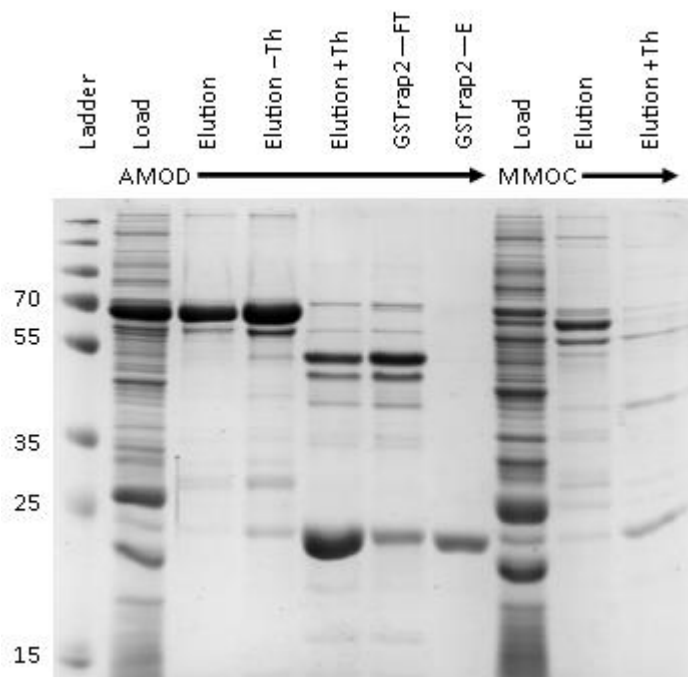


Figure 6.36: Polypeptide profiles of the purification of A) AmoD and B) MmoC as determined by SDS-PAGE. A) The *Escherichia coli* Rosetta 2 (pLysS) (pGEX-AMOD) soluble cell extract (Load) was applied to a 5 mL GSTrap affinity chromatography column and eluted with the addition of reduced glutathione (Elution). This was incubated in the presence and absence (+/-) of thrombin at room temperature overnight, followed by another GSTrap purification step, where both the flow through (FT) and elution (E) were analysed. B) The *Escherichia coli* Rosetta 2 (pLysS) (pGEX-MMOC) soluble cell extract (Load) was applied to a 5 mL GSTrap affinity chromatography column and eluted with the addition of reduced glutathione (Elution). This was incubated in the presence of thrombin at room temperature overnight (Elution+Th).

6.8. Comparison of activity of GST-reductase fusion proteins and the cleaved reductases

6.8.1. NADH:ferricyanide reductase activity assay

To check whether the reductases had a change in activity after cleaving from the GST fusion with thrombin, a comparison of cleaved and uncleaved protein was carried out with ferricyanide assays (as in section 6.6.2). The first trial was carried out on IsoF, which suggested that the fusion protein was inactive, whereas the cleaved protein was active (Figure 6.37). A low amount of ferricyanide reductase activity could be attributed to the presence of thrombin, though not to the level that was present in cleaved protein. The addition of more cleaved IsoF resulted in a higher rate of ferricyanide reduction. The

specific activity of the uncleaved GST-IsoF was calculated to be $2.07 \mu\text{mol min}^{-1} \text{mg}^{-1}$, whereas the two cleaved samples were calculated to have specific activities of $5.97 \mu\text{mol min}^{-1} \text{mg}^{-1}$ and $4.06 \mu\text{mol min}^{-1} \text{mg}^{-1}$ for the low and high protein concentrations respectively. This clearly demonstrates an increase in activity after the cleavage of the GST fusion, though these activities are very low even in comparison to that achieved in section 6.6.2, though this may not have been IsoF. The low activity could be attributed to the partial purification and the presence of cleaved GST in the reaction, which makes the total protein concentration not exclusively the IsoF protein. Despite this, the fact that IsoF cleaved from its GST fusion partner clearly had a higher activity than the complete fusion protein. This has also been recorded in the GST-fusion purification of alkene monooxygenase reductase of *Rhodococcus rhodochrous* sp. B-276 (Smith *et al.*, 1999).

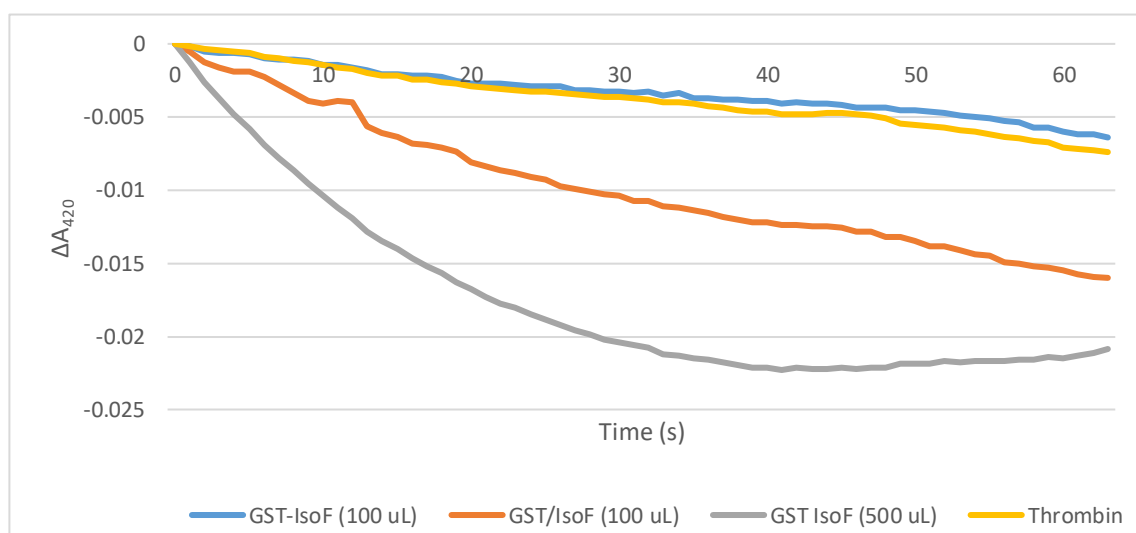


Figure 6.37: NADH:ferricyanide reductase activity of IsoF as a GST fusion (GST-IsoF), and after cleavage of the GST tag with thrombin (GST/IsoF) as monitored by the change in absorbance at 420 nm. The activity of thrombin alone was also monitored to account for the level which could be attributed to the presence of thrombin in the cleaved IsoF sample.

Following this, the activity of both recombinant MmoC and AmoD were assessed using the same method (Figure 6.38). The recombinant MmoC was found to be inactive in both fusion protein and cleaved formats, whereas the AmoD had a specific activity of $19.3 \mu\text{mol min}^{-1} \text{mg}^{-1}$ when still fused to GST, and $21.4 \mu\text{mol min}^{-1} \text{mg}^{-1}$ when cleaved. The previous recorded activities for MmoC on ferricyanide have often been using natively purified proteins. This sample was also the lowest concentration, so larger amounts of the protein may be capable of NADH:ferricyanide reductase activity. The activity of GST-AmoD fusion protein is in contrast to the literature, where it was previously recorded that the reductase

was only active when the GST tag was removed (Smith *et al.*, 1999). The specific activity of AmoD is within the parameters of other SDIMO NADH:ferricyanide reductase assays, where the specific activity of a range of natively purified reductases has been found to vary between 0.4 and 50 $\mu\text{mol min}^{-1} \text{mg}^{-1}$ (Lund *et al.*, 1985; Nakajima *et al.*, 1992; Miura and Dalton, 1995; Blazyk and Lippard, 2004). The specific activity of recombinant AmoD purified using the same vector as here resulted in a specific activity of 0.1 $\mu\text{mol min}^{-1} \text{mg}^{-1}$, though this was calculated using a reconstitution based assay which was not possible here.

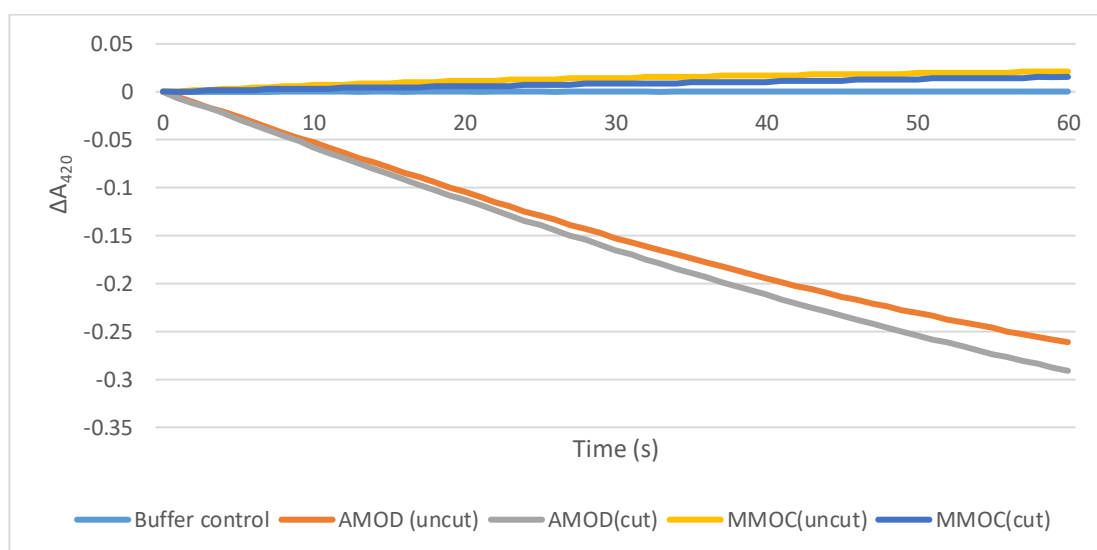


Figure 6.38: NADH:ferricyanide reductase activity of GST-AmoD and –MmoC fusion proteins (uncut) and those cleaved with thrombin (cut) as monitored by the change in absorbance at 420 nm. Volumes given are the amount of protein sample added to a 1 mL total reaction volume.

6.9. Purification of the reductase from toluene 4-monooxygenase of *Pseudomonas mendocina* sp. KR1

As a final comparison, the toluene 4-monooxygenase reductase protein, termed T4moF, was purified by Dr C. Lockwood (Murrell group, University of East Anglia). The construct used for protein expression was a generous gift from the Fox group (Wisconsin, USA), and encoded an N-terminal MBP fusion T4moF protein (Acheson *et al.*, 2015). Briefly, the construct was used to transform *Escherichia coli* BL21 chemically competent cells (section 2.3.2). Transformants were grown in 500 mL batch cultures containing 50 $\mu\text{g mL}^{-1}$ kanamycin to an $\text{OD}_{540} \sim 0.6$, followed by induction with 75 μM IPTG and incubation overnight at 20 °C. The cells were harvested by centrifugation (section 2.6), and stored at -80 °C until use.

Cells were resuspended in 50 mM HEPES 50 mM NaCl pH 7.5 (buffer A) and broken by three passes through a French pressure cell at 20,000 psi (137 MPa). Cell debris was removed by centrifugation at 11,000 x *g* for 30 min. The supernatant was further clarified by ultracentrifugation at 42,000 x *g* for 60 min. This clarified cell extract was applied to a 130 mL Q-Sepharose column (section 2.11.2) equilibrated in buffer A using an AKTApure HPLC system and UNICORN™ 7 software. After a 260 mL wash step, an elution gradient of 0 – 50 % Buffer B (50 mM HEPES 1 M NaCl pH 7.5) over 5.5 column volumes was performed. T4moF was identified to elute around 20 % Buffer B (200 mM NaCl) based on the brown colour of the fractions. These fractions were applied directly to a 5 mL MBPTrap column equilibrated in 50 mM HEPES 300 mM NaCl pH 7.5, and eluted using the addition of 10 mM maltose. The resulting purified T4moF protein was checked by SDS-PAGE analysis, where a polypeptide band of the expected 79 kDa mass was observed (Figure 6.39). Absorbance spectroscopy confirmed the presence of the expected characteristics for presence of both the FAD and [2Fe-2S] cofactors (Figure 6.40) (Acheson *et al.*, 2015).

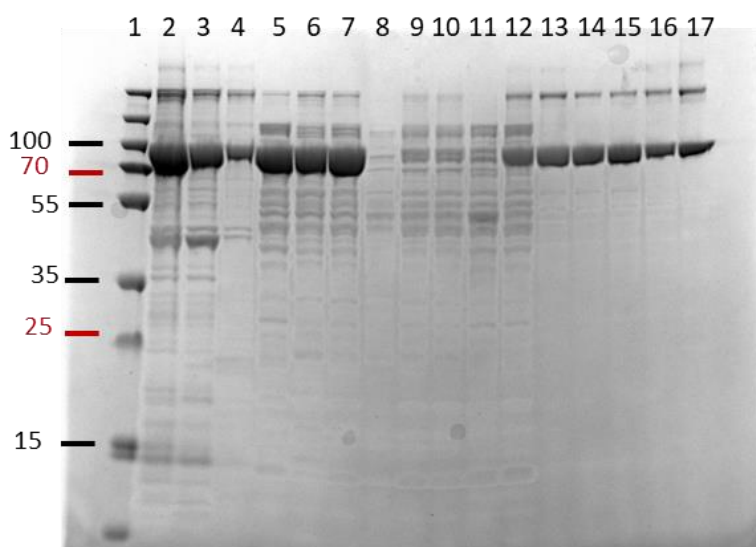


Figure 6.39: Polypeptide profiles of T4moF purification protocol. Lanes 2-7 are the Q-Sepharose elution fractions, Lanes 8-17 are the MBPTrap elution fractions. Image credit Dr C. Lockwood (Murrell Group, University of East Anglia).

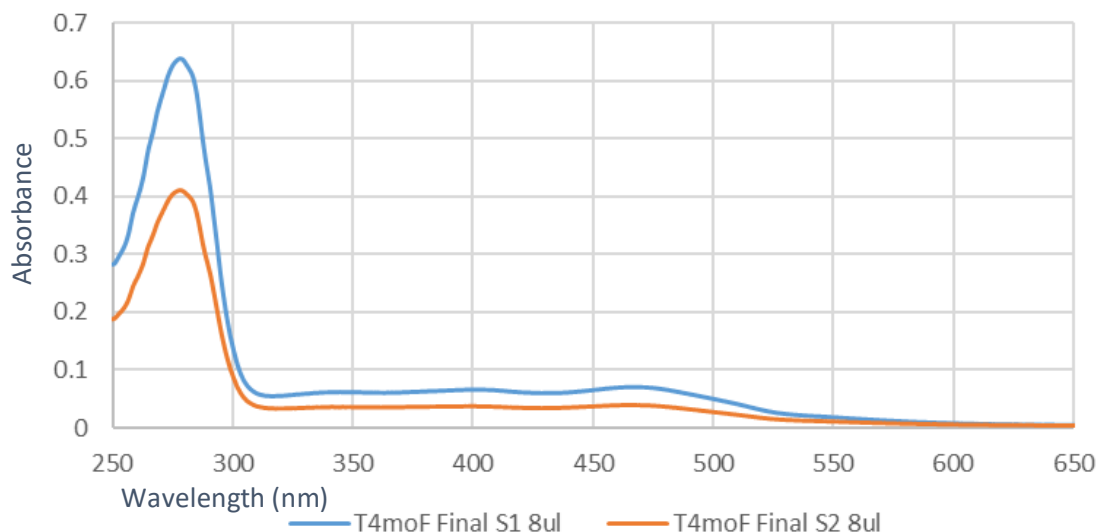


Figure 6.40: Absorbance spectrum of purified T4moF. Image credit Dr C. Lockwood (Murrell Group, University of East Anglia).

6.10. Reduction of purified IsoC using purified reductase fusion proteins

Due to the low yield and activity of the GST-IsoF fusion protein, the potential for use of alternative SDIMO reductases in reconstitution experiments was assessed by checking whether the GST-AmoD or MBP-T4moF were capable of reducing the IsoC (Rieske protein) component. This was based on the use of toluene 4-monooxygenase reductase to complement the alkene monooxygenase system when the alkene monooxygenase reductase proved impossible to purify (Champreda *et al.*, 2004).

To assess this, 800 μ L reactions were set up in reduced volume quartz cuvettes containing 3 μ M IsoC in buffer containing 50 mM HEPES 50 mM NaCl (pH 7.5). The absorbance spectrum was measured (section 2.12.1), and 1 mM NADH was added. Once the absorbance at 450 nm had stabilised the absorbance spectrum was measured again, and this process was repeated after the addition of 1 μ M of reductase, either MBP-T4moF or GST-AmoD. The results clearly demonstrated that the only changes in the absorbance spectrum occurred after the addition of MBP-T4moF, not NADH or GST-AmoD (Figure 6.41).

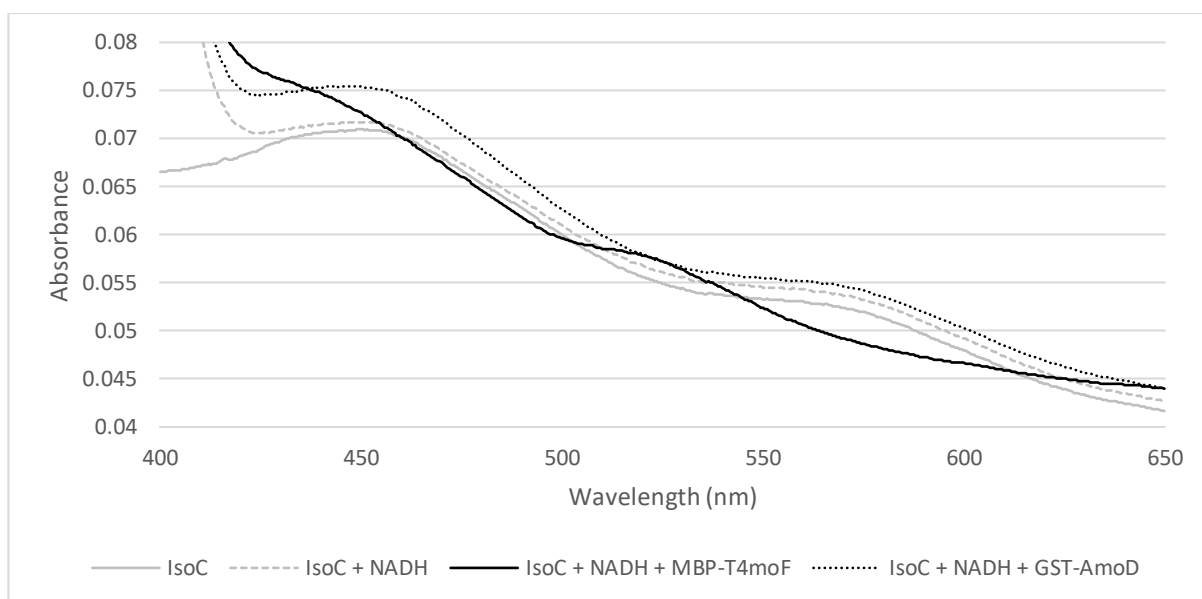


Figure 6.41: Reduction of purified IsoC by SDIMO reductases. MBP-T4moF is the maltose binding protein fusion to the toluene 4 monooxygenase reductase from *Pseudomonas mendocina* sp. KR1. GST-AmoD is the glutathione S-transferase protein fusion to the alkene monooxygenase reductase from *Rhodococcus rhodochrous* B-276

It is intriguing that the GST-AmoD was incapable of reducing IsoC, given that the protein was demonstrated to be active using potassium ferricyanide assays (section 6.6.2), and previous research has suggested that endogenous *Escherichia coli* reductases could compensate in the toluene 4-monooxygenase systems (Pikus *et al.*, 1996). Though these complementing reductases have never been identified, it would be expected that a reductase from within the SDIMO protein family would be more similar to IsoF than other types of reductase, and be more likely to complement the system. Given the findings outlined here and the low yield of attempted IsoF purification, it was deemed prudent to utilise the MBP-T4moF in the attempted reconstitution assays.

6.11. Conclusions

In this chapter, multiple approaches for the purification of the reductase component of isoprene monooxygenase from *Rhodococcus* sp. AD45 (IsoF) have been presented, and dismissed. The direct comparison of GST-fusions of alternative reductases from alkene monooxygenase and soluble methane monooxygenase to IsoF suggested that this may be due to the IsoF sequence, as this was the lowest expressed of the three fusion proteins and showed no FAD cofactor incorporation. The GST-IsoF protein and GST-AmoD proteins were

shown to be active using NADH:ferricyanide reductase assays, however the low yield of GST-IsoF meant this would be impractical to carry forward for reconstitution assays.

An alternative reductase from toluene 4-monooxygenase was also purified as an MBP fusion (MBP-T4moF), and this was shown to be capable of reducing the Rieske component of isoprene monooxygenase (IsoC), whereas the GST-AmoD could not perform this reduction which would be required for its use in reconstitution experiments.

In the next chapter, the purification of the final and largest component, the oxygenase, will be presented. In addition to this, the development of cell lysate and reconstitution assays to follow activity from whole cells to purified protein will be outlined, drawing together the purification of the components outlined in the previous three chapters.

7. Reconstitution of the active isoprene monooxygenase complex from *Rhodococcus* sp. AD45

7.1. Introduction

In previous chapters, the whole cell characterisation of isoprene monooxygenase in *Rhodococcus* sp. AD45 and the purification and characterisation of the smaller monooxygenase components have been presented. In this chapter, the focus will move to the larger active-site containing oxygenase component and reconstitution of an active purified isoprene monooxygenase complex.

Based on what is known about other SDIMOs, it is predicted that the isoprene monooxygenase oxygenase component will comprise the proteins IsoA, IsoB and IsoE with the active site lying next to the diiron cofactor site in the alpha subunit (IsoA). This, along with the beta (IsoE) and gamma (IsoB) subunits typically form a dimeric structure, with one of each subunit present per monomer. Based on this, the stoichiometric ratio has been demonstrated as two of the smaller coupling protein and Rieske protein subunits per hydroxylase dimer (Jahng and Wood, 1996; Cafaro *et al.*, 2002; Mitchell *et al.*, 2002; Champreda *et al.*, 2004; Bailey, Elsen, *et al.*, 2008). This previous work on reconstitution of SDIMO complexes was used to inform the development of both cell lysate and reconstitution assays.

The cloning of the genes encoding the oxygenase subunits and development of the oxygenase purification protocol was performed by Dr C. Lockwood (Murrell Group, University of East Anglia), and is presented here as a part of the wider work surrounding the cell lysate and reconstitution assays of isoprene monooxygenase.

In this chapter, the protocols used for cloning and purifying the oxygenase component from the isoprene monooxygenase of *Rhodococcus* sp. AD45 will be presented. The activity of isoprene monooxygenase from *Rhodococcus* sp. AD45 will be followed in whole cells, through to cell lysate and a reconstituted complex of purified protein to show activity of the complex throughout the various steps of purification. The effect of additional isoprene monooxygenase components on the isoprene degrading activity of cell lysate will be demonstrated.

7.2. Purification of the oxygenase component of isoprene monooxygenase from *Rhodococcus* sp. AD45.

7.2.1. Cloning *isoABE* from *Rhodococcus* sp. AD45 into the pTipQC2S2 vector for expression in *Rhodococcus* sp. AD45-ID

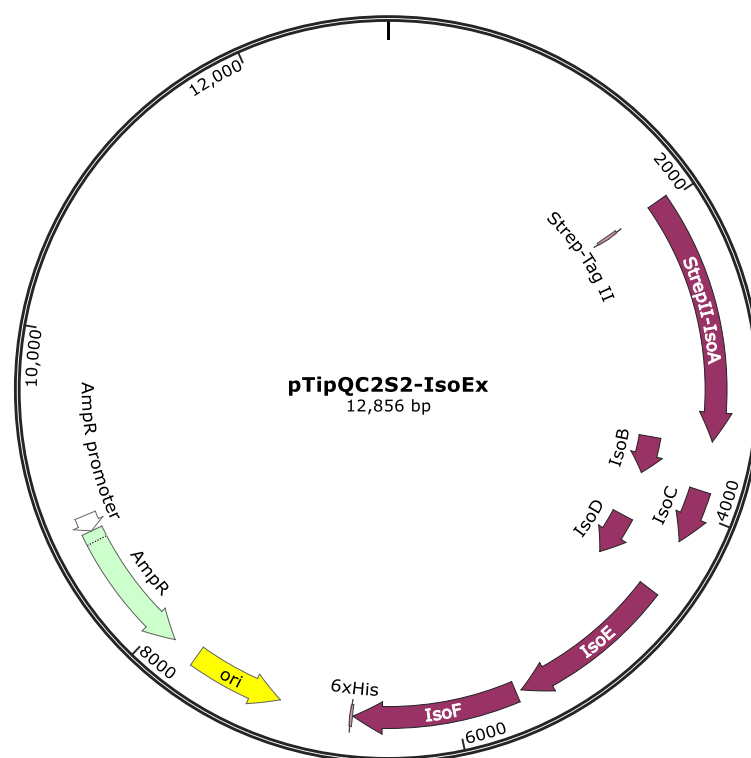


Figure 7.1: pTipQC2S2:IsoEx vector map for expression of *isoABCDEF* in *Rhodococcus* sp. AD45-ID, producing an N-terminally StrepII-tagged IsoA protein.

The pTip plasmid series was developed to enable expression of heterologous proteins over a wide range of temperatures in *Rhodococcus erythropolis* in order to overcome the inclusion bodies which often form in *Escherichia coli* (Nakashima and Tamura, 2004a). The pTipQC2 plasmid contains a multiple cloning site which has the potential to confer either an N or C terminal His tag to the expressed protein. This expression system was successfully used to express the *isoABCDEF* operon in *Rhodococcus* sp. AD45-ID, which has been outlined in Chapter 3. This construct produced a His-tagged IsoA, which Dr C. Lockwood (Murrell Group, University of East Anglia) attempted to purify using IMAC in conjunction with the IsoB and IsoE subunits forming the oxygenase, however this resulted in protein which could not restore isoprene monooxygenase activity to the flow through from the

column. This suggested that the oxygenase could bind the IMAC column, however eluted in an inactive form. Due to this, the vector was modified to introduce an N-terminal StrepII tag onto the IsoA protein, while still expressing with the rest of the operon in the same manner. This would overcome any negative effects the presence of imidazole or interaction with the IMAC column may have been having. This resulting construct, termed pTipQC2S2:IsoEx is shown in Figure 7.1

7.2.2. Purification protocol for IsoABE from *Rhodococcus* sp. AD45-ID (pTipQC2S2:IsoEx).

The purification protocol for the oxygenase component of isoprene monooxygenase was developed by Dr Lockwood (Murrell group, University of East Anglia). All purification steps were carried out using an AKTApure HPLC system and UNICORN™ 7 software.

The first step for purification of the oxygenase component was affinity chromatography using a StrepTactin-XT column. The purification buffers were as outlined in section 2.11.1, however the addition of 2 mM cysteine and 100 μM $(\text{NH}_4)_2\text{FeSO}_4$ was included, as this was found to maintain activity of the partially purified oxygenase in the StrepTactin-XT elution fractions, whereas this activity was not seen when these components were not included. This was in line with the purification of the oxygenase component from the toluene 2-monooxygenase from *Burkholderia cepacia* G4 (Newman and Wackett, 1995). The elution buffer contained 10 mM biotin for elution of the protein from the StrepTactin-XT column. The *Rhodococcus* sp. AD45-ID (pTipQC2S2:IsoEx) cells were grown in 6 x 1 L batch culture (section 2.3.3) on minimal medium with succinate as a carbon source and 35 $\mu\text{g mL}^{-1}$ chloramphenicol to maintain the plasmid. Once the cultures had reached an OD_{540} 0.6 – 0.8, isoprene monooxygenase operon expression was induced by the addition of 1 $\mu\text{g mL}^{-1}$ thiostrepton, followed by incubation at 25 °C overnight with shaking at 180 rpm. The cells were harvested by centrifugation and the cell pellet was resuspended in binding buffer. Following this, the cells were broken in a French pressure cell, and cell lysate prepared. The cell extract was filtered before applying to the StrepTactin XT column at 1 mL min^{-1} , and washed in 50 mL (10 CV) of binding buffer. The elution was paused for 20 minutes upon the beginning of the elution peak, as this was found to result in a cleaner peak of protein which eluted over a lower volume. The resulting AKTA trace from a 6 L batch of *Rhodococcus* sp. AD45-ID (pTipQC2S2:IsoEx) is presented in Figure 7.2. Samples of the load, flow through and elution were analysed by SDS-PAGE, and demonstrated clearly the

presence of polypeptides corresponding with the size of the two larger subunits of the oxygenase (IsoA and IsoE), though the smaller gamma subunit (IsoE) could not be visualised. This may be due to the small size making it less efficiently stained. There was also a number of contaminating bands, the majority of which were visible at 35 – 50 kDa.

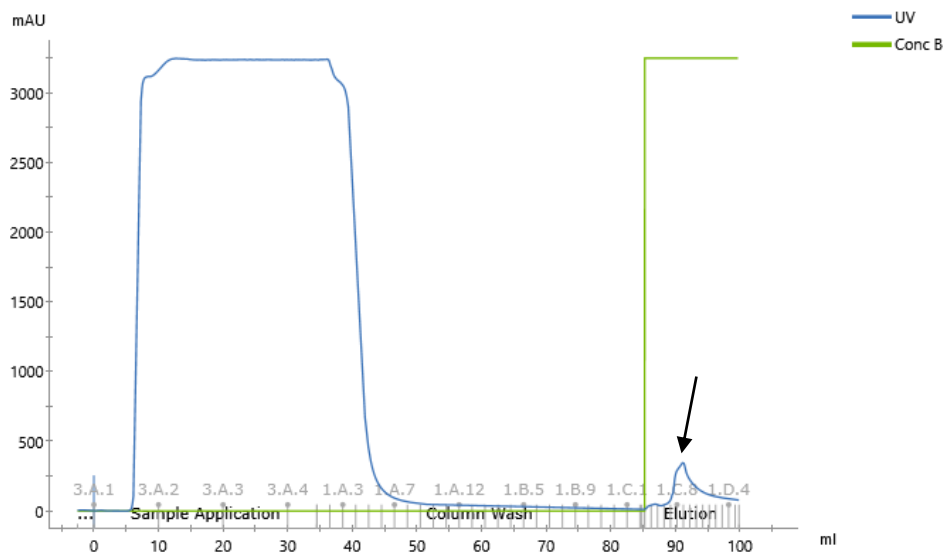


Figure 7.2: HPLC trace of a one-step elution of IsoABE from a 5 mL Strep-TactinXT column using an AKTApure system. The peak corresponding to the IsoABE elution has been highlighted with an arrow.

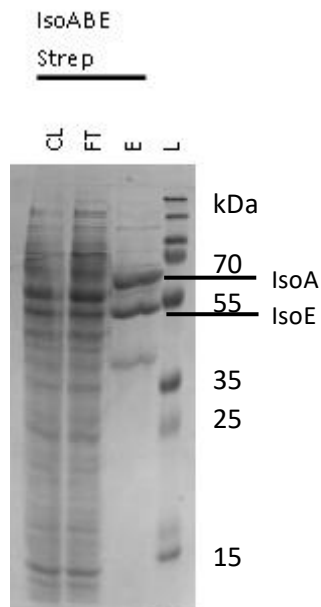


Figure 7.3: Polypeptide profile of IsoABE purification from *Rhodococcus* sp. AD45-ID (pTipQC2S2:IsoEx) using a 5 mL StrepTactin-XT column as visualised by SDS-PAGE and InstantBlue staining.

The elution fractions were combined, and this partially purified IsoABE sample was concentrated with a spin-concentrator column to approximately 2.5 mL. This concentrated sample was loaded onto a Superdex HiLoad 26/600 200 pg column equilibrated in the standard buffer (section 2.11.4), using a capillary loop. This gel filtration step was run at 1 mL min⁻¹ and 1 mL fractions were collected after 0.2 CV of buffer had been applied. This resulted in a cleaner profile for IsoABE and removal of most contaminating polypeptides according to samples run by SDS-PAGE (Figure 7.4).

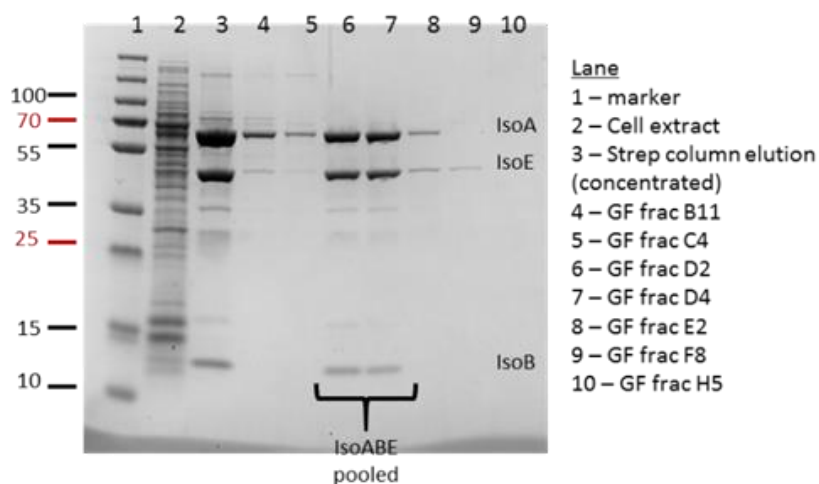


Figure 7.4: Purification of IsoABE using size exclusion chromatography. Polypeptide profiles of fractions were visualised using SDS-PAGE and InstantBlue staining. Image credit C. Lockwood.

7.3. Characterisation of purified IsoABE from *Rhodococcus* sp. AD45.

The purified oxygenase component was characterised using a variety of techniques, which aimed to identify the presence of the predicted diiron centre, the multimeric form of the protein component and how the spectroscopic characteristics compare to other SDIMO oxygenases.

7.3.1. Absorbance spectrum of purified IsoABE

The absorbance spectrum of IsoABE was recorded aerobically. The sample was analysed by diluting in a 2 mL quartz cuvette to ensure the absorbance at 280 nm was below 1 and

measuring the absorbance of the sample at wavelengths between 250 and 700 nm (Figure 7.5).

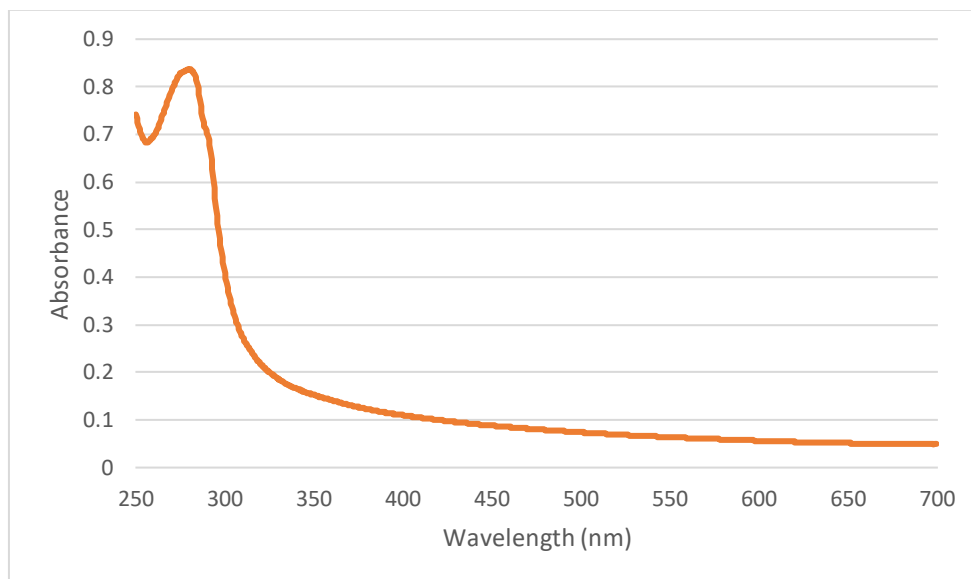


Figure 7.5: Absorbance spectrum of IsoABE as purified between 250 and 700 nm.

The IsoABE absorbance spectrum was featureless above 300 nm, which has been repeatedly reported in purified oxygenases from SDIMOs, including the soluble methane monooxygenase from *Methylococcus capsulatus* (Bath) (Merx and Lippard, 2002), the toluene 2-monooxygenase from *Burkholderia cepacia* G4 (Newman and Wackett, 1995), and the toluene/*o*-xylene monooxygenase from *Pseudomonas stutzeri* OX1 (Cafaro *et al.*, 2002).

7.3.2. ICP-MS analysis of IsoABE from *Rhodococcus* sp. AD45

As in Chapter 4 (section 4.6.3), ICP-MS analysis was used to quantify the presence of iron in purified IsoABE, and to check for the presence of other metals commonly found as enzyme cofactors. The samples were prepared as previously described (section 2.13.2), and results are presented in Table 7.1.

The initial ICP-MS analysis was performed on the elution from the StrepTactin column, followed by exchange into buffer containing 50 mM phosphate 150 mM NaCl (pH 7.0), using Spin-X UF concentrators (Corning). These results showed that approximately 4.32 equivalents of iron were present per monomer of IsoABE, which is higher than the predicted 2 equivalents of iron. Though iron quantification of the toluene 2-

monooxygenase of *Burkholderia cepacia* G4 found the component to contain 2.95 equivalents of Fe per monomer of protein (Newman and Wackett, 1995), the level found for the isoprene monooxygenase has not previously been recorded. The IsoABE protein sample was also analysed for the presence of other common metal cofactor components, magnesium, manganese, cobalt, nickel, copper, and zinc. Whilst most were absent, the results for copper and magnesium were mixed. ^{63}Cu analysis suggested the presence of 1.52 mol Cu per mol of protein, whereas ^{65}Cu analysis suggested that only 0.08 mol of Cu was present. In a similar level of inconsistency, ^{24}Mg analysis implied the presence of 1.1 Mg per monomer, whereas ^{25}Mg analysis suggested that only 0.21 mol was present. Anomalous ICP-MS readings of both ^{63}Cu and ^{24}Mg have previously been attributed to polyatomic interferences. ^{63}Cu interference is often due to ArNa species arising from high Na in the sample, for example due to the addition of salt to the preparation buffer. Anomalous ^{24}Mg data have been previously attributed to $^{12}\text{C}_2$ species, which can form due to the presence of dissolved gases such as CO_2 in the samples (Reed *et al.*, 1994; May and Wiedmeyer, 1998). Given these recognised limitations of ICP-MS, it is most likely that the high concentrations associated with certain copper and magnesium isotopes are the anomaly, and that IsoABE does not contain any metal cofactors except for the predicted diiron centre.

To confirm whether these anomalous values could alternatively be due to adventitious binding of metals, or contaminating proteins, a further size exclusion purification step was carried out (Section 2.11.4). ICP-MS analysis of this sample demonstrated reduction in all unexpected metals, and reduced the measured Fe content to 1.12 equivalents per monomer. This low iron content could cause reduced activity of the monooxygenase, due to apparent low incorporation of the catalytically important diiron site.

Table 7.1: Results of ICP-MS analysis of purified IsoABE, showing the number of moles of each element per mole of protein monomer. Where multiple isotopes of elements have been used the mean value is presented.

| Protein | Concentration (μM) | Fe | Mg | Mn | Co | Ni | Cu | Zn |
|---------|------------------------------------|------|------|------|------|------|------|------|
| IsoABE | 3.49 | 4.32 | 0.98 | 0.01 | 0.00 | 0.05 | 1.20 | 0.00 |
| | 72.69 | 1.12 | 0.01 | 0.00 | 0.00 | 0.01 | 0.11 | 0.04 |

The concentration of IsoABE was calculated to be 3.49 μM , compared to 3 μM as calculated by Bradford assay. Based on the concentration calculated by the ICP-MS analysis, the extinction coefficient of IsoABE at 280 nm was calculated to be 584,802 $\text{M}^{-1} \text{cm}^{-1}$. This value is in line with published values for other SDIMO oxygenase components, including the recorded 600,000 $\text{M}^{-1} \text{cm}^{-1}$ for toluene/*o*-xylene monooxygenase (Tinberg *et al.*, 2011), and 664,770 $\text{M}^{-1} \text{cm}^{-1}$ for soluble methane monooxygenase (Gassner and Lippard, 1999).

7.4. Following isoprene monooxygenase activity in *Rhodococcus* sp. AD45: from whole cells to purified protein

Whilst an assay for isoprene monooxygenase activity had been developed for whole cells of *Rhodococcus* sp. AD45 grown on isoprene and *Rhodococcus* sp. AD45-ID cells expressing the pTipQC1:IsoEx expression plasmid encoding the full *isoABCDEF* operon (Chapter 3), activity had not yet been achieved with cell lysate from either of these systems. It was important to establish whether the protein retained activity after cell lysis, since if this is where the issue lay, it may not be possible to purify active protein components for extensive characterisation and reconstitution assays. In this section, results of the development process for this cell lysate activity assay, and how this informed subsequent reconstitution attempts will be outlined.

7.4.1. Development of whole cell assays to monitor isoprene monooxygenase activity in *Rhodococcus* sp. AD45.

The optimisation of whole cell assays to analyse isoprene monooxygenase activity was presented in section 3.2. The assay protocol involved the resuspension of cells in 50 mM phosphate buffer at a final cell density of 0.25 mg mL^{-1} . The cells suspensions were incubated at 30 °C in a shaking water bath, and isoprene was added to a final headspace concentration of approximately 300 ppmv. Samples were taken every 3 min and the isoprene concentration was analysed using a Fast Isoprene Sensor (section 2.8). Repetition of this protocol with soluble extract of *Rhodococcus* sp. AD45 cells grown in a fermenter with isoprene as a carbon source resulted in no detectable activity, regardless of whether the soluble extract was used as prepared or further diluted with additional phosphate buffer.

7.4.2. Development of cell lysate assays to monitor isoprene monooxygenase activity in *Rhodococcus* sp. AD45.

Initially, the preparation of cell lysate resulted in a low protein concentration, so various approaches were used in order to break the *Rhodococcus* cells, including repeated cycles of freeze-thawing, sonication as was used for *Escherichia coli* (section 2.6), the addition of lysozyme (SigmaAldrich) according to manufacturer's instructions, and the French press method (section 2.6). The protein concentration of the resulting soluble cell extract was quantified using a Bradford assay, and the results suggested that the French pressure cell and sonication were the most effective cell lysis methods (Figure 7.6). Due to the ease of scaling up the French press method of cell lysis for large volumes of cell suspension, this technique was subsequently used.

Following this, the addition of a stabilising agent was attempted. Based on the previously published protocols for both cell lysate and reconstitution assays (Colby and Dalton, 1978; Whited and Gibson, 1991; Nakajima *et al.*, 1992; Small and Ensign, 1997; Merkx and Lippard, 2002; Champreda *et al.*, 2004, 2006), 5 mM DTT was added during assay preparation. This resulted in an activity of 0.23 nmol min⁻¹ mg protein⁻¹. This was still lower than the rate recorded in the paper the method was taken from, which was recorded as 0.45 nmol min⁻¹ mg protein⁻¹ (Nakajima *et al.*, 1992). Previous research focussing on soluble methane monooxygenases had identified that the use of 1 mM DTT was not high enough to stabilise the monooxygenase, and that 5 mM may be more appropriate (Nakajima *et al.*, 1992). This has been specifically implicated in increasing the stability of the reductase component (Colby and Dalton, 1978). In some cases, the addition of DTT had been performed before the cell breakage (Whited and Gibson, 1991; Small and Ensign, 1997), which was attempted next. Testing this resulted in an increase in activity to 0.44 nmol min⁻¹ mg protein⁻¹, and this was not increased by the addition of a higher (10 mM) DTT concentration, which is in agreement with the work on soluble methane monooxygenase of *Methylococcus capsulatus* (Bath) (Colby and Dalton, 1978). The addition of DTT after cell breakage resulted in no activity, so from this point forward the DTT was added at 5 mM before cell lysis and maintained at this level when diluting at later stages. The yield of protein was still low, and the cell suspension concentration had been demonstrated as a feature which affected calculated rates in the whole cell experiments (section 3.2.1). Due to this, the concentration of protein per assay was optimised next.

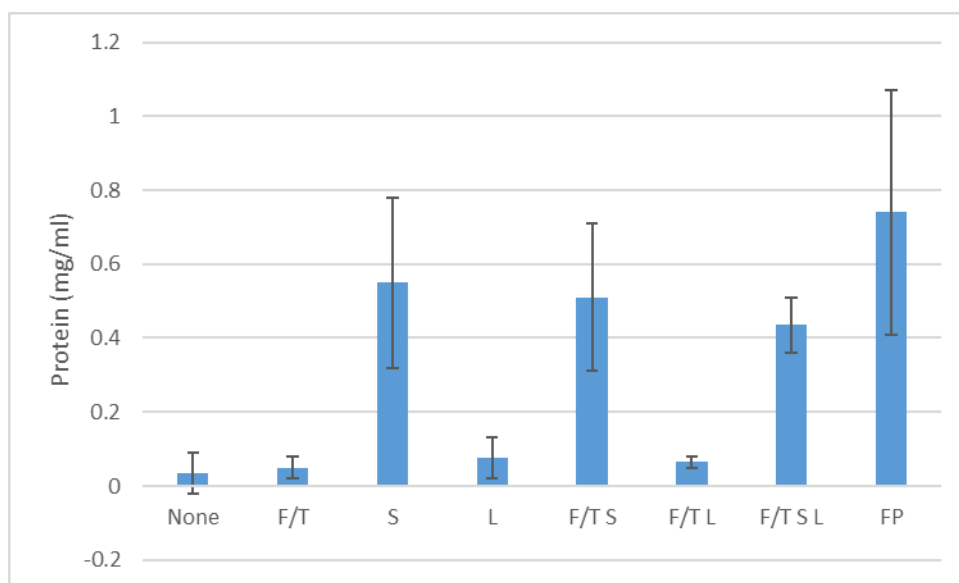


Figure 7.6: Protein yield of various cell lysis methods conducted on *Rhodococcus* sp. AD45 cells grown on isoprene (\pm SD, n=2). F/T – Freeze/Thaw 3x, S – Sonication, L – Lysozyme, FP – French Press.

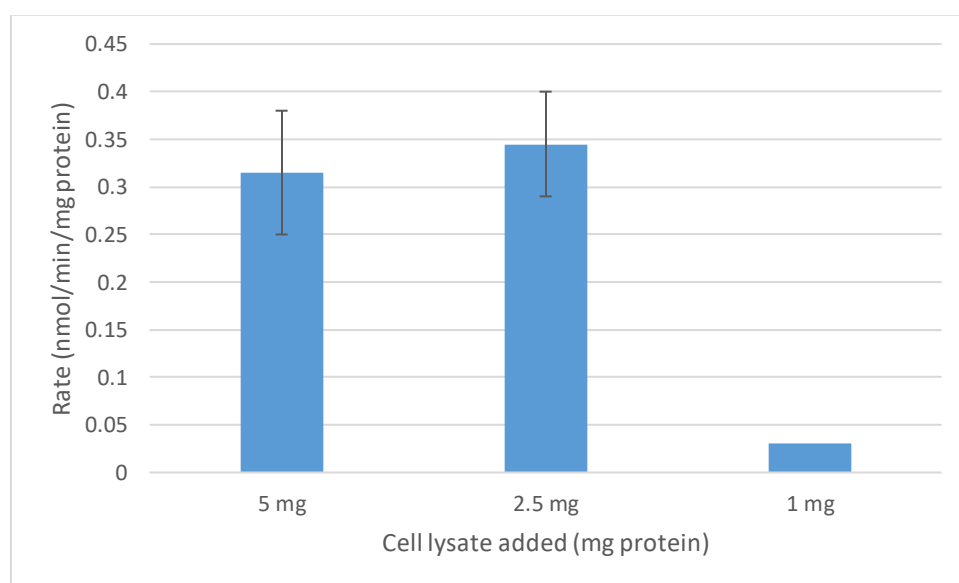


Figure 7.7: Difference in rate of isoprene degradation by *Rhodococcus* sp. AD45 cell lysate samples diluted to different protein concentrations using phosphate buffer (\pm SD, n=2 (5/2.5 mg), n=1 (1 mg)).

The typical yield of protein from the cell lysis was increased to approximately 6 mg mL⁻¹ by increasing the concentration of cell suspension used. The amount of protein used per 1 mL

assay was tested at 5 mg, 2.5 mg and 1 mg to identify whether altering this concentration could increase the activity level. The results of this suggested that 2.5 mg was the minimum that could be used while keeping an activity which was consistently measurable on the Fast Isoprene Sensor (Figure 7.7). This decreased protein requirement meant that the cell lysate could be used to perform more assays.

Due to the potential to run more assays with the cell lysate sample, the stability of activity in the cell extract was next monitored over several hours to identify whether it would quickly deplete when kept on ice after lysis. Assays were run every hour after the cells were lysed, and the results suggested that the activity was maintained at the same level for at least 6 hours (Table 7.2). Salt is often used in protein purification assays to mimic the osmotic environment within the cell, so the addition of 200 mM NaCl was attempted to increase the activity of the cell lysate assay. The addition of 200 mM NaCl was not found to increase the activity (Figure 7.8), so this was not carried forward.

Table 7.2: *Rhodococcus* sp. AD45 cell lysate isoprene degradation activity over as measured at timepoints (h) after cell breakage (n=1).

| Time (h) | Rate (nmol/min/mg protein) |
|---------------------|---------------------------------------|
| 3 | 0.54 |
| 4 | 0.4 |
| 5 | 0.47 |
| 6 | 0.64 |

The cell lysate assays were found to be highly variable, with cell lysate assays using the same parameters and from the same batch of isoprene-grown *Rhodococcus* sp. AD45 cells resulted in rates which varied between 0.3 and 1.7 nmol min⁻¹ mg protein⁻¹. This is similar to the findings of other research, particularly on the alkene monooxygenase of *Xanthobacter autotrophicus* sp. Py2, where the activity in cell lysate assays has been recorded between 5 – 55 nmol min⁻¹ mg protein⁻¹ (Small and Ensign, 1997). The addition of 10 % v/v glycerol, another component found to stabilise SDIMO activities in previous research (Hartmans *et al.*, 1991; Whited and Gibson, 1991; Newman and Wackett, 1995; Small and Ensign, 1997; Champreda *et al.*, 2004), did not result in any increased or more

consistent activity, and consistently prevented efficient removal of cell debris by centrifugation when added before cell breakage. Due to this, glycerol was not included in the future assays.

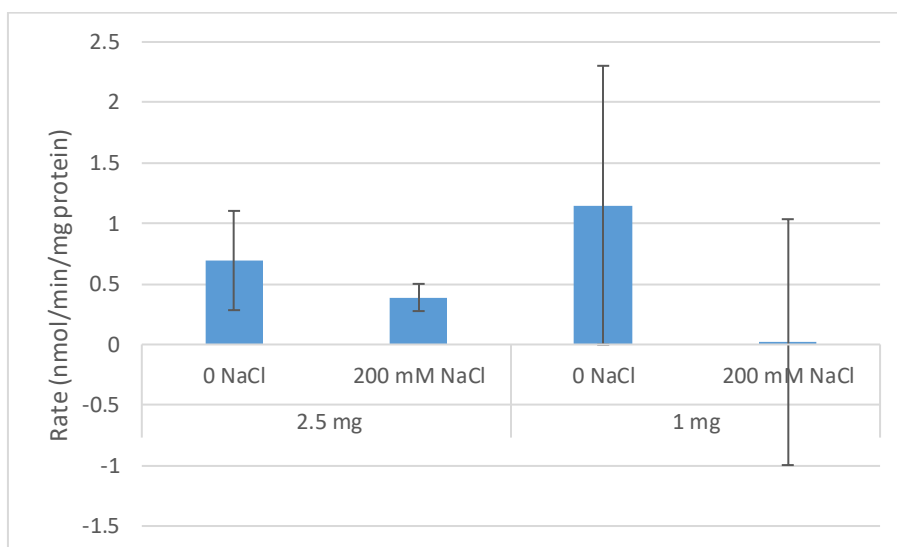


Figure 7.8: The effect of NaCl addition on the isoprene degradation activity of *Rhodococcus* sp. AD45-ID cell lysate (\pm SEM, $n=3$).

Following development of cell lysate assays for *Rhodococcus* sp. AD45 grown on isoprene, it was important to demonstrate that *Rhodococcus* sp. AD45-ID expressing the new pTipQC2S2:IsoEx plasmid could also demonstrate isoprene monooxygenase activity, as had previously been shown for the *Rhodococcus* sp. AD45-ID (pTipQC1:IsoEx) cells (section 3.2.4). The whole cell assays resulted in an activity of $0.06 \text{ nmol min}^{-1} \text{ mg dw cells}^{-1}$, which is half of the rate recorded for *Rhodococcus* sp. AD45-ID cells containing the pTipQC1:IsoEx plasmid (section 3.2.4). In contrast, the cell lysate assays following the same protocol as developed for *Rhodococcus* sp. AD45 cells grown on isoprene resulted in an isoprene degradation rate of $0.6 \text{ nmol min}^{-1} \text{ mg protein}^{-1}$, which is within the range observed for the isoprene-grown cells, which were previously shown to have a much higher isoprene degradation rate in whole cell assays (section 3.2.4). This seemingly increased rate in cell lysate assays may be due to the availability of NADH. The SDIMOs use the oxidation of NADH by the reductase to shuttle electrons through the Rieske protein to the diiron active site of the oxygenase (Liang and Lippard, 2014). In isoprene monooxygenase, it is predicted that this NADH pool is replenished by the reduction of NADH during a later step in the isoprene degradation pathway catalysed by IsoH (van Hylckama Vlieg *et al.*, 2000), which is

not on the pTipQC2S2:IsoEx plasmid. This means that the isoprene monooxygenase may rapidly deplete the available NADH in whole cell assays where IsoH is not present, whereas the addition of a large excess of NADH in the cell lysate assays can compensate for this. However, this does not explain why there is a comparatively high rate in the *Rhodococcus* sp. AD45-ID cells when expressing pTipQC1:IsoEx in comparison to pTipQC2S2:IsoEx.

7.4.3. Addition of purified protein components to isoprene monooxygenase activity assays using *Rhodococcus* sp. AD45-ID (pTipQC2S2:IsoEx).

Now that the activity of isoprene monooxygenase expressed using the pTipQC2S2:IsoEx plasmid had been demonstrated, the addition of purified oxygenase component to cell lysate assays was tested for increase in monooxygenase activity. This was predicted to increase the isoprene monooxygenase activity as multiple purified oxygenase components from SDIMOs have been demonstrated to confer low levels of monooxygenase activity even without the additional components (Froland *et al.*, 1992; Newman and Wackett, 1995; Cafaro *et al.*, 2002). The cell lysate assays were prepared as outlined above, using lysate from *Rhodococcus* sp. AD45-ID (pTipQC2S2:IsoEx) cells. IsoABE was added to the reaction after elution from the StrepTactin-XT column and after concentration and buffer exchange into the appropriate buffer for gel filtration (section 2.11.4). The rates were calculated per mg of IsoABE added (Table 7.3), and suggested that the protein was active when eluting from the StrepTactin-XT column but not after buffer exchanging. This may be due to a requirement for the additional iron and cysteine in the purification buffer, which was removed during the buffer exchange. This has been observed previously (Fox *et al.*, 1989; Newman and Wackett, 1995), and may be required for reconstitution of the active isoprene monooxygenase complex.

Table 7.3: Rate of isoprene degradation by cell lysate of *Rhodococcus* sp. AD45-ID (pTipQC2S2:IsoEx) with addition of IsoABE after various stages of purification. Experiments performed by Dr C. Lockwood (Murrell Group, University of East Anglia).

| Sample | Rate (nmol min ⁻¹ mg IsoABE ⁻¹) |
|-------------------------------|--|
| Strep column elution | 70 |
| Concentrated IsoABE (0.85 mg) | 15 |
| Concentrated IsoABE (1 mg) | 18 |

7.5. Reconstitution of the active isoprene monooxygenase complex from *Rhodococcus* sp. AD45

As the individual protein components were purified and characterised as individual units, the next step was to achieve reconstitution of the active complex. The oxygenase had been demonstrated as active based on addition to cell lysate assays (section 7.4.3), the Rieske protein had been shown to be capable of redox cycling (section 4.5), and the purified reductases from both the alkene monooxygenase of *Rhodococcus rhodochrous* sp. B-276 and the isoprene monooxygenase of *Rhodococcus* sp. AD45 were both capable of reducing potassium ferricyanide (section 6.8). The coupling protein was yet to be demonstrated as functional, however this was less of a concern as the coupling protein of soluble methane monooxygenase from *Methylocystis* sp. strain WI 14 was demonstrated to increase the level of monooxygenase activity dramatically, but was not required for low levels of activity (Grosse *et al.*, 1999) .

In the reconstitution assays, initial attempts comprised 5 μM of each IsoABE monomer, IsoD and IsoC, and 1 μM MBP-T4moF, as this was believed to have the highest chance of showing activity. This ratio of components similar to that used in other reconstitution assays for soluble methane monooxygenase (Jahng and Wood, 1996), toluene/*o*-xylene monooxygenase (Cafaro *et al.*, 2002), toluene 4-monooxygenase (Mitchell *et al.*, 2002) and alkene monooxygenase (Champreda *et al.*, 2004, 2006). When monitored by 50 μL headspace samples measured using the Fast Isoprene Sensor after every 3 minutes, the rate was found to be $0.85 \text{ nmol min}^{-1} \text{ mg IsoABE}^{-1}$, though the R^2 value for the line of best fit was calculated at 0.22, which makes this result less reliable. The reaction was monitored over a longer timeframe, and the new rate was found to be lower $0.37 \text{ nmol min}^{-1} \text{ mg IsoABE}^{-1}$, however the result was more reliable, with an R^2 value of 0.89 (Figure 7.9). This is in line with previous reconstitution of the alkene monooxygenase from *Xanthobacter autotrophicus* sp. Py2, , where a longer incubation of 180 min was used, and the rate of butene epoxidation was recorded as $6.25 \text{ nmol min}^{-1}$ in a reconstitution containing 1.5 nmol of reductase (Champreda *et al.*, 2006). This recorded rate for alkene monooxygenase, however, was much higher than that found for isoprene monooxygenase here, considering that a higher amount of oxygenase was utilised (2.5 nmol). Negative controls containing only buffer demonstrated a negligible rate of isoprene depletion, at $0.025 \pm 0.017 \text{ nmol min}^{-1}$ ($n=2$, \pm SD).

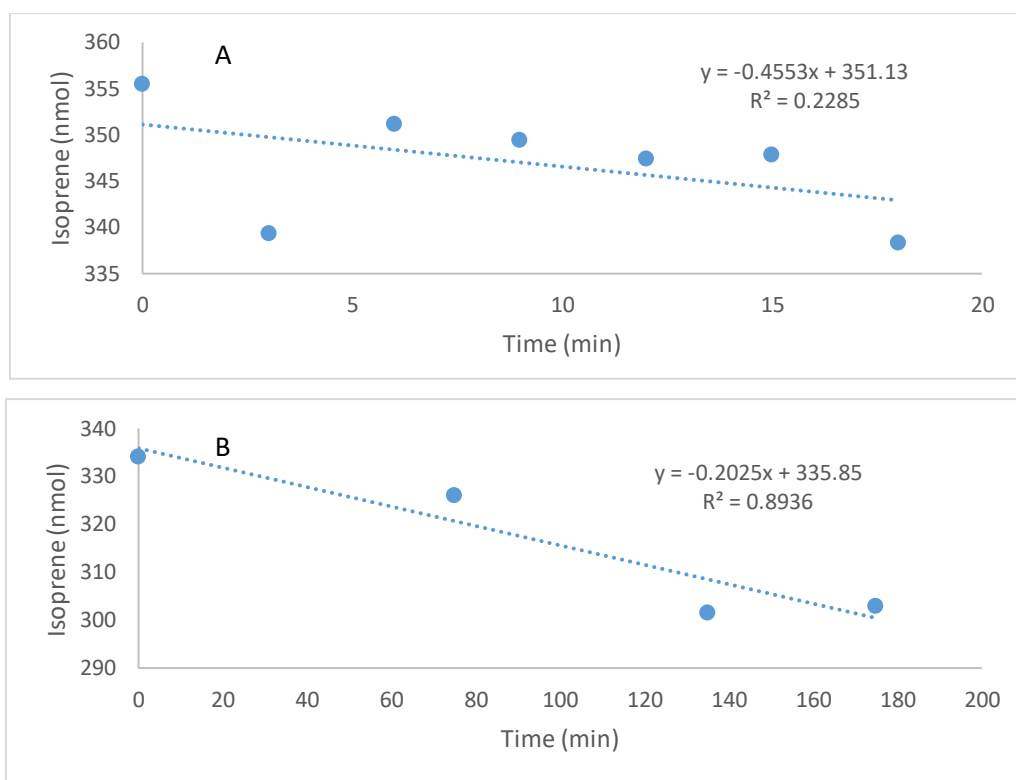


Figure 7.9: Attempted reconstitution of purified isoprene monooxygenase in 50 mM phosphate buffer pH 7.0 using purified protein (5 μ M each IsoABE, IsoC, IsoD, 1 μ M MBP-T4moF) as monitored by isoprene depletion using a Fast Isoprene Sensor over A) 18 min and B) 180 min.

Following this, the same reaction mixture was prepared, using a buffer containing 200 mM NaCl. This increased the rate of isoprene monooxygenase activity to $1.83 \text{ nmol min}^{-1} \text{ mg IsoABE}^{-1}$ over 18 min, however over 180 min this was similar to the previous rate of $0.31 \text{ nmol min}^{-1} \text{ mg IsoABE}^{-1}$. This suggested that the addition of 200 mM NaCl may be used to perform less time-consuming reconstitution assays. The addition of ferrous iron and L-cysteine was attempted as this seemed to improve the activity of the oxygenase previously (section 7.4.3), however this did not improve the rate of reaction (results not shown). The use of the alternative GST-AmoD reductase component yielded no rate, as expected due to its inability to reduce IsoC (section 6.10). The consistently low rates observed in attempted reconstitution assays of isoprene monooxygenase may be due to the absence of purified active reductase, IsoF, for use in the assays, or for the low iron incorporation into the oxygenase component (IsoABE), as suggested by the level of iron identified in ICP-MS analysis (Section 7.3.2)

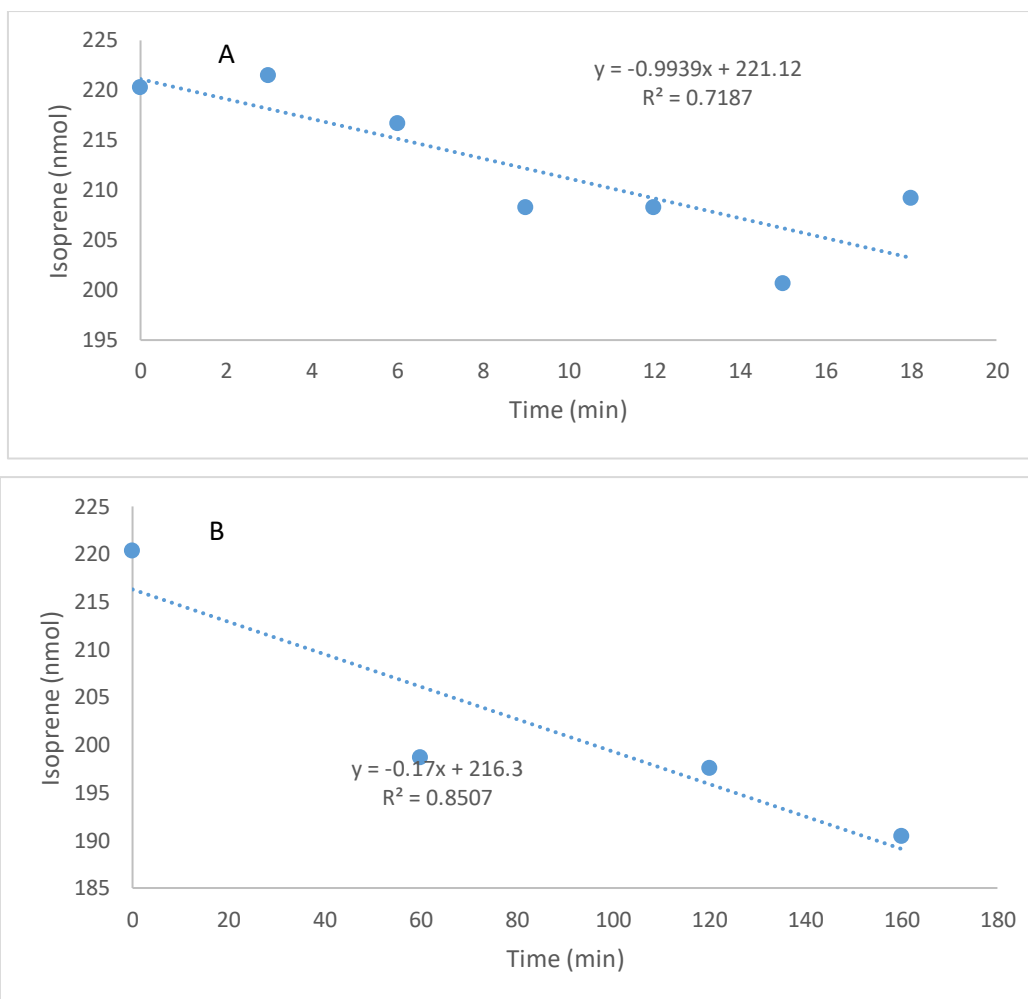


Figure 7.10: Attempted reconstitution of isoprene monooxygenase activity in 50 mM phosphate buffer pH 7.0 containing 200 mM NaCl, 5 μ M each IsoABE, IsoC, IsoD and 1 μ M MBP-T4moF. Isoprene depletion was monitored using a Fast Isoprene Sensor over A) 18 min and B) 180 min.

7.6. Conclusions

Overall, this chapter has presented the purification of the oxygenase component of isoprene monooxygenase from *Rhodococcus* sp. AD45 and followed the monooxygenase activity through from whole cells and cell lysate to the purified protein. The use of toluene 4-monooxygenase reductase was effective in reconstitution assays, however the low rates of reaction leave the potential for a wealth of optimisation, and ultimately future characterisation of the isoprene monooxygenase complex. Some ideas for this will be presented in the following, and final, chapter.

8. Conclusions and future prospects

8.1. Whole cell characterisation of isoprene monooxygenase

Chapter 3 detailed the development and optimisation of assays to quantify isoprene degradation by whole-cell suspensions of *Rhodococcus* sp. AD45. These assays were developed using a range of techniques, laying important groundwork for characterisation of the isoprene monooxygenase within the whole-cell system, which is most relevant to environmental studies. The whole cell kinetics of isoprene monooxygenase were calculated and compared to the closely related alkene monooxygenase in *Xanthobacter* sp. Py2. The substrate range was identified, and compared to the isoprene monooxygenase of *Variovorax* sp. WS11. These data were compared to the published substrate range of other SDIMOs, and could contribute to identification of the bioremediation potential of isoprene monooxygenase, due to the wide range of alkene and aromatic compounds which can be degraded. The profile of inhibition by varying chain-length alkynes was also identified, and crucially isoprene monooxygenases not inhibited by acetylene, unlike the soluble methane monooxygenases. This finding could present the opportunity to differentiate between environmental isoprene degradation by microorganisms containing isoprene monooxygenase, rather than co-oxidation by the soluble methane monooxygenase.

8.2. Purification and characterisation of the Rieske protein, IsoC

Chapter 4 described the purification and characterisation of IsoC, the Rieske-type protein component of the isoprene monooxygenase from *Rhodococcus* sp. AD45. IsoC was expressed using the *Rhodococcus* sp. AD45-ID homologous expression system, either as an N-terminally His-tagged protein or untagged as part of the isoprene monooxygenase operon. Both of these proteins were purified and shown to possess the same absorbance spectra characteristics, and midpoint potential based on cyclic voltammetry. The His-tagged protein was more extensively characterised, and the predicted Rieske-type cluster was proven to be present using absorbance, circular dichroism and electron paramagnetic resonance spectroscopy. LC-MS analysis was then used to confirm the size and purity of the protein, and the N-terminal methionine was found to be cleaved. ICP-MS proved that no other common metal cofactors were present, and was used to calculate the extinction coefficient for IsoC, which was found to be similar to other Rieske components of SDIMOs. The ICP-MS data also demonstrated that the protein had a high level of [2Fe-2S] cluster incorporation. All of these data supported the use of homologically expressed His-tagged

IsoC in future reconstitution attempts, and proved that the protein was capable of the redox cycling which is vital for its role in the isoprene monooxygenase catalytic cycle.

8.3. Purification and characterisation of the coupling protein, IsoD

In Chapter 5, the results of coupling protein (IsoD) purification and characterisation were presented. The homologous system was found to be ineffective for IsoD expression and purification, so an N-terminally StrepII-tagged IsoD was expressed in *Escherichia coli* instead. IsoD was successfully purified using a combination of affinity and gel filtration chromatography, and an anion exchange step was proven not to improve sample purity. Performing the purification protocol over a shorter timeframe also reduced protein aggregation. The purified IsoD was found to anomalously migrate on SDS-PAGE gels, regardless of buffer and protein concentration. Cleavage of the StrepII-tag was ineffective, however previous research suggested this may not pose a problem in reconstitution experiments (Brandstetter *et al.*, 1999; Champreda *et al.*, 2004; Moe *et al.*, 2006). Absorption spectroscopy proved the absence of optically active cofactors, as predicted, and LC-MS analysis revealed no evidence for an N-terminal truncation found to inactivate the coupling protein from a soluble methane monooxygenase (Lloyd *et al.*, 1997).

8.4. Purification of SDIMO reductases

Chapter 6 outlined the various attempts to purify the reductase component of isoprene monooxygenase from *Rhodococcus* sp. AD45, termed IsoF. Expression in the homologous system as an N-terminally His-tagged protein resulted in low yield of protein with no spectroscopic characteristics associated with the predicted FAD and [2Fe-2S] cofactors. Subsequently, untagged IsoF was produced as inclusion bodies in *Escherichia coli*, and an MBP-IsoF fusion protein rapidly precipitated after elution from the affinity chromatography column. Subsequent cleavage of the maltose binding protein resulted in a very low yield of protein which was not of the expected size according to LC-MS. Finally, a construct for expression of GST-IsoF fusion protein was produced. Protein production was directly compared between this and GST fusions of the reductases from alkene monooxygenase of *Rhodococcus rhodochrous* sp. B-276 (AmoD) (Smith *et al.*, 1999), and soluble methane monooxygenase from *Methylosinus trichosporium* sp. OB3b (MMOB) (Smith *et al.*, 2002). The GST-IsoF fusion protein was found to have the lowest yield of soluble protein based on the results of an affinity chromatography step. This protein had an absorbance spectrum

characteristic at 420 nm, suggesting the presence of the predicted [2Fe-2S] cluster, however the FAD characteristics were not observed. Both predicted cofactors were present in the GST-AmoD sample, and neither were present in the MMOB, based on the absorbance spectra. The GST-IsoF was only able to oxidise potassium ferricyanide after cleavage of the MBP fusion by thrombin, whereas the GST-AmoD was active with or without cleavage, and GST-MMOB was inactive in either state. Finally, another alternative reductase from toluene 4-monooxygenase (T4moF) was purified as an MBP-fusion protein (Acheson *et al.*, 2015). Comparison of the reduction of IsoC by the alternative reductases demonstrated that only the T4moF could complement the system, whereas AmoD could not, as either a fusion protein or after GST removal. These data influenced the reconstitution attempts, as only T4moF could be purified in large enough quantities and with IsoC reductase activity to be used in the reconstitution attempts.

8.5. Reconstitution of the active complex

Finally, Chapter 7 presented the purification of the active site-containing oxygenase component of isoprene monooxygenase (IsoABE), using the same homologous expression system used for the purification of the Rieske protein (IsoC, Chapter 4). The absorbance spectrum was in agreement with the previously purified oxygenase components of other SDIMO systems, and ICP-MS analysis confirmed the predicted presence of a diiron centre, and no other common metal cofactors. The development of an assay for isoprene degradation by *Rhodococcus* sp. AD45 cell lysate was also presented, to confirm that the enzyme activity could still be monitored when isoprene monooxygenase is outside the cell, and influencing the protocol for a reconstituted complex. The purified oxygenase component was demonstrated to increase the cell lysate activity, however the reconstitution of purified isoprene monooxygenase was incomplete, and only low rates of isoprene degradation was achieved over long time periods using the T4moF reductase.

8.6. Future prospects

The results of this study have opened some interesting avenues for future research to enhance our understanding of isoprene degradation by microbes and the biotechnological potential of SDIMOs. While a number of bacteria have been isolated which can grow on isoprene as a sole carbon source, the biochemical basis of isoprene degradation remains comparatively poorly understudied. An increased understanding of the whole-cell kinetics

of isoprene degradation by isoprene monooxygenase containing organisms could contribute to the understanding of the impact altering isoprene levels will have on the amount of isoprene degradation. Notably, the apparent K_M for isoprene degradation by whole cells suspensions of *Rhodococcus* sp. AD45 is considerably higher than recorded environmental isoprene levels at 2.88 μM , which would correspond to approximately 220 ppmv. This is much higher even than the isoprene concentrations found inside leaves, recorded at a maximum of 30 ppmv (Singsaas *et al.*, 1997). Atmospheric isoprene concentrations have been recorded much lower, at 1 – 5 ppbv over a range of isoprene emitting forests (Hewitt and Street, 1992; Klinger *et al.*, 1998; Harrison *et al.*, 2012), and around 40 ppbv below the forest canopy (Wiedinmyer *et al.*, 2001, 2005). Notably, *Rhodococcus* sp. AD45 was isolated from freshwater sediment (van Hylckama Vlieg *et al.*, 1998), and recent studies have suggested that some isoprene may be produced in plant roots (Miloradovic van Doorn *et al.*, 2020). Despite this, no studies have recorded the isoprene concentration in soil or sediments, despite these being a source of a number of environmental isolates. Interestingly, isolates found using lower isoprene concentrations are more varied (Larke-Mejía *et al.*, 2019), and it would be intriguing to identify whether these Gram negative isolates possess a different affinity for isoprene based on the whole-cell K_M . Isoprene co-oxidation has been recorded in bacteria containing other SDIMOs, including the alkene monooxygenase of *Xanthobacter autotrophicus* sp. Py 2 (van Ginkel *et al.*, 1986) and soluble methane monooxygenase from *Methylobacterium* sp. CRL-26 (Patel *et al.*, 1982). The alkyne inhibition profile outlined here could be used to aid in the identification of the proportion of isoprene degradation performed by the true isoprene degraders containing the isoprene monooxygenase, as opposed to organisms which contain alternative SDIMOs. In particular, acetylene can be used to remove co-oxidation by soluble methane monooxygenase containing bacteria, as it is a suicide substrate of this enzyme (Prior and Dalton, 1985). Alternatively, attempting inhibition with alkynes closer in structure to isoprene may yield a suicide substrate, which could be used to isolate the level of isoprene monooxygenase activity in environmental samples. The justification for this approach can be found in the literature, where studies have repeatedly shown that alkynes closer to the preferred substrates of SDIMOs act as more potent inhibitors. For example, propyne and butyne were more potent inhibitors of the alkene monooxygenase of *Rhodococcus rhodochrous* sp. B-276 (Fosdike *et al.*, 2005), aromatic alkynes were the most effective inhibitors of toluene 4-monooxygenase (Keener *et al.*, 2001), and propyne was

used as an inhibitor of the alkene monooxygenase of *Xanthobacter autotrophicus* sp. Py2; a bacterium which was isolated due to its ability to grow on propylene (Ensign *et al.*, 1992).

With consideration to the biotechnological potential for isoprene monooxygenase, and the wider SDIMO group, a number of future experiments would be informative. Firstly, the reconstitution of isoprene monooxygenase will need to be completed. This could be followed by identification of the enantiomers produced during epoxidation of compounds to identify the level of stereoselectivity, an important consideration in the formation of chiral compounds for industrial purposes. An enhanced understanding of the cross-reactivity between SDIMO components would also be beneficial. The successful complementation of some SDIMO systems with endogenous *Escherichia coli* reductases (Pikus *et al.*, 1996) is in direct contrast with the results obtained here, where the reductase from alkene monooxygenase of *Rhodococcus rhodochrous* sp. B-276 expressed as a GST-fusion protein (AmoD, Smith *et al.*, 1999) could not be used to reduce IsoC (section 6.10). This was unexpected as the AmoD had 50 % similarity to IsoF at the amino acid level, and 33 % of the residues were identical (Chapter 6). Other research groups have investigated the use of alternate coupling proteins to change the regioselectivity and stereoselectivity of SDIMOs (Champreda *et al.*, 2006), and the purification protocols outlined in this thesis for the components of isoprene monooxygenase offers further available components for this kind of investigation. Finally, studying the structure of isoprene monooxygenase and identifying key residues exclusive to this group of SDIMOs would enhance understanding of the link between structure and substrate specificity and the key differences between isoprene monooxygenases and other SDIMOs.

References

- Acheson, J.F., Bailey, L.J., Brunold, T.C., and Fox, B.G. (2017) In-crystal reaction cycle of a toluene-bound diiron hydroxylase. *Nature* **544**: 191–195.
- Acheson, J.F., Bailey, L.J., Elsen, N.L., and Fox, B.G. (2014) Structural basis for biomolecular recognition in overlapping binding sites in a diiron enzyme system. *Nat Commun* **5**: 5009.
- Acheson, J.F., Moseson, H., and Fox, B.G. (2015) Structure of T4moF, the Toluene 4-Monooxygenase Ferredoxin Oxidoreductase. *Biochemistry* **54**: 5980–5988.
- Allen, J.R., Clark, D.D., Krum, J.G., and Ensign, S.A. (1999) A role for coenzyme M (2-mercaptoethanesulfonic acid) in a bacterial pathway of aliphatic epoxide carboxylation. *Proc Natl Acad Sci* **96**: 8432–8437.
- Alvarez, L.A., Exton, D.A., Timmis, K.N., Suggett, D.J., and McGenity, T.J. (2009) Characterization of marine isoprene-degrading communities. *Environ Microbiol* **11**: 3280–3291.
- Anthony, C. (1986) Bacterial oxidation of methane and methanol. *Adv Microb Physiol* **27**: 113–210.
- Ashworth, K., Wild, O., and Hewitt, C.N. (2013) Impacts of biofuel cultivation on mortality and crop yields. *Nat Clim Chang* **3**: 492–496.
- Bäck, J., Aaltonen, H., Hellén, H., Kajos, M.K., Patokoski, J., Taipale, R., et al. (2010) Variable emissions of microbial volatile organic compounds (MVOCs) from root-associated fungi isolated from Scots pine. *Atmos Environ* **44**: 3651–3659.
- Bailey, L.J., Elsen, N.L., Pierce, B.S., and Fox, B.G. (2008) Soluble expression and purification of the oxidoreductase component of toluene 4-monooxygenase. *Protein Expr Purif* **57**: 9–16.
- Bailey, L.J., McCoy, J.G., Phillips, G.N., and Fox, B.G. (2008) Structural consequences of effector protein complex formation in a diiron hydroxylase. *Proc Natl Acad Sci U S A* **105**: 19194–19198.
- Batie, C.J., LaHaie, E., and Ballou, P. (1987) Purification and characterization of phthalate oxygenase and phthalate oxygenase reductase from *Pseudomonas cepacia*. *J Biol Chem* **262**: 1510–1518.

- Bentley, F.K., Zurbriggen, A., and Melis, A. (2014) Heterologous expression of the mevalonic acid pathway in Cyanobacteria enhances endogenous carbon partitioning to isoprene. *Mol Plant* **7**: 71–86.
- Blazyk, J.L. and Lippard, S.J. (2004) Domain engineering of the reductase component of soluble methane monooxygenase from *Methylococcus capsulatus* (Bath). *J Biol Chem* **279**: 5630–5640.
- Blazyk, J.L. and Lippard, S.J. (2002) Expression and characterization of ferredoxin and flavin adenine dinucleotide binding domains of the reductase component of soluble methane monooxygenase from *Methylococcus capsulatus* (Bath). *Biochemistry* **41**: 15780–15794.
- Borodina, E., Nichol, T., Dumont, M.G., Smith, T.J., and Murrell, J.C. (2007) Mutagenesis of the “leucine gate” to explore the basis of catalytic versatility in soluble methane monooxygenase. *Appl Environ Microbiol* **73**: 6460–6467.
- Brandstetter, H., Whittington, D.A., Lippard, S.J., and Frederick, C.A. (1999) Mutational and structural analyses of the regulatory protein B of soluble methane monooxygenase from *Methylococcus capsulatus*. *Chem Biol* **6**: 441–449.
- Bromberg, P.A. and Koren, H.S. (1995) Ozone-induced human respiratory dysfunction and disease. *Toxicol Lett* **82**: 307–316.
- Bu, X., Krause, S.M.B., Gu, X., Tian, J., and Zhou, X. (2019) Ethylene rather than acetylene inhibits soil methane oxidation rates in a subtropical evergreen forest. *Soil Biol Biochem* **135**: 10–12.
- Cafaro, V., Scognamiglio, R., Viggiani, A., Izzo, V., Passaro, I., Notomista, E., et al. (2002) Expression and purification of the recombinant subunits of toluene/o-xylene monooxygenase and reconstitution of the active complex. *Eur J Biochem* **269**: 5689–5699.
- Carlton, A.G., Wiedinmyer, C., and Kroll, J.H. (2009) A review of Secondary Organic Aerosol (SOA) formation from isoprene. *Atmos Chem Phys* **9**: 4987–5005.
- Carrión, O., Gibson, L., Elias, D.M.O., McNamara, N.P., Van Alen, T.A., Op den Camp, H.J.M., et al. (2020) Diversity of isoprene-degrading bacteria in phyllosphere and soil communities from a high isoprene-emitting environment: A Malaysian oil palm plantation. *Microbiome* **8**: 1–13.

- Carrión, O., Larke-Mejía, N.L., Gibson, L., Ul Haque, M.F., Ramiro-García, J., McGenity, T.J., and Murrell, J.C. (2018) Gene probing reveals the widespread distribution, diversity and abundance of isoprene-degrading bacteria in the environment. *Microbiome* **6**: 219.
- Champreda, V., Choi, Y.-J., Zhou, N.-Y., and Leak, D.J. (2006) Alteration of the stereo- and regioselectivity of alkene monooxygenase based on coupling protein interactions. *Appl Microbiol Biotechnol* **71**: 840–847.
- Champreda, V., Zhou, N.-Y., and Leak, D.J. (2004) Heterologous expression of alkene monooxygenase components from *Xanthobacter autotrophicus* Py2 and reconstitution of the active complex. *FEMS Microbiol Lett* **239**: 309–318.
- Chan Kwo Chion, C.K., Askew, S.E., and Leak, D.J. (2005) Cloning, expression, and site-directed mutagenesis of the propene monooxygenase genes from *Mycobacterium* sp. strain M156. *Appl Environ Microbiol* **71**: 1909–1914.
- Chang, S.L., Wallar, B.J., Lipscomb, J.D., and Mayo, K.H. (1999) Solution structure of component B from methane monooxygenase derived through heteronuclear NMR and molecular modeling. *Biochemistry* **38**: 5799–5812.
- Chatwood, L.L., Müller, J., Gross, J.D., Wagner, G., and Lippard, S.J. (2004) NMR structure of the flavin domain from soluble methane monooxygenase reductase from *Methylococcus capsulatus* (Bath). *Biochemistry* **43**: 11983–11991.
- Claeys, M., Graham, B., Vas, G., Wang, W., Vermeylen, R., Pashynska, V., et al. (2004) Formation of Secondary Organic Aerosols through Photo- Oxidation of Isoprene Materials and Methods. *Science (80-)* **303**: 1173–1176.
- Clark, L.C., Wolf, R., Granger, D., and Taylor, Z. (1953) Continuous recording of blood oxygen tensions by polarography. *J Appl Physiol* **6**: 189–193.
- Cleveland, C.C. and Yavitt, J.B. (1997) Consumption of atmospheric isoprene in soil. *Geophys Reseach Lett* **24**: 2379–2382.
- Cleveland, C.C. and Yavitt, J.B. (1998) Microbial consumption of atmospheric isoprene in a temperate forest soil. *Appl Environ Microbiol* **64**: 172–177.
- Colby, J. and Dalton, H. (1979) Characterization of the second prosthetic group of the flavoenzyme NADH-acceptor reductase (component C) of the methane monooxygenase from *Methylococcus capsulatus* (Bath). *Biochem J* **177**: 903–908.

- Colby, J. and Dalton, H. (1978) Resolution of the methane mono oxygenase of *Methylococcus capsulatus* (Bath) into three components. Purification and properties of component C, a flavoprotein. *Biochem J* **171**: 461–468.
- Colby, J., Stirling, D.I., and Dalton, H. (1977) The soluble methane monooxygenase of *Methylococcus capsulatus* (Bath). *Biochem J* **165**: 395–402.
- Coleman, N. V., Yau, S., Wilson, N.L., Nolan, L.M., Migocki, M.D., Ly, M.-A., et al. (2011) Untangling the multiple monooxygenases of *Mycobacterium chubuense* strain NBB4 , a versatile hydrocarbon degrader. *Environ Microbiol Rep* **3**: 297–307.
- Collins, W.J., Derwent, R.G., Johnson, C.E., and Stevenson, D.S. (2002) The oxidation of organic compounds in the troposphere and their global warming potentials. *Clim Change* **52**: 453–479.
- Crombie, A. and Murrell, J.C. (2011) Development of a system for genetic manipulation of the facultative methanotroph *Methylocella silvestris* BL2, 1st ed. Elsevier Inc.
- Crombie, A.T., El Khawand, M., Rhodius, V.A., Fengler, K.A., Miller, M.C., Whited, G.M., et al. (2015) Regulation of plasmid-encoded isoprene metabolism in *Rhodococcus*, a representative of an important link in the global isoprene cycle. *Environ Microbiol* **17**: 3314–3329.
- Crombie, A.T., El Khawand, M., Rhodius, V.A., Fengler, K.A., Miller, M.C., Whited, G.M., et al. (2015) Regulation of plasmid-encoded isoprene metabolism in *Rhodococcus*, a representative of an important link in the global isoprene cycle. *Environ Microbiol* **17**: 3314–3329.
- Crombie, A.T., Larke-Mejia, N.L., Emery, H., Dawson, R., Pratscher, J., Murphy, G.P., et al. (2018) Poplar phyllosphere harbors disparate isoprene- degrading bacteria. *Proc Natl Acad Sci U S A* **115**: 13081–13086.
- Cronn, D.R. and Nutmagul, W. (1982) Analysis of atmospheric hydrocarbons during winter MONEX. *Tellus* **34**: 159–165.
- Dalton, H. and Whittenbury, R. (1976) The acetylene reduction technique as an assay for nitrogenase activity in the methane oxidizing bacterium *Methylococcus capsulatus* strain Bath. *Arch Microbiol* **109**: 147–151.
- Dawson, R.A., Larke-Mejía, N.L., Crombie, A.T., Ul Haque, M.F., and Murrell, J.C. (2020) Isoprene oxidation by the Gram-negative model bacterium *Variovorax* sp. WS11.

Microorganisms **8**: 349.

- DeWitt, J.G., Rosenzweig, A.C., Salifoglou, A., Hedman, B., Lippard, S.J., and Hodgson, K.O. (1995) X-ray absorption spectroscopic studies of the diiron center in methane monooxygenase in the presence of substrate and the coupling protein of the enzyme system. *Inorg Chem* **34**: 2505–2515.
- Diner, B.A., Fan, J., Scotcher, M.C., Wells, D.H., and Whited, G.M. (2018) Synthesis of heterologous mevalonic acid pathway enzymes in *Clostridium ljungdahlii* for the conversion of fructose and of syngas to mevalonate and isoprene. *Appl Environ Microbiol* **84**: e01723-17.
- Elsen, N.L., Moe, L.A., McMartin, L.A., and Fox, B.G. (2007) Redox and functional analysis of the Rieske ferredoxin component of the toluene 4-monooxygenase. *Biochemistry* **46**: 976–986.
- Ensign, S.A., Hyman, M.R., and Arp, D.J. (1992) Cometabolic degradation of chlorinated alkenes by alkene monooxygenase in a propylene-grown *Xanthobacter* strain. *Appl Environ Microbiol* **58**: 3038–3046.
- Ewers, J., Freier-Schröder, D., and Knackmuss, H.-J. (1990) Selection of trichloroethene (TCE) degrading bacteria that resist inactivation by TCE. *Arch Microbiol* **154**: 410–413.
- Exton, D.A., Smith, D.J., McGenity, T.J., Steinke, M., Hills, A.J., and Suggett, D.J. (2010) Application of a Fast Isoprene Sensor (FIS) for measuring isoprene production from marine samples. *Limnol Oceanogr Methods* **8**: 185–195.
- Exton, D.A., Suggett, D.J., McGenity, T.J., and Steinke, M. (2013) Chlorophyll-normalized isoprene production in laboratory cultures of marine microalgae and implications for global models. *Limnol Oceanogr* **58**: 1301–1311.
- Fall, R. and Copley, S.D. (2000) Bacterial sources and sinks of isoprene, a reactive atmospheric hydrocarbon. *Environ Microbiol* **2**: 123–130.
- Fall, R. and Monson, R.K. (1992) Isoprene emission rate and intercellular isoprene concentration as influenced by stomatal distribution and conductance. *Plant Physiol* **100**: 987–992.
- Farinas, E.T., Alcalde, M., and Arnold, F. (2004) Alkene epoxidation catalyzed by cytochrome P450 BM-3 139-3. *Tetrahedron* **60**: 525–528.

- Fee, J.A., Findling, K.L., Yoshida, T., Hille, R., Tarr, G.E., Hearshen, D.O., et al. (1984) Purification and characterization of the Rieske iron-sulfur protein from *Thermus thermophilus*. *J Biol Chem* **259**: 124–133.
- Fosdike, W.L.J., Smith, T.J., and Dalton, H. (2005) Adventitious reactions of alkene monooxygenase reveal common reaction pathways and component interactions among bacterial hydrocarbon oxygenases. *FEBS J* **272**: 2661–2669.
- Fox, B.G., Froland, W.A., Dege, J.E., and Lipscombs, J.D. (1989) Methane Monooxygenase from *Methylosinus trichosporium* OB3b. *J Biol Chem* **264**: 10023–10033.
- Fox, B.G., Hendrich, M.P., Sureras, K.K., Andersson, K.K., Froland, W.A., Lipscomb, J.D., and Munck, E. (1993) Mossbauer, EPR, and ENDOR studies of the hydroxylase and reductase components of methane monooxygenase from *Methylosinus trichosporium* OB3b. *J Am Chem Soc* **115**: 3688–3701.
- Fox, B.G., Liu, Y., Dege, J.E., and Lipscomb, J.D. (1991) Complex formation between the protein components of methane monooxygenase from *Methylosinus trichosporium* OB3b. *J Biol Chem* **266**: 540–550.
- Froland, W.A., Andersson, K.K., Lee, S.-K., Liu, Y., and Lipscomb, D. (1992) Methane monooxygenase component B and reductase alter the regioselectivity of the hydroxylase component-catalyzed reactions. *J Biol Chem* **267**: 17588–17597.
- Funhoff, E.G., Salzmann, J., Bauer, U., Witholt, B., and van Beilen, J.B. (2007) Hydroxylation and epoxidation reactions catalyzed by CYP153 enzymes. *Enzyme Microb Technol* **40**: 806–812.
- Funk, J.L., Jones, C.G., Baker, C.J., Fuller, F.M., Giardina, C.P., and Lerdau, M.T. (2003) Diurnal variation in the basal emission rate of isoprene. *Ecol Appl* **13**: 269–278.
- Furuhashi, K., Shintani, M., and Takagi, M. (1986) Effects of solvents on the production of epoxides by *Nocardia corallina* B-276. *Appl Microbiol Biotechnol* **23**: 218–223.
- Furuya, T., Hayashi, M., and Kino, K. (2013) Reconstitution of active Mycobacterial binuclear iron monooxygenase complex in *Escherichia coli*. *Appl Environ Microbiol* **79**: 6033–6039.
- Gallagher, S.C., Callaghan, A.J., Zhao, J., Dalton, H., and Trewthella, J. (1999) Global Conformational Changes Control the Reactivity of Methane. *Biochemistry* **38**: 6752–6760.

- Gallagher, S.C., Cammack, R., and Dalton, H. (1997) Alkene monooxygenase from *Nocardia corallina* B-276 is a member of the class of dinuclear iron proteins capable of stereospecific epoxidation reactions. *Eur J Biochem* **247**: 635–641.
- Gassner, G.T. and Lippard, S.J. (1999) Component interactions in the soluble methane monooxygenase system from *Methylococcus capsulatus* (Bath). *Biochemistry* **38**: 12768–12785.
- Gelmont, D., Stein, R.A., and Mead, J.F. (1981) Isoprene - The main hydrocarbon in human breath. *Biochem Biophys Res Commun* **99**: 1456–1460.
- van Ginkel, C.G. and de Bont, J.A.M. (1986) Isolation and characterization of alkene-utilizing *Xanthobacter* spp. *Arch Microbiol* **145**: 403–407.
- van Ginkel, C.G., de Jong, E., Tilanus, J.W.R., and de Bont, J.A.M. (1987) Microbial oxidation of isoprene, a biogenic foliage volatile and of 1,3-butadiene, an anthropogenic gas. *FEMS Microbiol Ecol* **45**: 275–279.
- van Ginkel, C.G., Welten, H.G.J., and de Bont, J.A.M. (1986) Epoxidation of alkenes by alkene-grown *Xanthobacter* spp. *Appl Microbiol Biotechnol* **24**: 334–337.
- van Ginkel, C.G., Welten, H.G.J., and de Bont, J.A.M. (1987) Oxidation of gaseous and volatile hydrocarbons by selected alkene-utilizing bacteria. *Appl Environ Microbiol* **53**: 2903–2907.
- Green, J. and Dalton, H. (1986) Steady-state kinetic analysis of soluble methane monooxygenase from *Methylococcus capsulatus* (Bath). *Biochem J* **236**: 155–162.
- Green, M.J. and Hill, H.A.O. (1984) Chemistry of Dioxygen. *Methods Enzymol* **105**: 3–22.
- Grosse, S., Laramée, L., Wendlandt, K.-D., McDonald, I.R., Miguez, C.B., and Kleber, H.-P. (1999) Purification and characterization of the soluble methane monooxygenase of the Type II methanotrophic bacterium *Methylocystis* sp. strain WI 14. *Appl Environ Microbiol* **65**: 3929–3935.
- Guenther, A., Karl, T., Harley, P., Wiedinmyer, C., Palmer, P.I., and Geron, C. (2006) Estimates of global terrestrial isoprene emissions using MEGAN (Model of Emissions of Gases and Aerosols from Nature). *Atmos Chem Phys* **6**: 3181–3210.
- Guenther, A.B., Jiang, X., Heald, C.L., Sakulyanontvittaya, T., Duhl, T., Emmons, L.K., and Wang, X. (2012) The model of emissions of gases and aerosols from Nature version

- 2.1 (MEGAN2.1): an extended and updated framework for modeling biogenic emissions. *Geosci Model Dev* **5**: 1471–1492.
- Hanson, D.T., Swanson, S., Graham, L.E., and Sharkey, T.D. (1999) Evolutionary significance of isoprene emission from mosses. *Am J Bot* **86**: 634–639.
- Hantson, S., Knorr, W., Schurgers, G., Pugh, T.A.M., and Arneth, A. (2017) Global isoprene and monoterpene emissions under changing climate, vegetation, CO₂ and land use. *Atmos Environ* **155**: 35–45.
- Hardacre, C.J., Palmer, P.I., Baumanns, K., Rounsevell, M., and Murray-Rust, D. (2013) Probabilistic estimation of future emissions of isoprene and surface oxidant chemistry associated with land-use change in response to growing food needs. *Atmos Chem Phys* **13**: 5451–5472.
- Harley, P., Eller, A., Guenther, A., and Monson, R.K. (2014) Observations and models of emissions of volatile terpenoid compounds from needles of ponderosa pine trees growing in situ: Control by light, temperature and stomatal conductance. *Oecologia* **176**: 35–55.
- Harrison, S.P., Morfopoulos, C., Dani, K.G.S., Prentice, I.C., Arneth, A., Atwell, B.J., et al. (2013) Volatile isoprenoid emissions from plastid to planet. *New Phytol* **197**: 49–57.
- Harrison, S.P., Morfopoulos, C., Srikanta Dani, K.G., Prentice, I.C., Arneth, A., Atwell, B.J., et al. (2012) Volatile isoprenoid emissions from plastid to planet. *New Phytol* **197**: 49–57.
- Hartmans, S., Weber, F.J., Somhorst, D.P.M., and de Bont, J.A.M. (1991) Alkene monooxygenase from Mycobacterium: a multicomponent enzyme. *J Gen Microbiol* **137**: 2555–2560.
- Hemmi, H., Studts, J.M., Chae, Y.K., Song, J., Markley, J.L., and Fox, B.G. (2001) Solution structure of the toluene 4-Monooxygenase effector protein (T4moD). *Biochemistry* **40**: 3512–3524.
- Hendrich, M.P., Munck, E., Fox, B.G., and Lipscomb, J.D. (1990) Integer-spin EPR studies of the fully reduced methane monooxygenase hydroxylase component. *J Am Chem Soc* **112**: 5861–5865.
- Hewitt, C.N., Kok, G.L., and Fall, R. (1990) Hydroperoxides in plants exposed to ozone mediate air pollution damage to alkene emitters. *Nature* **344**: 56–58.

- Hewitt, C.N. and Street, R.A. (1992) A qualitative assessment of the emission of non-methane hydrocarbon compounds from the biosphere to the atmosphere in the U.K.: Present knowledge and uncertainties. *Atmos Environ* **26**: 3069–3077.
- Holmes, A.J. and Coleman, N. V. (2008) Evolutionary ecology and multidisciplinary approaches to prospecting for monooxygenases as biocatalysts. *Antonie Van Leeuwenhoek* **94**: 75–84.
- van Hylckama Vlieg, J.E.T., Kingma, J., Kruizinga, W., and Janssen, D.B. (1999) Purification of a glutathione-S-transferase and a glutathione conjugate-specific dehydrogenase involved in isoprene metabolism in *Rhodococcus* sp. strain AD45. *J Bacteriol* **181**: 2094–2101.
- van Hylckama Vlieg, J.E.T., Kingma, J., van den Wijngaard, A.J., and Janssen, D.B. (1998) A glutathione S-transferase with activity towards cis-1,2-dichloroepoxyethane is involved in isoprene utilization by *Rhodococcus* sp. strain AD45. *Appl Environ Microbiol* **64**: 2800–2805.
- van Hylckama Vlieg, J.E.T., Leemhuis, H., Spelberg, J.H.L., and Janssen, D.B. (2000) Characterization of the gene cluster involved in isoprene metabolism in *Rhodococcus* sp. strain AD45. *J Bacteriol* **182**: 1956–1963.
- Hyman, M.R. and Arp, D.J. (1988) Acetylene inhibition of metalloenzymes. *Anal Biochem* **173**: 207–220.
- Ibragimov, A., Sidique, S.F., and Tey, Y.S. (2019) Productivity for sustainable growth in Malaysian oil palm production: A system dynamics modeling approach. *J Clean Prod* **213**: 1051–1062.
- Iwasaki, T., Isogai, Y., Iizuka, T., and Oshima, T. (1995) Sulredoxin: a novel iron-sulfur protein of the thermoacidophilic archaeon *Sulfolobus* sp. strain 7 with a Rieske-type [2Fe-2S] center. *J Bacteriol* **177**: 2576–2582.
- Jacob, D.J. (1999) *Introduction to Atmospheric Chemistry*, Princeton University Press.
- Jahng, D. and Wood, T.K. (1996) Metal ions and chloramphenicol inhibition of soluble methane monooxygenase from *Methylosinus trichosporium* OB3b. *Appl Microbiol Biotechnol* **45**: 744–749.
- Jenkin, M.E., Young, J.C., and Rickard, A.R. (2015) The MCM v3.3.1 degradation scheme for isoprene. *Atmos Chem Phys* **15**: 11433–11459.

- Jiang, H., Chen, Y., Jiang, P., Zhang, C., Smith, T.J., Murrell, J.C., and Xing, X.-H. (2010) Methanotrophs: Multifunctional bacteria with promising applications in environmental bioengineering. *Biochem Eng J* **49**: 277–288.
- Johnston, A., Crombie, A.T., El Khawand, M., Sims, L., Whited, G.M., McGenity, T.J., and Murrell, J.C. (2017) Identification and characterisation of isoprene-degrading bacteria in an estuarine environment. *Environ Microbiol* **19**: 3526–3537.
- Jones, A.M.P., Shukla, M.R., Sherif, S.M., Brown, P.B., and Saxena, P.K. (2016) Growth regulating properties of isoprene and isoprenoid-based essential oils. *Plant Cell Rep* **35**: 91–102.
- Keener, W.K., Watwood, M.E., Schaller, K.D., Walton, M.R., Partin, J.K., Smith, W.A., and Clingenpeel, S.R. (2001) Use of selective inhibitors and chromogenic substrates to differentiate bacteria based on toluene oxygenase activity. *J Microbiol Methods* **46**: 171–185.
- Kesselmeier, J. and Staudt, M. (1999) Biogenic volatile organic compounds (VOC): An overview on emission, physiology and ecology. *J Atmos Chem* **33**: 23–88.
- El Khawand, M., Crombie, A.T., Johnston, A., Vavlline, D. V., McAuliffe, J.C., Latone, J.A., et al. (2016) Isolation of isoprene degrading bacteria from soils, development of isoA gene probes and identification of the active isoprene-degrading soil community using DNA-stable isotope probing. *Environ Microbiol* **18**: 2743–2753.
- El Khawand, M.E., Crombie, A.T., Johnston, A., Vavlline, D. V., McAuliffe, J.C., Latone, J.A., et al. (2016) Isolation of isoprene degrading bacteria from soils , development of isoA gene probes and identification of the active isoprene-degrading soil community using DNA-stable isotope probing. *Environ Microbiol* **18**: 2743–2753.
- Klinger, L.F., Greenberg, J., Guenther, A., Tyndall, G., Zimmerman, P., M'Bangui, M., et al. (1998) Patterns in volatile organic compound emissions along a savanna-rainforest gradient in central Africa. *J Geophys Res Atmos* **103**: 1443–1454.
- Kopp, D.A., Gassner, G.T., Blazyk, J.L., and Lippard, S.J. (2001) Electron-transfer reactions of the reductase component of soluble methane monooxygenase from *Methylococcus capsulatus* (Bath). *Biochemistry* **40**: 14932–14941.
- Kotani, T., Kawashima, Y., Yurimoto, H., Kato, N., and Sakai, Y. (2006) Gene structure and regulation of alkane monooxygenases in propane-utilizing *Mycobacterium* sp. TY-6

- and *Pseudonocardia* sp. TY-7. *J Biosci Bioeng* **102**: 184–192.
- Kuzma, J., Nemecek-Marshall, M., Pollock, W.H., and Fall, R. (1995) Bacteria produce the volatile hydrocarbon isoprene. *Curr Microbiol* **30**: 97–103.
- de Lacy Costello, B., Amann, A., Al-Kateb, H., Flynn, C., Filipiak, W., Khalid, T., et al. (2014) A review of the volatiles from the healthy human body. *J Breath Res* **8**:
- Laothawornkitkul, J., Paul, N.D., Vickers, C.E., Possell, M., Taylor, J.E., Mullineaux, P.M., and Hewitt, C.N. (2008) Isoprene emissions influence herbivore feeding decisions. *Plant Cell Environ* **31**: 1410–1415.
- Larke-Mejía, N.L. (2018) Molecular ecology of isoprene degradation in the terrestrial environment.
- Larke-Mejía, N.L., Crombie, A.T., Pratscher, J., McGenity, T.J., and Murrell, J.C. (2019) Novel isoprene-degrading proteobacteria from soil and leaves identified by cultivation and metagenomics analysis of stable isotope probing experiments. *Front Microbiol* **10**: 2700.
- Leahy, G.L., Batchelor, P.J., and Morcomb, S.M. (2003) Evolution of the soluble diiron monooxygenases. *FEMS Microbiol Rev* **27**: 449–479.
- Lee, S.J., McCormick, M.S., Lippard, S.J., and Cho, U.-S. (2013) Control of substrate access to the active site in methane monooxygenase. *Nature* **494**: 380–385.
- Liang, A.D. and Lippard, S.J. (2014) Component interactions and electron transfer in toluene/*o*-xylene monooxygenase. *Biochemistry* **53**: 7368–7375.
- Lindsay Smith, J.R. and Sleath, P.R. (1982) Model systems for cytochrome P450 dependent mono-oxygenases. Part 1. Oxidation of alkenes and aromatic compounds by tetraphenylporphyratoiron (iii) chloride and iodosylbenzene. *J Chem Soc Perkin Trans 2* 1009–1015.
- Link, T.A., Hatzfeld, O.M., Unalkat, P., Shergill, J.K., Cammack, R., and Mason, J.R. (1996) Comparison of the “Rieske” [2Fe-2S] center in the bc₁ complex and in bacterial dioxygenases by circular dichroism spectroscopy and cyclic voltammetry. *Biochemistry* **35**: 7546–7552.
- Lloyd, J.S., Bhambra, A., Murrell, J.C., and Dalton, H. (1997) Inactivation of the regulatory protein a of soluble methane monooxygenase from *Methylococcus capsulatus* (Bath)

- by proteolysis can be overcome by a Gly to Gln modification. *Eur J Biochem* **248**: 72–79.
- Lloyd, J.S., Finch, R., Dalton, H., and Murrell, J.C. (1999) Homologous expression of soluble methane monooxygenase genes in *Methylosinus trichosporium* OB3b. *Microbiology* **145**: 461–470.
- Lock, M., Nichol, T., Murrell, J.C., and Smith, T.J. (2017) Mutagenesis and expression of methane monooxygenase to alter regioselectivity with aromatic substrates. *FEMS Microbiol Lett* **364**: 13.
- Lountos, G.T., Mitchell, K.H., Studts, J.M., Fox, B.G., and Orville, A.M. (2005) Crystal structures and functional studies of T4moD, the toluene 4-monooxygenase catalytic effector protein. *Biochemistry* **44**: 7131–7142.
- Lund, J. and Dalton, H. (1985) Further characterisation of the FAD and Fe₂S₂ redox centres of component C, the NADH: acceptor reductase of the soluble methane monooxygenase of *Methylococcus capsulatus* (Bath). *Eur J Biochem* **147**: 291–296.
- Lund, J., Woodland, M.P., and Dalton, H. (1985) Electron transfer reactions in the soluble methane monooxygenase of *Methylococcus capsulatus* (Bath). *Eur J Biochem* **147**: 297–305.
- Magel, E., Mayrhofer, S., Muller, A., Zimmer, I., Hampp, R., and Schnitzler, J.-P. (2006) Photosynthesis and substrate supply for isoprene biosynthesis in poplar leaves. *Atmos Environ* **40**: S138–S151.
- Martin, K.E., Ozsvar, J., and Coleman, N. V. (2014) SmoXYB1C1Z of *Mycobacterium* sp. strain NBB4: A soluble methane monooxygenase (sMMO)-like enzyme, active on C₂ to C₄ alkanes and alkenes. *Appl Environ Microbiol* **80**: 5801–5806.
- Mattes, T.E., Alexander, A.K., and Coleman, N. V. (2010) Aerobic biodegradation of the chloroethenes: pathways, enzymes, ecology, and evolution. *FEMS Microbiol Rev* **34**: 445–475.
- May, T.W. and Wiedmeyer, R.H. (1998) A table of polyatomic interferences in ICP-MS. *At Spectrosc* **19**: 150–155.
- McClay, K., Fox, B.G., and Steffan, R.J. (2000) Toluene Monooxygenase-Catalyzed Epoxidation of Alkenes. *Appl Environ Microbiol* **66**: 1877–1882.

- McGenity, T.J., Crombie, A.T., and Murrell, J.C. (2018) Microbial cycling of isoprene, the most abundantly produced biological volatile organic compound on Earth. *ISME J* **12**: 931–941.
- Merkx, M. and Lippard, S.J. (2002) Why OrfY? Characterization of MMOD, a long overlooked component of the soluble methane monooxygenase from *Methylococcus capsulatus* (Bath). *J Biol Chem* **277**: 5858–5865.
- Miloradovic van Doorn, M., Merl-Pham, J., Ghirardo, A., Fink, S., Polle, A., Schnitzler, J., and Rosenkranz, M. (2020) Root isoprene formation alters lateral root development. *Plant Cell Environ* 1–17.
- Misztal, P.K., Owen, S.M., Guenther, A.B., Rasmussen, R., Geron, C., Harley, P., et al. (2010) Large estragole fluxes from oil palms in Borneo. *Atmos Chem Phys* **10**: 4343–4358.
- Mitchell, K.H., Studts, J.M., and Fox, B.G. (2002) Combined participation of hydroxylase active site residues and effector protein binding in a para to ortho modulation of toluene 4-monooxygenase regiospecificity. *Biochemistry* **41**: 3176–3188.
- Miura, A. and Dalton, H. (1995) Purification and characterization of the alkene monooxygenase from *Nocardia corallina* B-276. *Biosci Biotechnol Biochem* **59**: 853–859.
- Moe, L.A., Mccartin, L.A., and Fox, B.G. (2006) Component interactions and implications for complex formation in the multicomponent toluene 4-monooxygenase. *Biochemistry* **45**: 5478–5485.
- Müller, J., Lugovskoy, A.A., Wagner, G., and Lippard, S.J. (2002) NMR structure of the [2Fe-2S] ferredoxin domain from soluble methane monooxygenase reductase and interaction with its hydroxylase. *Biochemistry* **41**: 42–51.
- Murphy, G. (2017) Isoprene degradation in the terrestrial environment.
- Murrell, J.C., McGenity, T.J., and Crombie, A.T. (2020) Microbial metabolism of isoprene: A much-neglected climate-active gas. *Microbiology* **166**: 600–613.
- Nakajima, T., Uchiyama, H., Yagi, O., and Nakahara, T. (1992) Purification and properties of a soluble methane monooxygenase from *Methylocystis* sp. M. *Biosci Biotechnol Biochem* **56**: 736–740.
- Nakashima, N. and Tamura, T. (2004a) A Novel System for Expressing Recombinant Proteins

- Over a Wide Temperature Range From 4 to 35 °C. *Biotechnol Bioeng* **86**: 136–148.
- Nakashima, N. and Tamura, T. (2004b) Isolation and characterization of a rolling-circle-type plasmid from *Rhodococcus erythropolis* and application of the plasmid to multiple-recombinant-protein expression. *Appl Environ Microbiol* **70**: 5557–5568.
- Narancic, T., Djokic, L., Kenny, S.T., O'Connor, K.E., Radulovic, V., Nikodinovic-Runic, J., and Vasiljevic, B. (2012) Metabolic versatility of Gram-positive microbial isolates from contaminated river sediments. *J Hazard Mater* **215–216**: 243–251.
- Newman, L.M. and Wackett, L.P. (1995) Purification and characterization of toluene 2-monooxygenase from *Burkholderia cepacia* G4. *Biochemistry* **34**: 14066–14076.
- Newman, L.M. and Wackett, L.P. (1997) Trichloroethylene oxidation by purified toluene 2-monooxygenase: Products, kinetics, and turnover-dependent inactivation. *J Bacteriol* **179**: 90–96.
- Nguyen, T.B., Tyndall, G.S., Crouse, J.D., Teng, A.P., Bates, K.H., Schwantes, R.H., et al. (2016) Atmospheric fates of Criegee intermediates in the ozonolysis of isoprene. *Phys Chem Chem Phys* **18**: 10241–10254.
- Nichol, T., Murrell, J.C., and Smith, T.J. (2015) Controlling the activities of the diiron centre in bacterial monooxygenases: Lessons from mutagenesis and biodiversity. *Eur J Inorg Chem* **21**: 3419–3431.
- Nicholson, D. (2005) Products of isoprene metabolism. *Biochem Mol Biol Educ* **33**: 154–155.
- Oppenheimer, M., Pierce, B.S., Crawford, J.A., Ray, K., Helm, R.F., and Sobrado, P. (2010) Recombinant expression, purification, and characterization of ThmD, the oxidoreductase component of tetrahydrofuran monooxygenase. *Arch Biochem Biophys* **496**: 123–131.
- Orville, A.M., Joey, M., Lountos, G.T., Mitchell, K.H., and Fox, B.G. (2003) Crystallization and preliminary analysis of native and N-terminal truncated isoforms of toluene-4-monooxygenase catalytic effector protein. *Acta Crystallogr Sect D Biol Crystallogr* **D59**: 572–575.
- Osborne, C.D. and Haritos, V.S. (2019) Beneath the surface: Evolution of methane activity in the bacterial multicomponent monooxygenases. *Mol Phylogenet Evol* **139**: 106527.
- Owen, S.M. and Penuelas, J. (2005) Opportunistic emissions of volatile isoprenoids. *Trends*

Plant Sci **10**: 420–426.

- Pacifico, F., Harrison, S.P., Jones, C.D., and Sitch, S. (2009) Isoprene emissions and climate. *Atmos Environ* **43**: 6121–6135.
- Patel, R.N., Hou, C.T., Laskin, A.I., and Felix, A. (1982) Microbial oxidation of hydrocarbons: Properties of a soluble methane monooxygenase from a facultative methane-utilizing organism, *Methylobacterium* sp. Strain CRL-26. *Appl Environ Microbiol* **44**: 1130–1137.
- Paulsen, K.E., Stankovich, M.T., Liu, Y., Lipscomb, J.D., Fox, B.G., and Münck, E. (1994) Oxidation-reduction potentials of the methane monooxygenase hydroxylase component from *Methylosinus trichosporium* OB3b. *Biochemistry* **33**: 713–722.
- Perry, A. and Smith, T.J. (2006) Protocol for mutagenesis of alkene monooxygenase and screening for modified enantiocomposition of the epoxypropane product. *J Biomol Screen* **11**: 553–556.
- Pessione, E., Divari, S., Griva, E., Cavaletto, M., Rossi, G.L., Gilardi, G., and Giunta, C. (1999) Phenol hydroxylase from *Acinetobacter radioresistens* is a multicomponent enzyme: Purification and characterization of the reductase moiety. *Eur J Biochem* **265**: 549–555.
- Petkevičius, V., Vaitekūnas, J., Vaitkus, D., Čėnas, N., and Meškys, R. (2019) Tailoring a Soluble Diiron Monooxygenase for Synthesis of Aromatic N-oxides. *Catalysts* **9**: 356.
- Pikus, J.D., Mitchell, K.H., Studts, J.M., McClay, K., Steffan, R.J., and Fox, B.G. (2000) Threonine 201 in the diiron enzyme toluene 4-monooxygenase is not required for catalysis. *Biochemistry* **39**: 791–799.
- Pikus, J.D., Studts, J.M., Achim, C., Kauffmann, K.E., Munck, E., Steffan, R.J., et al. (1996) Recombinant toluene-4-monooxygenase: Catalytic and mossbauer studies of the purified diiron and Rieske components of a four-protein complex. *Biochemistry* **35**: 9106–9119.
- Prior, S.D. and Dalton, H. (1985) Acetylene as a suicide substrate and active site probe for methane monooxygenase from *Methylococcus capsulatus* (Bath). *FEMS Microbiol Lett* **29**: 105–109.
- Puntus, I.F., Borzova, O. V., Funtikova, T. V., Suzina, N.E., Egozarian, N.S., Polyvtseva, V.N., et al. (2019) Contribution of soil bacteria isolated from different regions into crude oil and oil product degradation. *J Soils Sediments* **19**: 3166–3177.

- Purves, D.W., Caspersen, J.P., Moorcroft, P.R., Hurtt, G.C., and Pacala, S.W. (2004) Human-induced changes in US biogenic volatile organic compound emissions: evidence from long-term forest inventory data. *Glob Chang Biol* **10**: 1737–1755.
- Raran-Kurussi, S., Cherry, S., Zhang, D., and Waugh, D.S. (2017) Removal of affinity tags with TEV protease. In *Methods in Molecular Biology*. pp. 33–43.
- Raran-Kurussi, S. and Waugh, D.S. (2012) The Ability to Enhance the Solubility of Its Fusion Partners Is an Intrinsic Property of Maltose-Binding Protein but Their Folding Is Either Spontaneous or Chaperone-Mediated. *PLoS One* **7**: e49589.
- Rasmussen, R.A. (1970) Isoprene: Identified as a forest-type emission to the atmosphere. *Environ Sci Technol* **4**: 667–671.
- Rasmussen, R.A. and Hutton, R.S. (1972) Utilisation of atmospheric organic volatiles as an energy source by microorganisms in the tropics. *Chemosphere* **1**: 47–50.
- Reed, N.M., Cairns, R.O., Hutton, R.C., and Takaku, Y. (1994) Characterization of polyatomic ion interferences in inductively coupled plasma mass spectrometry using a high resolution mass spectrometer. *J Anal At Spectrom* **9**: 881–896.
- Reij, M.W., Kieboom, J., de Bont, J.A.M., and Hartmans, S. (1995) Continuous degradation of trichloroethylene by *Xanthobacter* sp. strain Py2 during growth on propene. *Appl Environ Microbiol* **61**: 2936–2942.
- Rieske, J.S., MacLennan, D.H., and Coleman, R. (1964) Isolation and properties of an iron-protein from the (reduced coenzyme Q) -cytochrome C reductase complex of the respiratory chain. *Biochem Biophys Res Commun* **15**: 338–344.
- Rohmer, M. (1999) The discovery of a mevalonate-independent pathway for isoprenoid biosynthesis in bacteria, algae and higher plants. *Nat Prod Rep* 565–574.
- Roiban, G.-D., Agudo, R., and Reetz, M.T. (2013) Stereo- and regioselectivity in the P450-catalyzed oxidative tandem difunctionalization of 1-methylcyclohexene. *Tetrahedron* **69**: 5306–5311.
- Rosenstiel, T.N., Ebbets, A.L., Khatri, W.C., Fall, R., and Monson, R.K. (2004) Induction of Poplar Leaf Nitrate Reductase : A Test of Extrachloroplastic Control of Isoprene Emission Rate. *Plant Biol* **6**: 12–21.
- Rosenzweig, A.C. (2015) Breaking Methane. *Nature* **518**: 309–310.

- Rosenzweig, A.C. (2013) Metalloenzymes: Put a ring on it. *Nat Chem Biol* **9**: 220–221.
- Rosenzweig, A.C., Brandstetter, H., Whittington, D.A., Nordlund, P., Lippard, S.J., and Frederick, C.A. (1997) Crystal structures of the methane monooxygenase hydroxylase from *Methylococcus capsulatus* (Bath): Implications for substrate gating and component interactions. *Proteins* **29**: 141–152.
- Rosenzweig, A.C., Frederick, C.A., Lippard, S.J., and Nordlund, P. (1993) Crystal structure of a bacterial non-haem iron hydroxylase that catalyses the biological oxidation of methane. *Nature* **366**: 537–543.
- Sambrook, J. and Russell, D.W. (2001) Molecular cloning: A laboratory manual.
- Sander, R. (2015) Compilation of Henry's law constants (version 4.0) for water as solvent. *Atmos Chem Phys* **15**: 4399–4981.
- Sapan, C. V., Lundblad, R.L., and Price, N.C. (1999) Colorimetric protein assay techniques. *Biotechnol Appl Biochem* **29**: 99–108.
- Sazinsky, M.H., Bard, J., Di Donato, A., and Lippard, S.J. (2004) Crystal structure of the toluene/o-xylene monooxygenase hydroxylase from *Pseudomonas stutzeri* OX1. *J Biol Chem* **279**: 30600–30610.
- Schmidt, T.G.M. and Skerra, A. (2007) The Strep-tag system for one-step purification and high-affinity detection or capturing of proteins. *Nat Protoc* **2**: 1528–1535.
- Schöller, C., Molin, S., and Wilkins, K. (1997) Volatile metabolites from some gram-negative bacteria. *Chemosphere* **35**: 1487–1495.
- Schöller, C.E.G., Gürtler, H., Pedersen, R., Molin, S., and Wilkins, K. (2002) Volatile metabolites from actinomycetes. *J Agric Food Chem* **50**: 2615–2621.
- Sharkey, T.D., Chen, X., and Yeh, S. (2001) Isoprene increases thermotolerance of fosmidomycin-fed leaves. *Plant Physiol* **125**: 2001–2006.
- Sharkey, T.D. and Monson, R.K. (2014) The future of isoprene emission from leaves , canopies and landscapes. *Plant Cell Environ* **37**: 1727–1740.
- Sharkey, T.D., Wiberley, A.E., and Donohue, A.R. (2008) Isoprene Emission from Plants: Why and How. *Ann Bot* **101**: 5–18.
- Sharkey, T.D. and Yeh, S. (2001) Isoprene emission from plants. *Annu Rev Plant Physiol*

Plant Mol Biol **52**: 407–436.

Sheldon, R.A. and Woodley, J.M. (2018) Role of Biocatalysis in Sustainable Chemistry. *Chem Rev* **118**: 801–838.

Shennan, J.L. (2006) Utilisation of C₂–C₄ gaseous hydrocarbons and isoprene by microorganisms. *J Chem Technol Biotechnol* **81**: 237–256.

Shinohara, Y., Uchiyama, H., Yagi, O., and Kusakabe, I. (1998) Purification and characterization of component B of a soluble methane monooxygenase from *Methylocystis* sp. M. *J Ferment Bioeng* **85**: 37–42.

Sieber, V., Martinez, C.A., and Arnold, F.H. (2001) Libraries of hybrid proteins from distantly related sequences. *Nat Biotechnol* **19**: 456–460.

Sigdel, S., Hui, G., Smith, T.J., Murrell, J.C., and Lee, J.K. (2015) Molecular dynamics simulation to rationalize regioselective hydroxylation of aromatic substrates by soluble methane monooxygenase. *Bioorganic Med Chem Lett* **25**: 1611–1615.

Singh, A., Srivastava, N., and Dubey, S.K. (2019) Molecular characterization and kinetics of isoprene degrading bacteria. *Bioresour Technol* **278**: 51–56.

Singsaas, E.L., Laporte, M.M., Shi, J.-Z., Russell, K., Bowling, D.R., Johnson, K., et al. (1999) Kinetics of leaf temperature fluctuation affect isoprene emission from red oak (*Quercus rubra*) leaves. *Tree Physiol* **19**: 917–924.

Singsaas, L., Lerda, M., Winter, K., and Sharkey, T.D. (1997) Isoprene increases thermotolerance of isoprene-emitting species. *Plant Physiol* **115**: 1413–1420.

Siwko, M.E., Marrink, S.J., Vries, A.H.D., Kozubek, A., Schoot, A.J.M., and Mark, A.E. (2007) Does isoprene protect plant membranes from thermal shock? A molecular dynamics study. *Biochim Biophys Acta* **1768**: 198–206.

Small, F.J. and Ensign, S.A. (1997) Alkene monooxygenase from *Xanthobacter* Strain Py2. *J Biol Chem* **272**: 24913–24920.

Smith, T.J. and Dalton, H. (2004) Biocatalysis by methane monooxygenase and its implications for the petroleum industry. In *Petroleum Biotechnology: Developments and Perspectives*. pp. 177–192.

Smith, T.J., Lloyd, J.S., Gallagher, S.C., Fosdike, W.L.J., Murrell, J.C., and Dalton, H. (1999) Heterologous expression of alkene monooxygenase from *Rhodococcus rhodochrous*

B-276. *Eur J Biochem* **260**: 446–452.

Smith, T.J., Slade, S.E., Burton, N.P., Murrell, J.C., and Dalton, H. (2002) Improved system for protein engineering of the hydroxylase component of soluble methane monooxygenase. *Appl Environ Microbiol* **68**: 5265–5273.

Srikanta Dani, K.G. and Loreto, F. (2017) Trade-Off Between Dimethyl Sulfide and Isoprene Emissions from Marine Phytoplankton. *Trends Plant Sci* **22**: 361–372.

Srikanta Dani, K.G., Silva Benavides, A.M., Michelozzi, M., Peluso, G., Torzillo, G., and Loreto, F. (2017) Relationship between isoprene emission and photosynthesis in diatoms, and its implications for global marine isoprene estimates. *Mar Chem* **189**: 17–24.

Srivastva, N., Shukla, A.K., Singh, R.S., Upadhyay, S.N., and Dubey, S.K. (2015) Characterization of bacterial isolates from rubber dump site and their use in biodegradation of isoprene in batch and continuous bioreactors. *Bioresour Technol* **188**: 84–91.

Stirling, D.I. and Dalton, H. (1977) Effect of metal-binding agents and other compounds on methane oxidation by two strains of *Methylococcus capsulatus*. *Arch Microbiol* **114**: 71–76.

Stirling, D.I. and Dalton, H. (1979) Properties of the Methane Mono-oxygenase from Extracts of *Methylosinus trichosporium* OB3b and Evidence for Its Similarity to the Enzyme from *Methylococcus capsulatus* (Bath). *Eur J Biochem* **96**: 205–212.

Studts, J.M. and Fox, B.G. (1999) Application of fed-batch fermentation to the preparation of isotopically labeled or selenomethionyl-labeled proteins. *Protein Expr Purif* **16**: 109–119.

Studts, J.M., Mitchell, K.H., Pikus, J.D., McClay, K., Steffan, R.J., and Fox, B.G. (2000) Optimised expression and purification of toluene 4-monooxygenase hydroxylase. *Protein Expr Purif* **20**: 58–65.

Sullivan, J.P., Dickinson, D., and Chase, H.A. (1998) Methanotrophs, *Methylosinus trichosporium* OB3b, sMMO, and their application to bioremediation. *Crit Rev Microbiol* **24**: 335–373.

Sunda, W.G., Kieber, D., and Kiene, R.P. (2002) An antioxidant function of DMSP and DMS in marine algae oceanic dimethylsulfide (DMS) photolysis. *Nature* **418**: 317–320.

- Swift, R.J., Carter, S.F., Widdowson, D.A., Mason, J.R., and Leak, D.J. (2001) Expression of benzene dioxygenase from *Pseudomonas putida* ML2 in cis-1,2-cyclohexanediol-degrading pseudomonads. *Appl Microbiol Biotechnol* **55**: 721–726.
- Tao, Y., Bentley, W.E., and Wood, T.K. (2005) Regiospecific oxidation of naphthalene and fluorene by toluene monooxygenases and engineered toluene 4-monooxygenases of *Pseudomonas mendocina* KR1. *Biotechnol Bioeng* **90**: 85–94.
- Tee, L. and Schwaneberg, U. (2007) Directed evolution of oxygenases: Screening systems, success stories and challenges. *Comb Chem High Throughput Screen* **10**: 197–217.
- Terry, G.M., Stokes, N.J., Hewitt, C.N., and Mansfield, T.A. (1995) Exposure to isoprene promotes flowering in plants. *J Exp Bot* **46**: 1629–1631.
- Tinberg, C.E., Song, W.J., Izzo, V., and Lippard, S.J. (2011) Multiple roles of component proteins in bacterial multicomponent monooxygenases: Phenol hydroxylase and toluene/o-xylene monooxygenase from *Pseudomonas* sp. OX1. *Biochemistry* **50**: 1788–1798.
- Trainer, M., Williams, E.J., Parrish, D.D., Buhr, M.P., Allwine, E.J., Westberg, H.H., et al. (1987) Models and observations of the impact of natural hydrocarbons on rural ozone. *Nature* **329**: 705–707.
- Vickers, C.E., Gershenzon, J., Lerdau, M.T., and Loreto, F. (2009) A unified mechanism of action for volatile isoprenoids in plant abiotic stress. *Nat Chem Biol* **5**: 283–291.
- Wallar, B.J. and Lipscomb, J.D. (2001) Methane monooxygenase component B mutants alter the kinetics of steps throughout the catalytic cycle. *Biochemistry* **40**: 2220–2233.
- Walters, K.J., Gassner, G.T., Lippard, S.J., and Wagner, G. (1999) Structure of the soluble methane monooxygenase regulatory protein B. *Proc Natl Acad Sci* **96**: 7877–7882.
- Wang, W., Liang, A.D., and Lippard, S.J. (2015) Coupling Oxygen Consumption with Hydrocarbon Oxidation in Bacterial Multicomponent Monooxygenases. *Acc Chem Res* **48**: 2632–2639.
- Waugh, D.S. (2016) The remarkable solubility-enhancing power of *Escherichia coli* maltose-binding protein. *Postepy Biochem* **62**: 377–382.
- Went, F.W. (1960) Blue hazes in the atmosphere. *Nature* **187**: 641–643.
- West, C.A., Salmond, G.P.C., Dalton, H., and Murrell, J.C. (1992) Functional expression in

- Escherichia coli of proteins B and C from soluble methane monooxygenase of *Methylococcus capsulatus* (Bath). *J Gen Microbiol* **138**: 1301–1307.
- Whited, G.M. and Gibson, D.T. (1991) Toluene-4-monooxygenase, a three-component enzyme system that catalyzes the oxidation of toluene to p-cresol in *Pseudomonas mendocina* KR1. *J Bacteriol* **173**: 3010–3016.
- Wiedinmyer, C., Friedfeld, S., Baugh, W., Greenberg, J., Guenther, A., Fraser, M., and Allen, D. (2001) Measurement and analysis of atmospheric concentrations of isoprene and its reaction products in central Texas. *Atmos Environ* **35**: 1001–1013.
- Wiedinmyer, C., Greenberg, J., Guenther, A., Hopkins, B., Baker, K., Geron, C., et al. (2005) Ozarks Isoprene Experiment (OZIE): Measurements and modeling of the “isoprene volcano.” *J Geophys Res D Atmos* **110**: 1–17.
- van den Wijngaard, A.J., Prins, J., Smal, A.J.A.C., and Janssen, D.B. (1993) Degradation of 2-chloroethylvinylether by *Ancylobacter aquaticus* AD25 and AD27. *Appl Environ Microbiol* **59**: 2777–2783.
- Wise, R.R., Olson, A.J., Schrader, S.M., and Sharkey, T.D. (2004) Electron transport is the functional limitation of photosynthesis in field-grown Pima cotton plants at high temperature. *Plant, Cell Environ* **27**: 717–724.
- Xia, B., Pikus, J.D., Xia, W., McClay, K., Steffan, R.J., Chae, Y.K., et al. (1999) Detection and classification of hyperfine-shifted 1H, 2H and 15N resonances in the Rieske ferredoxin component of toluene 4-monooxygenase. *Biochemistry* **38**: 727–739.
- Ye, L., Lv, X., and Yu, H. (2016) Engineering microbes for isoprene production. *Metab Eng* **38**: 125–138.
- Yeager, C.M., Bottomley, P.J., Arp, D.J., and Hyman, M.R. (1999) Inactivation of Toluene 2-Monooxygenase in *Burkholderia cepacia* G4 by Alkynes. *Appl Environ Microbiol* **65**: 632–639.
- Yen, K.-M. and Karl, M.R. (1992) Identification of a new gene, *tmoF*, in the *Pseudomonas mendocina* KR1 gene cluster encoding toluene-4-monooxygenase. *J Bacteriol* **174**: 7253–7261.
- Yen, K.-M., Karl, M.R., Blatt, L.M., Simon, M.J., Winter, R.B., Fausset, P.R., et al. (1991) Cloning and characterization of a *Pseudomonas mendocina* KR1 gene cluster encoding toluene 4-monooxygenase. *J Bacteriol* **173**: 5315–5327.

Yoon, I.-K., Kim, C.-N., and Park, C.-H. (2002) Optimum operating conditions for the removal of volatile organic compounds in a compost-packed biofilter. *Korean J Chem Eng* **19**: 954–959.

Zhou, N.-Y., Jenkins, A., Chan Kwo Chion, C.K.N., and Leak, D.J. (1999) The alkene monooxygenase from *Xanthobacter* strain Py2 is closely related to aromatic monooxygenases and catalyzes aromatic monohydroxylation of benzene, toluene and phenol. *Appl Environ Microbiol* **65**: 1589–1595.

Appendix I

List of solubilities

Henry's constants for gaseous substrates and inhibitors. Taken from Sander, (2015)

| Compound | Henry's constant (M atm ⁻¹) |
|-----------|---|
| Isoprene | 1.3×10^{-2} |
| Ethylene | 4.7×10^{-3} |
| Propylene | 4.8×10^{-3} |
| Butene | 4.0×10^{-3} |
| Pentene | 2.5×10^{-3} |
| Hexene | 2.4×10^{-3} |
| Acetylene | 4.1×10^{-2} |
| Propyne | 9.2×10^{-2} |
| Butyne | 5.4×10^{-2} |

Solubility of compounds (<http://www.chemspider.com/>)

| Compound | Solubility (mM) |
|-------------------|-----------------|
| Hexene | 0.6 |
| Heptene | 0.2 |
| Octene | 0.04 |
| Decene | 0.004 |
| Dodecene | insoluble |
| Octadecene | insoluble |
| 1,3-butadiene | 13.6 |
| 1,4-pentadiene | 8.2 |
| Cyclohexene | 2.6 |
| Methylcyclohexene | 0.5 |
| Benzene | 22.9 |
| Toluene | 5.7 |
| Ethylbenzene | 1.6 |

| | |
|------------------|-----|
| Propylbenzene | 4.3 |
| Styrene | 3.0 |
| <i>o</i> -xylene | 1.0 |
| Hexyne | 4.4 |
| Heptyne | 0.9 |
| Octyne | 0.2 |